DIS3 and its Role in CircRNA Degradation

DISSERTATION

ZUR ERLANGUNG DES DOKTORGRADES
DER NATURWISSENSCHAFTEN (DR. RER. NAT.)
DER FAKULTÄT FÜR BIOLOGIE UND VORKLINISCHE MEDIZIN
DER UNIVERSITÄT REGENSBURG

vorgelegt von

Claudia Latini

aus Velletri (Rom, Italien)

Regensburg, 2021

Das Promotionsgesuch wurde eingereicht am:
23. 04.2021

Die Arbeit wurde angeleitet von:
Prof. Dr. Gunter Meister

Unterschrift:

To my family and Andrea, for their unconditional love and support.

To my grandmother Italia, an example of life.

Table of contents

Abstract

Circular RNAs (circRNAs) are covalently closed, single-stranded endogenous RNAs lacking 5′ end caps and 3′ poly(A) tails. Although the low abundance, these molecules show cell type-, tissue- or developmental stage-specific expression. For decades, circRNAs were considered as byproducts of aberrant splicing. Recent findings unrevealed their cellular functions such as microRNA (miRNAs) or RNA binding proteins (RBPs) sponges, scaffolds and decoys. Although circRNA biogenesis is considerably well understood, it remains intriguing how circRNAs are ultimately degraded, as they are stable and resistant to RNA exonucleolytic decay. Using a biochemical approach, we aim to identify the cellular degradation pathways of circRNAs and the endonucleases involved. To achieve this purpose, using an enzymatic ligation method, we performed *in vitro* synthesis of selected circRNAs and confirmed their circularity. Then, we measured the stability of the synthetic circRNAs and their linear counterpart in cell lysates of different purification approaches. Our data confirmed the high stability of circRNAs compared to the linear counterparts and showed high sensitivity of degradation for circular RNAs in cytoplasmic extracts suggesting cytoplasmic decay pathways. Next, we used mass spectrometry analysis to identify the endonucleases involved in circRNAs degradation and validated them with *in vitro* degradation assays. Furthermore, we characterized the function of DIS3 and its PIN domain using *in vitro* and *in vivo* experiments. *In vitro* experiments show that DIS3 can degrade synthetic circRNAs alone or associated with the exosome and that the PIN domain is responsible for its endoribonuclease activity. RNA-seq analysis from CRISPR/Cas9-mediated DIS3 knockout cells confirmed the potential role of DIS3 in degrading a subset of circRNAs. Among them, three candidates such as circOXCT1, circRERE and circFAM208, show upregulation in DIS3 knockout while their linear RNA counterparts do not change. Finally, proteomic studies of DIS3 function in the nucleus and cytoplasm elucidate the molecular mechanisms behind the regulation of DIS3, which might affect circRNA metabolism. Altogether our study adds a new aspect to the function of DIS3 in regulating circRNA degradation pathway.

1 Introduction

1.1 CircRNA history

The first circRNA was identified in 1976 by Sanger et al. in a study concerning the functions of plant viroids. Electron microscopy analysis suggested that viroids are single-strand covalently closed RNA molecules with a high structured rod-like shape (Sanger et al., 1976). A subsequent work confirmed the circle nature of viroids by Sanger sequencing (Gross et al., 1978). Even though circRNAs had been already discovered as a products of post splicing events in Tetranymena (Cech et al., 1981) and in Archea (Kjems & Garrett, 1988), but only in the 90s the first endogenous circRNAs were detected in complex organisms. Nigro et al. found that exons from the tumor suppressor gene DCC (Deleted in Colorectal Cancer) "were scrambled" during the splicing process generating unexpected transcripts whose ends were covalently closed (Nigro et al., 1991). Similarly, different studies demonstrated the production of highly stable circular transcripts by the human *ETS-1* and the mouse *Sry* (sex-determination region Y) genes (Cocquerelle et al., 1993)(Capel et al., 1993). During the following years, additional endogenous circRNAs were identified from the rat cytochrome P450 2C24 (Zaphiropoulos, 1996), the human cytochrome P450 2C18 (Zaphiropoulos, 1997) and the dystrophine genes (Surono et al., 1999). Nevertheless, with the only exception of the testis-specific circRNA Sry, which was suggested to have a possible role in mouse testis, the other observed circRNAs were usually considered splicing by-products, insignificant intermediates, or occasional events. Only recently, advances in high-throughput sequencing have led to a rebirth of circRNAs revealing their ubiquitous expression in all eukaryotes (Salzman et al., 2012; Hansen et al., 2013; Jeck et al., 2013; Memczak et al., 2013; Zhang et al., 2014; Westholm et al., 2014; Ivanov et al., 2015). Most circRNAs are generated from protein-coding genes, consist of a single exon or multiple exons and are evolutionary conserved (J. U. Guo et al., 2014). Although circRNAs are expressed at low levels, some can accumulate in specific cell types or tissues in a temporally and spatially controlled manner (Rybak-Wolf et al., 2014; You et al., 2015).

1.2 CircRNA biogenesis

CircRNAs are transcribed by RNA polymerase II (Pol II) and are presumably generated by pre-mRNA back-splicing (Y. Zhang et al., 2016). Back-splicing is an alternative type of splicing, in which

a downstream 5'splice site is joined to an upstream 3'splice site. This forms a 3'-5' phosphodiester bond that leads to the formation of a circular RNA (Ashwal-Fluss et al., 2014; Starke et al., 2015; Y. Wang & Wang, 2015) (Figure 1A). Back-splicing seems to be less efficient than canonical splicing, although both mechanisms depend on the same spliceosome machinery. Experiments with circRNA expression vectors and with the splicing inhibitor isoginkgetin confirmed that back-splicing requires the canonical splicing sites and factors (Ashwal-Fluss et al., 2014; Starke et al., 2015; Y. Wang & Wang, 2015). Interestingly, Liang et al. found that, in *Drosophila melanogaster* (*D. melanogaster*) cells, depletion of the core spliceosome or of the transcription termination factors increases the levels of circular respect to the linear RNAs (Liang et al., 2017). This suggested that when canonical pre-mRNA processing is slowed down or inhibited, nascent RNAs can be directed into alternative pathways that facilitate back-splicing. Moreover, there is not a clear correlation between linear and circular RNA relative levels, but in most cases, circRNA expression is lower than the linear counterpart (J. U. Guo et al., 2014).

Furthermore, circRNA production can also be associated with splicing intermediates known as lariats. In detail, circRNAs can derive from post-transcriptional back-splicing of a lariat during exon-skipping events or from splicing of an intronic lariat that escapes from debranching (Kelly et al., 2015; Y. Zhang et al., 2013) (Figure 1B). The gene *Saccharomyces pompe* (*S. pompe*) mrps16 is an example of exon skipping that leads to circRNA formation. In this case, the splicing of mrps16 gene results in the production of a mature linear mRNA and of an exon2-containing lariat that is subsequently back-spliced in a circRNA (Barrett et al., 2015).

CircRNAs are classified on the basis of intronic and/or exonic composition in three different types of circRNA: exonic, intronic and exonic-intronic circRNAs. Exonic circRNAs (EcircRNAs) consist of only exonic sequences and can contains one exon or multiple exons. In human, the most common ecircRNAs contain two or three exons and are localized in the cytoplasm (I. Chen et al., 2015) (Figure 1A). Alternatively, if the intron between the exons is retained, the resulting circRNA is an exon–intron circRNA (EIcircRNAs) (Li et al., 2015). Finally, intronic-circRNAs (ciRNAs) contain only intronic sequences and are derived from intron lariats that escape from debranching (Zhang et al., 2013)(Figure 1B).

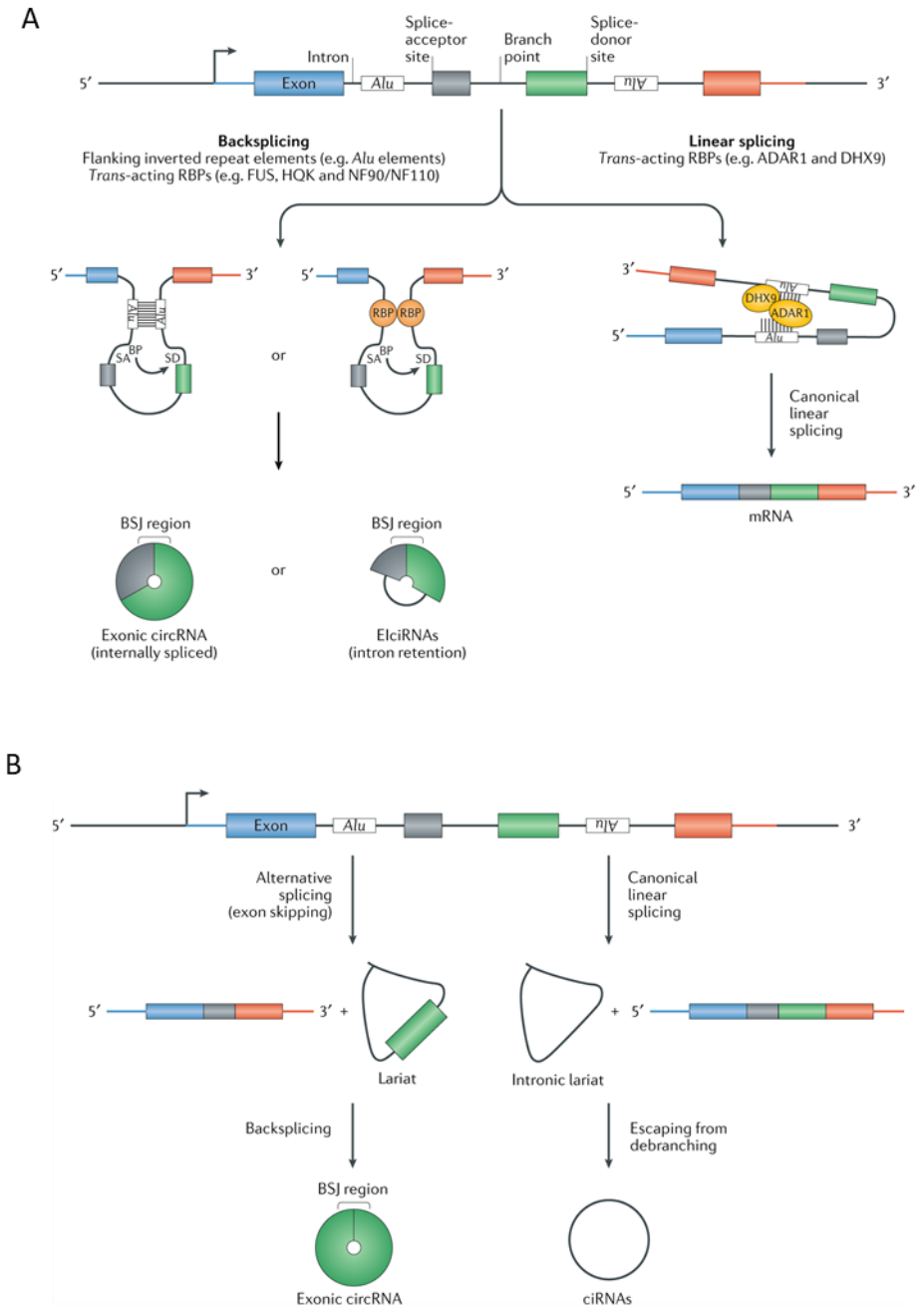

Figure 1. The biogenesis of circRNAs. (A) A pre-mRNA can be alternatively spliced to generate a linear or a circular RNA. When a 5'splice site (5'ss) is joined to an upstream 3'splice site (3'ss), a circRNA is generated and the ends are covalently closed by a 3'-5' phosphodiester bond. CircRNA formation is promoted by cis intron flanking inverted repeats and/or trans acting RNA Binding Proteins (RBPs). Back-splicing leads to the formation of exonic circRNAs (EcircRNAs) (when the intron is spliced out) or of exonic-intronic circRNAs (EIciRNAs) (when the intron is retained). (B) CircRNAs can also be generated from lariat precursors during an exon skipping event or from intronic lariats that escape debranching. Intronic circRNAs (ciRNAs) derive from intron lariat (modified from Kristensen et al. 2019).

1.3 Regulation of circRNA biogenesis

CircRNA production is modulated by introns with reverse complementary repeats (*cis*-regulators) and/or RNA-Binding Proteins (RBPs) (*trans*-regulators) (Figure 2). Both regulators enhance back-splicing by bringing the downstream splice-donor site in proximity to the upstream splice-acceptor site. This is coupled with the formation of a loop between flanking introns that facilitate the back-splicing. Most circRNAs are flanked by long introns that contain inverted repeats known as Alu elements. These repeats can form duplexes by RNA pairing and favour circular RNA production (Ivanov et al. 2015; Liang and Wilusz 2014; X. O. Zhang et al. 2014b) (Figure 2A). Even though short sequences of 30-40 bases are enough to enhances circRNA production, longer duplexes are more efficient (X. O. Zhang et al. 2014b; Liang & Wilusz, 2014). Not all exonic circRNAs are flanked by introns with inverted repeats, suggesting the presence of alternative mechanisms for circRNA formation. In addition to *cis*-regulators, *trans*-acting RBPs can promote circRNA biogenesis. In fact, in *D. melanogaster*, the splicing factor Muscleblind (Mbl) promotes the circularization of its own second exon by binding highly conserved regions in the flanking introns (Ashwal-Fluss et al., 2014) (Figure 1.2B). Similarly, the protein Quaking (QKI) promotes general circRNA formation during the human epithelial-mesenchymal transition by probably dimerizing and binding to intronic sequences of circRNA exons (S. J. Conn et al., 2015) (Figure 2C). In addition, FUS binds specifically the exon-intron junction and enhances general circRNA biogenesis in mouse embryonic stems cell-derived motoneurons (Errichelli et al., 2017). Interestingly, *cis* and *trans* regulators are not always independent of each other but they can also act synergistically for circRNA formation. This is the case of the laccase 2 circRNA, in *D. melanogaster*, whose biogenesis is regulated by a combination of intronic repeats and different RPBs including multiple hnRNPs (Heterogeneous nuclear ribonucleoproteins) and SR (Serine and arginine-rich) proteins (Kramer et al., 2015). The biogenesis of circRNAs can also be regulated negatively by RBPs. In fact, the double-stranded RNA (dsRNA) specific adenosine deaminase (ADAR) enzymes prevent back-splicing by editing adenosine to inosine (A-to-I editing) in the intronic inverted repeat Alu elements (Eisenberg & Levanon, 2018) (Figure D). Similarly, the ATP-dependent helicase A (also known as DHX9) represses circRNA production by unwinding RNA pairs between intronic inverted repeats (Aktaş et al., 2017).

A peculiar case of biogenesis regulation is mediated by the immune response factor NF90/NF110 which promotes back-splicing in the nucleus by associating with intronic flaking RNA duplexes. Interestingly, upon viral infection, NF90/NF110 is exported to the cytoplasm where it binds the viral mRNAs with consequent downregulation of circRNA levels (X. Li et al., 2017).

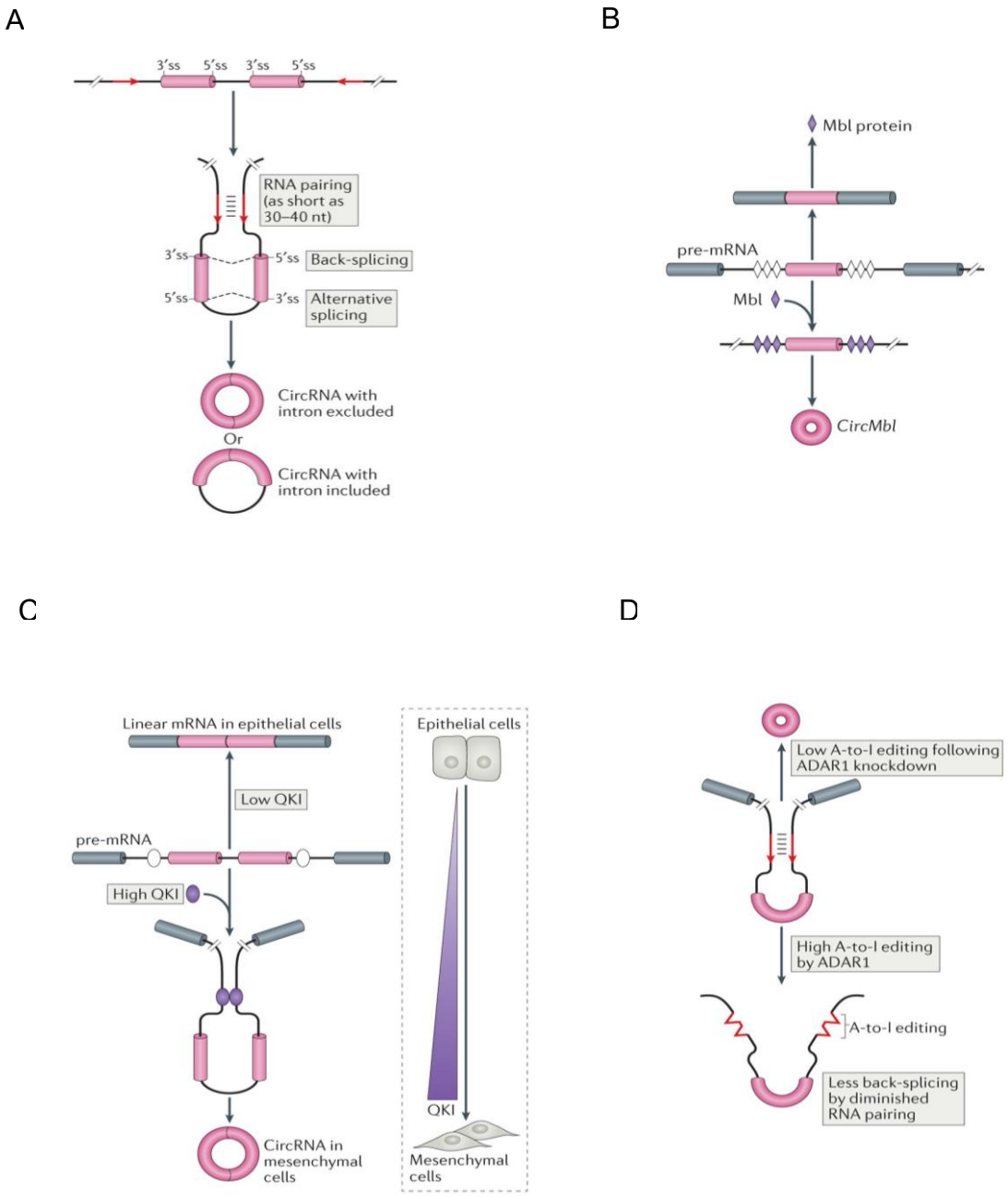

Figure 2. Regulation of circRNA biogenesis. (A) Base pairing between intronic repeats promotes the formation of the looping and back-splicing. (B) Muscleblind (Mbl) promotes back-splicing of its own pre-mRNA by binding the introns flanking sequences. (C) In epithelial cells, a low concentration of QKI protein promotes canonical linear splicing. In mesenchymal cells, a high concentration of QKI promotes back-splicing by dimerization and subsequent binding to the intronic flanking sequences of the QKI-regulated pre-mRNAs. (D) A-to I RNA editing mediated by ADAR1 represses circRNA biogenesis by blocking RNA duplexes formation in the intronic flanking sequences (Modified from L. L. Chen 2016).

1.4 Properties of circRNAs

1.4.1 *Cellular localization*

Once circRNAs are generated, they are mainly exported in the cytoplasm, except of circRNAs containing retained introns (Z. Li et al., 2015). Similar to many linear RNAs (Braunschweig et al., 2014), these circRNAs are sequestered in the nucleus. The work of Huang et al. provides the first evidence of how circRNAs are exported from the nucleus to the cytoplasm (Huang et al., 2018). In human cells, the nuclear RNA helicase URH49 (DDX39A) and the DEAD box protein UAP56 (DDX39B) mediate nuclear export in a length-dependent manner. UAP56 exports long circRNAs (>1200 nucleotides) while URH49 exports short circRNAs (<400 nucleotides). However, circRNAs with intermediate sizes might require a different mechanism (Huang et al., 2018).
Interestingly, circRNAs can have specific localizations. Many brain-enriched circRNAs are localized to synapses, axons and dendrites. CircStau2a is an example of synaptic circRNA. Different from its linear mRNA that is localized exclusively in the cytoplasm, circStau2a is enriched in synapses. Nevertheless, the biological function and the transport mechanism in the synapses remain to be clarified (Rybak-Wolf et al., 2014; You et al., 2015). Due to their high stability, circRNAs can also accumulate in extracellular compartments as body fluid. For instance, the population of circRNAs circulating in the blood is very abundant and more than 1000 circRNAs can also be detected in human serum exosomes and some of them specifically in patients with colon rectal cancer (Yan Li et al., 2015; Memczak et al., 2015).

1.4.2 *Stable structure*

CircRNAs are very stable due to their circular structure, which lacks 3’ and 5’ ends and is resistant to the exonucleolytic decay machinery. Half-life experiments with 4-thiouridine metabolic labelling show that most circRNAs have a longer half-life (19-24h) than the linear counterparts (4-7h) (Jeck & Sharpless, 2014). Additionally, circRNAs accumulate in cell types and tissues that do not divide or with low proliferation rate (Bachmayr-Heyda et al., 2015).

1.4.3 *Evolutionary conservation*

CircRNAs are expressed in all domains of life including Archaea, plants, yeast and metazoans (Danan et al., 2012; Salzman et al., 2013; P. L. Wang et al., 2014; Ye et al., 2015). Interestingly, many circRNAs are evolutionary conserved not only in terms of genes, but also in terms of expression, splice site and flanking sequences. For example, Jeck and Sharpless found that 457 (22%) human

circRNAs are also produced from murine testis pre-mRNAs, but only 69 (3%) of them contain homologous back-splice sites (Jeck & Sharpless, 2014). Similarly, another study demonstrates that circRNAs are very conserved between human and mouse brains at the level of splice sites and flanking regions (Rybak-Wolf et al., 2014). In fact, most of analysed circRNAs share the same splice sites and contain similar inverted repeats in the intron flanking sequences in mouse and human brains, demonstrating a very high degree of conservation within mammalian brain. An additional type of circRNA conservation has been reported: the circRNA/mRNA ratio across the evolution. One example is circRims2 that is two times more abundant than the linear counterpart in human and mouse brains suggesting potential conservation of the regulatory function (Rybak-Wolf et al., 2014).

1.4.4 *Tissue-specific expression*

Most circRNAs are expressed in a tissue-specific way. For instance, circRNAs accumulate at a very high level in neural tissue (Rybak-Wolf et al., 2014; Venø et al., 2015; You et al., 2015). The reasons for this enrichment can be found in the nature of neurons: cells that own the highest rate of alternative splicing and that generally do not divide. As products of alternative splicing and long-lived molecules, circRNAs find a fertile ground for specific expression in the brain. Interestingly, circRNA expression in brain is highly specific and does, in most cases, not dependent on the parental linear pre-mRNA expression (Rybak-Wolf et al., 2014; Venø et al., 2015; You et al., 2015). Furthermore, circRNAs accumulate in flies and mice in an age-dependent manner (Venø et al., 2015; Westholm et al., 2014; You et al., 2015). For example, in the brain of a 22 month old mouse, the expression of many circular RNAs such as mm9_circ_004501 and mm9_circ_013636 is increased compared to that of a 1-year-old mouse (Gruner et al., 2016). A handful of circRNAs is extremely regulated during the Epithelial-to-Mesenchymal Transition (EMT), suggesting a possible function in cell migration, invasion and metastasis (S. J. Conn et al., 2015). CircRNAs are also expressed in heart tissues. The first circRNA expression profiling in adult murine hearts was provided by the study of Jacobi et al., in 2016 (Jakobi et al., 2016). Subsequent work showed that between 7000 and 16000 different circRNAs are expressed in human heart (Tan et al., 2017; Werfel et al., 2016). Unlike brain, only 5% of the human circRNAs are also expressed in mouse heart suggesting a low conservation during evolution (Aufiero et al., 2018). In addition, more the 2400 circRNAs were found in human whole blood and several studies detected about 1000 circRNAs in exosome from human serum and more of 400 circRNAs in saliva (Bahn et al., 2015; Yan Li et al., 2015; Memczak et al., 2015). The stability of these circRNAs suggests a possible implication as disease biomarkers.

1.5 Biological functions of circRNAs

Recent studies have revealed that circRNAs can regulate gene expression at different levels. In the cytoplasm, circRNAs can act like microRNA sponges. Additionally, some circRNAs associate with RBPs and act as scaffolds, sponges or decoys. Although circRNAs are considered non-coding RNA, a handful of circRNAs might also be translated in a cap-independent manner. In the nucleus, intronic containing circRNAs can affect transcription and splicing. The currently known biological functions of circRNAs are summarized in Figure 3.

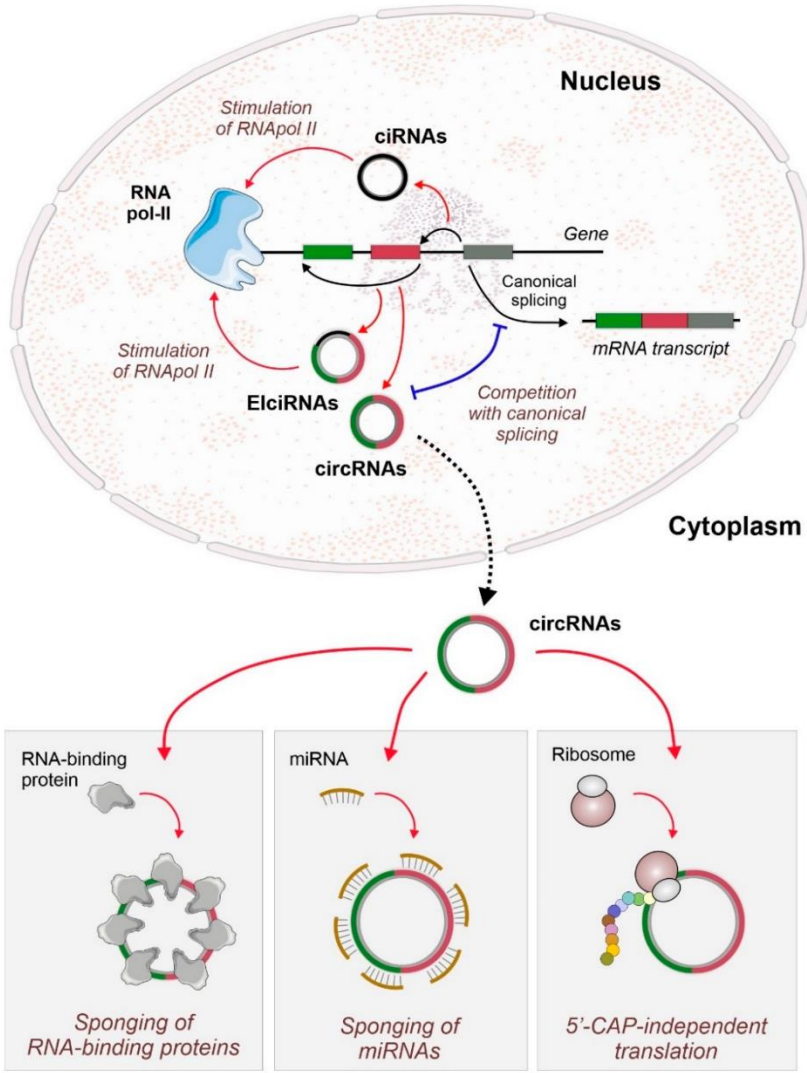

Figure 3. Biological function of circRNAs. In the nucleus, Exonic-Intronic ciRNAs can stimulate transcription by direct interaction with Pol II. In the cytoplasm, circRNAs can act as miRNA or RBP sponges and compete with the target mRNA. CircRNAs can also associate with ribosomes and translate into small peptides in a cap-independent manner (Gabriel et al., 2020).

1.5.1 *MiRNA sponges*

The initial search for conserved miRNA binding sites in highly abundant circRNAs together with the observation that circRNAs could be targeted by RNA interference suggested that they may compete with mRNA for miRNA binding and work, indeed, like miRNA sponges. The mouse Sex-determining region Y (Sry) and CDR1as (also known as ciRS-7) are the most well-known cases (Capel et al., 1993; Thomas B. Hansen, Jensen, et al., 2013; Thomas B Hansen et al., 2011). The Sry circRNA possesses 16 binding sites for mir-138, but the functional significance of this circRNA has not been elucidated so far (Thomas B. Hansen, Jensen, et al., 2013). In contrast, the ciRS-7 is highly expressed in brain and contains 73 binding sites for miR-7 but none of them is perfectly complementary, suggesting that this circRNAs can regulate miR-7 level and activity. Additionally, ciRS-7 also contains one perfect complementary binding site for miR-671 that can mediate the endonucleolytical cleavage of the circRNA by Argonaute 2 (AGO2) (Thomas B. Hansen, Jensen, et al., 2013; Thomas B Hansen et al., 2011). Piwecka et al. (2017) provides the first circRNA knockout mouse model to study the interaction between ciRS-7 and these miRNAs in the functional brain (Piwecka et al., 2017). When ciRS-7 genomic region is deleted, knockout mice are viable and fertile but display an impaired behaviour phenotype associated with neuropsychiatric disorders. At the molecular level, the expression of miR-7 is downregulated while miR-671 is up-regulated in all brain regions, suggesting that the presence of ciRS-7 stabilizes instead of titrates miR-7. This results in an increased expression of the miR-7 target genes, including immediate early genes, like Fos that is important for neuronal activity. A recent study reveals that ciRS-7 takes part in an even more complicated regulation network that includes the long-non-coding RNA (lncRNA) Cyrano, highlighting the importance of a thoroughly balanced gene expression for proper brain function (Kleaveland et al., 2018).

CircRNA sequences and analysis of AGO2 PAR-CLIP **(**photoactivatable ribonucleoside-enhanced crosslinking and immunoprecipitation) show that most circRNAs contain very few miRNAs binding sites (J. U. Guo et al., 2014). However, there are several other cases of circRNAs that can function as miRNA sponges. An example is circHIPK3 that, via luciferase screening, serves as a sponge for 9 miRNAs with 18 potential binding sites. Specifically, CircHIPK3 binds directly miR124 and suppresses its activity *in vivo* (Zheng et al., 2016). Another study shows that CircHIPK3 has two binding sites for miR-558 and can inhibit the migration, invasion and angiogenesis of bladder cancer cells by sponging miR-558 (Yawei Li et al., 2017). CircBIRC6 and circCORO1C, on their part, enhance the pluripotency of human embryonic stem cells by suppressing the well-known pluripotency genes NANOG, OCT4 and SOX2 via miRNA sponging (Yu et al., 2017). Instead, CircZNF91 is up-regulated during differentiation of epidermal stem cells and contains 24 binding sites for miR-23b-

3p, which is implicated in keratinocyte differentiation (Kristensen et al. 2018). However, as already mentioned in the work of Guo et al., 2014, further analyses are necessary to understand whether miRNA-sponge can be considered a general function of circRNAs or just a specific function of few isolated cases (J. U. Guo et al., 2014).

1.5.2 *RBP interactors*

In addition to miRNAs, circRNAs can also interact with RBPs and acts as RBP decoys, sponges or scaffolds (L. L. Chen, 2020). One of the first examples is circMbl, a circRNA that derives from the second exon's circularization of the splicing factor muscleblind (MBL/MBLN1), in flies and humans (Ashwal-Fluss et al., 2014). Notably, circMbl and its flanking introns contain conserved binding sites for the protein MBL. The alteration of MBL levels strongly affects circMbl production depending on the MBL binding sites. In detail, overexpression of MBL promotes the looping of the flanking introns and induces circRNAs biogenesis at the expense of its own mRNA production. This suggests that circMbl can act as protein sponge in normal condition and induce linear splicing by tethering MBL protein (Ashwal-Fluss et al., 2014). CircANRIL and circPABPN1 are other circRNA examples that function similarly (Abdelmohsen et al., 2017). In human cervical carcinoma Hela cells, CircPABPN1 represses the translation of its linear counterpart PABPN1 mRNA, by sequestering the RBP Hu-antigen R (HUR). This is the first example of competition of a circRNA and its own mRNA for an RBP that affects translation (Abdelmohsen et al., 2017).In addition, in vascular tissue, circANRIL sequesters PES1 (Pescadillo ribosomal biogenesis factor 1) and impars ribosomal RNA (rRNA) maturation, leading to nucleolar stress and apoptosis (Holdt et al., 2016).

CircFOXO3 represents the first case of circRNA acting as protein scaffold (Du et al., 2016). In murine NIH3T3 fibroblasts, circFOXO3 blocks cell cycle progression by forming a ternary complex with cyclin-dependent kinase inhibitor 1 (p21) and cyclin-dependent kinase 2 (CDK2). Notably, the formation of this circ-FOXO3-p21-CDK2 ternary complex inhibits the function of CDK2 and consequently blocks cell cycle progression (Du et al., 2016). CircFOXO3 also facilitates the interaction between the mouse double-minute 2 (MDM2) and p53, which promotes the degradation of p53 by ubiquitination and subsequently cell apoptosis (Du et al., 2017). Finally, circAmotl1 is another example of a protein scaffold. In primary cardiomyocytes, circ-Amotl1 interacts with the 3-phosphoinositide dependent protein kinase 1 (PDK1) and AKT1 (protein kinase b). This interaction leads to the PDK1 dependent-phosphorylation and subsequent localization of AKT1 in the nucleus, where it reduces apoptosis and promotes cardiac repair (Y. Zeng et al., 2017). Even though published data and several tools suggests possible circRNA-RBP interactions, the different isoforms of a

specific circRNA and the linear mRNA counterpart remain to be considered for the subsequent validation.

1.5.3 *Transcriptional regulators*

CircRNAs are mainly localized in the cytoplasm with the exceptions of the intron-circRNAs (ciRNAs) and exon-intron circRNAs (EIciRNAs). Even though nuclear retention mechanisms remain elusive, these circRNAs can regulate gene expression at transcriptional level by interaction with RNA polymerase II (PolII) and/or the U1 snRNP, an essential component of the pre-mRNA splicing machinery (Figure 4). One of the first hints for such function comes from a large polyA(-) RNA-seq screening study in human cells that identified ciRNAs. One abundant example is ci-ankrd52 that largely accumulates to its site of transcription and associates with the elongating Pol II machinery. Depletion of ci-ankrd52 decreases the transcription of the parental ankyrin repeat domain 52 (ANKRD52) gene suggesting that ankrd52 act as a positive regulator of Pol II transcription (Zhang et al., 2013) (Figure 4A). Another study reported a class of circRNAs associated with RNA polymerase II in human (Y. Zeng et al., 2017). Among them, knockdown of circEIF3J and circPAIP2 reduces transcription of their parental genes. Mechanistically, circEIF3J and circPAIP2 interact with U1 snRNP via specific RNA-RNA interaction and promote RNA pol II transcription of their own parental genes (Figure 4B). In Arabidopsis, the circRNA generated from the exon 6 of SEPELLATA, circular SEP3, forms an R-loop (RNA-DNA hybrid) at the parental locus that increases the expression of a linear cognate SEP3 with exon 6 skipped. It is possible that this R-loop may cause a pause during transcription elongation that helps to recruit alternative splicing factors (V. M. Conn et al., 2017)

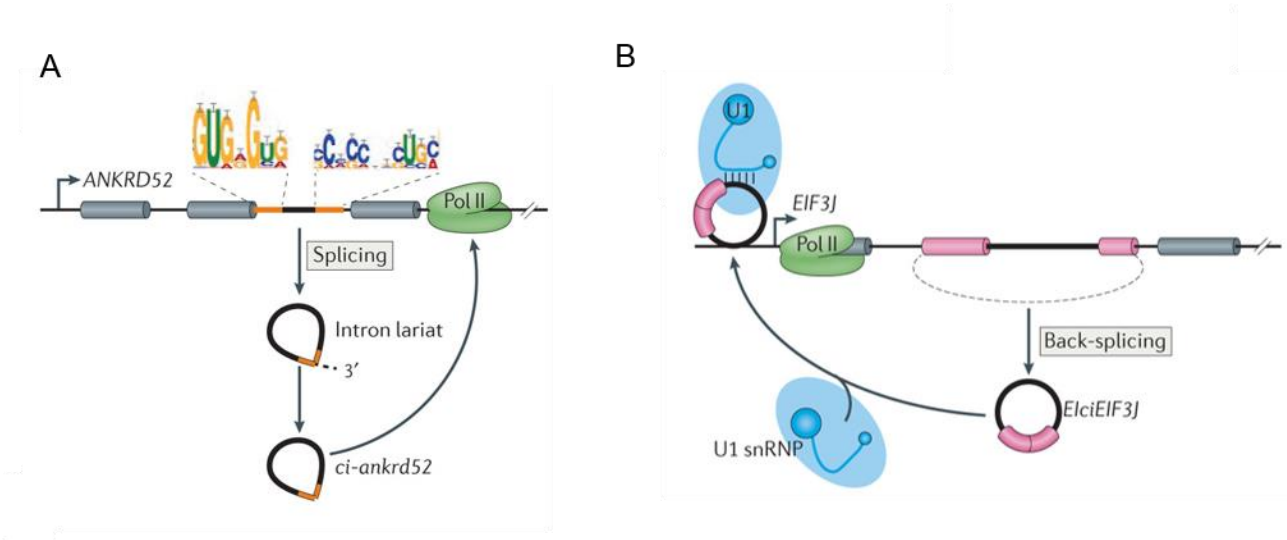

Figure 4. CircRNAs in trascription regulation. (A) The intronic circRNA ci-ankrd52 is generated from an intron lariat that escapes debranching depending on consensus sequences. Ci-ankrd52

localizes mainly in the nucleus where it interacts with Pol II and promotes transcription of its own gene. (B) EIciEIF3J is a back-spliced circRNA with a retained intron that interacts with U1 snRNP and the promoter of EIF3J gene to enhance transcription by Pol II (L. L. Chen, 2016).

1.5.4 *Translation*

CircRNAs lack 5'cap and poly(A) tails which are requirements for cap-dependent translation. Nevertheless, the presence of internal ribosomal entry sites (IRES) or N6-methyladenosine (m^6A) modification can promote cap-independent translation of artificial circRNAs *in vitro* (Chang You Chen & Sarnow, 1995) and *in vivo* (Abe et al., 2015; Meyer et al., 2015; Y. Wang & Wang, 2015). Even though early ribosome profiling studies failed to find endogenous circRNAs co-sedimentating with ribosomes, in 2017 three groups reported that circRNAs might be translated (Legnini et al., 2017; Pamudurti et al., 2017; Y. Yang et al., 2017). Firstly, Legnini et al. (2017) proved the existence of a circRNAs-derived peptide by different assays including ribosome profiling, artificial expression constructs and western blot. Specifically, the human circZNF609 contains an open reading frame that starts at the same start codon as the linear ZNF609 mRNA but ends three nucleotides after the back-splicing junction. Additionally, this study shows that the untranslated region (UTR) of the circRNA sequence may contain a potential IRES. Although knockdown of the circZNF609 represses myoblast differentiation, it is still unclear if this effect is due to the endogenous peptide, which could not be detected. Secondly, using a ribosome footprinting approach in fly heads, Pamadurti et al. found a group of circRNAs associated with ribosomes (Pamudurti et al., 2017). Many of them contain an IRES and share a start codon with the hosting mRNA whereas the stop codon is evolutionarily conserved and unique. Interestingly, they also confirmed by mass spectrometry a circRNA-derived protein from the gene locus muscleblind, circMBL (Pamudurti et al., 2017). Furthermore, through polysome profiling, computational prediction and mass spectrometry, Yang et al. (2017) identified m^6A enriched circRNAs with translation potential in cancer cell lines and human fibroblasts. Notably, they also found that the consensus m^6A motifs, such as RRACH (R can be either A or G, and H can be A, C or U) motifs, are enriched in circRNAs and a single m^6A site is sufficient to drive translation initiation. Interestingly, YTH domain-containing family protein 3 **(**YTHDF3) may recognize the m^6A modification on the circRNAs and recruit the translation initiation factors eIF4G2. This finding was further strengthened by two other studies showing that m^6A modification promotes translation of circRNA in cells (Di Timoteo et al., 2020; Zhao et al., 2019).

These three studies do not provide insights into the functional importance of the circRNA-derived peptides. Further investigations are required to understand if these circRNAs are really translated at a significant level or represent cellular noise. In this context, it is important to mention the recent

work of Ho-Xuan et al. (2020), which offers a comprehensive analysis of circRNA translation from overexpression constructs (Ho-Xuan, GlaÅar, et al., 2020). While it confirms that circZNF609 can be translated from overexpression constructs and encoded for a subset of peptides, this study points out that most of the apparent circ-ZNF609 translation products derive from linear trans-splicing by-products of the overexpression plasmids. Furthermore, this finding together with the evidence that endogenous peptides are not always detected, suggests that circRNA overexpression constructs need to be considered carefully for functional studies and since such standards have not always been applied, circRNA translation remains still controversial. Indeed, comprehensive bioinformatics analysis has shown that circRNAs are generally not the template of translation (J. U. Guo et al., 2014; T. B. Hansen, 2021; Stagsted et al., 2019).

Nevertheless, there is more and more evidence that circRNAs can be translated in cells and even encode for functional proteins. Indeed, circRNA-derived peptides are often N-terminal truncated versions of the full-length protein encoded by the linear cognate. These truncated versions may have dominant negative functions or act as decoys or scaffolds. An example is the SHPRH-146aa peptide that derives from the circSHPRH and acts as a tumour suppressor. Mechanistically, the SHPRH-146aa peptide seems to protect the full-length SHPRH protein from ubiquitination and subsequent degradation (M. Zhang et al., 2018). Another example is SMO-193a.a., a novel protein encoded by circular SMO (circ-SMO). SMO-193a.a is essential for Hedgehog signaling activation in glioblastoma, guides glioblastoma tumorigenesis and represents a potential target for glioblastoma treatment (Wu et al., 2021).

1.6 CircRNA and disease

In-depth analyses of RNA sequencing data sets reveal that circRNAs are expressed in all human tissues. This widespread expression together with the unusual high stability make circRNAs important biomarkers for disease with potential therapeutic implications. The well-known circRNA, CDR1as (circRNA sponge for miR-7), is involved in neurogenerative diseases like Alzheimer disease as well in diabetes and atherosclerosis (Lukiw, 2013; Weng et al., 2017). Notably, circHIPK3 and CDR1as regulate insulin secretion and cells function in diabetes mellitus by acting as miRNA sponges (Stoll et al., 2018). In addition, CircANRIL, the circular antisense transcript of the INK4/ARF tumour suppressor locus, prevents atherosclerosis by regulating ribosomal RNA maturation (Holdt et al., 2016). Recently, two high-throughput-RNA studies identified new circRNAs as a potential biomarker in systemic lupus erythematosus (Miao et al., 2019) and in psoriasis (Moldovan et al., 2019).

CircRNAs have also been characterized in solid tumours where they can act as oncogenes or tumour suppressors. For example, circPVT1 plays an oncogenic role in head and neck squamous cell carcinoma (HNSCC) by modulating the expression of miR-497-5p and genes involved in the control of cell proliferation (Verduci et al., 2017). CircZNF609 also functions as oncogene to regulate several types of cancer, for example rhabdomyosarcoma (Rossi et al., 2019) hepatocellular carcinoma (He et al., 2020) or colorectal cancer (Ho-Xuan, Lehmann, et al., 2020). On the other hand, the circSMARCA5 and the protein derived by the circ-SHPRH show a tumour suppressor function in glioblastoma (Barbagallo et al., 2018; Begum et al., 2018). Curiously, some circRNAs can have different roles depending on the cell tumour type-specificity. One of such cases is circHIPK3 that acts as oncogene in colon rectal cancer (K. Zeng et al., 2018) and as tumour suppressor in bladder cancer (Yawei Li et al., 2017). Another interesting aspect of circRNAs in cancer is that there is a correlation between circRNAs abundance and proliferation rate of cells. Bachmayr-Heyda et al., (2015) were the first to report a general reduction of circRNAs expression in different cancer cells (colorectal, ovarian and idiopathic lung fibrosis) respect to normal tissue suggesting a model of how circRNAs may accumulate in non-proliferative cells (Bachmayr-Heyda et al., 2015).

1.7 Degradation of circRNAs

CircRNAs lack free ends and for this, they escape the canonical RNA exonucleolytic decay pathways. Furthermore, due to the high stability, circRNAs have long half-life and preferentially accumulate in cells with low proliferation rates like neurons. It is possible that when the proliferation rate is high, circRNAs are not newly transcribed but diluted (Y. Zhang et al., 2016). Nevertheless, it is very likely that general pathways exist to ultimately degrade circRNAs. One untested hypothesis is that specific endonucleases could initiate the circRNA degradation and once the circular structure is open, a combination of endo- and exonuclease could take part. Macke in 1998 and Schaeffer et al. in 2009 suggested that two endoribonucleases, RNase E and Rrpp44, respectively, were able to cleave synthetic circRNAs *in vitro* (Mackie, 1998; Schaeffer et al., 2009). Only recently, some insights into circRNA degradation *in vivo* have been reported. An initial study suggested that a subset of m^6A-containing circRNAs can be subject to endonucleolytic cleavage by the ribonuclease P (RNase P)/multidrug resistant-associated protein 1 (MRP) complex (Park et al., 2019). The degradation of m^6A-containing circRNAs is mediated by the interaction of the m^6A reader protein YTHDF2 with the adaptor protein HRSP12 (also known as heat-responsive protein 12) that facilitates the recruitment of RNase P/MRP (Park et al., 2019) (Figure 5C). Notably, 11 m^6A-containing circRNAs are enriched in YTHDF2 immunoprecipitation but only three of them are up-regulated in YTHDF2 or HRSP12

knockdown. This study suggests that a subset of m^6A-containing circRNAs might be endoribonucleolytically cleaved by a YTHDF2-HRSP12-RNase P/ MRP axis but further mechanistic insights are still missing. Another relevant study in this field found that circRNAs are globally degraded by the endoribonuclease RNase L upon poly (I:C) (polyinosinic:polycydylic acid) stimulation, which mimics viral infection (Figure 5B). In detail, authors show that endogenous circRNAs tend to form 16-26 bp imperfect RNA duplexes and act as inhibitors of the double-stranded RNA (dsRNA)-activated protein kinase (PKR) related to innate immunity. Viral infection leads to activation of RNase L, which endoribonucleolytically cleaves circRNAs, with subsequent release and activation of PKR (C. X. Liu et al., 2019)(Figure 5B). Furthermore, the ATP-dependent RNA helicase upstream frameshift 1 (UPF1) and its associated endonuclease G3BP1 can mediate degradation of highly structured circRNAs (Fischer et al., 2020). Although the mechanism has not been elucidated so far, depletion of either proteins increased steady-state levels of mRNAs with highly structured 3′ UTRs as well as highly structured circular RNAs (Figure 5D). UPF1 plays a crucial role in nonsense-mediated mRNA decay (NMD) and is involved in other diverse mRNA decay pathways mediated by a variety of RNA-binding proteins (Y. K. I. Kim & Maquat, 2019).

It is important to consider that all the above-mentioned endonucleases are not specific for circRNA degradation. For example, RNase L cleaves also viral and linear transcripts or YTHDF2-HRSP12-RNase P/MRP and UPF1-G3BP1 complexes mainly degrade m^6A-cointaning linear mRNAs and highly structured 3'UTR containing linear mRNAs, respectively.

Until now, circRNA CDR1as is the unique example of degradation mediated by RNA interference (RNAi) (Figure 5A). Interestingly, the miR-671 binds a full complementary site on CDR1as and activate its cleavage by AGO2 that is a key factor in RNAi. This mechanism is supported by the fact that deletion of this site causes an increase in CDR1as levels.

Several studies have found circRNAs enriched in exosomes suggesting that exocytosis might also be a mechanism of circRNA removal (Dou et al., 2016; Lasda & Parker, 2016). However, it is not clear whether the secretion by vesicles really contributes to the reduction of the endogenous circRNAs levels. What is known so far is that vesicle-mediated export prefers smaller circRNAs and might be important for cell communication (Yan Li et al., 2015; Preußer et al., 2018).

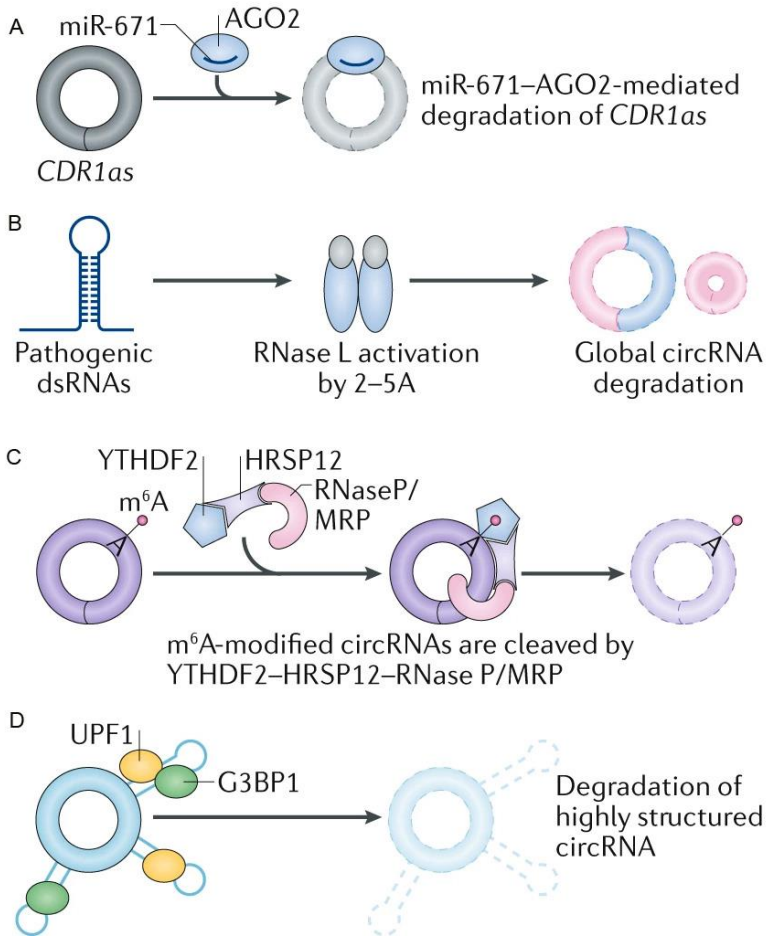

Figure 5. Degradation of circRNAs. (A) CDR1as is the unique case in which circRNA degradation is mediated by miR-671-directed AGO2 cleavage. (B) Pathogenic double-stranded RNAs (dsRNA) activate the endonuclease RNase L and cause global degradation of circRNAs. (C) M^6A modified-circRNAs can be bound by the reader YTHDF2 and the adaptor HRSP12 which recruits the endonuclease complex RNase P/MRP and thus promotes degradation of a subset of circRNAs. (D) The ATP-dependent RNA helicase upstream frameshift 1 (UPF1) and its associated endonuclease G3BP1 can bind and degrade highly structure circRNAs (L. L. Chen, 2020).

1.8 Degradation of mRNAs

Eukaryotic mRNAs contain two important stability structures: the 5' 7-methyguanosine cap and 3' poly(A) tail that are incorporated during and after transcription respectively (Ahn et al., 2004; Moteki & Price, 2002). In the cytoplasm, the 5' cap is recognized by the eukaryotic translation initiation factor 4E (eIF4E) and the poly(A) by the poly(A)-binding protein (PABP). Next, eIF4E associates in a complex and interacts with PABP to form a closed loop that protects the transcripts from exoribonucleases and mediates translation initiation (Jackson et al., 2010). The mRNA degradation starts either when one of this structure is removed or when the mRNA is cleaved internally by

endoribonucleases. Therefore, there are three mRNA degradation mechanisms: deadenylation-dependent, deadenylation-independent or endonuclease-mediated mRNA decay (Figure 6).

Deadenylation-dependent mRNA decay (Figure 6a). The majority of RNAs initiates degradation through poly(A) shortering. The poly(A) tail is removed by the deadenylase activity of CCR4-NOT and Pan2-Pan3 complexes. Interestingly, Pan2-Pan3 is only responsible for initial poly(A) trimming since it does not degrade poly(A) tail completely (Yamashita et al., 2015). Deadenylation is considered as a "rate-limiting" step for starting mRNA decay in both 5'-3' and 3'-5' directions. In fact, deadenylation can lead to 5' decapping by the Dcp1-Dcp2 complex with subsequent Xrn1 exonuclease mediated-decay in the 5'-3' direction (Braun et al., 2012). Alternatively, the unprotected 3' end can be attacked by the large complex exosome that degrades mRNA in 3'-5' direction (Houseley et al., 2006). In this case, the remaining 5' cap fragment is then hydrolysed by the scavenger-decapping enzyme Dcps (H. Liu et al., 2002).

Deadenylation-independent mRNA decay (Figure 6b). Although most mRNAs go through the deadenylation-dependent pathway, some specific mRNAs seem to bypass it. In *Saccharomyces cerevisiae* (*S. cerevisiae*), two transcripts, RPS28B and EDC1 mRNAs make an exception. In one case, the protein Rps28B binds to a stem-loop structure in the 3'UTR of its own mRNA and enhance decapping by recruiting Edc3, a decapping-enhancer (Badis et al., 2004). In the other case, the 3' UTR of EDC1 mRNA contains secondary structures that inhibit the binding of deadenylases (Muhlrad et al., 2005). Moreover, the 3'-uridylation can also be considered as a deadenylation-independent mRNA decay. The addition of uridine to the poly(A) tail of mRNAs enhances either decapping via the LSM1-7/Pat1 complex or 3'-5' degradation by the exoribonuclease Dis3L2 (Song et al., 2007; Malecki et al., 2010; Thomas et al., 2015).

Endoribonuclease-mediated mRNA decay (Figure 6c). Another way to degrade an RNA is through endonucleolytic cleavage. This produces two fragments with unprotected ends that can be degraded by either 5'-3' exoribonucleases or 3'-5' exoribonucleases. Several cellular endoribonucleases that target mRNAs have been identified including PMR1, IRE1 and the nucleolar ribosomal RNA (rRNA)-processing enzyme RNase MRP.

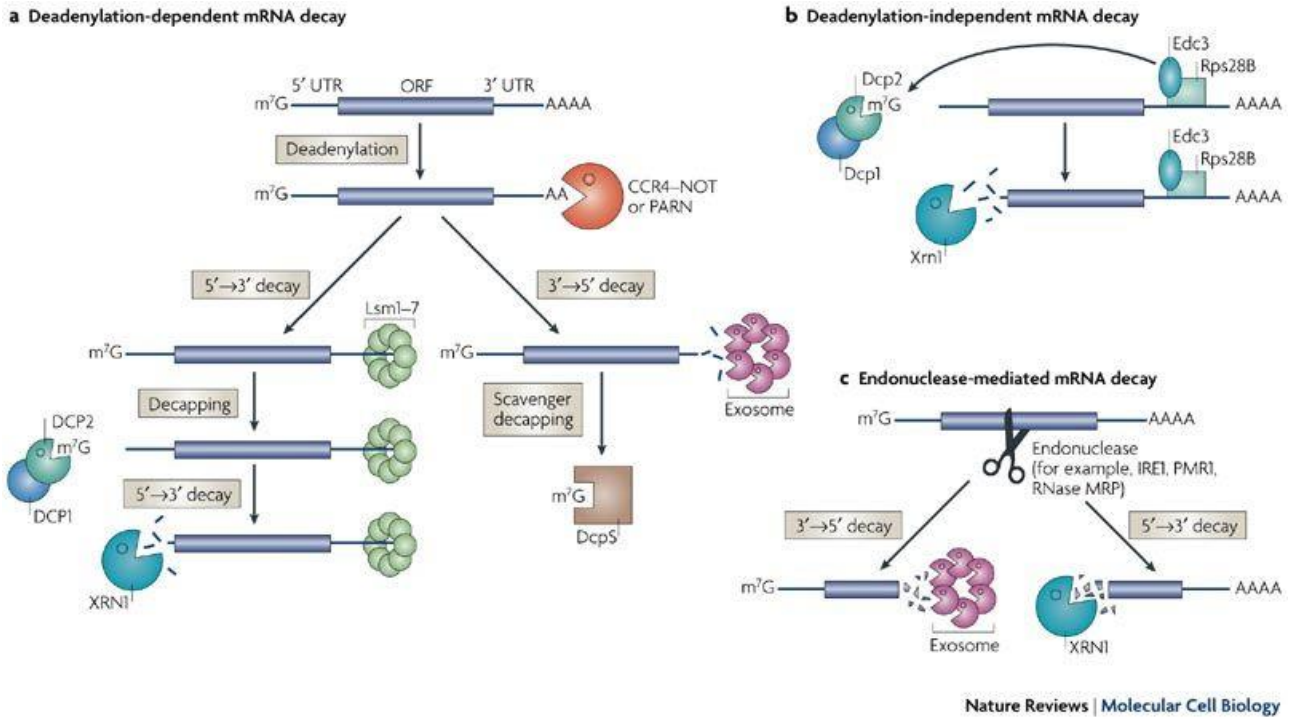

Figure 6. Different mechanisms of mRNA decay. (a) The most common way for mRNA degradation is the deadenylation-dependent pathway. The first step is the deadenylation that is mediated by deadenylases (here CCR4-NOT or PARN). After the poly(A) tail shortening, two mechanisms can degrade the mRNA: either decapping followed by 5'-3 decay or 3'-5' decay. In the 5'-3' decay, the Lsm1-7 complex associates with the 3' end of the mRNA and promotes decapping by the Dcp1-Dcp2 complex. The mRNA can be degraded in the 5'-3' direction by the exonuclease Xrn1. In the 3'-5 decay, the deadenylated mRNA can be degraded in 3'-5' direction by the exosome. The remaining cap structure is hydrolysed by the scavenger-decapping enzyme DcpS. (b) In *S.cerevisiae*, the mRNA decay can also be independent from deadenylation. Here, the RPS28B protein with the decapping-enhancer Edc3 to recruit the decapping complex. After decapping, the mRNA is degraded in 5'-3'direction by Xrn1. (c) In the endonuclease-mediated mRNA decay, endonucleases such as IRE1, PMR1 or RNase MRP, can cut RNAs internally, leaving two fragments with free ends to be targeted by both 5'->3' and 3'->5' exonucleases (Garneau et al., 2007).

1.9 Overview of known endonucleases

The endonuclease-mediated mRNA decay remains an emerging field. Even though endonuclease cleavage was the first mRNA decay mechanism to be identified, until recently, it took a subordinate role to the exonuclease-mediated mRNA. This was also partly due the difficulty of their identification and to the absence of a real functional significance. Recent studies demonstrate the involvement of endonucleases in many aspects of RNA metabolism: translation-dependent RNA quality control, RNAi, tRNA and rRNA processing. Here, the following chapters summarize the best characterized endoribonucleases that cleave mRNA *in vitro* and/or *in vivo* (Figure 7).

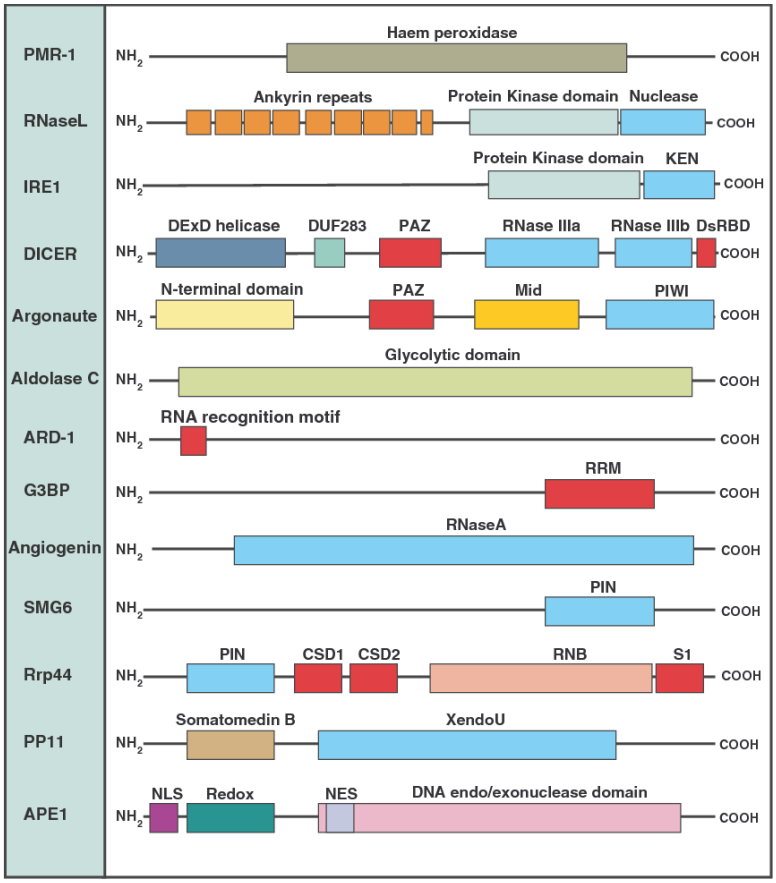

Figure 7. Summary of the domain structures of the eukaryotic endonucleases. Domains containing endoribonuclease activity are indicated in blue and domains with RNA-binding properties are indicated in red. Notably, PMR-1, aldolase C, ARD-1 and G3BP do not contain endoribonuclease domains but show to cleave RNA molecules (W. M. Li et al., 2010).

1.9.1 *Polysome ribonuclease 1 (PMR1)*

PMR1 was first identified as a polysome-associated endonuclease that destabilizes serum protein mRNAs after estrogenic induction in Xenopus liver (Pastori, Moskaitis, & Schoenberg, 1991; Pastori, Moskaitis, Buzek, et al., 1991). Although PMR1 belongs to the peroxidase family, showing a 50% sequence identity to myeloperoxidase, it lacks peroxidase activity (Chernokalskaya et al., 1998). However, PMR1 is associated with polysomes where it is involved in the endonuclease mediated decay of the albumin mRNA by forming a specific RNA-PMR1 complex of 680 kDa (Cunningham et al., 2001; F. Yang & Schoenberg, 2004). Interestingly, phosphorylation of PMR1 mediated by c-Src, is crucial for the association with polysomes and for the cleavage of albumin mRNA (F. Yang & Schoenberg, 2004). In breast cancer cells, human PMR1 overexpression stimulates cell motility by down regulating miR-200 miRNA family suggesting a new role for PMR1 in the post-transcriptional regulation of miRNAs (Gu et al., 2016). In mammalian erythroid cells, an endoribonuclease activity

similar to PMR1 can mediate the decay of the human β globin mRNA (Bremer et al., 2003; Stevens et al., 2002). However, the human protein responsible for this activity has been identified only recently as a 53 kDa protein which results from alternative splicing of the gene PXDNL (Gu et al., 2012).

1.9.2 *Inositol-requiring enzyme 1 (IRE1)*

IRE1 is a key sensor of the unfolded protein response to endoplasmic reticulum (ER) stress (Ron & Hubbard, 2008). In the presence of misfolded proteins, IRE1 oligomerizes and activates its kinase and endoribonuclease domains. The endoribonuclease domain is responsible of the correct splicing of the X-box-binding protein 1 (XBP1) gene which homologue in yeast is HAC1. XBP1 promotes the expression of different target genes such as ER chaperones and enzymes for protein folding (Calfon et al., 2002; Sidrauski & Walter, 1997; Yoshida et al., 2001). In addition to this "splicing" role, IRE1 is also responsible for the endonucleolytical cleavage of other mRNAs localized in the ER, including its own mRNA (Tirasophon et al., 2000). Interestingly, by sequence alignment, IRE1 is similar to RNase L (see chapter below). In fact, they both show a kinase domain and an endoribonuclease domain also known as a kinase extension nuclease (KEN) domain (Calfon et al., 2002). Unlike RNase L, the endonuclease activity of IRE1 necessitates autophosphorylation for activation (K. P. K. Lee et al., 2008).

1.9.3 *RNase L*

RNase L is a highly regulated, latent endoribonuclease (hence the "L" in RNase L) that is expressed in most mammalian tissue. It is one of the essential proteins involved in the host antiviral response induced by double-stranded RNA via the 2-5A pathway. Upon viral infection, RNase L is activated by 2-5A, small oligonucleotides producted by the oligoadenylate synthetases (OAS), and catalyses the cleavage of viral and cellular single-strand RNAs (Bisbal & Silverman, 2007; Khabar et al., 2003; Scherbik et al., 2006). RNase L contains a series of 9 ankyrin repeats (R1-R9), a linker, several protein kinase-like motifs, and a ribonuclease domain homologous to IRE1 (see chapter above)(Dong et al., 2001). Structurally, the ankyrin repeats R2-R4 are responsible for 2-5A binding. This binding causes a conformational change in the protein: from an inactive monomeric to active dimeric endoribonuclease (Dong & Silverman, 1997; Tanaka et al., 2004). In addition to its role in degradation of linear single-strand RNAs upon viral infection, RNase L has also been implicated in circRNA degradation (see chapter 1.7) (C. X. Liu et al., 2019).

1.9.4 *Aldolase A and C*

Aldolases A and C are glycolytic enzymes expressed in brain and nervous tissue (Cañete-Soler et al., 2005). In addition to their role in glycolysis and gluconeogenesis, both enzymes were found to have a secondary function as endonucleases. In response to an extracellular stimulus, Aldolase A and C can bind and cleave the light-neurofilament (NF-L) mRNA at UG sites (Cañete-Soler et al., 2005). Specifically, Aldolase C shows zinc dependent-endonuclease activity *in vitro*. Surprisingly, even without an identifiable RNA binding motif, they regulate NF-L mRNA stability in response to an extracellular stimulus. It is not clear whether the active site for glycolysis is the same for ribonuclease activity (Cañete-Soler et al., 2005).

1.9.5 *Activator of RNA Decay 1 (ARD-1)*

ARD-1 was first discovered as a human protein able to replace the endonuclease function of RNase E in bacteria (M. Wang & Cohen, 1994) and is considered as a mammalian analogue of *Escherichia coli* (*E. coli*) RNase E (Claverie-Martin et al., 1997). *In vitro* assays with the recombinant protein ARD-1 confirmed that it can bind and cleave several RNase E substrates in a magnesium-dependent manner. Specifically, ARD-1 cleaves single strand RNA 3' to purines and pyrimidines in A+U-rich regions and generates 5'-phosphate termini at the site of cleavage (Claverie-Martin et al., 1997; M. Wang & Cohen, 1994). Interestingly, in human ARD-1 is a product of alternative splicing of the gene Protein Phosphatase 1 Regulatory Subunit 8 (PPP1R8) (Chang et al., 1999; Van Eynde et al., 1999). In detail, this gene encodes three different isoforms. Two of the protein isoforms are specific inhibitors of type 1 serine/threonine protein phosphatases and can bind but not cleave RNA. The third protein isoform lacks the phosphatase function and is the one that corresponds to the endoribonuclease ARD-1 (Chang et al., 1999; Van Eynde et al., 1999). However, the role of ARD-1 and its target in human remain to be characterized.

1.9.6 *Stress Granule Assembly Factor (G3BP)*

Ras-GTPase-activating protein (SH3 domain)-binding proteins (G3BP, also known as Rasputin) are a family of RNA binding proteins with multifunctions (Irvine et al., 2004). The G3BP family is formed by three proteins: G3BP1, G3BP2a and G3BP2b. Their main role is associated with stress granules where they regulate gene expression in response to environmental stresses by controlling mRNA stability and translation (Gallouzi et al., 1998). However, the phosphorylation of serine 149 acts as a signal for nuclear import and promotes the integration of G3BP into nuclear mRNP

complexes with an eventual RNA endonucleolytic-degradation role (Tourrière et al., 2001). Indeed, it was found that G3BP has a phosphorylation-dependent RNase activity, which specifically cleaves the 3'-untranslated region of human c-myc mRNA *in vitro* (Gallouzi et al., 1998). This hypothesis was supported by the fact that c-myc mRNA decay is delayed in RasGAP-deficient fibroblasts, which contain a defective isoform of G3BP that is not phosphorylated at serine 149 (Tourrière et al., 2001). Further investigations show that G3BP specifically interacts through its c-terminal RNA recognition motif (RRM) and cleaves between cytosine and adenine (CA) (Tourrière et al., 2001). G3BP is an essential gene and its absence causes delays in fetal growth and neuronal cell death (Zekri et al., 2005). These studies support the hypothesis that G3BP may play an important role in post-transcriptional regulation of selected mRNAs but the catalytic mechanism for RNA cleavage remains to be identified. Finally, a recent work show that G3BP1 together with UPF1 can mediate degradation of highly structured circRNAs (see chapter 1.7) (Fischer et al., 2020).

1.9.7 *Angiogenin*

Angiogenin is a very small polypetide secreted in blood vessels (Gao & Xu, 2008). It is a member of the RNase A family, sharing 33% of amino acid sequence with the pancreatic ribonuclease A (Holloway et al., 2002). Originally characterized for its angiogenic role, angiogenin was also found to cleave rRNA and tRNA *in vitro* (Saxena et al., 1992). More recently, two groups showed that angiogenin is required for tRNA cleavage in the cytosol under stress condition such as nutrient deprivation, heat shock and UV radiation (Fu et al., 2009; Yamasaki et al., 2009). Specifically, in this degradation pathway, angiogenin cleaves a specific class of tRNAs into 5’ and 3’ halves within the anticodon loop to generate tRNA-derived stress-induced RNAs (tiRs) (Fu et al., 2009; Yamasaki et al., 2009). Surprisingly, angiogenin knockout do not decrease the level of tiRs under stress condition, suggesting either that angiogenin is not essential for tRNA cleavage or that tRNA halves can also be generated by angiogenin independent mechanisms (Su et al., 2019).
Unlike RNase A, angiogenin has a weak endoribonuclease activity. This is due to the presence of a glutamine (glutamine 117) that partially occupies the nucleotide binding site (Russo et al., 1994).

1.9.8 *Apurinic/Apyrimidinic Endodeoxyribonuclease 1 (APE1)*

APE1 is a multifunctional protein involved in several cellular events including DNA-base-excision repair where it shows apurinic/apuridinic DNA endonuclease activity (Demple & Sung, 2005; Kanno et al., 1999; Kuninger et al., 2002; Wilson et al., 1995). In addition to DNA endonuclease, APE1 also can act as 3’-5’exonuclease, 3’phosphodiesterase, 3’-phosphatase and RNase H (Barzilay et al., 1995;

Chou et al., 2000, 2000). Regarding the RNase H activity, it was suggested that APE1 could also cleave not only DNA but also RNA targets. Indeed, Barnes et al. (2009) discovered that APE1 cleaves c-myc mRNA *in vitro* (Barnes et al., 2009). Additionally, knockdown of APE1 in HeLa cells leads to increased steady-state level of c-*myc* mRNA and its half-life. Specifically, APE1 cleaves between the C/A and U/A dinucleotides showing a mechanism like the apurinic/apuridinic endonuclease activity on the DNA. In support of this hypothesis, studies using the catalytic mutants E96A and H309N suggested that the endoribonuclease activity for c-myc uses the same active center of the AP-DNA endonuclease activity (Barnes et al., 2009). Furthermore, APE1 cleavage is not restricted to *c-myc*, as miRNAs (miR-21, miR-10b), CD44 mRNA, and three RNA components of the SARS-corona virus RNA are also cleaved by APE1 (W. C. Kim et al., 2010). Finally, APE1 knockout causes embryonic lethality in mice, indicating that the APE1 gene is essential (Izumi et al., 2005).

1.9.9 *Poly(U)-specific endoribonuclease ENDOU or PP11*

PP11 is a glycoprotein and was previously classified as serine protease specifically expressed in the syncytiotrophoblasts and in several tumor tissues (Grundmann et al., 1990). However, it has been subsequently demonstrated that PP11 lacks serine protease activity but has endoribonucleolytic activity. PP11 shares a significant sequence homology and predicted secondary structure with XendoU (Laneve et al., 2008). This enzyme is an amphibian endoribonuclease that participates in the biosynthesis of small nucleolar RNAs, a class of noncoding RNAs involved in ribosome biogenesis. Like XendoU, recombinant human PP11 binds and cleaves single stranded RNA in a Mn^{2+}-dependent manner to produce molecules with 2′,3′-cyclic phosphate ends. Mutagenesis and structural analyses lead to the identification of the catalytic center within the conserved amino acids that are crucial for catalytic activity (Laneve et al., 2008).

1.9.10 *The Nonsense Mediated MRNA Decay Factor SMG6*

SMG6 is one of the catalytic enzymes required for the non-sense mediated mRNA decay (NMD). NMD is a surveillance mechanism that prevents the production of truncated proteins by identifying and degrading transcripts that contain premature termination codons (PTCs) (Behm-Ansmant et al., 2007; Isken & Maquat, 2007). Moreover, it has been demonstrated that NMD can be initiated by a PTC-proximal endonucleolytic cleavage. SMG6 is the responsible endoribonuclease that cleaves in proximity of the premature termination codons (Eberle et al., 2009; Huntzinger et al., 2008) (Huntzinger et., 2008). Indeed, SMG6 possesses a C-terminal PIN domain similar to the nuclease domain of the FLAP, family which includes the t4 bacteriophage RNase H and the Taq polymerase

(Eberle et al., 2009; Glavan et al., 2006; Huntzinger et al., 2008). SMG6 PIN domain displays manganese-dependent endoribonuclease activity *in vitro* on linear and circular RNA substrates. Moreover, mutations of conserved aspartate residues in its PIN domain abolishes endonucleolytic activity *in vivo* and *in vitro* (Eberle et al., 2009).

1.9.11 *RNase for mitochondrial RNA processing (RNase MRP) and its close related RNase P*

RNase MRP and its close related RNase P are multi-component protein complexes with an RNA catalytic core that function as endoribonuclease (Esakova & Krasilnikov, 2010). Specifically, mammalian RNase P and RNase MRP contain seven common protein components (POP1, RPP38, POP5, RPP25, RPP20, RPP30, and RPP40), several unique protein components with their unique non-coding RNA components termed RPPH1 and RMRP respectively. Initially, RNase MRP and RNase P were identified as site-specific endoribonuclease involved in rRNA, mitochondrial RNA and tRNA processing. The processing of the 5′-end of the precursor tRNA (pre-tRNA) is indeed the best-characterized and ubiquitous function of RNase P. The recognition of pre-tRNAs by RNase P requires conserved features that act in a cooperative manner (Kirsebom, 2007). In addition, interactions between eukaryotic RNase P and substrate pre-tRNA appear to be influenced by La (or, in yeast, La-like) proteins bound to the pre-tRNA (Fan et al., 1998; Yoo & Wolin, 1997). However, subsequent studies demonstrated that they are responsible of the cleavage of different substrates. Specifically, it was shown in *S. cerevisiae* that MRP cleaves CLB2 mRNA in its 5’ UTR to promote 5’-3’ degradation by Xrn1 nuclease. Surprisingly, the decay of CLB2 mRNA occurs in a specific type of P body such as temporal asymmetric MRP (TAM) body, which contains only RNase MRP and Xrn1 (Gill et al., 2004). Similarly, RNase P was found to process the long non-coding RNA MALAT1 (Wilusz et al., 2008) and to participate in the maturation of the box C/D intron-encoded snoRNAs (Coughlin et al., 2008).

A recent study has shown that RNase P and MRP can cleave m^6A-containing mRNAs and circRNAs via YTHDF2 (m^6A reader protein) and HRSP12 (adaptor protein) interaction (see chapter 1.7) (Park et al., 2019).

1.10 Defective in sister chromatid disjoining 3 (DIS3)

1.10.1 *Brief introduction*

Human DIS3 (Defective in sister chromatid disjoining 3), also known as Dis3/Rrp44 in yeast and *Drosophila*, is a highly conserved exoribonuclease and one of the exosome catalytic subunits, a multi-protein complex involved in nuclear and cytoplasmic 3'-5' degradation and processing of different RNA species. However, DIS3 also possesses endoribonuclease activity, which is facilitated by its PIN domain. Mutant phenotype studies in *S. pompe*, *S. cerevisiae* and *D. melanogaster* revealed that Dis3 is involved in cell-cycle progression and microtubule assembly. Recently, high-throughput sequencing analysis have shown also that DIS3 is mutated in a range of cancers with a specific impact in multiple myeloma. However, it remains to be investigated the precise role of DIS3 in cancer.

1.10.2 *Conservation and structure*

Dis3/Rrp44 was first discovered in *S. pompe* mutants (Ohkura et al., 1988). Dis3 belongs to RNase II/RNR superfamily, whose members show high conservation in terms of sequence, function and domain organization (Zuo & Deutscher, 2001). Human DIS3 contains a N-terminal Cys residues motif (CR3), an exonucleolytic RNB domain, two cold-shock domains (CSDs), a S1 domain, which non-specifically binds RNA and a C-terminal endonucleolytic PIN domain (Tomecki et al., 2010). In human, there are two further orthologues of DIS3: DIS3L1, which contains a catalytic inactive PIN domain and DIS3L2, which lacks a PIN domain and a CR3 motif (Lubas et al., 2013; Malecki et al., 2013; Staals et al., 2010) (Figure 8).

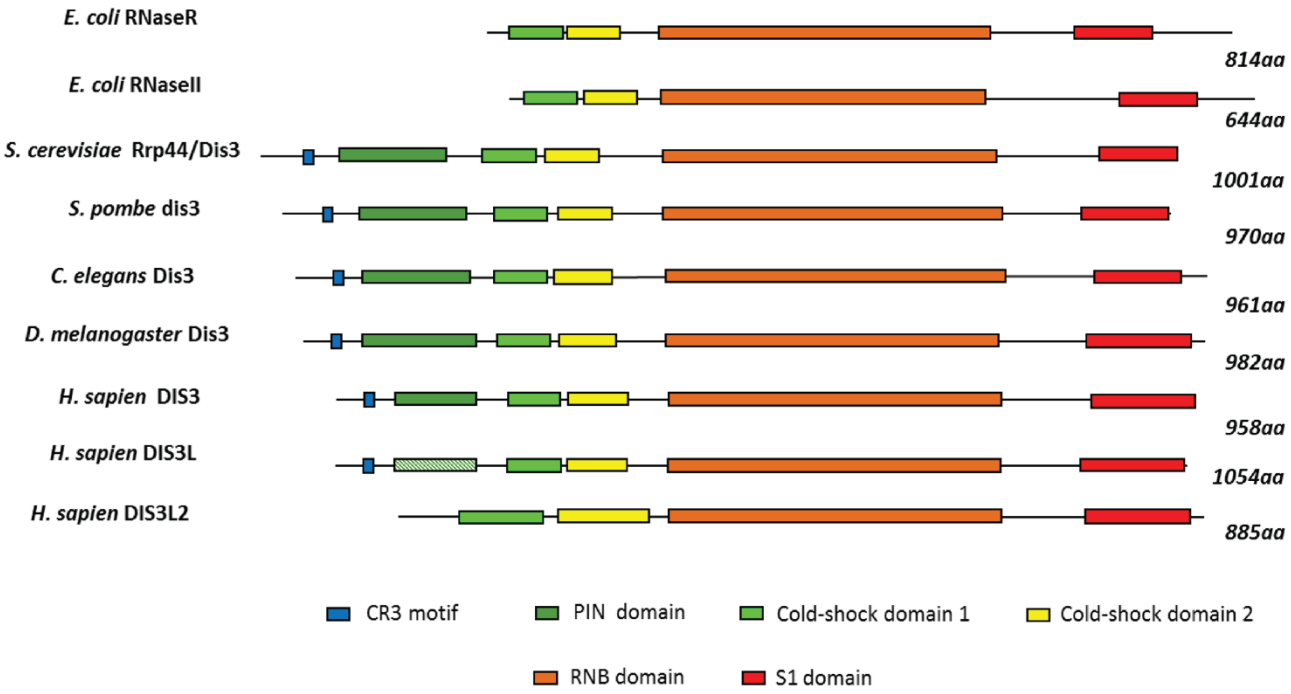

Figure 8. Domain organization of RNR/RNase II superfamily. Members of this family have a similar modular domain organization: although the N-terminal region is variable, all the members contain a cold-shock domain 1, a cold-shock domain 2, an RNB domain and a S1 domain. DIS3 in yeast, Drosophila and human show a conserved CR3 motif and an endoribonuclease PIN domain. However, The PIN domain is inactive in DIS3L and absent in DIS3L2, both are the human orthologues of DIS3 (Robinson et al., 2015).

1.10.3 *DIS3 and the exosome*

DIS3 is one of three catalytic subunits of the exosome, along with DIS3L1 and RRP6, a distributive exonuclease, which is a member of the RNase D family (Makino et al., 2013; Wasmuth & Lima, 2012) (Figure 9). The exosome consists in a two layered barrel of 9 catalytically inert subunits (also known as EXO-9 complex). The upper layer of EXO-9 is composed of a cap of three proteins (EXOSC1/Csl4, EXOSC2/Rrp4, and EXOSC3/Rrp40) with S1 or KH RNA-binding domains. The cap sits on a ring of six proteins (EXOSC4/Rrp41, EXOSC5/Rrp46, EXOSC6/Mtr3, EXOSC7/Rrp42, EXOSC8/Rrp43, and EXOSC9/Rrp45) that are homologues to RNase PH from Eubacteria (Symmons & Luisi, 2009). The active nuclease DIS3/Dis3 is located at the base of the ring-forming EXO-10 complex. Eventually, in the nucleus EXOSC10/Rrp6 can associate with the exosome cap to form the EXO-11 complex (Figure 9A). Crystal structure studies of the exosome in *S. cerevisiae* showed that Dis3 interacts at the bottom of the ring with Rrp41 via its PIN domain (Makino et al., 2013). Furthermore, the N-terminal CR3 motif (a small domain with three conserved Cysteines) mediates additional interactions between Dis3 and EXO-9 (Schneider et al., 2009). *In vitro* evidence suggests

that DIS3 can degrade RNA independently of the exosome, but this has not been demonstrated *in vivo* (Wasmuth & Lima, 2012).

The EXO-9 complex forms a central channel that permits the entry only to ssRNA. The Trf4/Air2/Mtr4p Polyadenylation complex (TRAMP)/PAPD5-ZCCHC7-hMTR4/SKIV2L2 and the Ski complex (Ski2–Ski3–Ski8/SKIV2L-TTC37-WDR61) are exosome cofactors that unwind secondary structured RNA in the nucleus and in the cytoplasm, respectively (Halbach et al., 2013; LaCava et al., 2005). The RNA substrate is usually threaded through the central channel and then degraded by DIS3 (Figure 9B). Alternatively, some highly structured substrates can directly enter to the catalytic centre of DIS3 rather than passing through the exosome barrel (Phil Mitchell, 2014; Schneider et al., 2012).

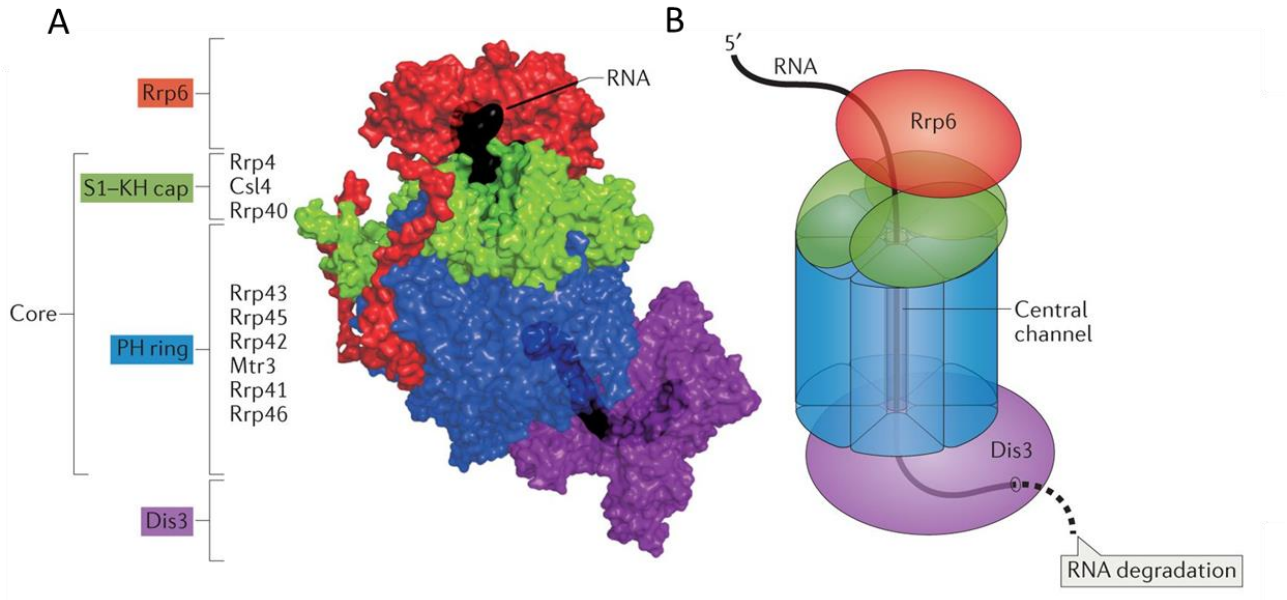

Figure 9. Structure of the exosome. A) A model of the Exosome EXO11 complex: Dis3 is located at the bottom whereas Rrp6 at the top of the barrel-core EXO9. (B) Schematic representation of an RNA molecule threading through the central channel of the cap and PH ring to the DIS3 exonuclease center, where it is degraded in 3'-5' direction (Kilchert et al, 2016).

1.10.4 *Mechanistic function*

As already mentioned, DIS3 is a multi-domain protein with two distinct catalytic activities: a 3'-5' exonucleolytic activity depending on the RNB domain and an endonucleolytic depending on the N-terminal PIN domain. Both activities have been well characterized with the support of structural analyses and RNase protection experiments (Schaeffer et al., 2009). Concerning the exonucleolytic activity, DIS3 is a processive enzyme that hydrolases ssRNA in a 3'-5' direction, one nucleotide at a time and releasing a final product of 2–5 nucleotides. The exonucleolytic active site contains four conserved aspartic amino acid residues that form two binding sites for two magnesium ions

(Lorentzen et al., 2008). Interestingly, Although the RNB active site is located at the bottom of the exosome narrow channel and only accessible for ssRNA (at least 7 nt long), DIS3 can unwind and degrade duplex and structured RNAs when they contain 4-5 single-stranded overhangs at their 3' ends (G. Lee et al., 2012). Regarding the endonucleolytic activity, the PIN domain is a compact domain of 100 amino acids which is present in many RNA processing enzymes including SMG6 for example (see chapter 1.9.10). The endonucleolytic active site consists of 4 amino acids that coordinate a divalent metal ion with a preference for manganese. This ion serves to catalyse the internal cleavage of the RNA with subsequent release of 5' monophosphate products. Specifically, the PIN domain can cleave circular and linear RNAs *in vitro*. Mutation studies revealed that the endo- and exonucleolytic activities of DIS3 are not independent but cooperate for efficient processing of several exosome substrates. Indeed, it has been hypothesized that the endonucleolytic activity of DIS3 can provide an alternative entry site and cleavage for highly structured RNAs (Lebreton et al., 2008; Schneider et al., 2009; Schaeffer et al., 2009).

1.10.5 *Subcellular localization*

The subcellular localization of DIS3 and of the exosome complex has been investigated solely in two studies in Drosophila (Graham et al., 2006, 2009) and in one study in human HeLa and HEK293 cells (Tomecki et al., 2010). However, it is a common agreement that in yeast Dis3 is localized either in the nucleus in association with Rrp6 (EXO-11) or in cytoplasm (EXO-10) (Figure 10A). Interestingly, in *Drosophila* S2 cells, the localization of Dis3 differs from cell to cell and in several cells, Dis3 is restricted to the cytoplasm (Graham et al., 2006). Additionally, flag-tagged Dis3 co-localises with the nuclear lamina but the significant relevance of this nucleo-peripheral localisation remains unknown (Graham et al., 2006). Unlike in humans, DIS3 is mainly localized in the nucleus, excluded from the nucleolus and present only in small amounts in the cytoplasm. The homologue DIS3L1 associates with the core exosome only in the cytoplasm whereas Rrp6 associates simultaneously with the exosome and Dis3 in the nucleus and only with the exosome in the nucleolus (Tomecki et al., 2010) (Figure 10B).

The nuclear localization of yeast/Drosophila Dis3 and human DIS3 depends on the two nuclear localization signals at the C-terminal of the protein. N-terminal domains can also contribute to the nuclear localization although they do not contain specific sequences (Graham et al., 2009). It is known that DIS3 targets both nuclear and cytoplasmic substrates. Still, it remains to be investigated if there are distinct pools of DIS3 protein in each compartment or if there is only one pool shuttling between the nucleus and cytoplasm depending on cellular conditions.

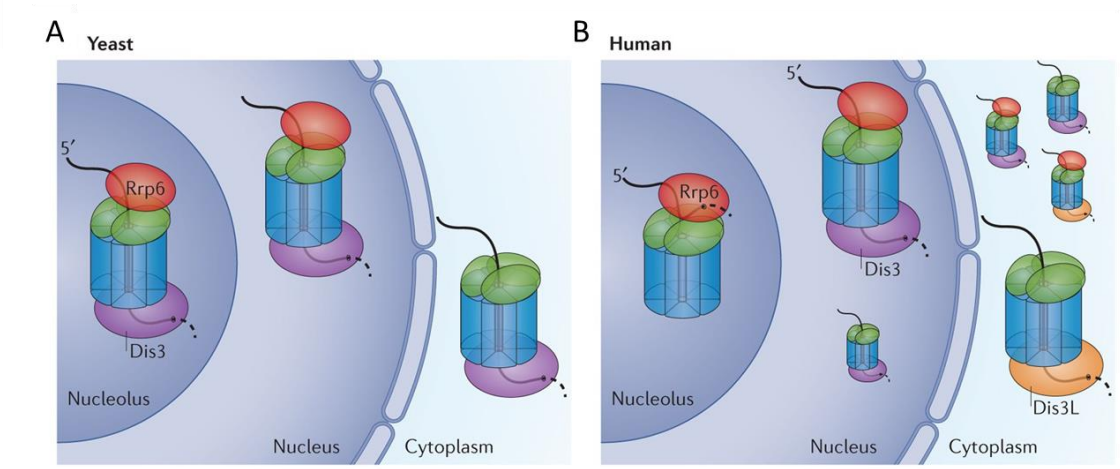

Figure 10. Subcellular localization of the different exosome complexes. (A) In *S. cerevisiae*, exosome complex with Rrp6 is exclusively localized to the nucleus whereas exosome complex with Dis3 can be found throughout the cell. (B) In human, DIS3 is mainly nuclear and excluded from nucleolus. In addition, small amounts of exosome with DIS3 can be found in the cytoplasm. DIS3L1 also associated with the exosome core and is restricted to the cytoplasm (Kilchert et al., 2016).

1.10.6 *Molecular functions of DIS3*

The exosome has a central role in RNA quality control pathways in the nucleus and the cytoplasm. Specifically, it has been shown that DIS3 is involved in the degradation of un-spliced pre-mRNA such as mRNAs with retained introns and mRNAs with defective poly(A) tail, at 3' end (Bousquet-Antonelli et al., 2000; Milligan et al., 2005). There is evidence that this mRNA quality control mediated by the exosome occurs co-transcriptionally. The exosome also degrades mRNA with defects on the chromatin or in packing into RNPs in *S. cerevisiae* (Rougemaille et al., 2007). A recent study in human cells has shown that DIS3 and EXOSC10 are both essential but DIS3 degrades most of the nuclear exosome substrates (Davidson et al., 2019). Among them, one of the major classes is constituted by products of the pervasive antisense transcription such as cryptic unstable transcripts (CUTs) in yeast or promoter upstream transcripts/upstream antisense RNAs (PROMPTs/uaRNAs) in humans (Davidson et al., 2019; Preker et al., 2008; Szczepińska et al., 2015). Furthermore, DIS3 is also involved in the degradation of a specific a class of noncoding RNA, the enhancer RNAs (eRNAs), which are products of divergent transcription at intergenic enhancer sequence elements (Andersson et al., 2014). In addition, DIS3 downregulation results in the accumulation lncRNA NEAT1 and in the enhanced formation of paraspeckles, nuclear bodies organized around NEAT1 (Szczepińska et al., 2015). More recently, products of premature cleavage and polyadenylation (PCPA) were also revealed as exosome substrates in mouse embryonic stem cells (mESCs)(Chiu et al., 2018).

Concerning the RNA quality control pathway in the cytoplasm, NMD substrates seem to be preferentially degraded by Rrp6 in *Drosophila* C2 cells (Kiss & Andrulis, 2010). However, in *yeast* and in mammalian cells, mRNAs that fail to signal translational termination, are detected in a ribosome-depending manner by the Ski complex and subsequently degraded by the exosome (Frischmeyer et al., 2002). Generally, the exosome cooperates with Xrn1 in the regular cytoplasmic RNA decay that is usually initiated by poly(A) tail shortening. Additionally, it has been found that the exosome can degrade mRNAs that contain the full poly(A) tail. This is the specific case of mRNAs with AU-rich elements (AREs) in their 3'UTRs. These ARE sequences recruit ARE-binding proteins (AUBPs), which destabilize the mRNAs and promote degradation by CCR4-NOT/complex and subsequently by DIS3-exosome (Ching Yi Chen et al., 2001; Mukherjee et al., 2002).

Not all the exosome substrates are the target for complete degradation. Indeed, DIS3 and the exosome play a crucial role in rRNA processing and snoRNA, snRNA and tRNA maturation. Generally, DIS3 is required for trimming the 3'end of the precursors of these RNA classes (Kadaba et al., 2004; Philip Mitchell et al., 1996; Schneider et al., 2007). Accordingly, recent analyses established that DIS3-exosome seem to be responsible for the 3' end trimming of the 5.8S rRNA (Kobyłecki et al., 2018; Tafforeau et al., 2013). Indeed, depletion of the exosome subunits or of the exosome cofactors causes the accumulation of diverse intermediate processing fragments between the 12S and 7S pre-rRNAs, which are 5.8S rRNA precursors (Pirouz et al., 2019; Schilders et al., 2007).

1.10.7 *Biological Functions of DIS3*

Although the molecular function of DIS3 in RNA metabolism has been well-characterized, a little is known about its biological functions at a cell and organism level. Several studies in *S. pompe* and *S. cerevisiae* showed that Dis3 plays a role in cell-cycle progression. Indeed, the ribonuclease activity of Dis3 is required for mitotic progression and the correct kinetochore formation in *S. pompe* (Murakami et al., 2007). Similarly, Dis3 dysfunction in *S. cerevisiae* blocks mitotic progression by affecting microtubule organization and structure and knockdown of Dis3 in *Drosophila* S2 cell deregulates cell-cycle related genes (Smith et al., 2011). Interestingly, in *Drosophila* ubiquitous Dis3 knockdown causes larval lethality whereas spatial Dis3 knockdown results in a severe no wing phenotype (Towler et al., 2015).

DIS3 is frequently mutated in multiple myeloma and other cancers (Chapman et al., 2011; Walker et al., 2012). Approximately 10%–15% of multiple myeloma cases have specific hemizygous or homozygous mutations in the DIS3 RNB domain, leading to DIS3 dysfunction but not complete inactivation. Indeed, HEK-293 cells expressing DIS3 variants with multiple myeloma-associated

mutations show a slower proliferation rate and impaired RNA degradation. Additionally, these mutations are synthetically lethal with the PIN domain catalytic mutations suggesting that the PIN domain can be a potential drug target for cancers (Tomecki et al., 2014).

1.10.8 *Post-translational modifications of yeast and Drosophila Dis3*

Post-translational modifications (PTMs) are chemical modifications at amino acid residues that occur after protein synthesis. PTMs contribute to regulate protein functions like enzymatic activity, structural conformation, cellular localization, interactions and stability. Most common PTMs include phosphorylation, acetylation, ubiquitination, glycosylation and methylation.

Little is known about DIS3 post-translational modifications. Until now, phosphorylation has been the only one well characterized in budding and fission yeast and in *Drosophila*. Mass spectrometry analysis of PMTs of the RNA exosome complex revealed 7 phospho-sites on Dis3 in *S. pompe*, whereas no phospho-sites were so far detected on Dis3 in *S. cerevisiae* (Synowsky et al., 2006; Telekawa et al., 2018). Interestingly, functional characterization of phosphorylated Ser-809 and Tyr-814 on Dis3 *S. pompe* shows that these residues are important for controlling Dis3 activity. Specifically, phospho-mimetic versions of Dis3 display impaired exosome function *in vivo* and reduction of Dis3 exonucleolytic activity *in vitro*. In addition, the localization of Ser-809 and Tyr-814 close to the catalytic center of Dis3 supports the idea that phosphorylation of these residues could affect the positioning of the negatively charged RNA in the catalytic site. As consequence, exonucleolytic activity and RNA degradation are affected (Telekawa et al., 2018).

Phosphorylation of Ser-786, the equivalent to *S. pompe* Ser-809, was also identified in *Drosophila*. Ser-786 is an evolutionary conserved phosphorylation site modified by CDK1. Like in *S. pompe*, when this residue is phosphorylated, it inhibits Dis3 exonucleolytic but not endonucleolytic activity. Additionally, inhibition of the Dis3 exonucleolytic activity by phosphorylation impairs mitotic cell division (Snee et al., 2016). Finally, phosphorylations on human DIS3 has not been investigated so far.

2 Aim of the thesis

Deep sequencing analysis and newly developed computational annotation approaches have allowed for the identification of thousands of different circRNAs in all domains of life. Although studies on circRNA biogenesis and its biological function are being conducted rapidly, many questions remain to be answered. An interesting question is how circRNAs are ultimately degraded, as they have long half-lives and are resistant to RNA exonucleolytic decay. Only recently, initial insights into circRNA degradation have been reported. Although it has been found that RNase L can degrade circRNAs upon viral infection and that RNase P may cleave a subset of m^6A containing circRNAs, other mechanisms by which circRNAs are degraded remain largely unknown. Therefore, the main aim of my PhD thesis was to identify the general pathways of circRNA degradation and the associated endonucleases. In detail, we combined *in vitro* RNA degradation assays using cell extracts of different purification steps with mass spectrometric analyses. From several endonucleases found from mass spectrometry, DIS3, the catalytic subunit of the exosome, was chosen as the most promising candidate. To better understand its involvement in circRNA turnover, we studied different aspects of DIS3 regulation, including catalytic activity, localization, post-translational modification, and association with the exosome. Finally, we generated several CRISPR/Cas9-mediated DIS3 knockout cells and we performed RNA-seq analysis to identify the putative targets of DIS3 *in vivo*.

3 Results

3.1. Biochemical strategy to identify potential endonuclease candidates

In this first part of the results, I illustrate a comprensive biochemical approach to identify endonucleases involved in circRNA degradation. The steps we followed are summarized below (figure 11):

1) Identification and validation of circRNA expression
2) *In vitro* synthesis of circRNA candidates
3) Confirmation of circularity
4) *In vitro* RNA degradation assays using different cell lysates of different purification stages
5) Identification of endonucleases by Mass Spectrometry
6) *In vitro* and *in vivo* validation of endonuclease candidates

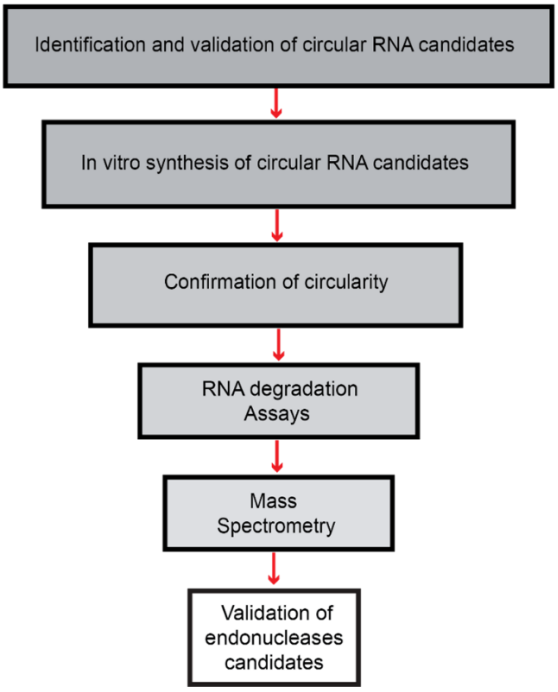

Figure 11. Biochemical strategy to identify endonucleases.

3.1.1 *Identification and validation of circRNA candidates in different cell lines*

Before starting with *in vitro* experiments, we selected a set of circRNAs from RNA-seq data available in the lab in collaboration with the Rajewsky group (Max Delbrück Center, MDC, Berlin, Germany). We chose four exonic circRNAs: CircNRIP1, CircGSE1, CircCORO1C and CircDOPEY2. These circRNAs are expressed in different cell lines, derive from – or + strand and have a length between 200 and 300 nt as summarized in the table below (Table 1).

Table 1. Overview of the circRNAs selected for this study.

CircRNA	Organism	Position (hg19)	Strand	Cell lines	Host gene	Property	Lenght	circRNA study
CircGSE1	Homo sapiens	chr16:85667519-85667738	+	LN229, T98G, Hela, HT29, HEK	GSE1	Exonic	219 bp	Jeck2013, Memczak2013, Rybak2015
CircNRIP1	Homo sapiens	chr21:16386664-16415895	-	HT29, LN229, HEK293	NRIP	Exonic	203 bp	Jeck2013, Rybak2015, Salzman2013
CircDOPEY2	Homo sapiens	chr21:37619814-37620866	+	HT29, HEK293, LN229	DOPEY2	Exonic	301 bp	Memczak2013, Rybak2015, Salzman2013
circCORO1C	Homo sapiens	chr12:109046047-109048186	-	HEK293, HT29, Hela, LN229	CORO1C	Exonic	251 bp	Memczak2013, Rybak2015, Salzman2013

For the selected four circRNAs, we confirmed that they were circular by divergent reverse-transcription PCR (RT-PCR) in HEK293 cells and subsequent Sanger sequencing of the splice junctions (figure 12 A-B).

To further demonstrate their circularity, we also used RNAse R treatment. RNase R is a 3'-5' exoribonuclease that degrades all linear RNAs but not circRNAs. Accordingly, Real-time PCR from total RNA showed resistance of CircNRIP1, CircGSE1, CircCORO1C and CircDOPEY2 to RNase R digestion in HEK293 cells. The linear RNAs GAPDH, MALAT1, TUBULIN and HRTPK are used as controls for RNase R activity (figure 12 C-D).

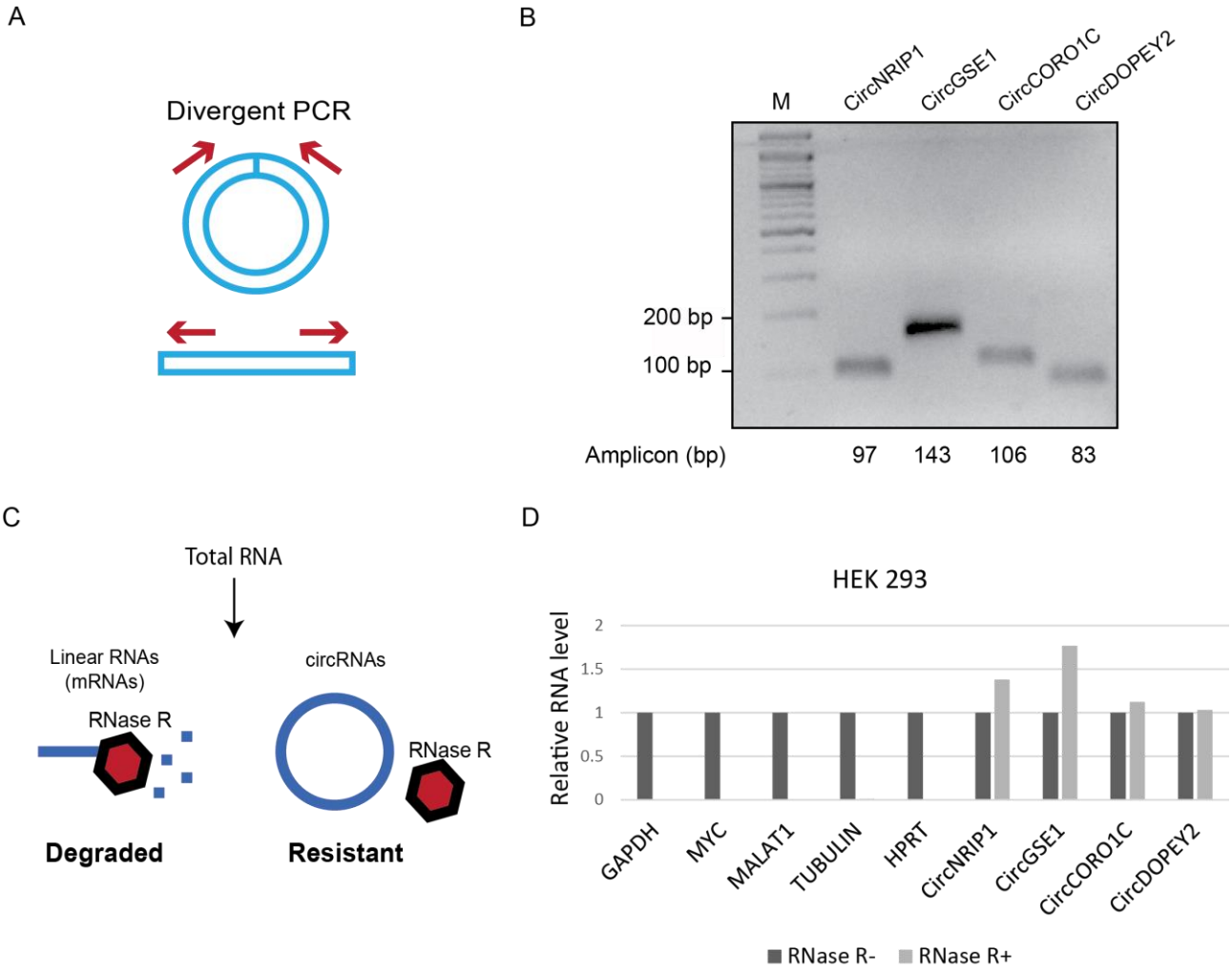

Figure 12. Characterization and validation of circRNA candidates. (A) Divergent primers, designed to span the circRNA backspliced junction sequence, can specifically amplify the circRNAs but not the linear counterparts. (B) RT-PCR products with divergent primers showing circularization of the four circRNAs in HEK-293 cells. (C) Experimental procedure to validate circRNAs with RNase R treatment. Total RNA is treated with RNase R: CircRNAs are resistant while linear RNAs are degraded. (D) Real-time PCR in HEK-293 cells showing that the four circRNA candidates are resistant to RNase R digestion differently from the linear negative controls GAPDH, MALAT1, TUBULIN, MYC and HPRT.

3.1.2 *In vitro synthesis of circRNA candidates*

After identification and *in vivo* validation of the four circRNAs, we proceeded with generating circRNAs *in vitro*. RNA circularization involves the intramolecular formation of a 3'-5'-phosphodiester bond requiring close proximity of the 3'- and 5'-terminus of the linear precursor. There are different *in vivo* and *in vitro* strategies to generate circRNAs. We chose and optimized the T4 RNA ligase 1- mediated ligation method because it was suitable for small and medium-size RNAs (RNA < 500 nt). This protocol consists of four different steps: *in vitro* transcription of the linear RNA,

dephosphorylation of 5’ end, re-phosphorylation of the 5’ end, and ligation of the 3’-5 ends by T4 RNA ligase 1 (Figure 13). Specifically, the T4 RNA ligase 1 can produce circRNAs from a linear precursor with 3’-hydroxyl and 5’ monophosphate termini. Generally, a 5’ monophosphate end can be generated by dephosphorylation and re-phosphorylation (with γ-32P-ATP or unlabeled ATP) of the 5’ triphosphate terminal of the linear substrate resulting from *in vitro* transcription. Alternatively, these two enzymatic steps can be circumvented by a GMP-primed *in vitro* transcription that directly leads to 5’monophosphorylated linear substrates (Suppl. Figure 1).

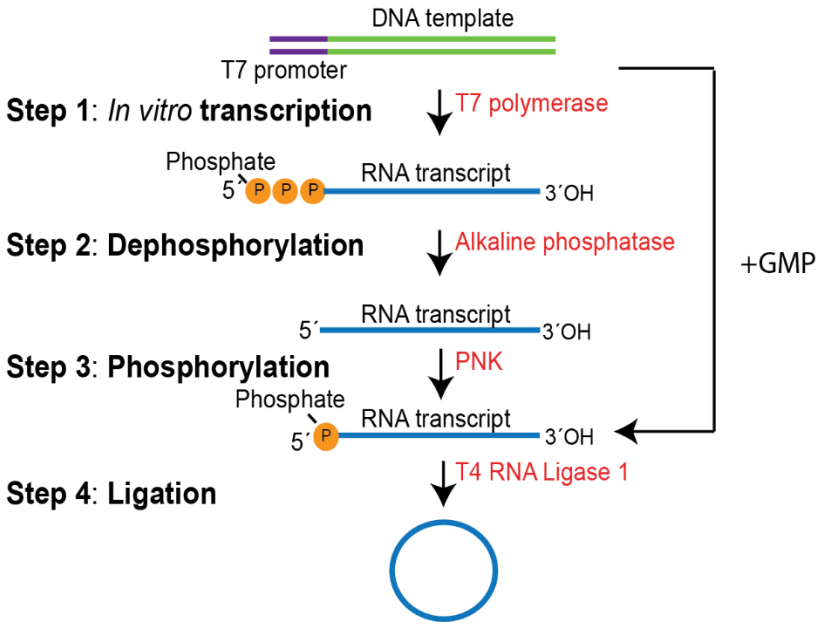

Figure 13. Schematic representation of in vitro circularization using T4 RNA Ligase 1. T4 RNA ligase 1 can form circRNAs from a linear precursor with 5’ monophosphate and 3’-hydroxyl. Generally, the 5’ triphosphate linear RNA resulting from *in vitro* transcription is first dephosphorylated by an alkaline phosphatase and then re-phosphorylated by Polynuclotide Kinase using γ-32P-ATP or unlabeled ATP. GMP-guided *in vitro* transcription can be an alternative way to obtain a 5’monophospharylated linear RNA substrates that can be directly used for ligation.

We tried both approaches and we could successfully obtain radioactivily-labelled synthetic circRNA products. After ligation by T4 RNA ligase 1, the generated circRNAs were loaded onto 6% polyacrylamide (PAA) gels (figure 14 and Suppl. Figure 1). It is known that circRNAs run slower in PAA gels compared to the linear counterparts beacuse they are retained in the gel matrix (Jeck & Sharpless, 2014). Since our products run slower as well, we concluded that the linear RNAs were successfully ligated (*). However, in such reactions, dimers of the two linear products can occasionally be produced. Thus, we further confirmed their circularity with different approaches.

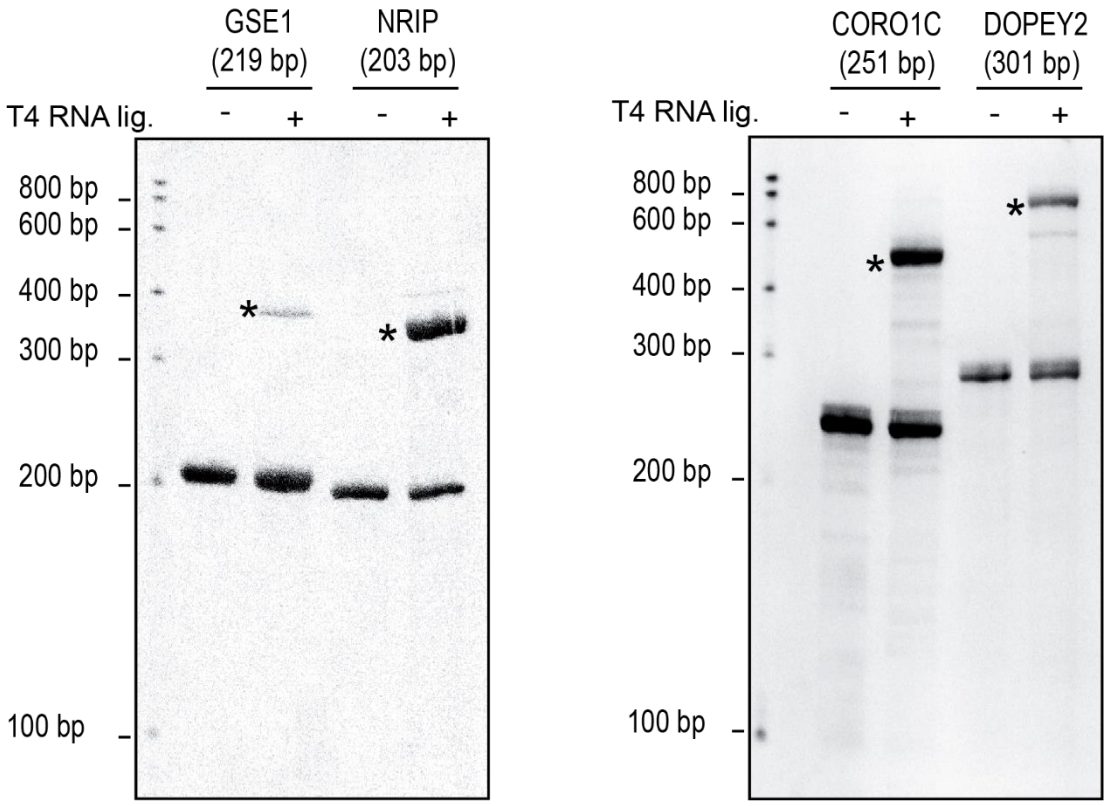

Figure 14. *In vitro* synthesis of circRNA candidates. *In vitro* circularization was analyzed by 6% denaturing polyacrylamide gel electrophoresis (PAGE). The mobility of the putative circular RNAs is indicated with asterisks (*). CircRNAs migrate slower compared to their linear counterparts.

3.1.3 *Confirmation of circularity*

To confirm that the selected RNA products obtained from the ligation were circular, we decided to use two different strategies: RNase R and RNase H treatment. As previously described, RNase R is a 3'-5 exoribonuclease that generally degrades linear RNAs leaving circRNAs intact (Figure 15A). Accordingly, we digested the linear RNAs and the corresponding circRNAs with RNase R for 30 min. Northern blots of the digestions showed that the selected circRNAs were resistant to RNase R digestion, while linear RNAs were degraded (Figure 15B). Unlike RNase R, RNase H is an endoribonuclease that can cleave RNA within RNA-DNA hybrids. In the presence of an antisense DNA oligo, the RNase H cleaves the RNA of interest into two products if it is linear or in one single product (of the predictable linear size) if it is circular (Figure 15C). Therefore, we digested the linear RNAs and the corresponding circRNAs with RNase H using specific antisense oligos and performed northern blots (Figure 15D). Northern blot analyses revealed two RNA fragments corresponding to the products digested from linear RNAs (GSE1, NRIP1 and CORO1C). In case of linear DOPEY2, only the longer digestion product was detected since the smaller one runned out of the gel. Expectedly, digestion of the all tested circRNAs gave only one fragment, which migrates approximately to the

corresponding size of their linear counterparts. In sum, in conjunction with the RNase R resistance, these RNase H cleavage/northern blot assays conclusively demonstrate the circular configuration of the synthetic circRNA candidates.

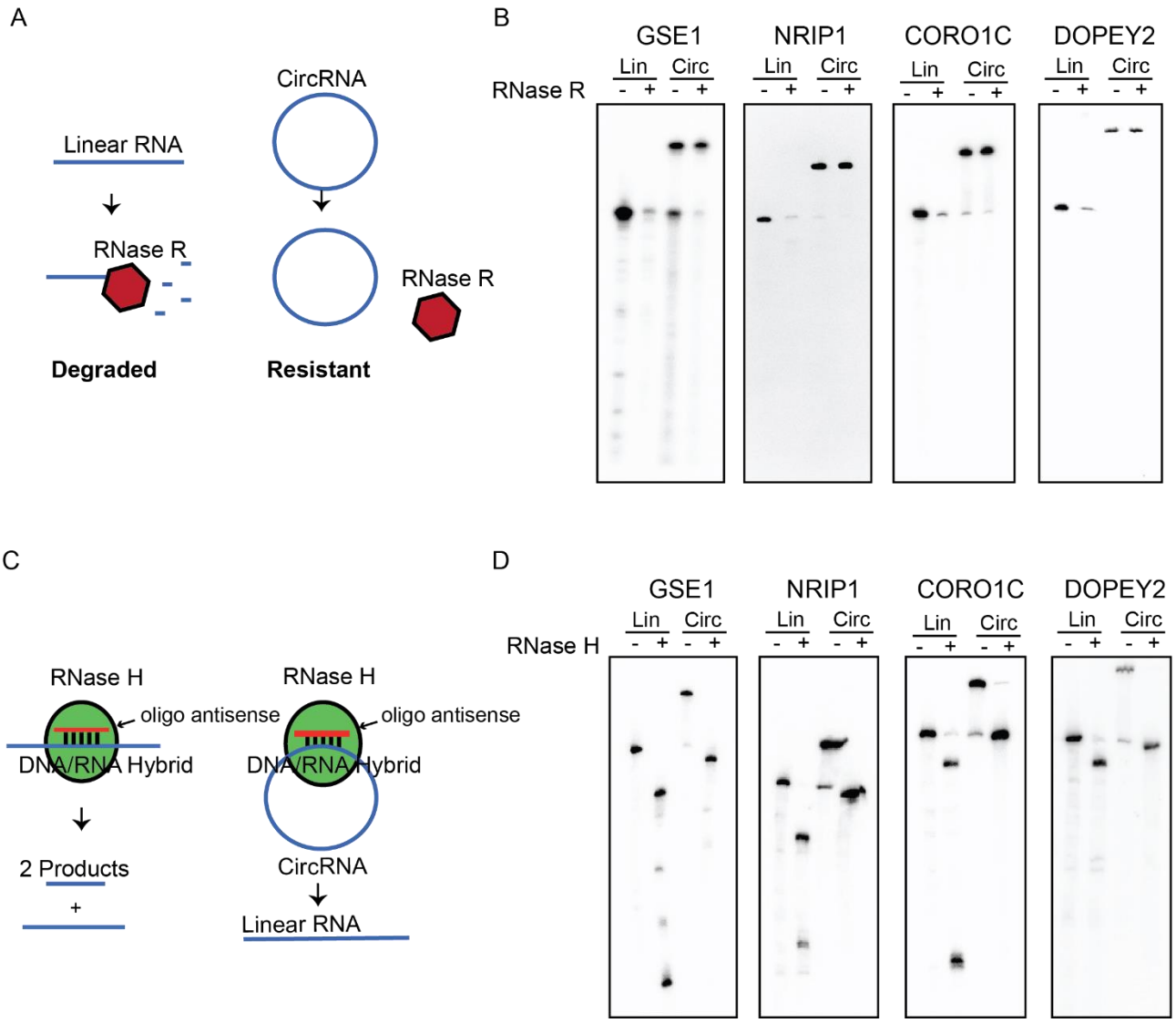

Figure 15. Confirmation of circularity of synthesized circRNAs. (A) Schematic representation of RNase R strategy to demonstrate the circularity. (B) Circular and linear RNAs were treated for 30 min with RNase R and analysed by northern blotting. CircRNAs are resistant to RNase R digestion, while linear RNAs are degraded. The following northern blot analysis show two RNA products for linear RNAs and only one linear fragment for circRNAs whose size correspond approximately to the linear counterpart. (C) Schematic representation of RNase H strategy to demonstrate the circular configuration of circRNAs. (D) Linear and circular RNAs were treated with RNase H in the presence of an antisense DNA oligonucleotide. The following northern blot analysis revealed two RNA fragments for linear RNAs and only one linear fragment for circRNAs whose size correspond approximately to the linear counterparts.

3.1.4 *CircRNAs preferentially degraded in cytoplasmic extracts*

After the optimization of *in vitro* synthesis of circRNAs, we started measuring the turnover of the synthetic circRNAs and their linear counterparts in cell lysates of different purification stages. First, we performed nuclear/cytoplasmic fractionation of HEK293T cells and validated the subcellular fractionation efficiency by western blot. Western blot using beta-tubulin and GAPDH, as cytoplasmic markers as well as Lamin A/C and NONO, as nuclear markers, confirmed our succesful fractionation procedure (Figure 16A). Subsequentely, we performed *in vitro* RNA degradation assays by incubating four selected radioactive labelled circRNAs and linear RNAs with cytoplasmic and nuclear extracts at different time points (Figure 16B). As expected, linear RNAs are degraded in cytoplasmic and nuclear extracts since the exoribonuclease-mediated decay is present in both compartiments. Interestingly, all four tested circRNAs are more stable than their linear RNA counterparts and are preferentially degraded in cytoplasmic extracts (Figure 16B). In conclusion, we confirmed that our selected circRNAs have higher stability than the linear RNA counterparts and that circular RNAs are stronger degraded in cytoplasmic extracts compared to nuclear extracts.

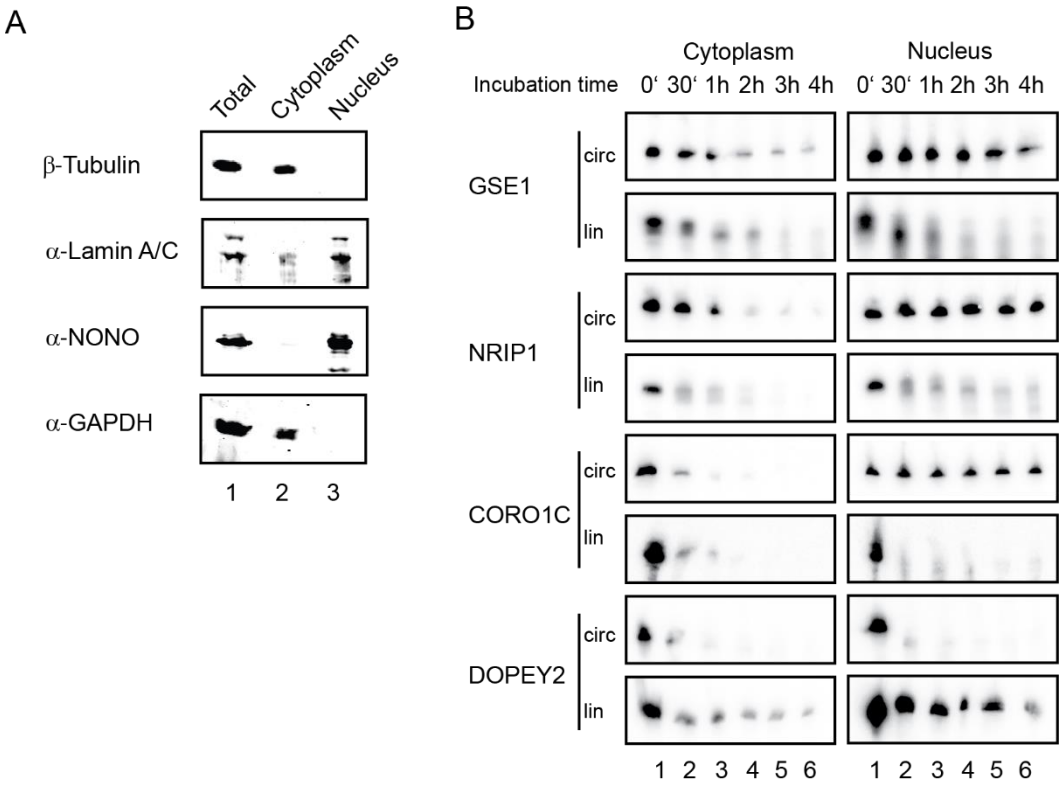

Figure 16. CircRNAs are predominantly degraded in cytoplasmic extracts. (A) Validation of the efficiency of the nuclear and cytoplasm fractionation by western blot. Beta-Tubulin and GAPDH were used as cytoplasmic markers, while Lamin A/C and NONO served as nuclear markers. (B) Circular and linear synthetic version of GSE1, NRIP1, CORO1C and DOPEY2 were incubated with

cytoplasmic and nuclear extracts at different time points. The PAGE analysis shows that circRNAs are more stable than their linear counterparts and more sensitive to degradation in cytoplasmic extracts.

3.1.5 *Identification of endoribonuclease candidates*

Based on the previous results, cytoplasmic extract was selected for further biochemical fractionations followed by degradation activity. To confidently identify endonuclease candidates, we performed two serial fractionation/purification steps: Ammonium Sulfate (AS) precipitation and glycerol density gradient ultracentrifugation. First, we performed an AS precipitation test: the cytoplasmic extract was precipitated with different AS concentrations and then tested for *in vitro* RNA degradation assays. Since all four candidates yielded similar degradation efficiency in several test experiments (data not shown), we mainly focused on two selected circRNAs, circNRIP1 and circGSE1, in the subsequent RNA degradation assays. Interestingly, as shown in the urea PAGE gel, circRNAs were preferentially degraded at 20% and 30% of AS saturation and around 20-30 % AS saturation (Figure 17A). Surprisingly, we also found degradation activity at a higher concentration of AS, around 50-70% AS saturation (Figure 17A). As a starting point, 30% saturated precipitate was selected for the next purification step. In detail, we performed a 10-40% glycerol density gradient ultracentrifugation of the 30% AS precipitate and we collected about 14 fractions. Each fraction was used to test circRNA degradation activity by performing *in vitro* RNA degradation assays (upper panel, Figure 17B). Two hours were selected as incubation time based on several pilot experiments (data not shown). Interestingly, we found that the fractions 2-5 could efficiently degrade the two tested circRNAs, circNRIP1 and circGSE1. These four fractions were pooled together and tested again for degradation activity using one-hour incubation time course (lower panel, Figure 17B). The pool was then analysed by mass spectrometry to identify potential endonuclease candidates migrating within these fractions.

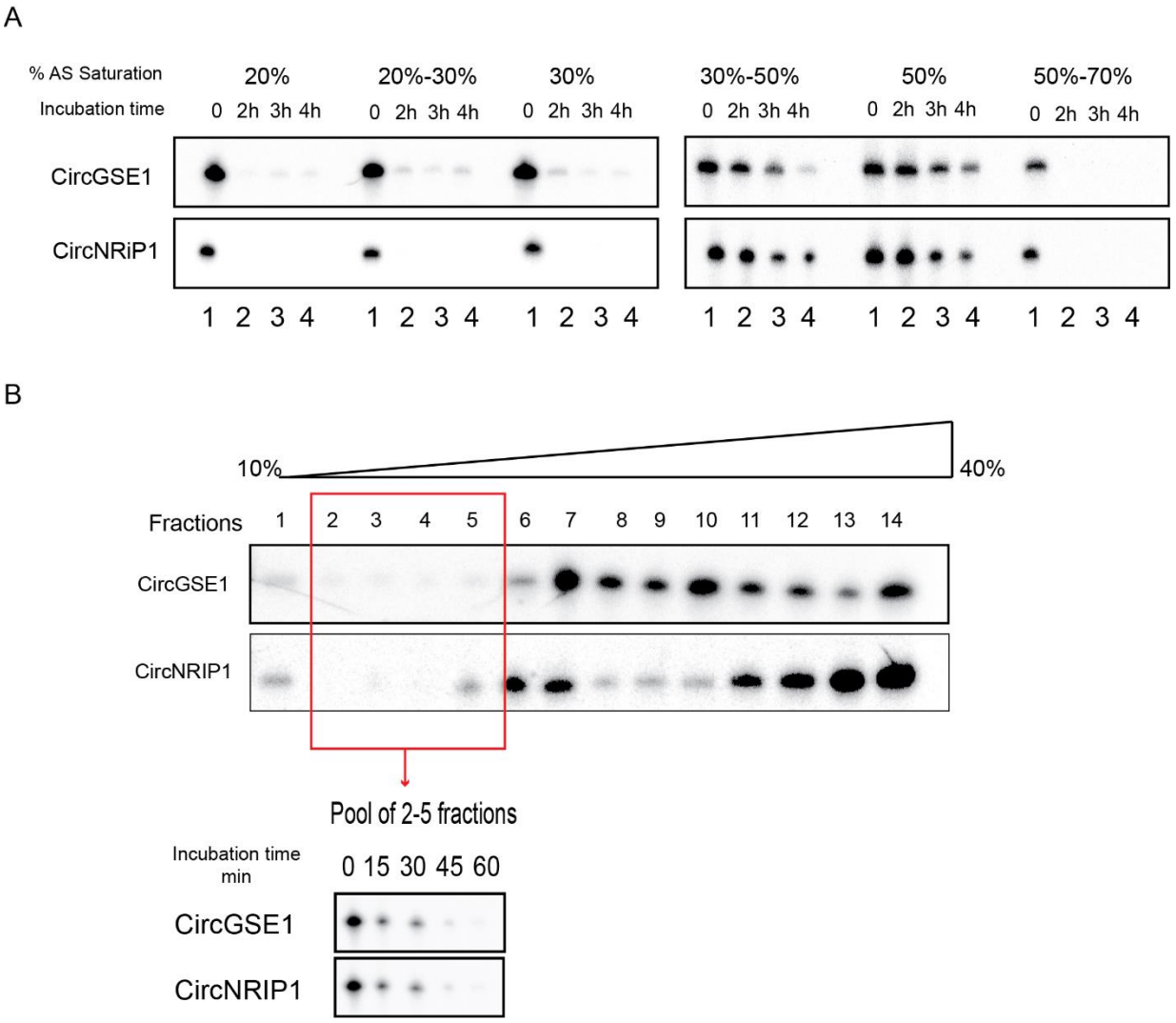

Figure 17. Serial fractionation steps to identify endonuclease candidates. (A) Synthetic circular GSE1 and NRIP were incubated with different Ammonium Sulfate saturated precipitates. PAGE gel analysis show that circRNAs were preferentially degraded at 20% and 30% of Ammonium Sulfate (AS) saturation and around 20-30% AS and 50-70% AS saturation. (B) A 10%-40% glycerol gradient of 30% ammonium sulfate precipitate was performed and 14 fractions were collected. Each fraction was tested for circRNAs degradation as shown in the PAGE gel. CircRNP1 and circGSE1 were mainly degraded in fractions 2-5. These fractions (red rectangle) were pooled together and tested for degradation activity using shorter incubation times.

3.1.6 *Mass spectrometry analysis reveals potential endonuclease candidates*

In collaboration with Bruckmann lab (Biochemistry I, University of Regensburg), we performed mass spectrometry analysis of the four fractions competent for circRNA degradation. Figure 18A shows the coomassie gel of the pool of the fractions analysed. Several putative endonuclease candidates were identified: Aldolase A, APEX, ARD1/ppp18, G3BP1 and DIS3 (Figure 18B and Suppl. Table 1). Although Aldolase A, ARD-1 and G3BP1 do not have a specific endonuclease domain, these proteins have been demonstrated to cleave RNA molecules (Figure 18B). Aldolase A is a glycolytic

enzyme and its homologue Aldolase C was found to have a secondary function as endoribonuclease (Cañete-Soler et al., 2005). APE1 is involved in DNA-base-excision repair where it shows apurinic/apuridinic DNA endonuclease activity. It was suggested that APE1 can not only cleave DNA but also RNA. ARD1 is considered a mammalian analogue of *E. coli* RNase E but its role in human still remain to be characterized (Claverie-Martin et al., 1997; M. Wang & Cohen, 1994). G3BP has multi-functions. Among them, an eventual RNA endoribonucleolytic degradation role (Irvine et al., 2004). And finally, DIS3 is the catalytic component of the exosome and has also endoribonuclease activity, which is mediated by its PIN domain (Figure 18B).

A

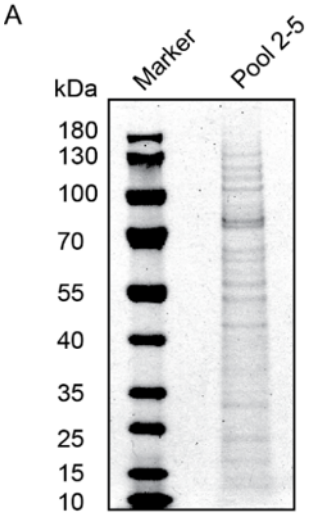

B

Candidates	Molecular weight (KDa)	Domains
Aldolase A	38,4	
G3BP	52,1	
ARD1	38,5	
APE1	35,5	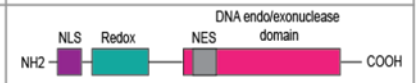
Dis3/Rrp44	108,9	

Figure 18. Identification of endoribonuclease candidates by mass spectrometry analysis. (A) Coomassie gel staining of the purified 2-5 fractions pool. (B) Summary table of the five promising endonuclease candidates found by mass spectrometry. The domain structures and the molecular weights of the five eukaryotic endoribonucleases are shown. Despite no known endoribonuclease domains have been identified in aldolase A, ARD-1 and G3BP, these proteins have been demonstrated to cleave RNA molecules. To note that the domain structures and the relative sizes of the proteins are not drawn to scale.

3.1.7 *DIS3 and ARD1 are promising candidates for circRNA degradation*

Our mass spectrometry data suggested both well-characterized and also less well-characterized endonucleases, which have other main roles. We wondered if these candidates were real endonucleases and if they could cleave circRNAs. To validate them, we combined protein immunoprecipitation experiments with *in vitro* RNA degradation assays. First, we overexpressed Flag-HA tagged versions of all endonuclease candidates in HEK293T cells and performed anti-Flag immunoprecipation of the proteins. Flag-HA GFP was used as negative control. After confirmation

of the immunoprecipitation efficiency by western blot (Figure 19A), radioactively labeled circRNAs and linear RNAs were incubated with the immobilized proteins at different time points. The results were analysed by northern blot (Figure 19B). Interestingly, not all endonucleases candidates were able to degrade our selected circRNAs. In detail, both ARD1 and DIS3 could degrade linear and circular RNAs (NRIP1 and GSE1). As DIS3 contains an N-terminal PIN domain, it was expected to cleave circular RNAs. Surprisingly, although APEX1 has an apurinic/apuridinic DNA endonuclease domain, it does not degrade both linear and circular NRIP1. This suggests that APEX1 is not involved in general RNA degradation. Unfortunately, for G3BP1 and ALDOA we did not get clear signals (data not shown). These preliminary data suggested that DIS3 and ARD1 could be promising candidates for circRNA degradation. ARD1 was object of study of the Master Thesis of Sabrina Mandl. In this thesis, we decided to focus mainly on DIS3, since it is the catalytic component of the exosome and its cytoplasmic role in circRNA degradation in human has not been fully analysed.

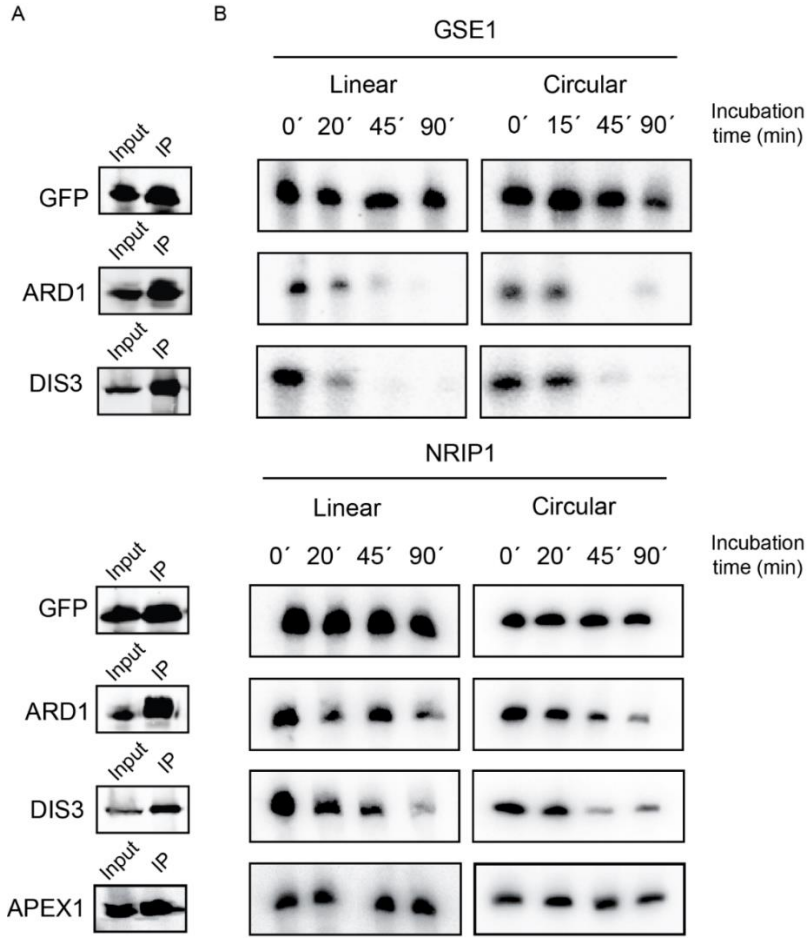

Figure 19. *In vitro* RNA degradation assays for validation of endonuclease candidates. (A) Flag-HA tagged endonucleases were immunoprecipitated with flag beads and detected by western blot using anti HA antibodies. (B) Urea Gel-electrophoresis analyses represent the incubation of labelled linear and circular NRIP1 and GSE1 with resin-immobilized indicated proteins at different time points. ARD1 and DIS3 but not APEX1 degrade *in vitro* circRNAs. GFP served as negative control.

3.1.8 *DIS3L1 and EXOSC10 and other exosome components can't degrade circRNA in vitro*

As already mentioned in the introduction, DIS3 is one of three catalytic subunits of the exosome along with DIS3L1 and EXOSC10. The core exosome consists of 9 conserved subunits, six of them (EXOSC4-9) form a central barrel-like structure (EXOSC4-6) on which a three subunits-cap lean on (EXOSC1-3). We wondered if the components of the cap or the core of the exosome were involved in circRNA degradation. Moreover, we also want to verify if the other catalytic subunits, DIS3L1 and EXOSC10, could degrade circRNAs *in vivo* and *in vitro*. To answer this question, we performed immunoprecipitation of different exosome components followed by *in vitro* RNA degradation assays using linear and circular NRIP1 (Figure 20). First, the efficient immunoprecipitation of the different exosome components was confirmed by western blot (Figure 20A). When we look at the degradation assay from UREA gels, we found that the catalytic subunits of the exosome, DIS3L1 and EXOSC10, efficiently degraded linear NRIP1 but not its circular counterpart (Figure 20B). This is expected because EXOSC10 is a 3'-5' exoribonuclease and DIS3L1 is a homolog of DIS3 but contains a catalytic inactive endoribonuclease PIN domain (Lykke-Andersen et al., 2011). Interestingly, as shown in the urea PAGE gels/northern blot, all the immunoprecipitated exosome cap components (EXOSC1-3) were able to degrade linear NRIP1 but not its circular form implying that DIS3 might not co-immunoprecipitated with the cap components of the exosome in our immunoprecipitations. Taken together, these results show that immunoprecipitated cap components as well as other catalytic components of the exosome, can degrade linear but not circular RNAs. We also confirmed that DIS3L1 and EXOSC10 do not have endonuclease activity, at least for the tested circRNA.

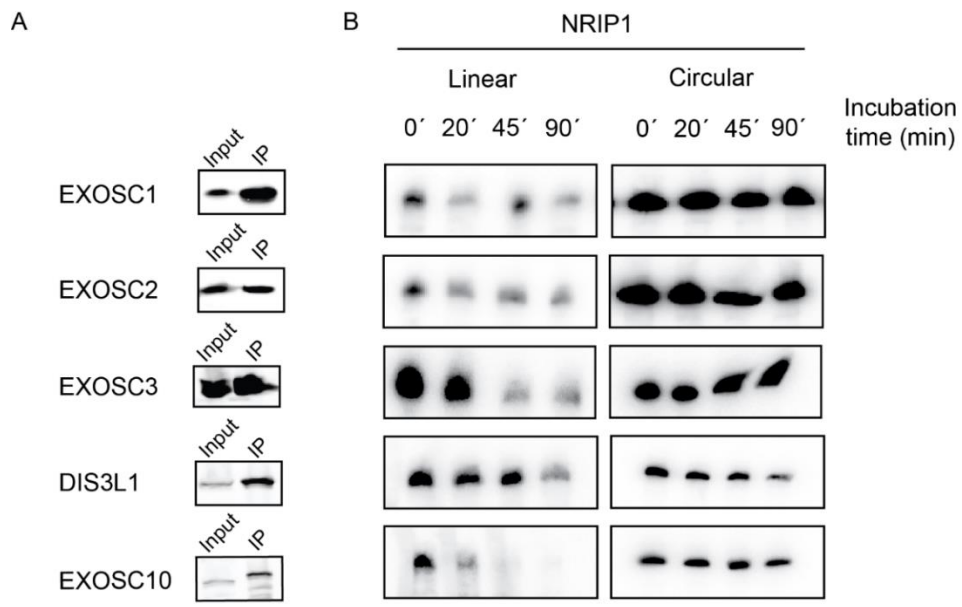

Figure 20.Validation of exosome components by performing in vitro RNA degradation assays. (A) Western blots of the anti-Flag immunoprecipitations of different exosome components were performed with anti-HA. (B) Urea Gel-electrophoresis analysis from the degradation assay after incubation of labelled linear and circular NRIP1 with resin-immobilized proteins at different time points. Unlike linear NRIP1, circRNP1 is not degraded by the catalytic subunits, EXOSC10 and DIS3L1, and the exosome's cap components.

3.2 Validation of DIS3 function in circRNA degradation by *in vitro* RNA degradation assays

Motivated by our Mass spectrometry results and initial *in vitro* degradation assays, we further characterized DIS3 as a potential candidate for circRNA degradation. The following experiments investigated DIS3 endoribonucleolytic function by *in vivo* and *in vitro* RNA degradation assays with linear and circular RNAs. Since DIS3 is conserved between humans and yeast, we also investigated the corresponding yeast dis3/rrp44 protein and its PIN domain responsible for the endoribonucleolytic activity. For this purpose, in collaboration with Sprangers lab (Biophysics I, University of Regensburg), we purified recombinant wild-type and mutant versions of the DIS3 protein or we immunoprecipitated from human cells several Flag-HA tagged versions of DIS3 and we also studied the impact of DIS3 and whole exosome on circRNA degradation *in vitro*.

3.2.1 *S. cerevisiae recombinant Dis3/Rrp44 alone or associated with the exosome can degrade circRNAs in vitro*

The eukaryotic RNA exosome is a conserved multisubunit protein complex that catalyzes 3′-to-5′ RNA degradation. In *S. cerevisiae*, the exosome includes a nine-subunit core (Exo9) that interacts with Dis3/Rrp44 to form a 10-subunit complex (Exo10) (Figure 21A). The Exo9 core lacks catalytic activity, while Dis3/Rrp44 catalyses endoribonuclease and 3′-to-5′ exoribonuclease activities (Dziembowski et al., 2007; Lebreton et al., 2008; Q. Liu et al., 2006). To test whether yeast Dis3/rrp44 and the whole exosome could affect circRNA degradation *in vitro*, we received from Sprangers lab (Biophysics 1, University of Regensburg), yeast Dis3/Rrp44, yeast exosome (Exo10) and an inactive catalytic exosome lacking Dis3/Rrp44 (Exo9) (Figure 21A). The efficient purification of yeast Dis3/rrp44 and of different exosome complexes was confirmed by Coomassie staining (Figure 21B). All exosome core subunits were present in purified Exo9 and Exo10 while Rrp44/Dis3 was purified alone and was present only in Exo10 as expected. Next, we performed RNA degradation assays by incubating our tested RNAs with purified proteins. Reactions were carried out in a high manganese concentration buffer which favours endoribonucleolytic activity (Lebreton et al., 2008). The following *in vitro* RNA degradation assays with linear and circular NRIP1 and GSE1 showed that Dis3/Rrp44 alone could degrade circRNAs and linear RNAs *in vitro* (upper left panel, Figure 21C). Indeed, the liner and circular RNA signal intensity are reduced over time. When Dis3/Rrp44 is assembled in the exosome (Exo10), the complex exhibits the ability to degrade linear and circRNAs *in vitro* but with less efficiency (upper right panel, Figure 21C) comparing to Dis3/Rrp44 alone. The catalytic inert exosome Exo-9 (without Dis3/Rrp44) cannot degrade circRNAs *in vitro* and present a weak degradation activity on the linear RNAs after long incubation (down panel, figure 21C).
Together, we showed that the *S. cerevisiae* Dis3/Rrp44 alone or in association with the exosome could degrade circRNAs *in vitro*. The catalytic inert exosome Exo9 (without Dis3/Rrp44) cannot degrade *in vitro* circular and linear RNAs.

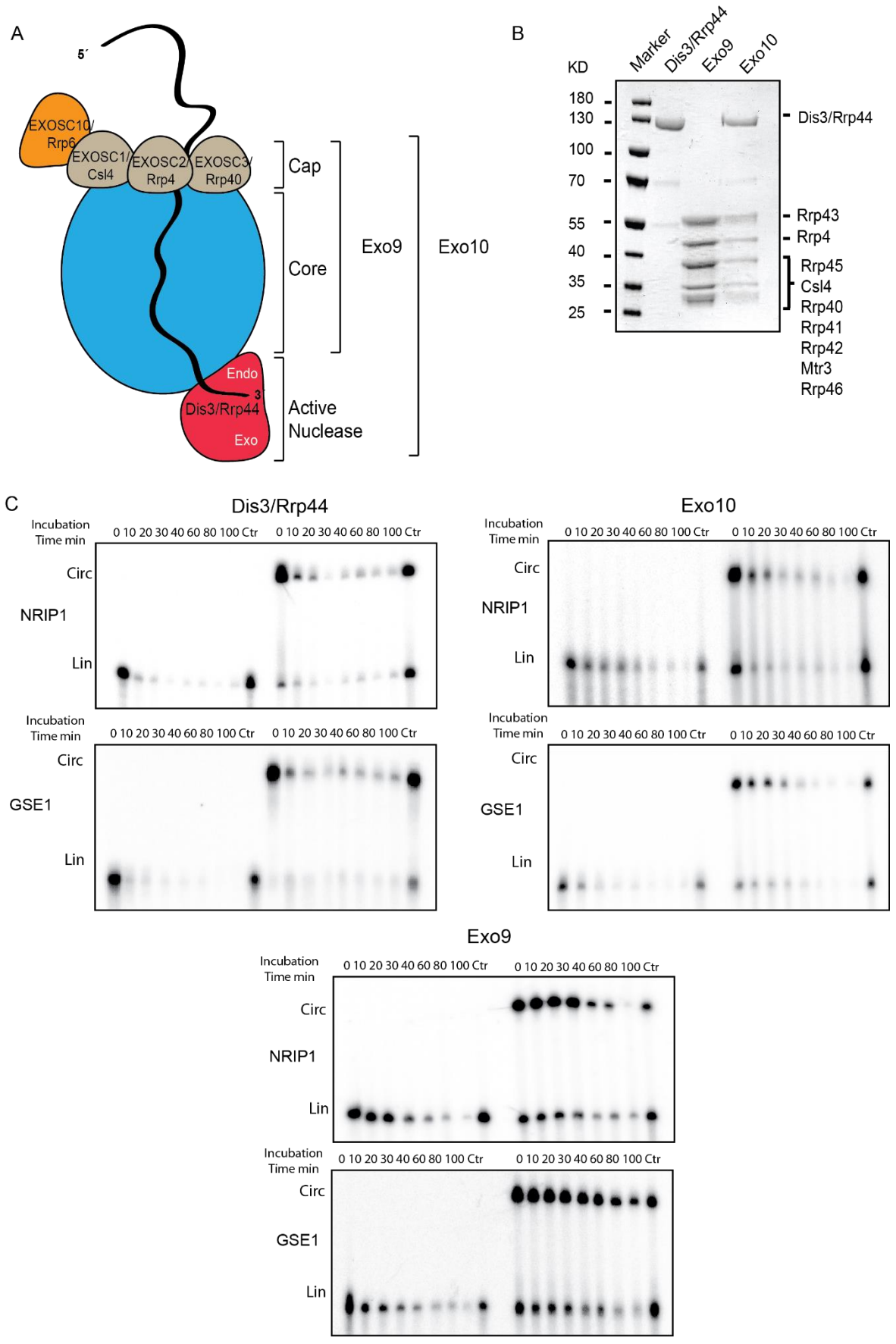

Figure 21. Yeast Dis3/Rrp44 and exosome impact on circRNA degradation. (A) Exosome components and composition of exosome subcomplexes Exo9 (cap+core), Exo10 (cap+core+Dis3)

in eukaryotes. (B) Coomassie Gel staining showing Yeast Dis3/Rrp44 recombinant protein and exosome complexes Exo10 and Exo9. (C) Gel-electrophoresis analysis generated by the incubation of labelled linear and circular NRIP or GSE1 with recombinant Dis3/Rrp44 and exosome complexes. Dis3/Rrp44 alone or assembled into the exosome, can degrade circRNAs *in vitro*. The catalytic inert exosome Exo9 (without Dis3/rrp44) cannot degrade *in vitro* circRNAs.

3.2.2 *Biochemical analyses of the endonuclease activity of the human recombinant DIS3*

DIS3 is conserved from bacteria to humans. The *S. cerevisiae* rrp44/Dis3 and the human DIS3 show the same domain organization: A N-terminal CR3 motif, an RNB domain responsible for exoribonucleolytic activity, two cold-shock domains (CSDs), an S1 domain, which non-specifically binds RNA and a C-terminal PIN domain (Figure 22A) (Tomecki et al., 2010). Mutation of a conserved aspartate in the PIN domain, D146N in *Homo sapiens* and corresponding D171N in *S. cerevisiae* respectively, abolishes its endoribonucleolytic activity (Lebreton et al., 2008). Furthermore, the D487N mutation in the exoribonucleolytic RNB domain abolishes its 3'-5' exoribonucleolytic activity (Tomecki et al., 2014). To analyse the biochemical role of DIS3 on circRNA degradation and its endoribonucleolytic activity *in vitro*, we compared the activity of the human recombinant wild-type protein DIS3 with single mutants of the PIN (DIS3 PIN D146N) and RNB (DIS3 RNB D487N) domains. All three variants of recombinant human DIS3 were purified from yeast by the Sprangers lab and tested for endoribonuclease activity using the four selected circular RNA substrates (Figure 22). First, we checked the purity of recombinant human DIS3 proteins by Coomassie staining (Figure 22B). In the RNA degradation experiments, wild type DIS3 and the RNB mutant version, DIS3 RNB D487N, show endoribonucleolytic activity as the level of the four tested circRNAs decreases over time (Figure 22C). In concordance, the PIN domain mutant version of DIS3, DIS3 PIN D146N, does not show endoribonuclease activity *in vitro*. Taken together, these results demonstrated that the human DIS3 could degrade circRNAs *in vitro* and the PIN domain is crucial for its endoribonucleolytic function. Indeed, when the PIN domain is mutated, DIS3 cannot degrade circRNAs.

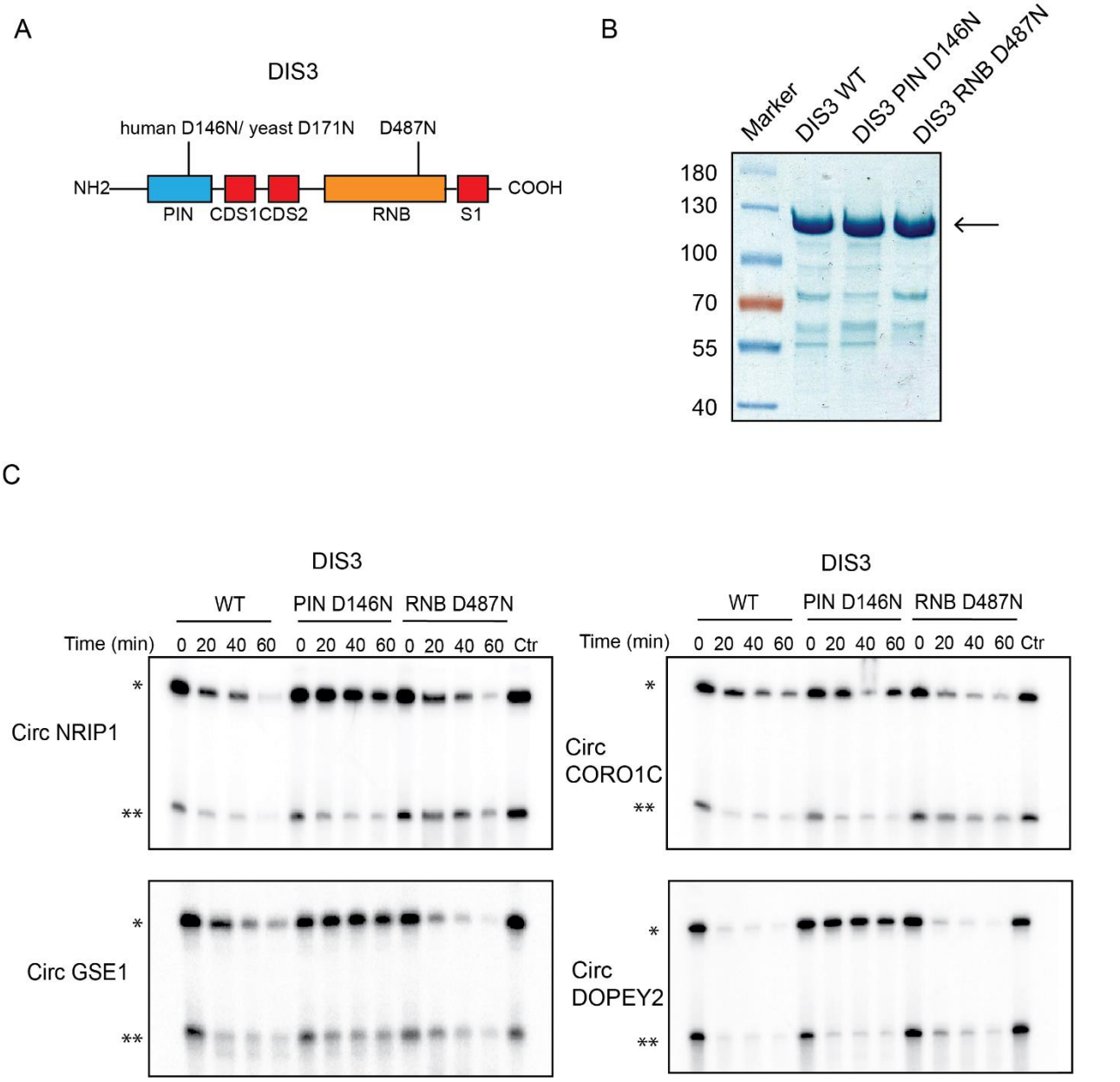

Figure 22. Endoribonuclease activity of the recombinant human DIS3. (A) Domain organization of human DIS3 and yeast Dis3/Rrp44. RNB domain has exoribonucleolytic activity and the N-terminal PIN Domain has endoribonucleolytic activity. Mutations of conserved aspartates, D146N in *H. Sapiens* and D171N in *S. cerevisiae* respectively, abolish its endoribonucleolytic activity. The D487N mutation in the exoribonucleolytic domain (RNB) abolishes its exoribonucleolytic activity. (B) Coomassie Gel staining showing of different recombinant human DIS3 protein: Wild type DIS3 (DIS3 WT), PIN domain mutant (DIS3 PIN D146N) and exoribonuclease mutant (DIS3 RNB D487N). (C) Gel-electrophoresis analysis of labelled circular NRIP1, GSE1, CORO1C and DOPEY2 RNAs (*) incubated with DIS3 WT, DIS3 PIN D146N and DIS3 RNB D487N at different time points in the presence of 3mM manganese (MnCl2). Only DIS3 protein versions that contain an intact PIN domain (DIS3 WT and DIS3 RNB D487N) can cleave circRNAs *in vitro*. Linear substrate molecules (**) result from spontaneous cleavage or breakage during handling before the reaction.

3.2.3 *The S. cerevisiae and H. sapiens DIS3 PIN domain can cleave circRNAs in vitro*

To test whether only the PIN domain of the DIS3 is sufficient for cleavage of circRNAs, we purified *S. cerevisiae* and human wild type PIN domain and its mutants (D146N in humans and D171N in *S. cerevisiae*) (Figure 23). After confirming successful preparation of recombinant PIN domains by Coomassie staining (Figure 23A), we performed RNA degradation assays with *S. cerevisiae* PIN domain (Figure 23B) and then with human PIN domain (Suppl. Figure 2). The efficient purification of yeast and human domains was confirmed by Comassie SDS-PAGE (Figure 23A). As shown in the urea PAGE analysis, the yeast wild-type PIN domain has endoribonucleolytic activity on both linear and circular RNAs (Figure 23B) of all four tested RNAs. On the other hand, the PIN D171N mutant is not able to digest both linear and circular RNAs as the mutation abolishes the activity of the PIN domain protein completely (Figure 23B). This result demonstrated that the PIN domain is responsible for the endoribonuclease activity of DIS3 and that it can act independently from the other DIS3 domains.

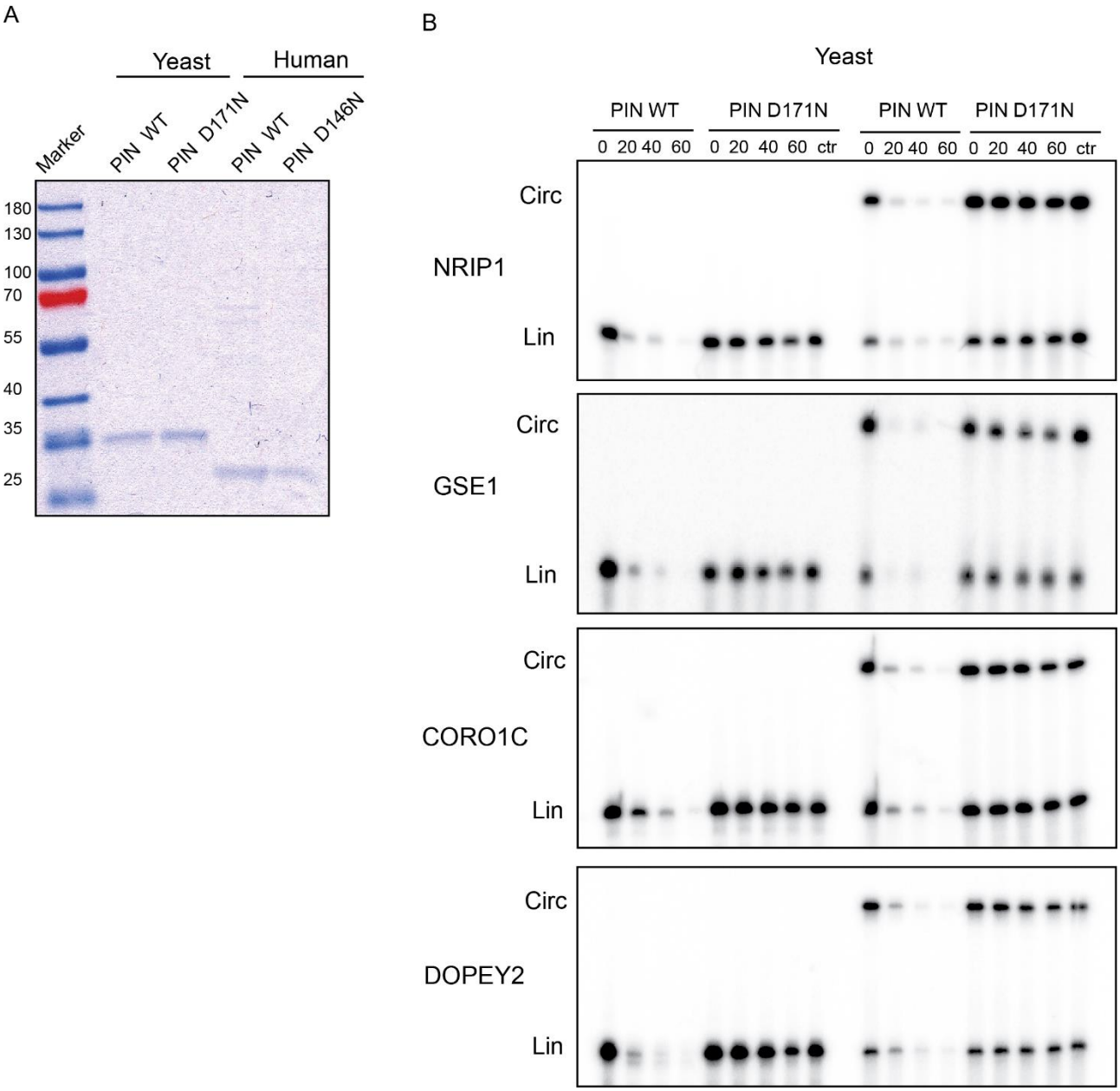

Figure 23. Endonucleolytic activity of DIS3 PIN domain. (A) Coomassie Gel staining showing *S. Cerevisiae* and *Homo sapiens* recombinant PIN domains wild type (yeast PIN WT or human PIN WT) and mutants (yeast PIN D171N or human PIN D146N). (B) Gel- electrophoresis analysis generated by the incubation of labelled linear and circular NRIP1, GSE1, CORO1C and DOPEY2 with different versions of yeast PIN domain at different time points. When the PIN domain of Dis3 is mutated (PIN D171N), circRNAs and linear cannot be cleaved.

3.2.4 *DIS3 catalytic mutant inhibits circRNA degradation in vivo*

To test whether the *in vitro* activity results also reflected the situation in a cellular context, we cloned and overexpressed Flag-HA tagged wild type DIS3 (DIS3 WT) and its catalytic mutants in HEK293 cells, DIS3 PIN D146N and DIS3 RNB D487N. In addition to the single mutants, D146N and D487N,

we created a double mutant, in which both endo- and exo-ribonucleolytic activities are inhibited i.e. DIS3 D146N/D487N (Figure 24A). Flag-HA GFP protein was used as the negative control (GFP). After the immunoprecipitation, the proteins were eluted with commercial Flag peptide and the successful elution was confirmed by western blotting (Figure 24B). Next, we tested *in vitro* degradation assays of the immunoprecipitated proteins using circNRIP1 as an example. The assays were analysed by urea gel electrophoresis (Figure 24C). Comparison of the activities of the wild type protein with the mutants demonstrated that circNRIP1 digestion occurs only in presence of the wild type protein or of the single mutant of the RNB domain. Notably, we observed only a mild degradation activity: the level of circNRIP1 slightly decreases over time. This less degradation efficiency could be due either to a low concentration of the proteins or to the short incubation time course. Moreover, the single mutant of the PIN domain and the double mutant were not able to digest a circular RNA similar to the negative control represented by Flag-HA GFP. Taken together, these results agreed with the previous *in vitro* activity results and confirmed that DIS3 could play a role in circRNA degradation *in vitro* and *in vivo*.

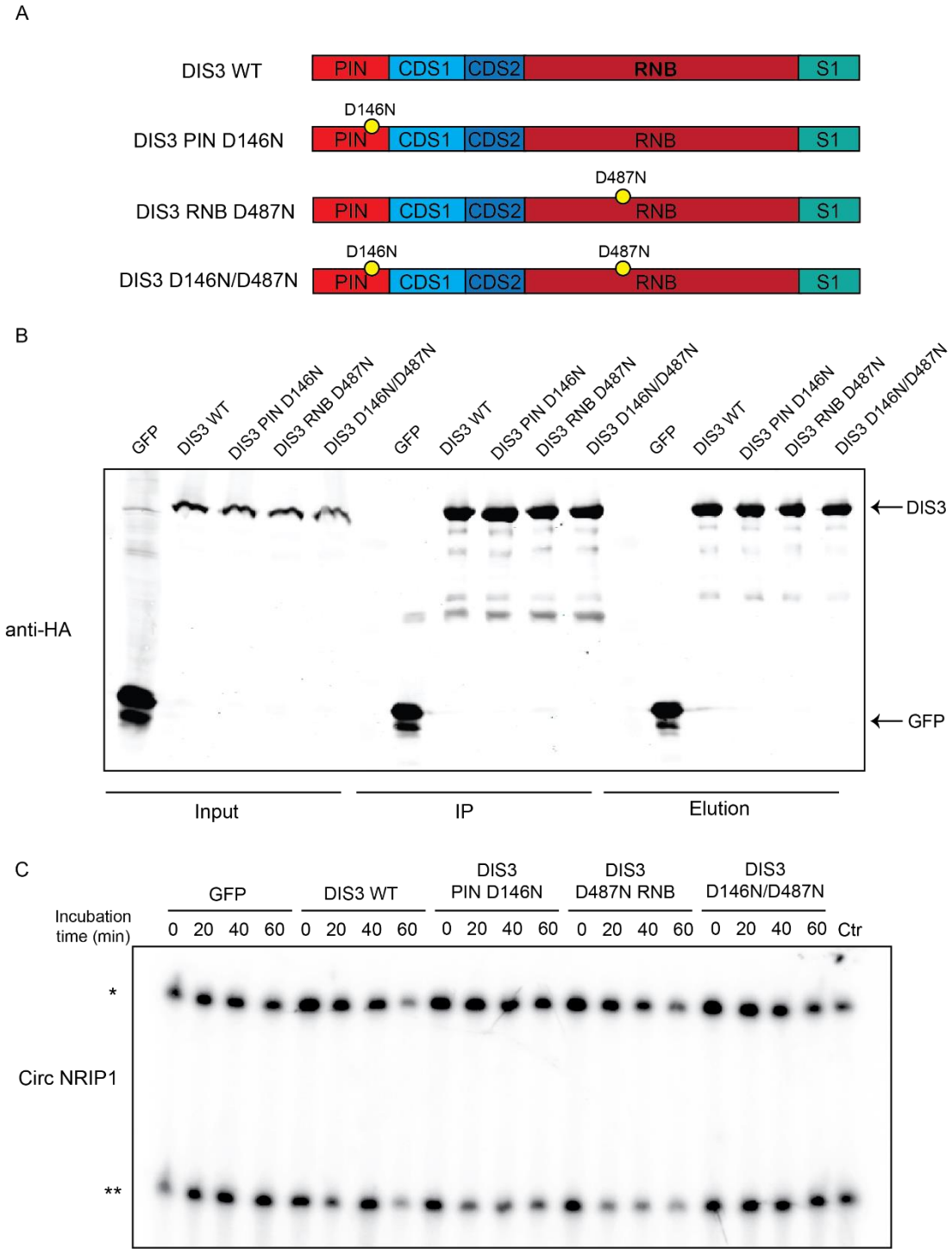

Figure 24. DIS3 activity *in vivo* on circRNAs degradation. (A) Schematic representation of DIS3 wild type protein (DIS3 WT) and its mutant versions (DIS3 PIN D146N, DIS3 RNB D487N and DIS3 D146N/D487N) overexpressed in HEK293 cells. (B) Western blot with anti-HA antibody confirmed the correct overexpression, immunoprecipitation and elution of DIS3 proteins. (C) Gel-electrophoresis analysis from degradation assay generated by the incubation of labelled circular NRIP1 with different versions of DIS3 (DIS3 WT, DIS3 PIN D146N, DIS3 RNB D487N and DIS3 D146N/D487N) at different time points. Flag-HA GFP protein was used as negative control (GFP). CircNRIP1 (*) level faintly decreases only in the presence of DIS WT or the single exonucleolytic mutant DIS3 RNB D487N. Linear substrate molecules (**) result from spontaneous cleavage or breakage during handling before the reaction.

3.3 *In vivo* validation of DIS3 effects on circRNA degradation

In vitro degradation assays showed that DIS3 can degrade circRNAs alone or associated with the exosome and that the PIN domain is responsible for its endoribonuclease activity. Accordingly, DIS3 alone has the potential to degrade circRNAs. We wondered how this works *in vivo* and which circRNAs are regulated by DIS3. To answer this question, we generated several CRISPR/Cas9-mediated DIS3 knockout cell lines and performed RNA sequencing (RNA-seq) analysis of the obtained cell lines.

3.3.1 *CRISPR/Cas9 knockout strategy to study circRNA degradation in vivo*

To study the physiological relevance of DIS3 in circRNA degradation *in vivo*, we performed knockout experiments using the CRISPR/Cas9 system. As reported previously, DIS3 is essential in yeast (Gudipati et al., 2012; Schneider et al., 2012) and in *Drosphila* (Hou et al., 2012). Initially, we tried to create DIS3 knockout HEK293T cells using the traditional single-guide RNA (gRNA) CRISPR/Cas9 method. However, we could obtain only one heterozygous DIS3 partial knockout HEK293 clone and we were not able to obtain any homozygous DIS3 knockout HEK293T cell lines (data not shown) confirming that DIS3 is essential gene in human cells as well (Davidson et al., 2019). To overcome this problem, we applied an alternative approach for depletion of DIS3 via CRISPR/Cas9. First, we generated Flp-In T-REx-293 stable cell line expressing exogenous Flag-HA DIS3 WT or Flag-HA DIS3 D146N, its PIN catalytic mutant. We are aware that the Flp-In T-REx-293 cells exhibit a mild leaky expression of the exogenous proteins even in the absence of doxycycline. Therefore, we take advantage of this to create DIS3 knockout cells. After obtaining Flp-In T-REx-293 stable cell lines, we performed knockout experiments using the dual-guide RNAs CRISPR/Cas9 editing system (Figure 25). Since the cells already contain the exogenous coding sequence of DIS3, we designed two gRNAs that target the intron of the DIS3 locus. Specifically, the two gRNAs flank the second exon of DIS3 where the PIN domain is located. After that, the CRISPR/Cas9 KO clones were genotyped by PCR using specific primers flanking the deletion, which is about 677 bp long. PCR using these primers, gave a single band of 677 bp in case of wild-type clones, a single smaller band in case of homozygous KO clones and a double band in case of heterozygous KO clones (Figure 25A). Using this approach, we could obtain eight homozygous KO clones from 16 clones tested for Flp-In T-REx-293 stable cell lines expressing Flag HA DIS3 WT (Figure 25B). Unfortunately, two clones (Clone 9 and Clone 11) did not give any signals while two clones (Clone 15 and Clone 16) give non-specific signals and will be needed to investigate in the future (Figure 25B). The same approach applied to the Flp-In T-REx-293 stable cell lines expressing

Flag HA DIS3 D146N mutant. We could obtain only one homozygous DIS3 KO clone (clone 2) showing a single band at the expected size of the deleted fragment (Figure 25C).

Taken together, these results indicated that we could successfully obtain different DIS3 KO clones in the background of Flp-In T-REx-293 stable cell lines expressing exogenous FLAG-HA-tagged DIS3 proteins.

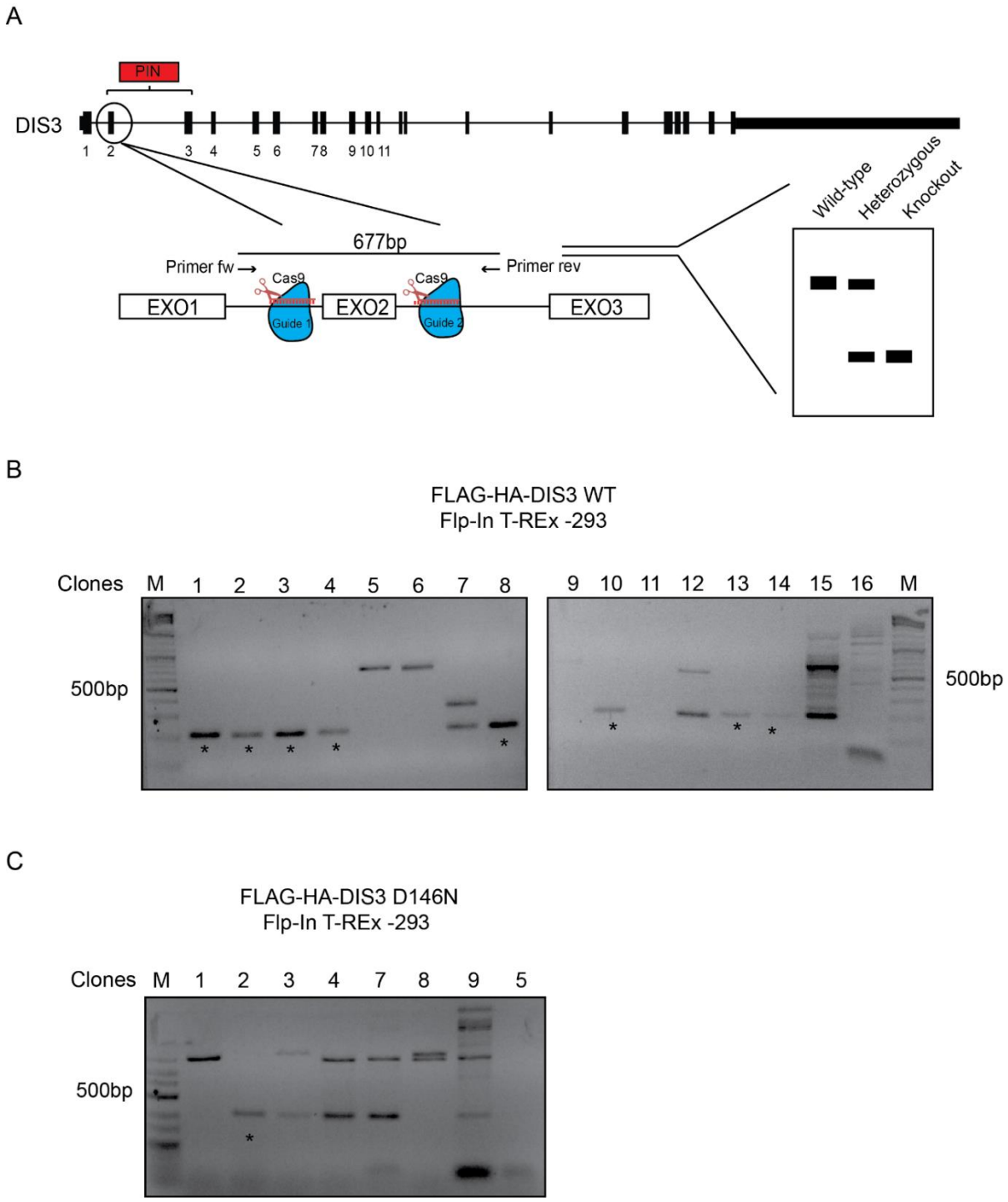

Figure 25. CRISPR/Cas9 strategy for knockout of DIS3. (A) Diagram of location of dual target sites and of the CRISPR/Cas9 dual gRNAs in DIS3 locus. Schematic representation of the genotyping

PCR used for validation. Two gRNAs are indicated by red scissors and gene-specific primers used for PCR genotyping are indicated by arrows. Genotyping PCR results in a single band of 677bp for wild-type clones, a single smaller band for homozygous KO clones and a double band in case for heterozygous KO clones (B) Gel electrophoresis of PCR amplicons using specific primers flanking the deletion in FLAG-HA-DIS3 WT Flp-In T-REx -293 cells. The asterisks indicate positive clones. (C) Gel electrophoresis of PCR amplicons using specific primers flanking the deletion in Flag-HA-DIS3 D146N in Flp-In T-REx -293 cells. DIS3 D146N KO clone 2 (*) is the only positive.

3.3.2 *Validation of inducible DIS3 CRISPR/cas9 knockout cell lines by western blotting*

After verification of positive clones by PCR, we wanted to confirm the DIS3 knockout clones by western blot using an anti-DIS3 antibody (Figure 26). For DIS3 WT KO generated from Flag HA DIS3 WT (FH-DIS3 WT) Flp-In T-REx-293, we randomly selected three knockout clones: 1, 8, and 13 (left panel, Figure 26A). For DIS3 D146N KO cells generated from Flag-HA DIS3 D146N (FH-DIS3 D146N) Flp-In T-REx-293, we selected the only homozygous clone, clone 2 and an additional heterozygous one, clone 7 (left panel, Figure 26B). Comparing the level of DIS3 in the knockout clones with the respective wild-type stable cell lines, we could nicely observe a strong reduction of the endogenous DIS3 in all the homozygous knockout clones tested and a mild reduction in the heterozygous clone, clone 7, as expected. Of note, a faint band was recognized in DIS3 WT KO clones, which represented the leaky expression of exogenous Flag-HA DIS3 WT. According to this observation, we could detect the faint band using an anti-HA antibody confirming leaky expression of exogenous DIS3.

We next tested the ectopic expression of DIS3 from the inducible promoters upon doxycycline induction (right panels, Figure 26A and 26B). After inducing cells for 48 hours with doxycycline, we analysed the expression of DIS3 by western blot using anti-DIS3 and anti-HA antibodies. In contrast to the non-treated samples, Flag-HA DIS3 WT or Flag-HA DIS3 D146N protein expression levels were significantly increased in all the knockout clones after two days of doxycycline treatment.

Taken together we could validate the inducible DIS3 knockout cell lines by western blot and thus confirm that their suitability for further analysis.

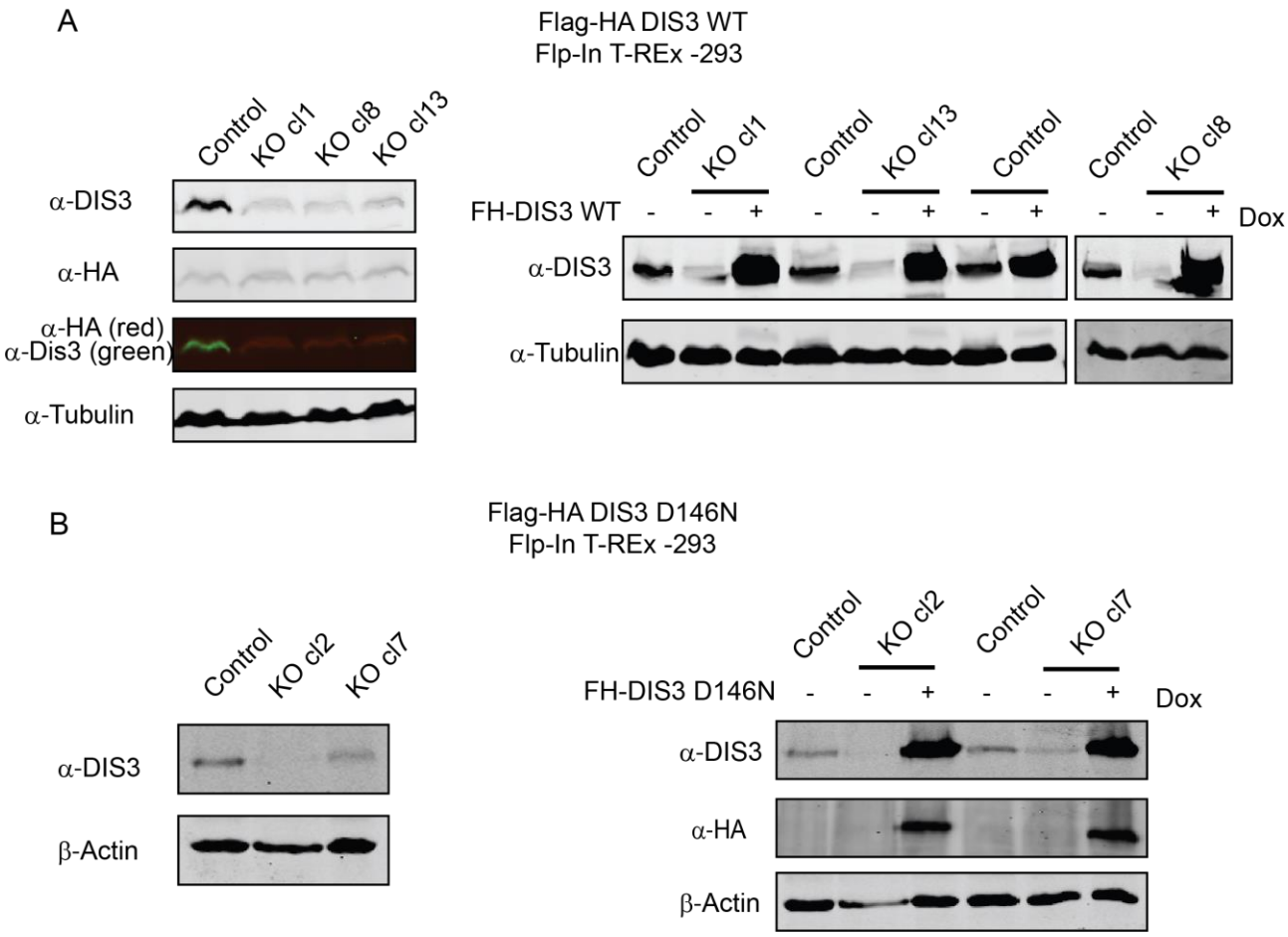

Figure 26. Validation of DIS3 CRISPR/Cas9 knockout cells by western blot. (A) (Left panel) western blot showing reduction of DIS3 protein in three different DIS3 WT KO clones (cl1, cl8, cl13). (Right panel) Western blot showing reconstitution of Flag-HA DIS3 WT by induction of doxycycline for 2 days. DIS3 proteins were detected using anti-DIS3, anti-HA antibodies. Alfa-Tubulin was used as loading control. (B) (Left panel) Validation by western blot of the DIS3 D146N KO clones. DIS3 protein was not detectable only in the homozygous clone 2 (cl2). (Right panel) Western blot showing reconstitution of Flag-HA DIS3 D146N protein by adding doxycycline for 2 days. DIS3 proteins were detected using anti-DIS3 and anti-HA antibodies. Beta-Actin was used as loading control.

3.3.3 *DIS3 CRISPR/Cas9 knockout cell lines affect 5.8S rRNA biogenesis*

After verifying the DIS3 KO clones, we further characterized them by examining the expression of known targets of DIS3. First, we assessed 5.8S rRNA transcripts because it was shown that DIS3 contributes to the processing of 5.8S biogenesis (Kobyłecki et al., 2018; Tafforeau et al., 2013). The biogenesis of 5.8S rRNA is a multistep process. The 12S pre-rRNA, the precursor of the 5.8S is sequentially cleaved by a combination of diverse endoribonuclease and 3-5' exoribonucleases, including the core exosome and its catalytic subunit DIS3, the catalytic subunit RRP6/EXOSC10, the exonuclease ISG20L2 and Eri1 (Schillewaert et al., 2012; Tafforeau et al., 2013) (Figure 27A). It has

been extensively studied in budding yeast and mammals, but the exact number of steps in this process and the molecular length of each rRNA intermediate is still not clear in human. However, recent analyses established that the core exosome together with its catalytic subunits DIS3 seem to be responsible for the 3' end trimming of either the 12S pre-rRNA or the 7S pre rRNA. Depletion of exosome subunits or the exosome cofactors causes the accumulation of diverse intermediate processing fragments between the 12S and 7S pre-rRNAs (Schilders et al., 2007; Pirouz et al., 2019). We consequently wondered whether the 5.8S biogenesis was also affected in our DIS3 knockout cells. For this purpose, we extracted RNA from DIS3 WT KO clones and performed northern blotting. Probing the northern blots with a radiolabelled antisense oligonucleotide overlapping the 3′ end of 5.8S rRNA revealed various discrete intermediates products (figure 27B). Indeed, depletion of DIS3 caused accumulation of some of these RNA intermediates (black arrows, figure 27B). Notably, the long and the short forms of 5.8S rRNA were not affected by the perturbation of DIS3 (Figure 27B, lower panel). Next, to deeply analyse the intermediates accumulated in DIS3 WT KO cells, we assessed northern blots using a set of different probes spanning the 3'end of 5.8S precursor as shown in Figure 27C. Probe 4 detects 5.8S rRNA and all the 3'-extended 5.8S species, probe 1 detects only the 3-extended 5.8S species. Probes 2 and 3 used to detect 5.8S rRNA with longer extensions. Probing with these specific antisense oligonucleotides overlapping different regions of the 3'end of 5.8S rRNA precursor revealed two stabilized intermediates that could correspond to the 7S and 12S rRNA precursors (Figure 27D). In detail, all probes (1-4) showed accumulation of a longer precursor of 5.8S that could correspond to a 12S rRNA intermediate in DIS3 KO cells. 7S accumulation was detected using probe 1, probe 3 and probe 4 as expected for their positioning. Probe 2 could detect only the 12S rRNA intermediate since it hybridizes at the very 3'end of the 5.8S precursor. Notably, the other products corresponding to the 7Sa (an intermediate product between 7S and 5.8S) and the 5.8S rRNA were not affected by DIS3 perturbation. In the northern blots presented, hybridization with probes specific to 7SL, the RNA component of human SRP, and to U6, the non-coding small nuclear RNA (snRNA) component of U6 snRNP (small nuclear ribonucleoprotein), serve as loading controls (Figure 27E).

Taken together, these results confirmed that DIS3 is indeed involved in 5.8S biogenesis, specifically in the processing of the 7S and 12S intermediates. Thus, our inducible DIS3 KO cells represent a functional knockout line to study DIS3 effect on RNA metabolism, especially circRNA turnover.

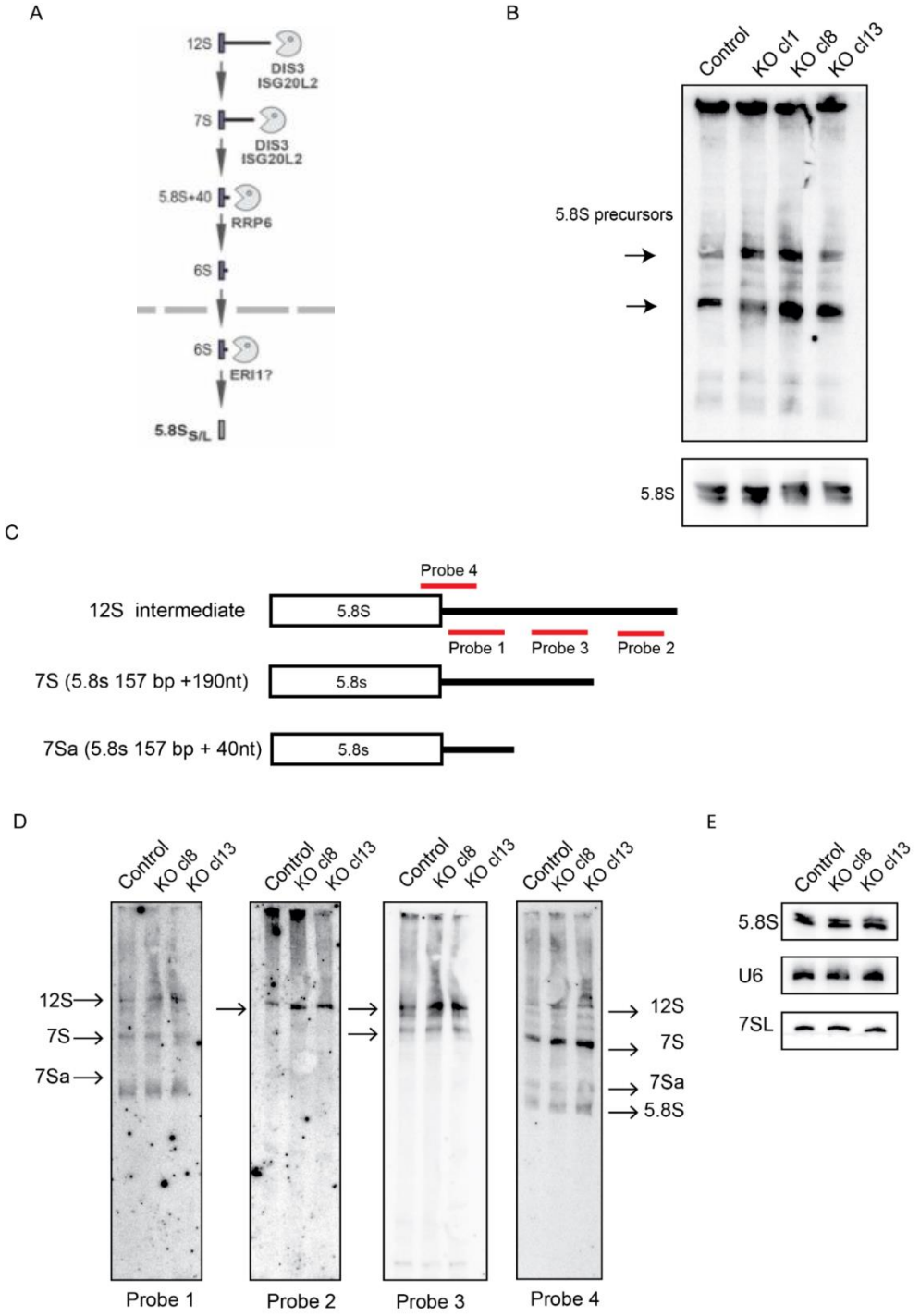

Figure 27. Characterization of DIS3 role in 5.8S biogenesis using DIS3 CRISPR/cas9 knockout cell lines. (A) Schematic representation of human 5.8S rRNA processing pathway modified from (Aubert et al., 2018). (B) Analysis of pre-rRNA processing by northern blotting in DIS3 WT knockout cells. Total RNA was separated by denaturing acrylamide gel electrophoresis and hybridized with probes specific for 3'end of 12S or the mature 5.8S rRNA. (C) Schematic overview of different probes used for northern blot analyses in this study. Red bars represent the antisense DNA oligos used as northern blot probes. Probe 4 detects 5.8S rRNA and all the 3'-extended 5.8S species, probe 1 detects only the 3-extended 5.8S species. Probes 2 and 3 used to detect 5.8S rRNA with longer extension are represented. (D) Northern blot analysis of pre-rRNA processing in DIS3 WT knockout cells using the mentioned probes specific for 5.8S intermediates. (E) Northern blots from (D) was probed with 7SL, U6 and 5.8S to serve as a loading control.

3.3.4 *DIS3 CRISPR/Cas9 knockout cell lines affect the stability of 5.8S rRNA precursors*

We consequently wondered whether DIS3 depletion affects the stability of the previously described pre-rRNA 5.8S intermediates. To assess the RNA stability, we measured the RNA decay rate using *in vivo* transcription. Actinomycin D is a DNA intercalator that binds to the DNA duplex at the transcription initiation complex and inhibits transcription by preventing RNA polymerase elongation. To determine if DIS3 influences the pre-rRNA intermediates stability, we treated DIS3 WT and different knockout cell lines with a low dose of actinomycin D for different time points and then we measured the abundance of selected RNAs by northern blot. Interestingly, we found that in all tested DIS3 knockout clones, 5.8S rRNA precursors is more stable comparing to the corresponding DIS3 wild type control cells during the Actinomycin D treatment time-course (Figure 28). Furthermore, the decay pattern of 5.8S intermediates was slower in the knockout cells over time. Notably, we confirmed again that at time point 0h, DIS3 depletion caused accumulation of different 5.8S precursors in all knockout clones. Northern blots with probes specific to 5.8S, 7SL, 7SK and U6 provided loading controls. 5.8S, 7SL, 7SK levels are constant during the Actinomycin D treatment time-course in all cell lines. Surprisingly, DIS3 depletion affects the stability of U6 RNA on a steady-state level. Indeed, the northern blot showed a delay in U6 decay in DIS3 knockout cells respect to the DIS3 wildtype cells during the Actinomycin D treatment suggesting that DIS3 could also be involved in the U6 turnover or biogenesis.

Collectively, these data from our DIS3 knockout clones confirm a role of DIS3 in 5.8S biogenesis suggesting that our DIS3 knockout cells are a valid tool for further analysis.

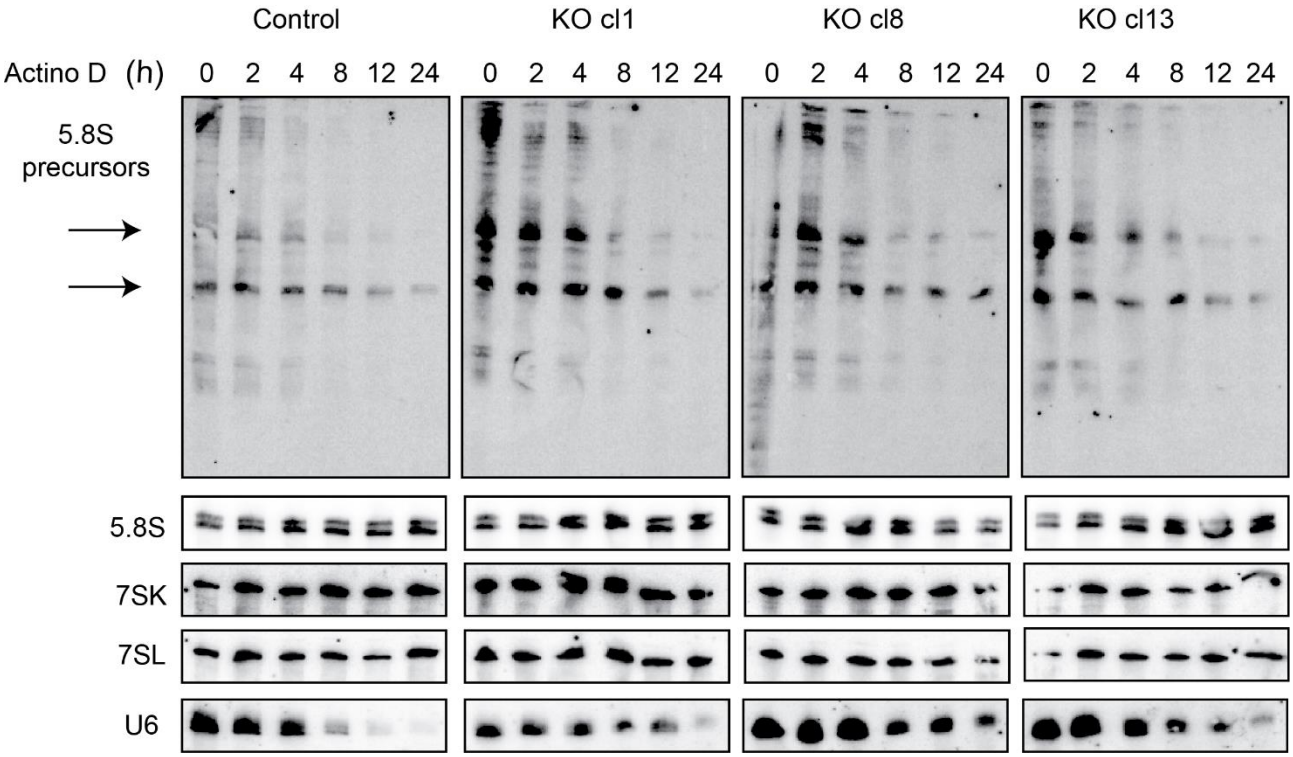

Figure 28. DIS3 affects 5.8S precursors stability during actinomycin D time-course. DIS3 WT KO cell lines were treated with 10 nM of actinomycin D and RNA was extracted at the indicated times. RNA samples were analysed by northern blotting. The same membrane was incubated with probes specific for the 5.8S precursors and for 7SL, 7SK, U6 and 5.8S RNAs. These last hybridizations serve as a loading control.

3.3.5 *DIS3 knockout moderately affects the four circRNA expression*

We first investigated the effect of DIS3 depletion on the circRNA candidates selected for the biochemical part of the thesis. We hypothesized that since DIS3 could degrade *in vitro* these circRNAs, DIS3 knockout would also affect the expression of them *in vivo*. We extracted total RNA from several DIS3 WT knockout cell clones (cl1, cl10, cl13, cl8), and we determined circRNA expression levels by qPCR (Figure 29). Although there was high variability between different KO clones, we found that DIS3 depletion causes only mild effects on these circRNA candidates (Figure 29A). Not all the four circRNAs were up-regulated as expected in DIS3 WT KO clones. CircGSE1 was the most up regulated among the four circRNA candidates and was the only one found deregulated in all of the KO clones tested. To exclude the possibility of off targets, we performed rescue experiments by adding doxycycline to DIS3 WT KO clones (Figure 29B). In the rescue experiments, almost all the mild effects on circRNA levels caused by DIS3 knockout were restored. Most circRNA levels could be rescued to the normal control condition with the only exception of circGSE1. In conclusion, we found that the *in vitro* situation does not fully recapitulate the *in vivo* situation. DIS3 KO affects moderately the 4 circRNA expression levels *in vivo* with more effect on

circGSE1. These mild effects generated by DIS3 depletion could be partially rescue with overexpression experiments. We hypothesized that *in vivo* there are additional factors that might influence circRNA degradation.

A

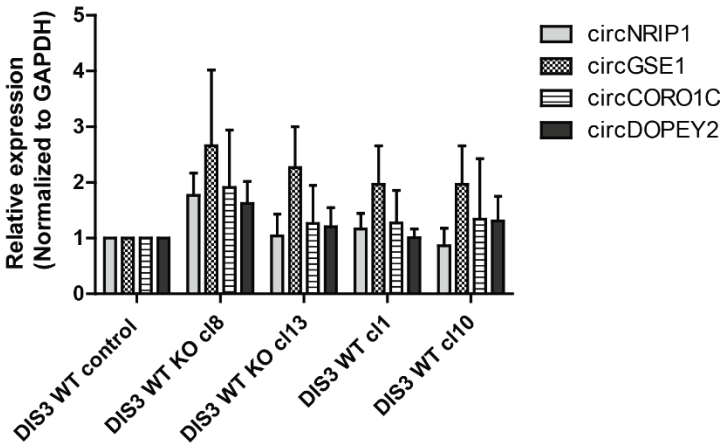

B

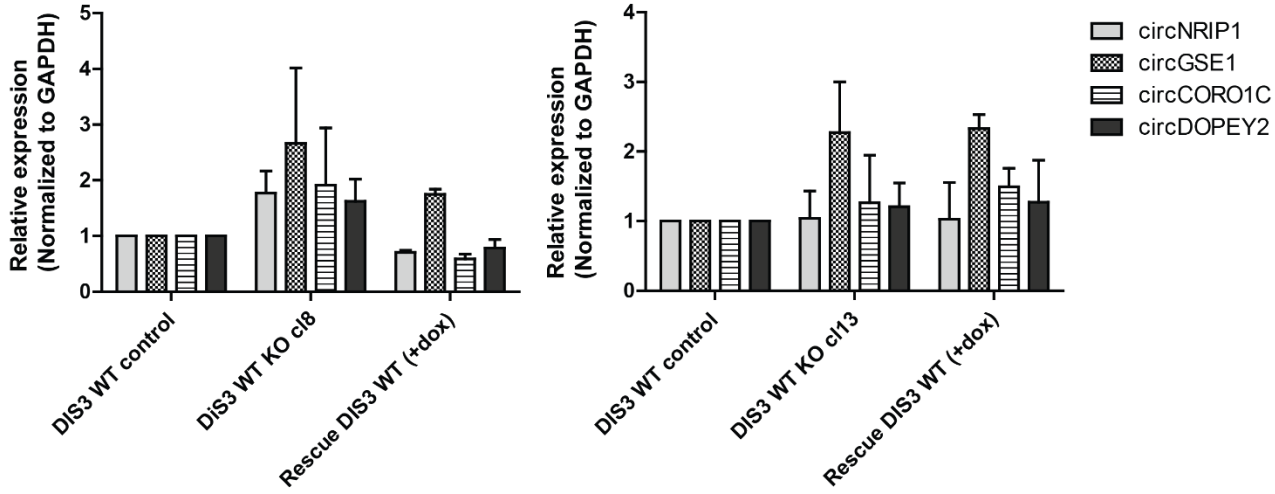

Figure 29. DIS3 depletion effect *in vivo* on the four circRNA candidates. (A) CircNRIP1, circGSE1, circCORO1C and circDOPEY2 expressions were analysed in several DIS3 WT KO clones by qRT-PCR. CircRNAs were normalized against GAPDH mRNA levels and DIS3 WT control were set to a value of 1. (B) CircRNA levels were analysed in rescue experiments (+dox) and normalized against GAPDH mRNA levels and DIS3 WT control cells were set to a value of 1.

3.3.6 *Library preparation for the identification of endogenous circRNAs potentially regulated by DIS3*

Our DIS3 KO cell lines exhibit 5.8S biogenesis defects, which confirms functional inactivation of DIS3. To identify new circRNA candidates that could be regulated by DIS3, we performed RNA-sequencing (RNA-seq) analysis of DIS3 WT KO clones and DIS3 WT cells as control. To achieve this purpose, we profiled differential expression of RNA from rRNA-depletion library. Specifically, we performed RNA-seq from DIS3 WT control cells and two DIS3 WT KO clones: cl8 and cl13. Rescue experiments were performed by inducing DIS3 WT KO cells for 72h with doxycycline. In addition, to better understand the role of DIS3 PIN domain in regulation of circRNAs, we also performed RNA-seq analysis of DIS3 D146N cell lines and the corresponding DIS3 D146N KO clone 2. Rescue experiments of the DIS3 D146N mutant were performed as described for DIS3 WT cell lines. Total RNA was extracted from two biological replicates for each condition and the library was prepared using the Universal RNA-Seq with Nuquant (TECAN). The RNA-seq was performed using Illumina NovaSeq. We obtained about 70-100 million reads which represent a profound coverage of RNA-seq reads for further analysis. We also found that rRNA depletion was efficient in all samples (Suppl. Table 2 and 3). Thus, we proceeded with the bioinformatic analysis.

3.3.7 *RNA-seq analysis for differential expression of linear RNAs upon depletion of DIS3*

As protein coding genes were affected by DIS3 depletion (Preker et al., 2008; Szczepińska et al., 2015), we first investigated changes of mRNA levels in DIS3 knockout cell lines. Bioinformatical analysis for identification and quantification of differentially expressed linear RNAs was performed by Gerhard Lehmann (Biochemistry I, University of Regensburg). Principal component analysis from our RNA-seq data and distance plot revealed consistent clustering as shown in suppl. data (Suppl. Figure 3 and 4). We initially focused on the analysis of the differentially expressed mRNA between DIS3 WT control and two DIS3 WT KO clones (-dox) (figure 30 and Suppl. Figure 5). The log ratios-mean average (MA) plot of upregulated and downregulated genes can be found in Figure 30A, while only the most significantly regulated genes are highlighted in blue. Interestingly, only a few protein-coding genes were found to be upregulated in DIS3 KO conditions. This could be due to the fact that most mRNAs undergo XRN1-mediated degradation (Nagarajan et al., 2013). DIS3 has been reported to degrade inherently unstable mRNAs containing specifically AU-rich elements (AREs) within their 3' untranslated regions and promoter upstream transcripts (PROMPTs) (Davidson et al. 2019; Szczepińska et al. 2015). In this thesis we did not have time to fully analyse if these transcripts are regulated by DIS3, which however will be further investigated in the future. Importantly, it was

previously shown that DIS3 depletion leads to an increase of MYC levels (Segalla et al., 2015). In agreement with this, we found that MYC was one of the most significantly up-regulated genes in DIS3 KO cells (Figure 30). MYC was selected for further validation by qPCR (Figure 30B). qPCR analyses confirmed that MYC is up regulated DIS3 KO cells. No evidence for general accumulation of lncRNAs was observed, and only a few lncRNAs accumulated robustly in DIS3 depleted cells (Suppl. Figure 5).

Taken together, we found several mRNAs, including MYC, showing changes in DIS3 knockout, confirming the published data about the function of DIS3 in regulating these targets. This motivated us to continue our further analysis of circRNAs upon depletion of DIS3.

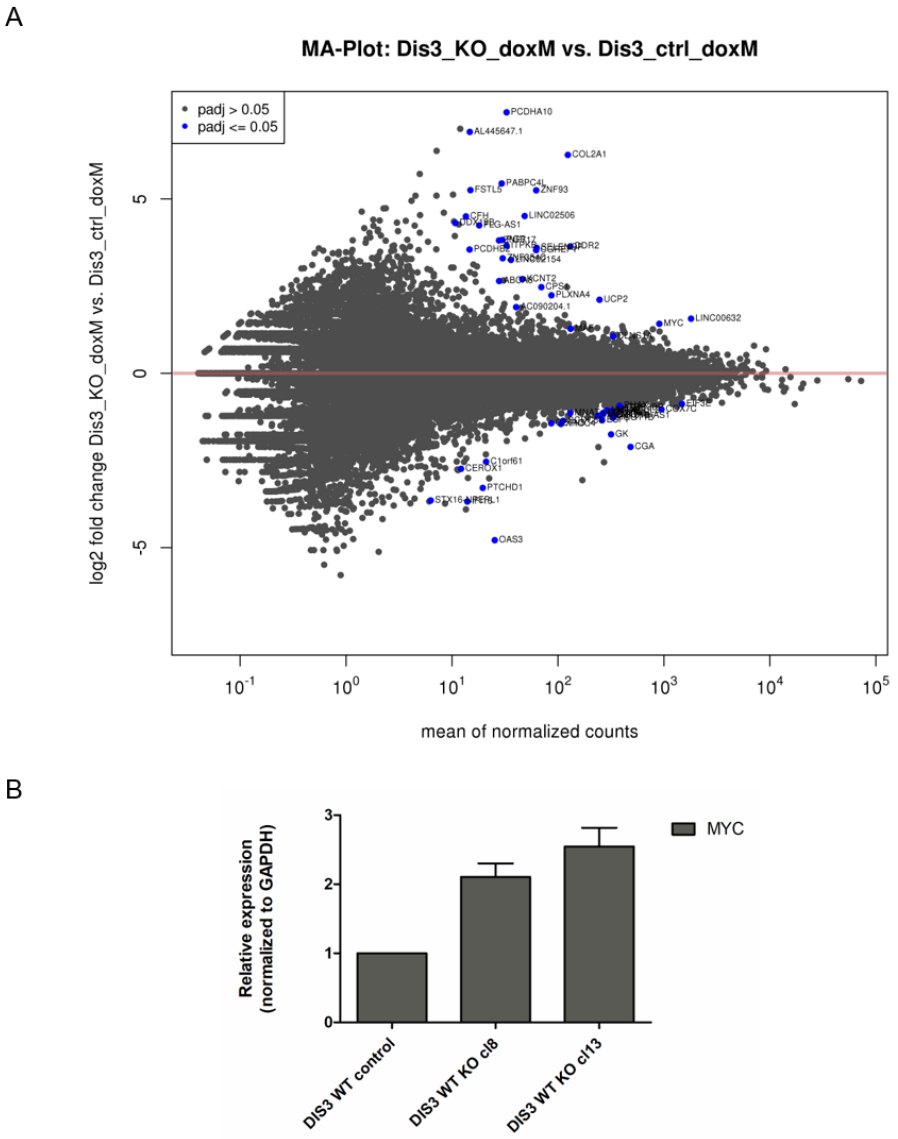

Figure 30. Identification of differential expressed linear RNAs in DIS3 depleted cells. (A) Log ratios-mean average (MA) plot of differentially expressed mRNAs in DIS3 WT KO clones 8 and 13 vs normal DIS3 WT control cells. Blue dots represent significant genes. (B) MYC expression was analysed by qRT-PCR in DIS3 KO cl8 and cl13 cells (- dox). MYC levels were normalized against GAPDH mRNA levels.

3.3.8 *Identification and validation of differentially expressed circRNAs in DIS3 depleted cells*

After verifying the differential expression of mRNAs in DIS3 KO cells, we analysed the expression of circRNAs. Bioinformatical analysis for identification and quantification of circRNA expression was performed in collaboration with the laboratory of Nikolaus Rajewsky. Principal component analysis from our RNA-seq data and clustering of the 500 most variable genes for all sequencing samples are shown in supplementary data (Suppl. Figure 6 and 7). CircRNAs were identified by detecting reads overlapping head-to-tail junctions, indicative of circular splicing. First, we started to analyse the circRNA expression in DIS3 WT KO cells compared to DIS WT control cells. Using this strategy, we found a subset of circRNAs differential expressed in DIS3 knockout cells (Figure 31A). Analysis and validation of DIS3 D146N cells are still ongoing and will give as a comprehensive view of DIS3 endoribonucleolytical domain impact on circRNA expression.

In our initial analysis, we aim to identify circRNAs that are upregulated upon knockout of DIS3 because these RNAs might be candidates for DIS3 degradation (Figure 31B). First, we selected circRNAs with Log2-fold changes > 0 in both DIS3 WT KO clones and p-adjusted value < 0.05. This filtering allowed us the selection of 9 circRNAs that were up regulated in DIS3 KO condition (Figure 31C). Principal characteristics of the 9 circRNAs are summarized in Suppl. Table 4.

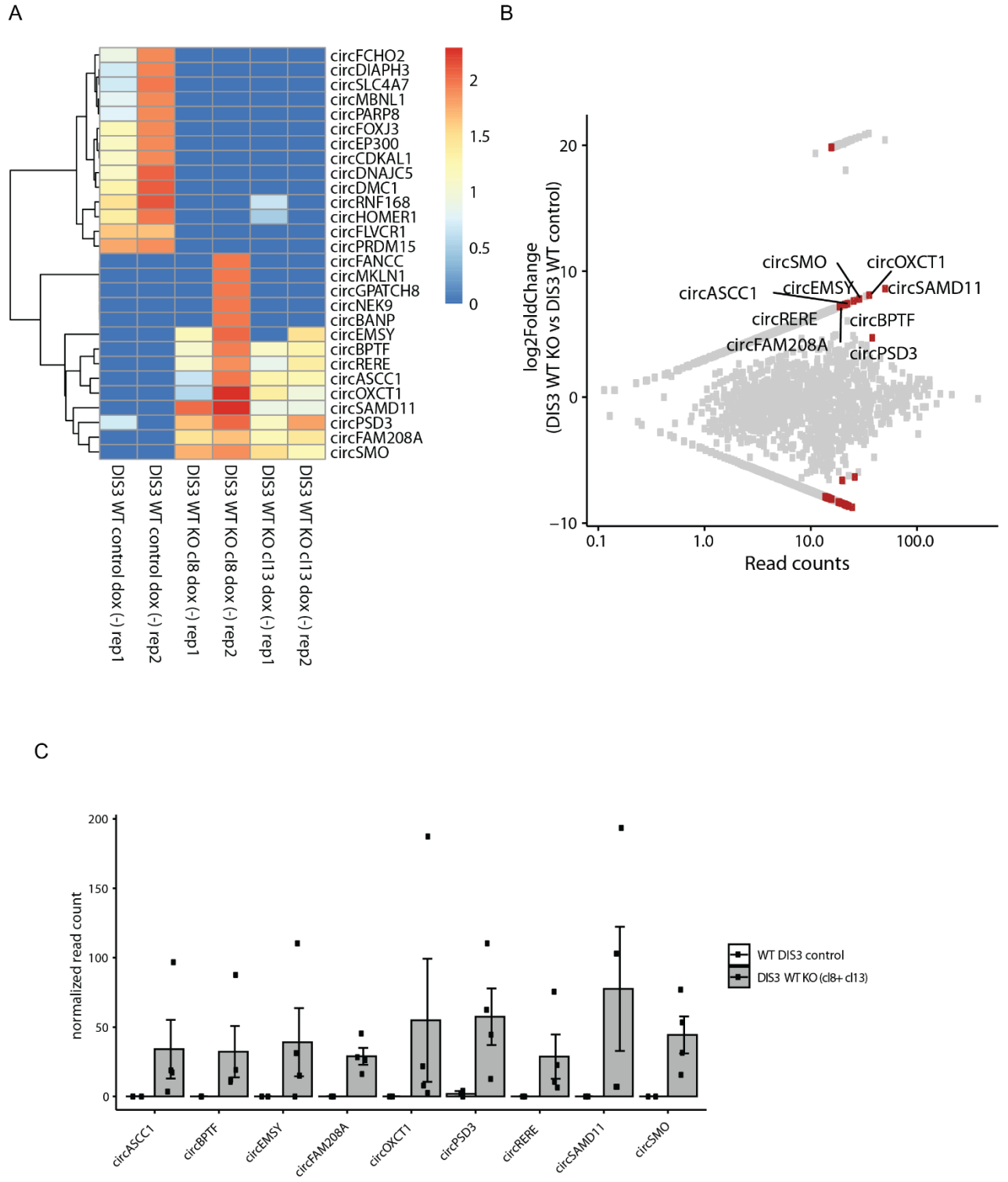

Figure 31. Identification of differential expressed circRNAs in DIS3 depleted cell lines. (A) Heatmap of differentially expressed circRNAs in DIS3 WT control and in DIS3 WT KO cl1 8 and 13. The total number of reads supporting a particular head-to-tail junction was used as an absolute measure of circRNA abundance. Normal: control. (B) Scatter plot of circRNA expression in DIS3 WT control versus combined DIS3 WT KO clones. Red dots represent significant up regulated circRNAs. (C) Bar plot and individual data points showing the normalized read counts of the 9 selected circRNAs.

After identification of upregulated circRNAs, we performed qPCR experiments on the 9 circRNAs candidates using circRNA-specific primer pairs (Figure 32). Although we found many variabilities, most of the selected circRNAs were up-regulated in a similar way as observed in our RNA-seq data except for circSAMD11 and circBPTF in both DIS3 KO clones. Notably, DIS3 depletion caused more effects in circRNA expression in DIS3 KO cl8 than in DIS3 KO cl13.

To exclude the possibility of off target effects caused by CRISPR/Cas9, we analysed the effect of DIS3 WT rescue on circRNA expression. For this purpose, we induced the expression of DIS3 WT protein in the selected KO clones and performed qPCR experiments on the same target circRNAs (Figure 32A). As expected, induction of DIS3 successfully rescues the expression levels of some circRNAs, including circSMO, circRERE, circOXCT1, circASCC1 respect to the control condition in both clones. We also noticed that the rescue effect of DIS3 WT in KO clone 8 was more efficient compared to KO clone 13.

Interestingly, several circRNAs showed differential expression while their cognate mRNAs did not change in DIS3 KO condition. This inverse correlation was confirmed by qPCR experiments for three circRNAs, including OXCT1, RERE and FAM208. As shown by qPCR (Figure 32B), DIS3 specifically affects the levels of the circRNAs but not of their linear counterparts. The modulation of the corresponding linear transcripts was also measured in rescue experiments (+ dox).

In sum, DIS3 depletion does not affect the expression of circRNAs broadly. Indeed, DIS3 depletion caused an increase in the expression of a specific subset of circRNAs. Re-expression of DIS3 in the two KO clones succeeds in rescue the correct expression level of some circRNAs. Furthermore, in three tested cases, depletion of DIS3 affects specifically circRNAs, while the linear counterparts are unaffected.

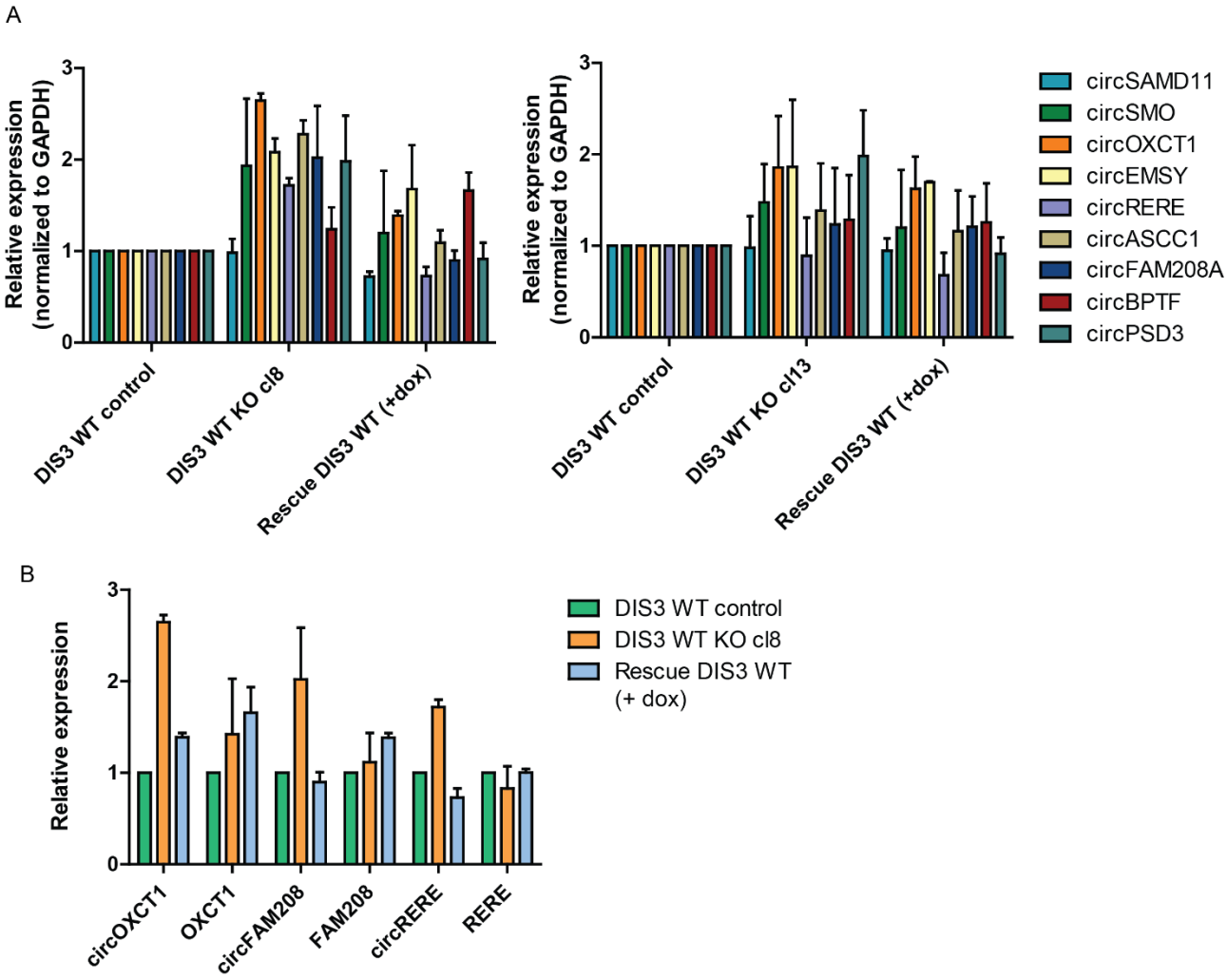

Figure 32. Validation of selected circRNAs upon DIS3 depletion. (A) CircRNA expression level analysed by qRT-PCR in DIS3 KO cl8 and cl13 (- dox) cells and the corresponding WT DIS3 rescue cells (+ dox). CircRNA levels were normalized against GAPDH mRNA levels and compared to DIS3 WT control cells (- dox). (B) CircRNA and linear RNA expression was analysed by qRT-PCR, in DIS3 KO cl8 and cl13 (- dox) cells and in the corresponding WT DIS3 Rescue cells (+ dox). CircRNA and linear RNA levels were normalized against GAPDH mRNA levels and DIS3 WT control cells were set to a value of 1.

3.4 Towards the understanding of DIS3 cytoplasmic and nuclear function

Our findings showed that DIS3 has the potential to degrade circRNAs *in vitro* and *in vivo* but raised many questions about the molecular mechanism behind it. First, we wondered whether DIS3 can act independently. Indeed, it remains to be determined whether DIS3 exists on its own as a monomer or is acting within the exosome. Second, since DIS3 is mainly nuclear and only a small pool is cytoplasmic, it is not clear how DIS3 preferentially degrades circRNAs in the cytoplasm. The following studies permit us to gain new insights into DIS3 cytoplasm and nuclear function and DIS3 post transcriptional regulation.

3.4.1 *Subcellular localization of DIS3*

As reported previously (Tomecki et al., 2010), DIS3 is predominately localized to the nucleus, with a small portion in the cytoplasm in human cells. To test the subcellular localization of DIS3, we performed subcellular fractionation in HEK293 cells. The following total, cytoplasmic and nuclear fractions were analysed by western blot (Figure 33). The purity of the fractionation was verified by different cytoplasmic markers: beta-tubulin and GAPDH and nuclear markers: Lamin A/C and NONO. Using a commercial anti-DIS3 antibody, we found that DIS3 localized to both the nuclear and cytoplasmic compartments. Even though the exact partitioning of DIS3 was subjected to some experimental variations, we found that DIS3 is not preferentially localized to the nucleus as expected from published data (Tomecki et al., 2010). We also checked the subcellular localization of other components of the exosome (Figure 33). EXOSC3 and EXOSC9 were found in both fractions, whereas EXOSC10 mainly in the nucleus. In sum, using a subcellular fractionation approach, we could conclude that DIS3 is localized in both compartments in HEK293 cells.

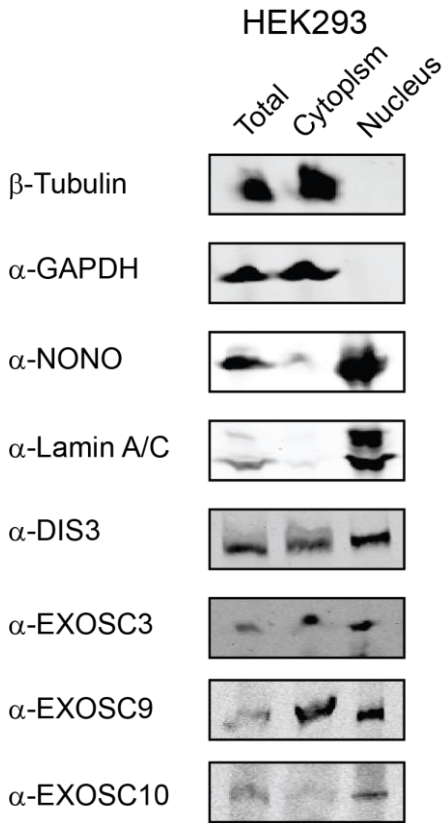

Figure 33. Subcellular localization of DIS3. Western blot analysis of the distribution of DIS3 in subcellular fraction of HEK293 cell line. Beta-tubulin and GAPDH were used as cytoplasmic markers, while Lamin A/C and NONO as nuclear markers. DIS3 and the three exosome components, EXOSC3, EXOSC9 and EXOSC10, were detected using specific antibodies.

3.4.2 *DIS3 partially co-sediments with the exosome components*

To investigate the association of DIS3 with the exosome, we performed a glycerol density gradient ultracentrifugation. Flag-HA DIS3 WT and Flag-HA DIS3 D146N were expressed in HEK293 cells and the lysates were separated onto a 10–40% glycerol gradient and fractionated by centrifugation for 18h. Fractions were then analysed by western blotting using antibodies against DIS3 and three components of the exosome: the cap-component EXOSC3, the core-component EXOSC9 and one of the catalytic subunit, EXOSC10 (Figure 34). The western blot analysis showed that both Flag-HA DIS3 WT (upper panel) and Flag-HA DIS3 D146N (lower panel) predominantly migrated in the fractions with low glycerol density (fractions 4-6) (Figure 34). In addition, a small portion of DIS3 was found in higher molecular weight fractions in a complex with the other exosome components. Differently, EXOSC3, EXOSC9 and EXOSC10 migrated predominantly in the higher density fractions and co-sedimented in fractions 9-11 (Figure 34). Notably, using a commercial anti-EXOSC3 antibody, a second higher molecular weight band was detected in the western blot. This band migrated

preferentially in the lower fractions and could be another isoform or non-specific. Further investigations are still needed to better understand the sedimentation of EXOSC3.

Taken together, our data showed that only a small amount of DIS3 is associated with the exosome. The high amount of free DIS3 could be explained as a consequence of dissociation of DIS3 from the exosome during ultracentrifugation. However, a pool of DIS3 that exists on its own and might act alone is also conceivable.

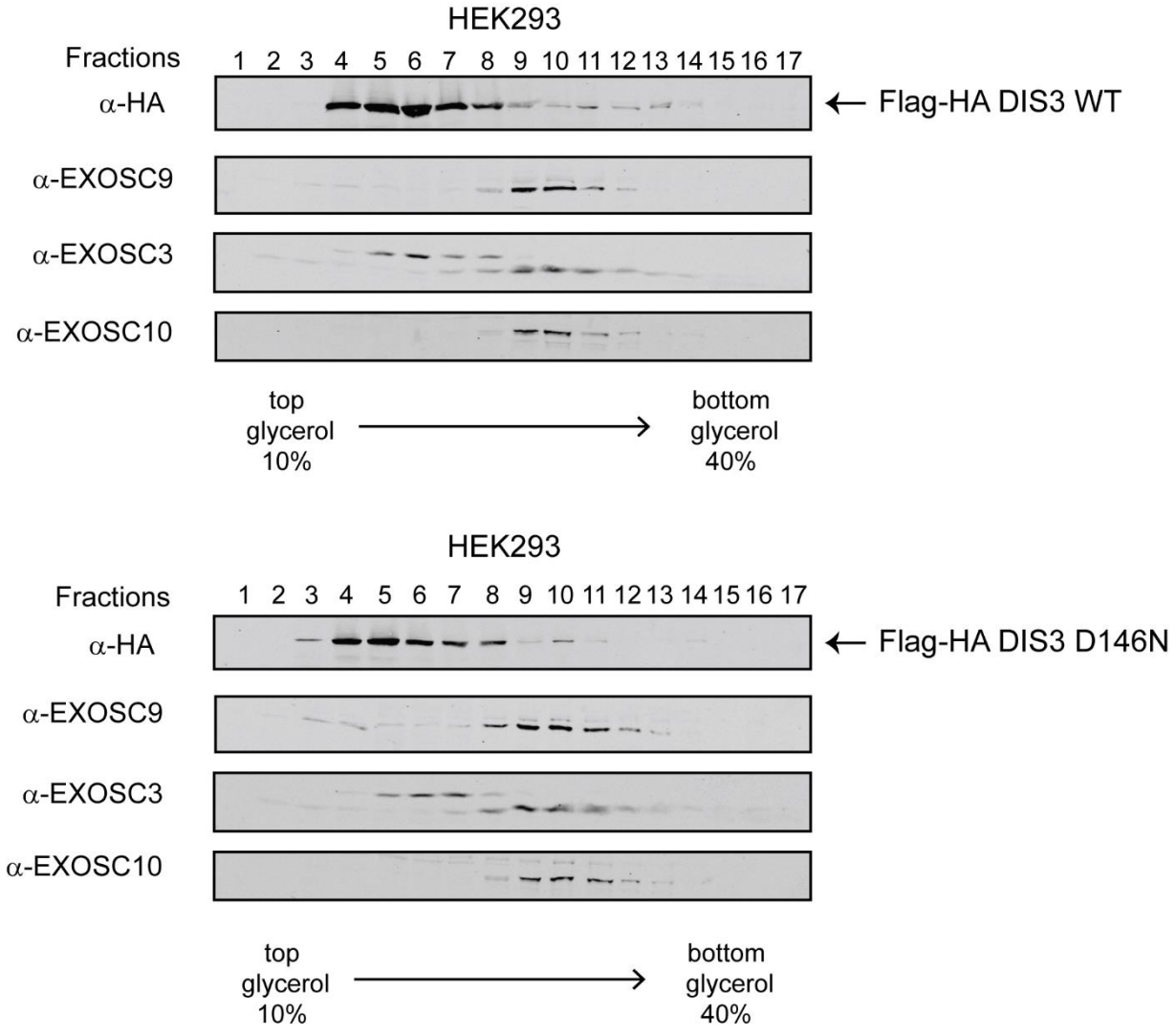

Figure 34. DIS3 partially co-sediments with the exosome complex. HEK293 cell lysates expressing Flag-HA DIS3 WT (upper panel) and Flag-HA DIS3 D146N (lower panel) were separated by glycerol gradient centrifugation. The sedimentation of Flag-HA DIS3 WT and Flag-HA DIS3 D146N were analysed by western blotting using HA antibodies. Endogenous EXOSC3, EXOSC9 and EXOSC10 were analysed using the specific antibodies.

3.4.3 *DIS3 distribution in nuclear and cytoplasmic gradients*

Since we found that DIS3 is localized in both cytoplasmic and nuclear extracts, we further characterized how DIS3 migrates on a glycerol gradient when extracts for the different compartments are separated. Because we did not observe any differences in migrating behaviour between Flag-HA DIS3 WT and Flag-HA DIS3 D146N, we only test the migration of Flag-HA DIS3 WT. HEK 293 cell lysates expressing Flag-HA DIS3 WT were separated by centrifugation as described above. Individual fractions were analysed by western blot using anti-HA antibody for detection of DIS3 and the three mentioned exosome components (EXOSC3, EXOSC9 and EXSC10) (Figure 35).

Interestingly, cytoplasmic and nuclear extracts yielded similar results. Flag-HA DIS3 WT from both cytoplasmic and nuclear extracts migrated preferentially in low-density fractions. The amount of DIS3 in low-density fractions was more in the cytoplasm than in the nucleus. Furthermore, a small portion of DIS3 was found in higher density fractions co-migrating with the other exosome components. On the other hand, the three tested exosome components co-migrated in the higher molecular weight fractions (Figure 35). According to the previous study, EXOSC10 was only detected in the nucleus. Notably, the signals of these exosome components were more intense in the nuclear extract whereas the DIS3 signal was more intense in the cytoplasmic extract.

In summary, we found that only a minor portion of DIS3 migrates with exosome complex in both compartments. A higher amount of DIS3 is found in low density fractions of cytoplasmic extracts suggesting that a pool of free DIS3. However, we still have to consider that this could occur partly due to Flag-HA DIS3 overexpression.

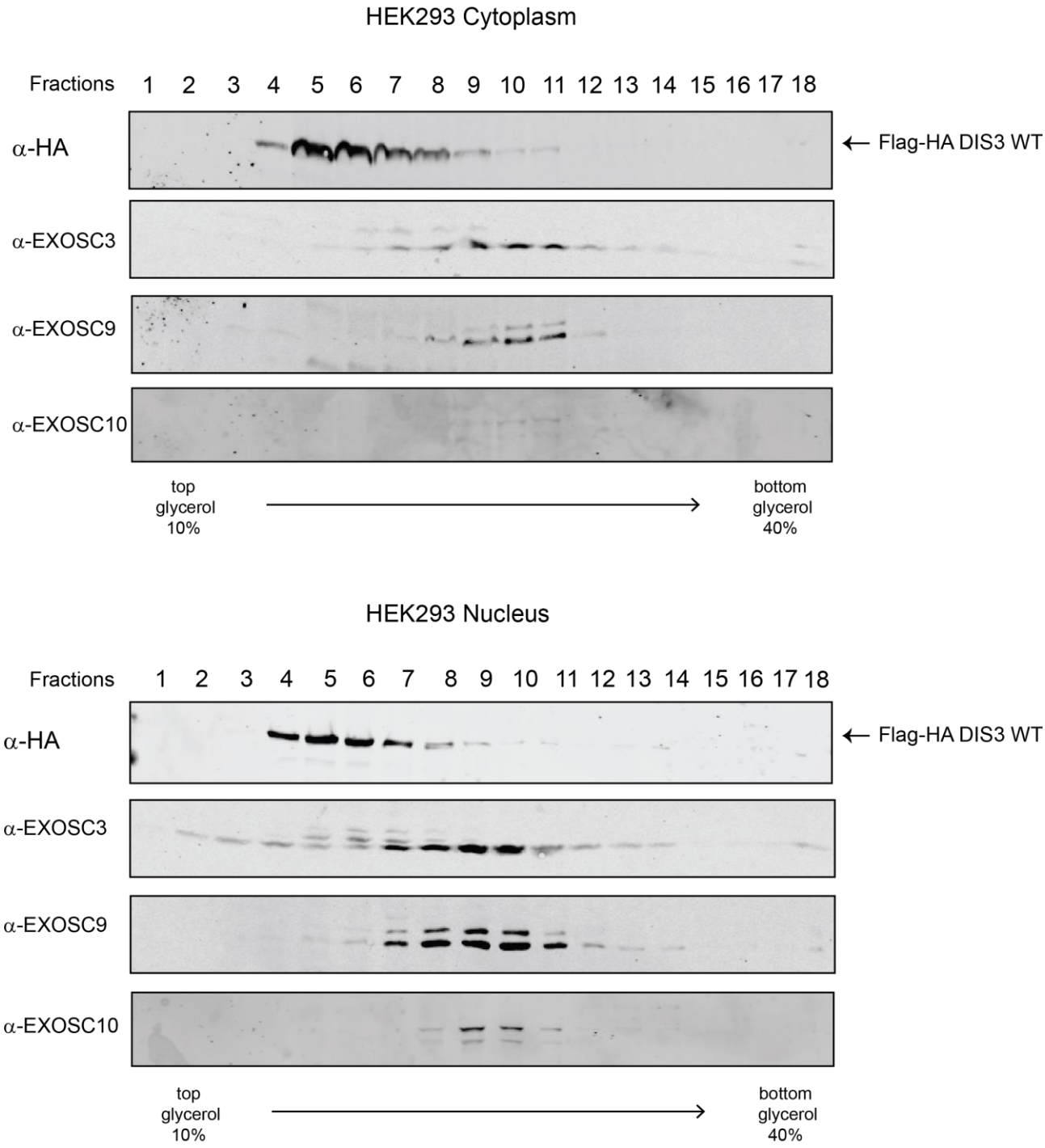

Figure 35. DIS3 distribution in nuclear and cytoplasmic fractions. Nuclear and cytoplasmic gradients from HEK293 lysates expressing Flag-HA DIS3 WT were analysed by western blot using anti-HA and anti-EXOSC3, anti-EXOSC9, anti-EXOSC10 antibodies.

3.4.4 *DIS3 is not co-immunoprecipitated with the other components of the exosome*

To better understand how DIS3 associates with the exosome, we studied in-depth the interactions between DIS3 and the exosome components. In detail, we overexpressed different Flag-HA tagged exosome components in HEK293T cells and we performed co-immunoprecipitation experiments. The presence of DIS3 and other exosome proteins in the immunoprecipitates was detected by western blotting (Figure 36). Surprisingly, DIS3 was not co-immunoprecipitated with any of the proteins tested, including the cap-components of the exosome (EXOSC1-3), the core-component EXOSC9 and the other catalytic subunits (DIS3L and EXOSC10). This suggests that DIS3 could dissociate from the exosome during the co-immunoprecipitation or that the interaction between DIS3 and with the exosome is rather transient. Interestingly, DIS3L1 was co-immunoprecipitated with the cap and core components (Figure 36). DIS3L1 was also found to interact with the homologs DIS3 and DIS3L2 but these interactions are false positive because they seem to be due to cross reactivity of the polyclonal antibody. Similarly, EXOSC10 interacts with all exosome components analysed but not with DIS3 and DIS3L2. Finally, we confirmed that EXOSC3 co-immunoprecipitated with the other cap components (EXOSC1 and EXOSC2), with the catalytic subunits EXOSC10 and DIS3L but not with DIS3 and DIS3L2.

In summary, we conclude that DIS3 association with the RNA exosome is weak and it could be lost during the immunoprecipitation. Additionally, it is possible that DIS3 interacts more with some exosome components than others. However, this result, together with the circRNA degradation assays, indicates that DIS3 does not necessarily need all the exosome components to degrade circRNAs *in vivo*.

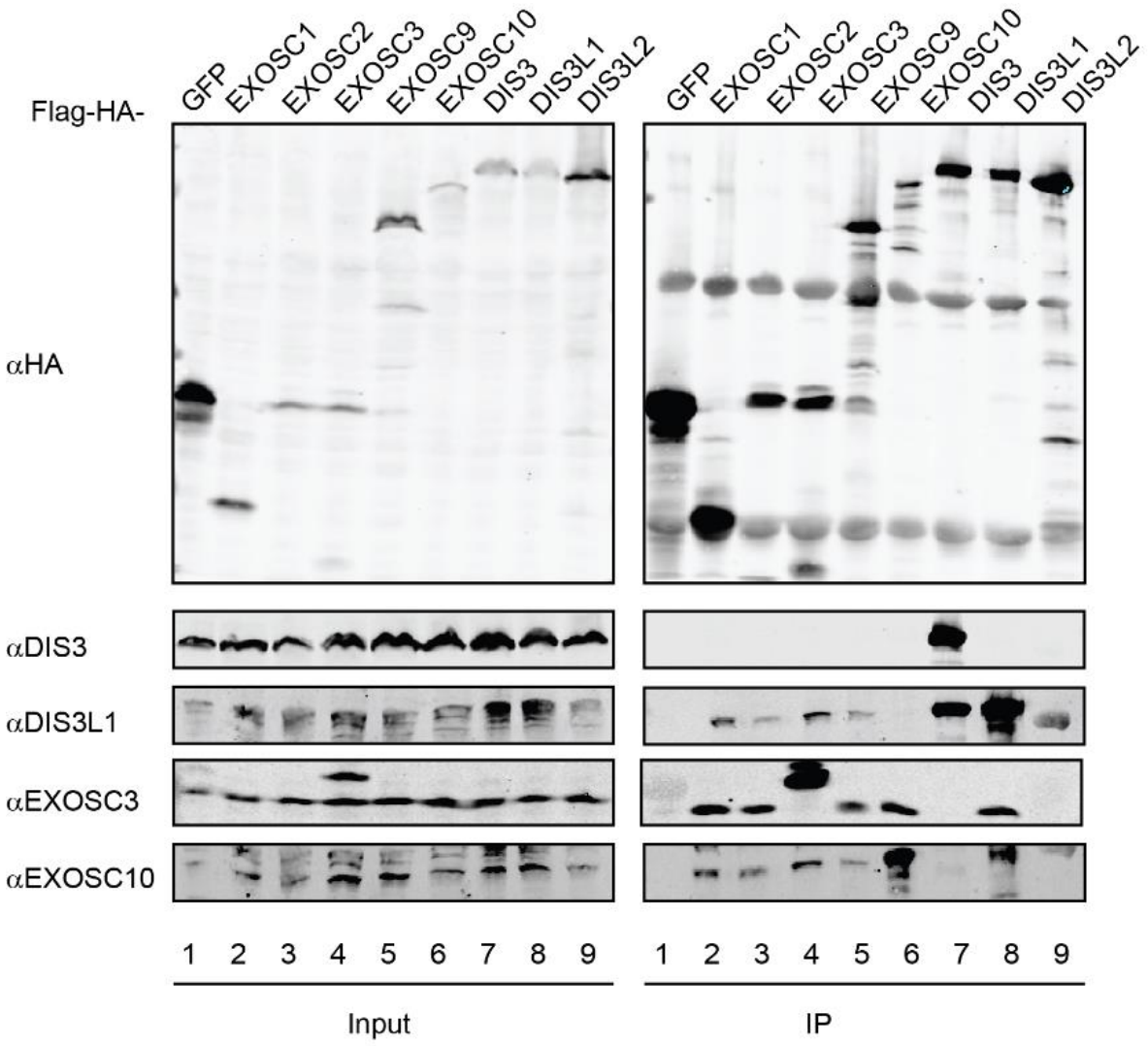

Figure 36. Immunoprecipitation of exosome components. Western blots of the immunoprecipitations were performed with anti-HA, anti-DIS3, anti-DIS3L, anti-EXOSC3 and anti-EXOSC10.

3.4.5 *Identification of DIS3 cytoplasmic and nuclear interaction partners*

In order to investigate the role of cytoplasmic DIS3 in circRNA degradation, we identified cytoplasmic and nuclear partners of DIS3 using immunoprecipitation followed by mass spectrometry. We transiently overexpressed Flag-HA DIS3 wild type and Flag-HA GFP as a control in HEK293 cells and the lysates were separated by subcellular fractionations. The deriving cytoplasmic and nuclear fractions were immunoprecipitated with anti-Flag antibodies and the co-immunoprecipitated proteins were analysed by SDS-PAGE and mass spectrometry (Figure 37A). As control for successful immunoprecipitation, the immunoprecipitated samples were subjected to western blotting using anti-HA antibody (Figure 37B).

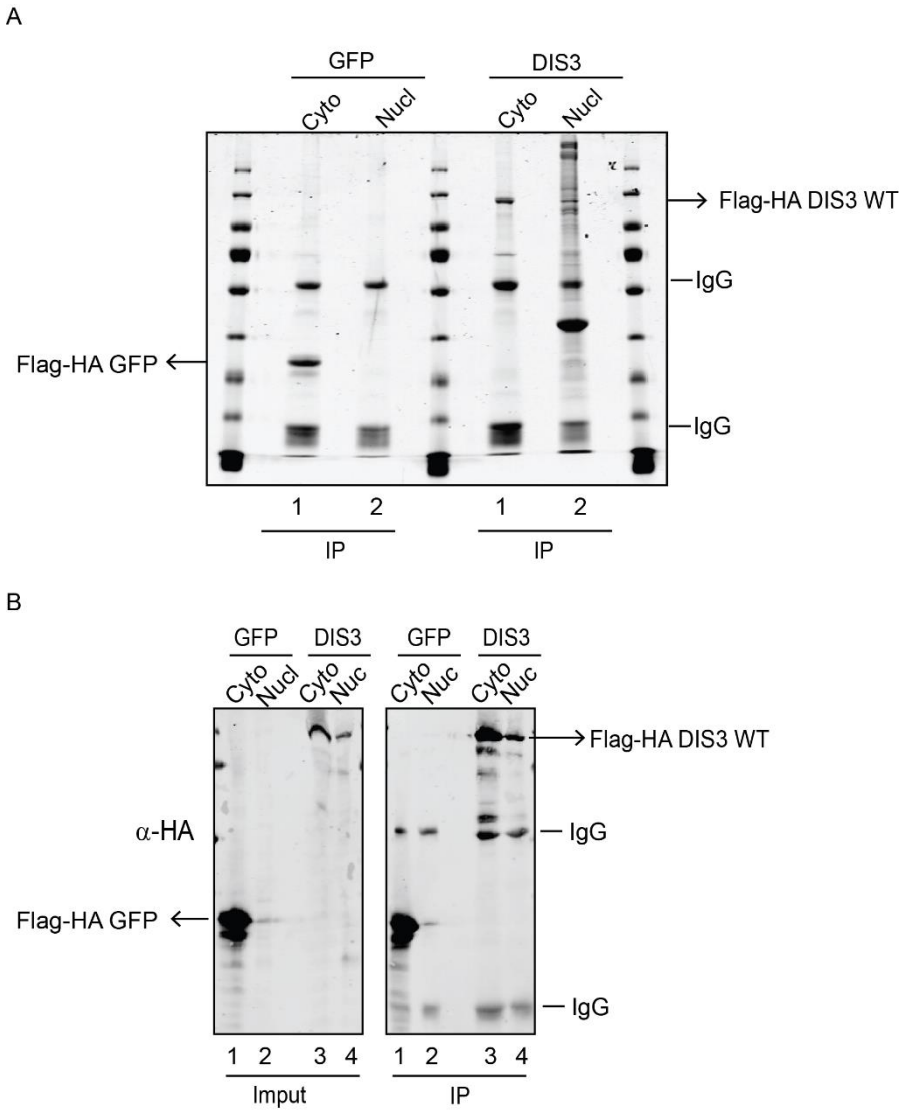

Figure 37. Proteomic analysis of nuclear and cytoplasmic interactors of DIS3. (A) Cytoplasmic and nuclear lysates from HEK293 cells containing Flag-HA DIS3 wild type and Flag-HA GFP were immunoprecipitated using anti-FLAG antibodies. Immunoprecipitated proteins were separated by SDS-PAGE and probed for anti-HA antibody. IgG as well as Flag-HA DIS3 bands are indicated with black and red arrows, respectively. (B) Immunoprecipitated proteins in cytoplasmic and nuclear extracts were detected by western blotting using α-HA antibodies. IgG as well as Flag-HA DIS3 bands are indicated with black arrows and segments, respectively.

As expected from the Coomassie staining, mass spectrometry analysis confirmed that DIS3 has different number of interactors between cytoplasm and nucleus. Using GFP as negative control, we calculated nuclear-, cytoplasmic-specific and common interactors of DIS3. Notably, the Venn diagram of this analysis showed that although DIS3 has about 477 common interactors, nuclear-specific interactors (about 1833 proteins) are much more than cytoplasmic-specific ones (about 338

proteins), (Figure 38). This difference could be read as a consequence of the mayor role of DIS3 in the nucleus.

In the table below (Table 1), we carefully examined the exosome components immunoprecipitated with DIS3 in both compartments. Preliminary data showed that, although the number of peptides of each exosome component was similar between the nucleus and cytoplasm, the number of peptides of DIS3 was much higher in the cytoplasm. Indeed, DIS3 was found about six times more in the cytoplasm than in the nucleus. This indicated that not all the DIS3 protein found in the cytoplasm is associated with the exosome, but a small pool of free DIS3 independent of the exosome. Regarding the exosome association, only the core-components EXOSC4, EXOSC5, EXOSC6, EXOSC9 and the cap-component EXOSC2 were found in both compartments. DIS3 core-component EXOSC8 and the cap-component EXOSC3 were found exclusively in the nucleus while the core-component EXOSC7 was seen only in the cytoplasm. These results suggested different interaction levels between DIS3 and the exosome components in the nucleus and the cytoplasm. Moreover, as already mentioned, the association of DIS3 with the RNA exosome complex appears to be weak, explaining its absence in the previous data of exosome co-sedimentation and immunoprecipitations.

To sum the analyses, we provide further support for our hypothesis that DIS3 exists independently of the exosome, preferentially in the cytoplasm at least under overexpression conditions. However, further quantitative analyses are required for better understanding the association of DIS3 with other components of the exosome.

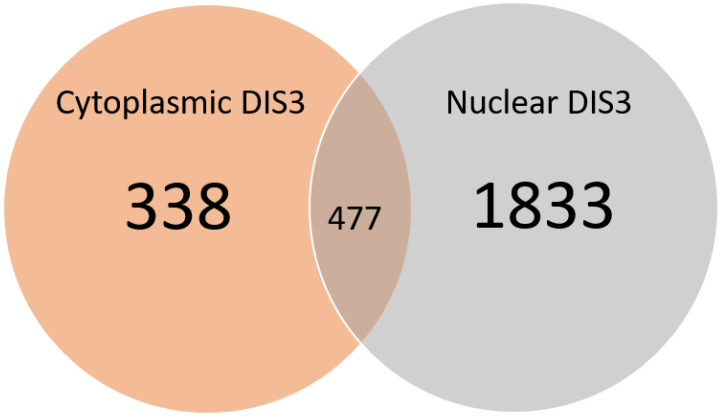

Figure 38. The venn diagram of the interactors of DIS3 in cytoplasm and nucleus.

Table 2.Exosome components associated with DIS3 in cytoplasm and nucleus

Protein Name	Cytoplasm Scores	Nucleus Scores	Ratio Cyto/Nucleus	Number Peptides cyto	Number Peptides nucleus	SC (C) [%]	SC (N) [%]
DIS3	13331.8	2126.9	6,268183742	146	38	79,4	43,6
EXOSC9	36.5	31.9	1,144200627	1	1	2,5	2,5
EXOSC6	138.5	88.6	1,563205418	3	2	18,4	9,6
EXOSC5	66.7	51.9	1,285163776	1	1	5,1	5,1
EXOSC4	84.7	93.9	0,902023429	2	2	12,7	12,7
EXOSC2	96.5	115.9	0,832614323	3	2	13,0	9,2

SC: Sequence Coverage. C: cytoplasm. N: nucleus.

Further analysis of mass spectrometry data identified several proteins as specific interactors of DIS3 in the cytoplasm or the nucleus (Table 3 and Suppl. Tables 5 and 6). In the cytoplasm, we found proteins involved in the protein degradation system like the proteasome components and the ubiquitination machinery (Table 3 and Suppl. Table 5). The high concentration of DIS3 in the cytoplasm due to overexpression condition may facilitate its own degradation by the ubiquitin-proteasome system (UPS). Notably, RioK1, was found at the top of the list of DIS3 cytoplasmic interactors together with NOB1 and PNO1. RioK1 is an atypical serine/threonine kinase and it is known to be involved in the final steps of cytoplasmic maturation of the 40S ribosomal subunit together with the endonuclease NOB1 and its partner PNO1 (Widmann et al., 2012). In addition to its role in ribosomal biogenesis, RioK1 acts as an adapter protein for the Protein Arginine Methyltransferase PRMT5 complex. We also identified all the components of the PRMT5 complex that consists of a core structure PRMT5, WD45/MEP50 (WD repeat domain 45/methylosome protein 50) and one of the adaptor proteins plCln (chloride channel sensitive nucleotide sensitive 1A).

Next, we analysed nuclear DIS3 interaction partners (Table 3 and Suppl. Table 6). Interestingly, mass spectrometry analysis identified all the components of the nuclear PTW/PP1 phosphatase complex. PTW/PP1 is a stable multimeric protein serine/threonine phosphatase complex composed of regulatory subunits PNUTS, Tox4, and Wdr82 and a PP1 catalytic subunit (PPP1CA, PPP1CB or PPP1CC) (J. H. Lee et al., 2010). All six subunits were found consistently as nuclear interactors suggesting a possible implication in phosphorylation of DIS3.

Table 3. Cytoplasmic and nuclear interactors of DIS3

Principal cytoplasmic DIS3 interactors					
Accession No.	**Name gene**	**Description**	**Score**	**Peptides**	**SC (%)**
sp|Q9Y2L1|RRP44_HUMAN	DIS3	Exosome complex exonuclease	13331.8	146	79.4
Proteasome					
sp|Q99460|PSMD1_HUMAN	PSMD1	26S proteasome non-ATPase regulatory subunit 1	547.8	11	13.3
sp|O00231|PSD11_HUMAN	PSD11	26S proteasome non-ATPase regulatory subunit 11	479.7	9	29.1
sp|O00232|PSD12_HUMAN	PSD12	26S proteasome non-ATPase regulatory subunit 12	243.4	6	16.2
sp|Q9UNM6|PSD13_HUMAN	PSD13	26S proteasome non-ATPase regulatory subunit 13	271.3	6	25.3
sp|O43242|PSMD3_HUMAN	PSMD3	26S proteasome non-ATPase regulatory subunit 3	497.0	12	26.8
sp|Q15008|PSMD6_HUMAN	PSMD6	26S proteasome non-ATPase regulatory subunit 6	231.3	6	17.2
sp|P51665|PSMD7_HUMAN	PSMD7	26S proteasome non-ATPase regulatory subunit 7	288.6	7	28.4
sp|P48556|PSMD8_HUMAN	PSMD8	26S proteasome non-ATPase regulatory subunit 8	264.2	6	19.7
sp|P62333|PRS10_HUMAN	PSMC6	26S proteasome regulatory subunit 10B	344.9	7	30.1
sp|P43686|PRS6B_HUMAN	PSMC4	26S proteasome regulatory subunit 6B	274.2	6	27.0
sp|P35998|PRS7_HUMAN	PSMC2	26S proteasome regulatory subunit 7	394.8	9	21.9
sp|P62195|PRS8_HUMAN	PSMC5	26S proteasome regulatory subunit 8	445.1	10	32.0
Ubiquitination machinery					
sp|P19474|RO52_HUMAN	TRIM21	E3 ubiquitin-protein ligase TRIM21	872.5	17	35.2
sp|O95071|UBR5_HUMAN	UBR5	E3 ubiquitin-protein ligase UBR5	655.0	14	7.3
PRMT5 complex					

sp|P54105|ICLN_HUMAN	CLNS1A	Methylosome subunit pICln	855.9	15	59.5
sp|O14744|ANM5_HUMAN	PRMT5	Protein arginine N-methyltransferase 5	5420.9	67	73.8
sp|Q9BQA1|MEP50_HUMAN	WDR77	Methylosome protein 50	2180.9	29	93.6
sp|Q9BRS2|RIOK1_HUMAN	RIOK1	Serine/threonine-protein kinase RIO1	1794.9	31	37.0
sp|Q9ULX3|NOB1_HUMAN	NOB1	RNA-binding protein NOB1	65.2	2	7.8
sp|Q9NRX1|PNO1_HUMAN	PNO1	RNA-binding protein PNO1	40.9	1	5.6
sp|P19338|NUCL_HUMAN	NCL	Nucleolin	391.1	10	19.0
Principal nuclear DIS3 interactors					
PTW/PP1 complex					
sp|Q9Y2L1|RRP44_HUMAN	DIS3	Exosome complex exonuclease	2126.9	38	43.6
sp|P62140|PP1B_HUMAN	PPP1CB	Serine/threonine-protein phosphatase PP1-beta catalytic subunit	2072.6	32	67.9
sp|P36873|PP1G_HUMAN	PPP1CC	Serine/threonine-protein phosphatase PP1-gamma catalytic subunit	1964.5	30	66.6
sp|Q6UXN9|WDR82_HUMAN	WDR82	WD repeat-containing protein 82	193.8	5	12.8
sp|Q96QC0|PP1RA_HUMAN	PPP1R10/PNUTS	Serine/threonine-protein phosphatase 1 regulatory subunit 10	119.7	3	5.9
sp|O94842|TOX4_HUMAN	TOX4	TOX high mobility group box family member 4	61.8	1	1.6

3.4.6 *Validation of DIS3 nuclear interaction partners*

In order to validate DIS3 interaction with the PTW/PP1 complex, different co-immunoprecipitation experiments were performed. In a first approach, Flag-HA tagged versions of the PP1 regulatory subunits PNUTS and Tox4 and of the PP1 catalytic subunit PPP1CA, PPP1CB or PPP1CC were immunoprecipitated from transiently transfected HEK293 cell lysates using anti-FLAG antibodies. Flag HA-GFP protein was used as control. The efficiency of the immunoprecipitation and the association with the endogenous DIS3 were analysed by western blotting using anti-HA and anti-DIS3 specific antibodies (figure 39A). Surprisingly, DIS3 was strongly co-immunoprecipitated with one component of the complex, Flag-HA-PNUTS. A weak DIS3 signal was also detected in Flag-

HA-PPP1CA, Flag-HA-PPP1CC and Flag-HA-Tox4 immunoprecipitated samples. The predominant interaction of DIS3 with the regulatory subunit PNUTS could be due to its role in the complex. As previously described, PNUTS indeed mediates PTW/PP1 complex formation by providing a binding platform for each component of the complex and the target protein (J. H. Lee et al., 2010).

In a second approach, nuclear and cytoplasm extracts containing Flag-HA DIS3 wild type and Flag-HA GFP as control were prepared from HEK293 cells. The fractions were immunoprecipitated using anti-FLAG antibodies and the samples were analysed by western blotting for two co-purified endogenous components of PTW/PP1 complex, PNUTS and PPP1CA proteins (Figure 39B). anti-HA antibody was used to control the efficiency of the immunoprecipitation. The data showed that PNUTS interacts with Flag-HA DIS3 but not with the Flag-HA GFP control, and this interaction is only in the nucleus. On the other hand, PPP1CA was co-precipitated with Flag-HA DIS3 in both compartments but more in the nucleus.

In summary, the interaction of DIS3 with the PTW/PP1 complex was successfully confirmed by co-immunoprecipitations. We found that DIS3 interacts strongly in the nucleus with the regulatory subunit of the complex PNUTS and in both compartments with the phosphatase PPP1CA.

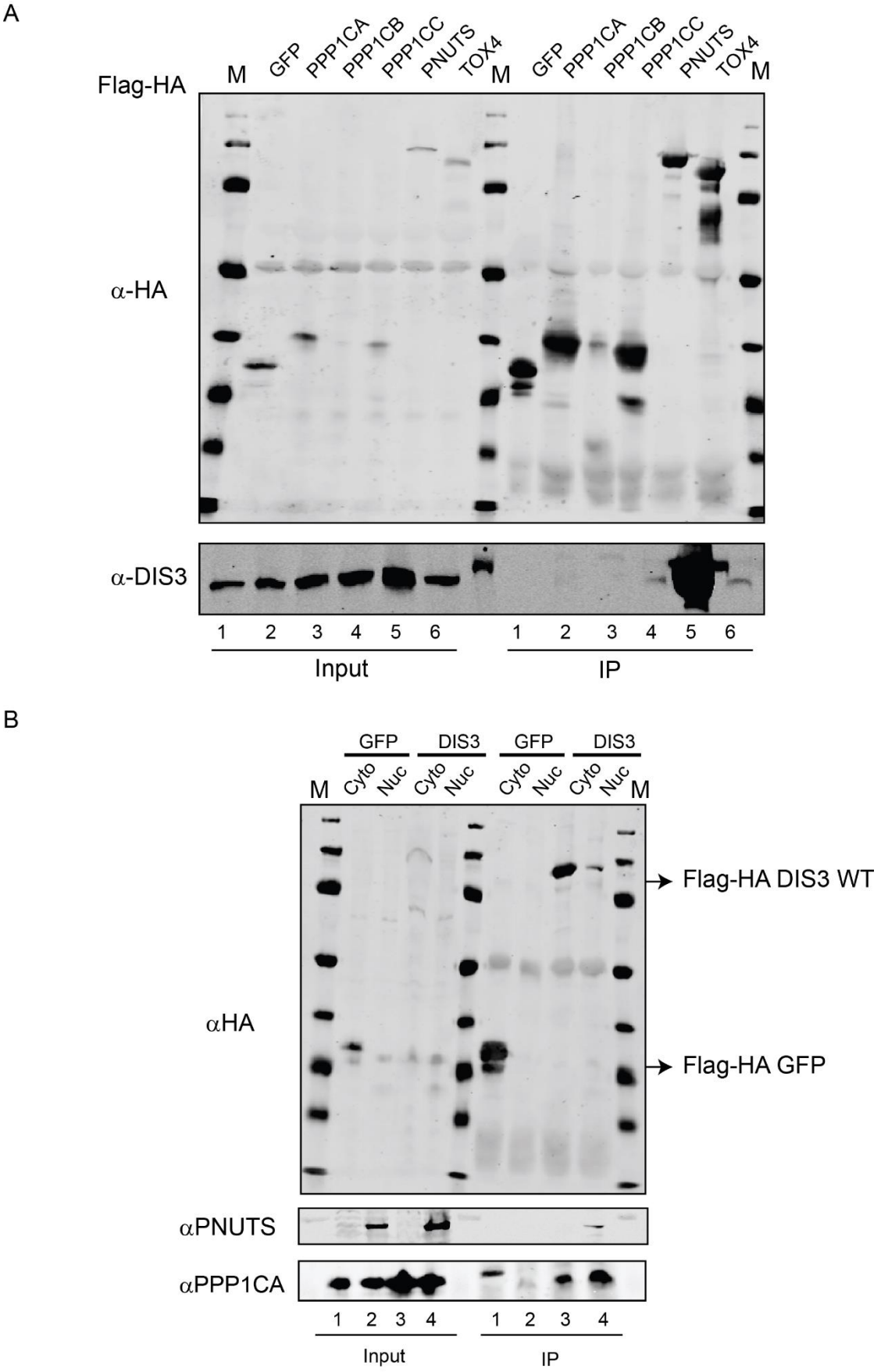

Figure 39. Verification of DIS3 nuclear interactions by co-immunoprecipitation. (A) HEK293 cells were transfected with Flag-HA-tagged proteins as indicated. FLAG-HA-tagged subunits of

PTW/PP1 complex were immunoprecipitated with anti-Flag antibodies and probed with specific antibodies against HA and DIS3. (B) Cytoplasmic and nuclear lysates from HEK293 cells expressing Flag-HA DIS3 wild type and Flag-HA GFP were immunoprecipitated using anti-FLAG antibodies. Interactions were analysed by western blotting using antibodies against PNUTS and PPP1CA.

3.4.7 *Sedimentation of co-purified nuclear interactors of DIS3*

To confirm DIS3 nuclear association with PTW/PP1 complex, we examined PTW/PP1 components for specific co-sedimentation with DIS3-containing fractions in glycerol gradients. Nuclear and cytoplasm extracts containing Flag-HA DIS3 WT were separated onto a 10–40% glycerol gradient as described above. Fractions were then analysed by western blotting using specific antibodies against PNUTS and PPP1CA components (Figure 40). Flag-HA DIS3 was detected with anti-HA antibody. Consistent with the mass spectrometry data, DIS3 co-migrated with both PNUTS and PPP1CA proteins in low molecular weight fractions in the nucleus only (Figure 40). Notably, PPP1CA but not PNUTS was found co-sedimenting with DIS3 in the cytoplasmic fractions. As already mentioned, PNUTS plays a crucial role as a platform for the assembly of all the components of PTW/PP1 complex (J. H. Lee et al., 2010). Its localization restricted to the nucleus explains the formation of PTW/PP1 complex exclusively in this cellular compartment.

In summary, we further support a potential link between DIS3 and PTW/PP1 complex. Furthermore, we found that ectopically expressed DIS3 co-sedimented with both PNUTS and PPP1CA by gradient centrifugation of nuclear extracts.

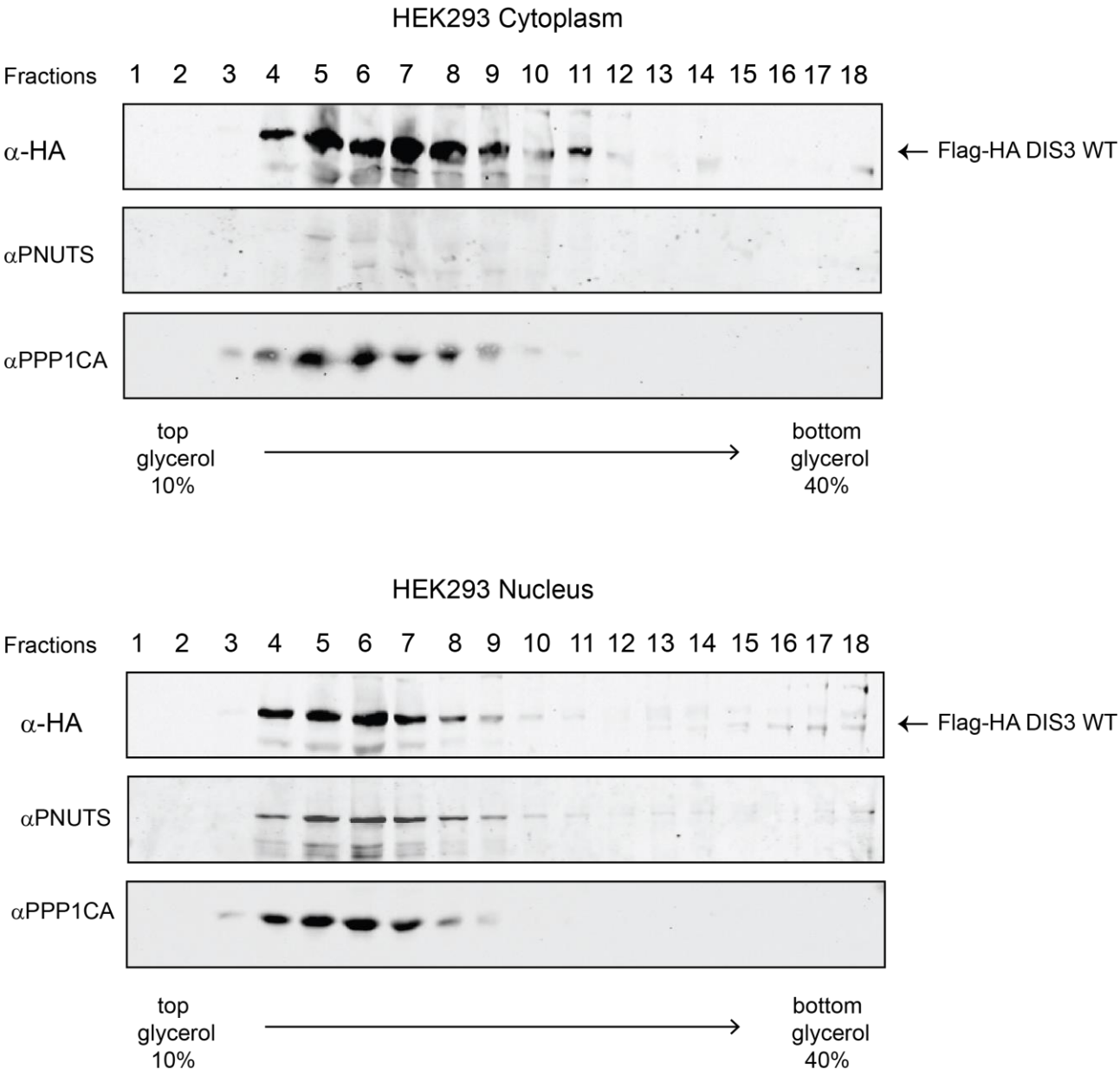

Figure 40. Co-migration of PTW/PP1 components with DIS3. Nuclear and cytoplasmic gradients from HEK293 lysates containing Flag-HA DIS3 wild type were analysed by western blot using anti-HA for DIS3 protein and PNUTS and PPP1CA specific antibodies.

3.4.8 *Detection of DIS3 phosphorylation sites*

The interaction of DIS3 with the phosphatase complex PTW/PP1 preferentially in the nucleus drove us to investigate the presence of phosphorylations on nuclear and cytoplasmic DIS3. We immunoprecipitated Flag-HA DIS3 from the cytoplasmic and nuclear fractions and phosphorylation of DIS3 was measured using mass spectrometry. To eliminate technical artifacts, we performed our measurements in triplicates and only the most frequent phosphorylation sites were considered.

Figure 41 summarizes the results of three different measurements and shows the potential phospho-sites on DIS3. Interestingly, we found phospho-sites only in the cytoplasmic DIS3, although we had similar sequence coverage for both cytoplasmic and nuclear DIS3. We observed in total five phospho-sites, one following the PIN domain (S215) and the other four in the exonucleolytic domain (S633, S634, S730 and S732). In detail, in the RNB domain, we could identify two clusters, in which individual residues were repeatedly phosphorylated. The first cluster is composed of two consecutive serines, S633 and S634, whereas the second cluster by serine S730 and tyrosine T732. For both clusters, no multiple phosphorylated peptides were found. The most reliable phospho-sites were serines S634 and S732 since they were found in three out of three biological experiments. Furthermore, we compared the phospho-sites found with the ones listed at PhosphoSitePlus® (www.phosphosite.org) and we confirmed all of them except for T732.

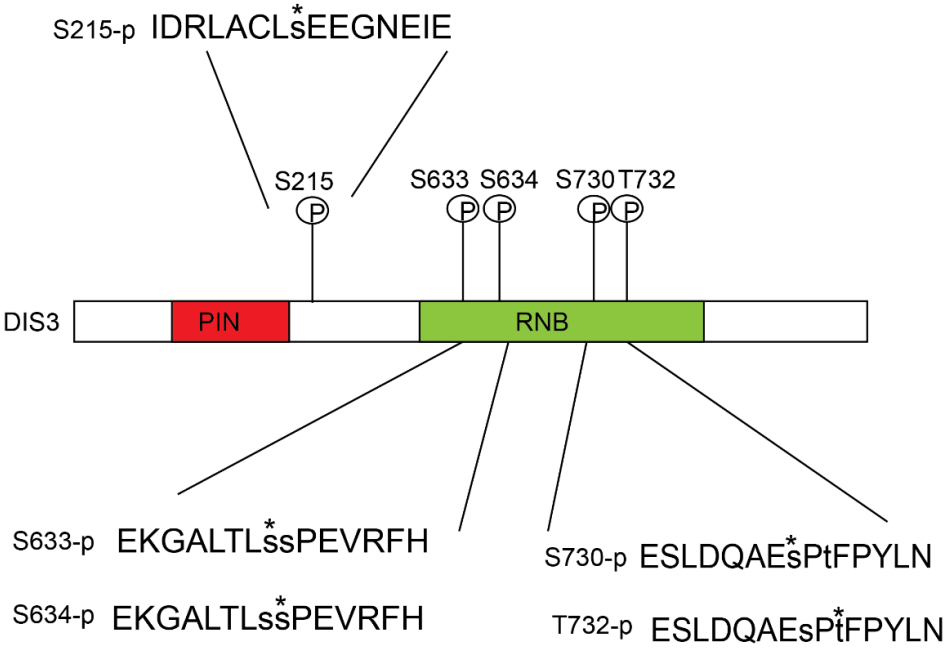

Cytoplasmic DIS3 Phospho-site	Times found by Mass Spec	Annotated in PhosphoSitePlus®
S633-p	I	X
S634-p	III	X
S730-p	III	X
T732-p	II	
S215-p	II	X

Figure 41. Identification of phosphorylation sites in DIS3 protein. Schematic representation of the DIS3 domain organization with the positions of the identified phosphor-sites. In the lower panel, a summary of the frequency of phosphorylation sites found in three biological replicates and of the phospho-sites annotated in PhosphoSitePlus® (www.phosphosite.org).

3.4.9 *Location of potential phosphorylation sites on DIS3 protein structure*

The two phosphorylation clusters are both localized in the exoribonucleolytic domain (RNB) of DIS3 (Figure 42). Interestingly, S633 and S634 are located in the catalytic center of DIS3 in close proximity to the target RNA (yellow arrow). These phospho-sites could potentially affect the binding of RNA and the activity of the exoribonucleolytic catalytic center. Phosphorylations S730 and T732 instead are located at the surface of DIS3 in a flexible and exposed loop (red arrow). In sum, the localization of S633 and S634 in the catalytic center of cytoplasmic DIS3 as well as S730 and T732 in the flexible loop supports the idea that phosphorylation of these residues could affect the positioning of the negatively charged RNA, consequently the exoribonucleolytic activity in the cytoplasm. Indeed, it has been reported previously that phosphorylations in the RNB domain of Ser-786 and Ser-809, in drosophila and *S. pompe* respectively, inhibit DIS3 exoribonucleolytic activity (Snee et al., 2016; Telekawa et al., 2018).

Figure 42. Position of RNB domain phospho-sites on the human DIS3. Residues S633 and S634 are located in the catalytic center and indicated with a yellow arrow. Residues S730 and T732 are located in a flexible loop and indicated with a red arrow. The structure is based on the model 6d6r (Synowsky et al., 2006).

3.4.10 *A phosphomimetic mutant of DIS3 inhibits its exoribonuclease activity*

Phosphorylations in the RNB have been shown to inhibit DIS3 exoribonuclease activity but not its endoribonuclease in yeast and Drosophila (Snee et al., 2016; Telekawa et al., 2018). After finding phosphorylations only in the RNB of cytoplasmic DIS3, we wondered if that was also our case. We hypothesized that the inactivation of exonuclease domain favours endonuclease activity in the cytoplasm. To test our hypothesis, we selected the most frequent phospho-sites such as S634 and S730 and we generated four Flag-HA tagged forms of DIS3 phospho-mutants (Figure 43A):

1) Flag-HA DIS3 S634A mutant, a non-phosphorylatable form in which we mutated the serine S634 to A (Alanine)
2) Flag-HA DIS3 S634E mutant, a phosphomimetic form in which we mutated the S634 to E (Glutamic acid)
3) Flag-HA DIS3 S730A mutant, a non-phosphorylatable form in which we mutated the serine S720 to A (Alanine)
4) Flag-HA DIS3 S730E mutant, a phosphomimetic form in which we mutated S720 to E (Glutamic acid)

To measure exonuclease activity, we combined protein immunoprecipitation experiments with *in vitro* RNA degradation assays. Specifically, we assayed the ability of different DIS3 mutants in degrading GSE1 linear RNA *in vitro*. Especially, our degradation assay was performed in the presence of Mg++, which is required for optimal exonuclease activity, but not Mn++, which is required for optimal endonuclease activity. Flag-HA DIS3 WT was used as positive control. The western blot analysis of the immunoprecipitation of the different versions of Flag-HA tagged DIS3 is shown in Figure 43B. The degradation assays showed that DIS3 WT and the two non-phosphorylable forms (DIS3 S634A and DIS3 S730A) exhibit significant exonuclease activity as GSE1 linear RNA signal decreases over time (Figure 43C). Surprisingly, the DIS3 phosphomimetic S730E, but not S634E, does not efficiently degrade the GSE1 RNA, suggesting effects on exonuclease activity. Currently, we are testing the effect of DIS3 phosphorylations on endonuclease activity using different systhetic circRNAs. In sum, we found that the phosphorylation on S730 but not on S634 inhibits DIS3 exonuclease activity *in vitro,* suggesting an exciting aspect of DIS3 regulation on RNA metabolism.

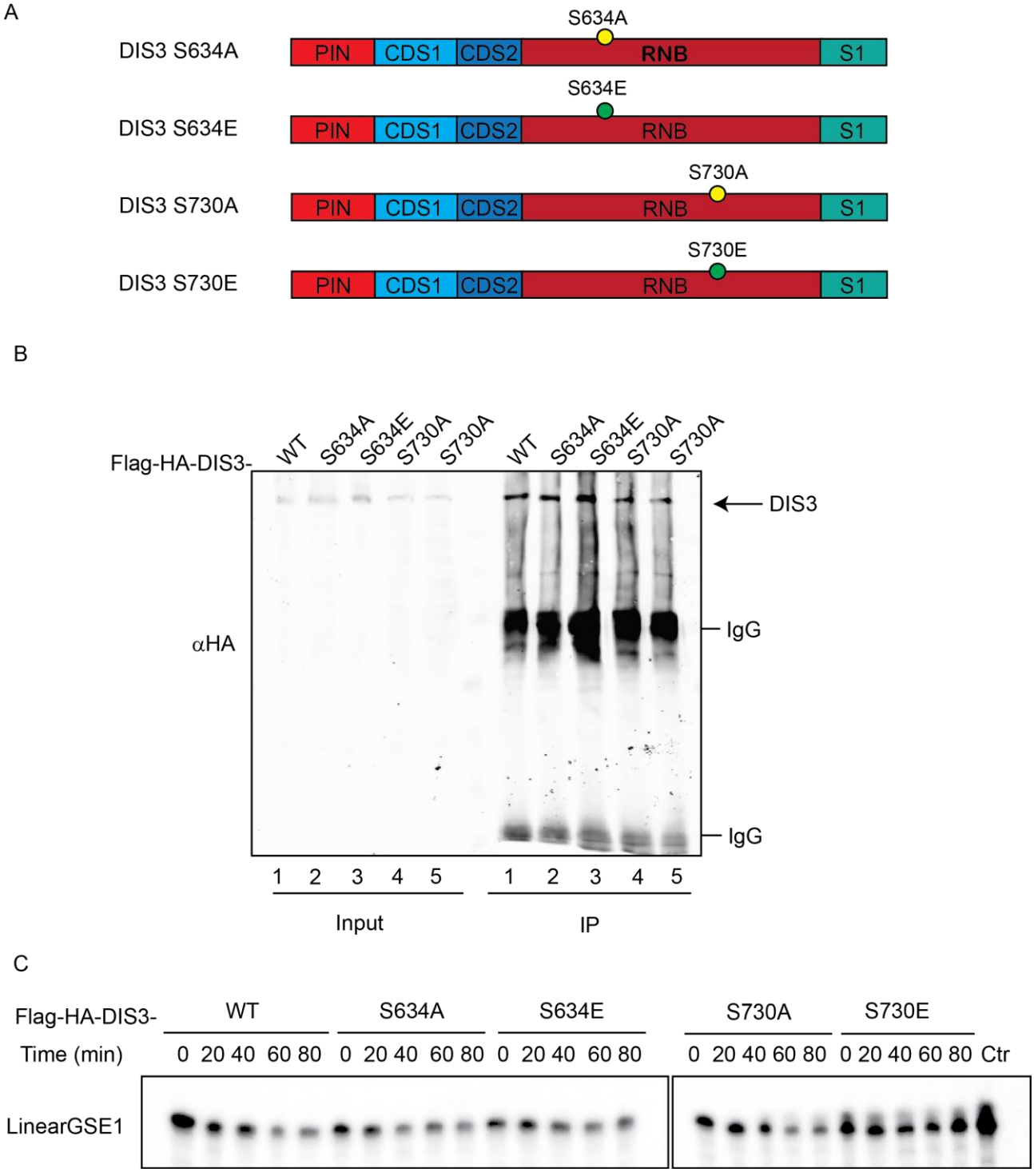

Figure 43. The phosphomimetic mutant S730E abolishes exoribonucleolytic activity of DIS3 *in vitro*. (A) HEK293 cells were transfected with different FLAG-HA-tagged DIS3 constructs as indicated. (B) FLAG-HA-tagged forms were immunoprecipitated with anti-Flag antibodies and probed with anti-HA antibodies against HA to detect the expression of DIS3 (C) Urea Gel-electrophoresis analysis of RNA degradation assay by incubating labelled GSE1 linear RNA with different immunoprecipitated DIS3 protein versions at different time points.

.

4 Discussion

CircRNAs are generated via a non-canonical splicing event known as backsplicing. Once produced, circRNAs are covalently closed, single strand molecules that exhibit tissue and cell-type-specific expression patterns. Despite their general low abundance, many circRNAs have been reported to regulate gene expression by modulating transcription and splicing, acting as miRNA and protein sponges and being a template for translation. Furthermore, several studies have revealed that circRNAs are implicated in diseases such as cancer, cardiovascular disease and neurological disorders and serve as a potential biomedical marker.

Differently from biogenesis and function, the turnover of circRNAs has only recently been investigated. The circular nature of circRNAs makes them more stable than the linear counterpart and resistant to exonuclease-mediated degradation. Few endonucleases such as RNase L, RNase P/MRP and G3BP1 have been shown to degrade a subset of circRNAs in addition to the well-known target RNAs in specific cell conditions. However, further endonucleases and pathways responsible for circRNA degradation in different conditions remain elusive.

In this PhD thesis, I combined biochemical and proteomic approaches to identify endonuclease candidates for circRNAs degradation. Interestingly, we confirmed the innate stability of some tested circRNAs compared to their linear counterparts and we found that circRNAs are mainly degraded in cytoplasmic extracts. We selected DIS3, the catalytic component of the exosome, as a promising candidate for circRNA turnover in HEK293 cells. We confirmed its potential to degrade selected circRNAs with *in vivo* and in *vitro* RNA degradation experiments. Combining an inducible CRISPR/Cas9 strategy system with RNA-seq analysis, we also found that depletion of DIS3 affects the expression of a subset of circRNAs *in vivo.* Furthermore, we investigated DIS3 function in in the cytoplasm and in the nucleus. We found that DIS3 localizes to both cellular compartments, is weakly associated with the exosome, and tends to exist on its own mainly in the cytoplasm. Finally, mass spectrometry analysis identified specific nuclear and cytoplasmic interaction partners and phosphorylation-sites on DIS3 protein. Taken all these results together, we could hypothesize a mechanistic model for DIS3 with a preference to degrade circRNAs in the cytoplasm.

4.1 *In vitro* synthesis of circRNAs and validation of their circularity

To identify endonuclease candidates, we applied a biochemical strategy. One of the first step of this biochemical strategy was to synthetize *in vitro* selected circRNAs. Different *in vitro* and *in vivo* methods of circularization are available (Abe et al., 2018; Y. G. Chen et al., 2017; Ho-Xuan, GlaÅar, et al., 2020; Müller & Appel, 2017; Obi & Chen, 2021; Petkovic & Müller, 2018; Wesselhoeft et al., 2018, 2019). Since the circRNAs selected for this study (circNRIP1, circGSE1, circCORO1C and circDOPEY2) were in a range of length between 200 and 300 nucleotides, we chose the enzymatic T4 RNA ligation method as the most suitable for producing *in vitro* small circRNAs. We optimized the conditions for all four designed circRNAs and we could successfully obtain synthetic circRNAs. CircRNA ca be identified on a 6% Urea PAGE since they run slower compared to the linear RNAs of the same size.

One of the adverse effects of the T4 ligation method is that, by chance, RNA dimers and concatemers can also be produced. Careful confirmation of the circular configuration of the *in vitro* molecules with different tools is necessary and important for further functional analysis. We used two different methods for circRNA confirmation, including RNase R and RNase H treatment. We adapted the two strategies to our *in vitro* conditions and we conclusively demonstrated the circularity of our selected synthetic circRNAs. Rnase R is the most common treatment used to purify circRNAs. Even though RNase R is a possible approach to confirm circularity, it still needs to be controlled carefully. Notably, excess of RNase R can also degrade long circRNAs or linear RNAs with secondary structure can be resistant to RNase R (Xiao & Wilusz, 2019). RNase H treatment combined with northern blots was firstly used by Starke et al., 2015 to demonstrate *in vivo* the circular configuration of endogenous circRNAs. Obviously, the RNase H approach can be considered crucial to prove circular configuration of endogenous and synthetic circRNAs. Indeed, biochemical assays using RNase H have been reported to be useful also for studying circular RNA concatemers (Thomas B. Hansen, 2018).

4.2 CircRNAs are stable and mainly degraded in the cytoplasm

The synthetic circRNAs produced by T4 ligation as starting point, were used for biochemical assays to identify endonuclease candidates. At the beginning, we incubated the selected synthetic circRNAs and their linear counterpart in nuclear and cytoplasmic extracts. Interestingly, we confirmed that *in vitro* circRNAs are more stable than their linear RNA cognate in cellular lysates. The high stability of circRNAs is due to the their own circular nature that makes them resistant to degradation by

exonuclease-mediated RNA decay. The work of Enuka et al., 2016, supported our data reporting similar results *in vivo* with selected circRNAs (Enuka et al., 2016). The circRNAs they examined have a long life with a median half-life between 18.8 and 23.7 hours compared to 4 and 7.4 hours of their respective linear RNAs.

Another interesting aspect we found is that circRNAs are preferentially degraded in cytoplasmic extracts. Differently, linear RNAs can be degraded in the cytoplasm and nucleus since components of the exonuclease mediated machinery are present in both compartments. It is possible that endonucleases are expressed more prevalent in the cytoplasm. Most circRNAs are cytoplasmic (Jeck et al., 2013; Salzman et al., 2012), except the intron-containing circRNAs (Z. Li et al., 2015; Y. Zhang et al., 2013). Consequently, in the cytoplasm, there should be pathways or additional endonucleases responsible for maintaining the appropriate steady-state levels of the circRNAs.

4.3 Identification of endonuclease candidates by biochemical and proteomic approaches

The cytoplasmic extract mentioned above was subjected to two serial purification steps, including ammonium sulfate precipitation and glycerol density gradient ultracentrifugation. Both purifications were combined with RNA degradation assays to find fractions competent for circRNA degradation. This biochemical method proved to be valid for *in vitro* identification of endonuclease candidates and could be used as support to the common *in vivo* experiments. Indeed, the following mass spectrometry analysis permits us to successfully identify several endonucleases candidates for circRNA degradation, such as Aldolase A, APEX, ARD1/PPP18, G3BP1 and DIS3.

The following immunoprecipitation experiments combined with *in vitro* RNA degradation assays suggested that not all the putative endonucleases have the potential to degrade circRNAs *in vitro*. Notably, although we could not confirm its endonuclease activity *in vitro*, G3BP1 has recently been reported to affect the decay of highly structured circRNA *in vivo* together with the helicase UPF1 (Y. Guo et al., 2020). The exact molecular mechanism behind circRNA decay by G3BP1/UPF1 has not elucidated so far and awaits identification. However, the finding of G3BP1 in the mass spectrometry data is an additional confirmation of the validity of our biochemical approach as a tool to identify endonuclease candidates. Furthermore, we could not verify the putative role as endonucleases of the other two candidates APEX and aldolase A. It is possible that these proteins are not responsible for degrading circRNAs and they are mainly focused on their biological function. Nevertheless, to exclude any possibility, further *in vivo* investigations are necessary since we could not have any effect *in vitro*.

Even though we have not observed evident degradation results for the mentioned endonucleases, ARD1 and DIS3 showed degradation activity on our tested synthetic linear and circular RNAs. ARD1 is considered as a mammalian analogue of *E. coli* RNase E and it is interesting to investigate in the future. DIS3 was selected as a promising candidate to study circRNA degradation for different reasons. Firstly, DIS3 is the catalytic component of the exosome and its endonucleolytic domain await investigation especially in human. Secondly, its cytoplasmic role has not been analysed so far. Finally, although the first hint for circRNA degradation was already shown *in vitro* for DIS3 (Schaeffer et al., 2009), the authors tested only artificial small circular RNA molecules and the DIS3 activity on cleavage of these circRNA species was very low efficient.

4.4 *In vitro* validation of DIS3

As a first approach to validate DIS3 as candidate mediating circRNA turnover, we performed *in vitro* RNA degradation assay with recombinant versions of human and yeast DIS3/Rrp44 full-length and the DIS3/Rrp44 PIN domain. The *in vitro* assays demonstrated that human DIS3 and its yeast homolog Dis3/Rrp44 could degrade linear and circular substrates *in vitro*. This degradation is independent of the RNA sequence because all selected targets were degraded in a time-dependent manner. Importantly, the endoribonucleolytic activity of DIS3 was already demonstrated *in vitro* with artificial circular RNAs consisting of only 17 adenines (Lebreton et al., 2008; Schaeffer et al., 2009). At that time, circRNAs were not systematically discovered yet. In this study, we can clearly show for the first time that DIS3 cleaves synthetic longer circular RNAs that are expressed in human cells. Notably, a high concentration of manganese was always required for circRNA degradation since it is necessary for activating the endoribonucleolytic activity (Lebreton et al., 2008). Comparing the activity of the human recombinant DIS3 wild-type protein with DIS3 D146N (PIN domain mutant) and DIS3 D487N (RNB domain mutant) mutants, we also confirmed that DIS3 requires an active PIN domain to display its endoribonucleolytic activity on circRNAs. Indeed, inactivation of the PIN domain of DIS3 protein by point mutation (D146N) abolishes circular but not linear RNA degradation. Furthermore, the *in vitro* assays with wild type and the single mutant of the PIN domain confirmed that not only the PIN domain is responsible for the endoribonucleolytic cleavage but also it can act independently from the exoribonucleolytic domain.

Next, since DIS3 is one of the catalytic components of the exosome, we investigated the endoribonucleolytic activity of DIS3 in the exosome complex and examined the impact of the exosome on circRNA degradation. *In vitro* RNA assays with different subcomplexes of yeast exosome showed that Dis3/Rrp44 could degrade circRNAs alone or in association with the exosome.

However, circRNA degradation mediated by DIS3 in combination with exosome is slower and less efficient. Interestingly, when the cap or catalytic components of the exosome were immunoprecipitated and tested for *in vitro* RNA assays, they could degrade linear but not circular RNAs. These results were in accordance with the *in vivo* co-immunoprecipitation experiments between exosome components. The interaction between DIS3 and the exosome seems to be very weak compared to the other components and it might get lost during the immunoprecipitation. We suggested that the current model of DIS3 associated with the exosome should therefore be revisited. Furthermore, it is possible that DIS3 displays its endoribonucleases activity on its own because it does not necessarily need all the exosome components to degrade circRNAs *in vivo*. Indeed, it was shown that the cap and core components are necessary for the 5'end recognition and positioning of linear RNAs (Bonneau et al., 2009; Lorentzen et al., 2007; Makino et al., 2013; Malet et al., 2010). CircRNAs do not have access to the exosome core until an endonuclease-mediated cleavage. However, it is still not clear if circRNAs, once cleaved, are loaded to the exosome.

4.5 *In vivo* validation of DIS3

Our *in vitro* experiments showed that DIS3 has a potential to degrade circRNAs and its endoribonuclease domain is the main feature for this degradation activity. As an approach to validate DIS3 *in vivo*, a dual gRNA RNA CRISPR-Cas9 editing system was used. Since DIS3 is an essential gene (Gudipati et al., 2012; Hou et al., 2012; Schneider et al., 2012), we deleted endogenous DIS3 PIN domain region on stable cell lines expressing DIS3 wild type or the catalytic mutant DIS3 D146N upon doxycycline induction. We generated a conditional DIS3 knockout in which we hope that the leaky expression of the target protein maintains the cells alive. This model results to be a useful tool for studying essential genes such as DIS3 and provides several advantages that complement previous RNAi approaches. First, the effect of DIS3 depletion is constant and does not get diluted after a given time. Moreover, it avoids the typical off-target effects observed with interfering RNA because we could rescue the effect of DIS3 knockout by induction of the protein expression using doxycycline. Third, it permits us to study the effects on RNA targets with long turnovers, such as circRNAs.

We were initially concerned that the leaky expression of DIS3 may prove problems for testing the impact of its loss. However, several observations alleviated this concern. First, we observed that DIS3 knockout results in a grown defect phenotype and needs a more careful handling (data not shown), suggesting functional knockout cells. Second, we showed by northern blot and actinomycin D experiments that DIS3 knockout causes accumulation of 5.8S rRNA precursors. The role of DIS3 in 5.8S has been extensively reported during the past years in eukaryotes (Allmang et al., 1999; Philip

Mitchell et al., 1996; Schilders et al., 2007; Schillewaert et al., 2012; Tafforeau et al., 2013). Further analysis is still necessary to understand the exact number of steps in this process and the molecular length of each rRNA intermediates. However, this result confirmed the role of DIS3 in trimming the 3'end of 5.8S rRNA precursors in human cells and indicates the validity of DIS3 knockout cells for studying RNA metabolism, especially circRNA degradation.

Although DIS3 depletion did not have a strong effect on the four selected circRNAs *in vivo* (except circGSE1), RNA-seq analysis revealed a subset of 9 circRNAs significantly enriched in DIS3 KO cells. Many of them were successfully validated by qPCR and with rescue experiments. Notably, we found high variability between the two CRISPR-Cas9 selected clones, clone 8 and clone 13, not only in the RNA-seq results but also in the validation.

We have initially expected a global effect on circRNA expression upon DIS3 KO, but it turned out to be specific only for a few cases. This seems to be a peculiarity of endonucleases that tend to degrade target RNAs in a selective way. Examples of this kind are the RNAse P which degrades only few methylated circRNAs *in vivo* or G3BP which prefers highly structured circRNAs (Fischer et al., 2020; Ok Hyun Park et al., 2019). Differently, the RNAse L globally degraded circRNAs but only in stressed condition upon viral infection (C. X. Liu et al., 2019). Furthermore, it should be considered that the endonuclease function can be redundant since most of circRNAs seems to be degraded in a not sequence-specific way. Another reason can be found in the limit of our model system. We should carefully consider that our knockout model is a milder depletion rather than a full knockout. Maybe the leaky expression of DIS3 wild type protein is enough for mediating circRNAs decay. Notably, DIS3, and potentially all the endonucleases mentioned above, do not play roles only in circRNA decay but are involved in other major cellular pathways. Finally, the subcellular localization of these circRNAs should be another interesting aspect to investigate, and that can give us more hints about DIS3-specific circRNA degradation.

Another interesting funding was that for three cases tested (OXCT1, RERE and FAM208), DIS3 depletion affects only circRNAs but not the linear counterparts. This inverse correlation confirmed that the endoribonucleolytic activity of DIS3 is specific for these three circRNAs. The reason why DIS3 preferentially degrades selected circRNAs *in vivo* still awaits answers. According to the *in vitro* assays, DIS3 endoribonuclease activity does not show sequence specificity since it is able to cleave all four circRNAs used for this study. One possibility is that *in vivo*, DIS3 endoribonuclease domain recognizes specific secondary structures of the circRNAs. Indeed, it has been already suggested that the PIN domain of DIS3 can be an alternative entry site for structured RNAs (Lebreton et al., 2008; Schneider et al., 2009; Schaeffer et al., 2009). CircRNAs, therefore, might have special topological structures to distinguish themselves from the linear cognates, which allow binding and cleavage to

DIS3. RNA SHAPE studies can be performed to prove this hypothesis. However, the presence of adaptor proteins such as helicases that can facilitate the substrate recognition should also not be excluded.

Although them main interest of this thesis was circRNA decay, we also analysed by RNA-seq differential expressed protein coding genes in DIS3 knockout conditions. Also, in this case, only few mRNAs were upregulated in DIS3 depletion. We were not surprised since DIS3 is known to be more involved in small RNA biogenesis (tRNA, rRNA and snoRNA)(Allmang et al., 1999; Gudipati et al., 2012) and in the degradation of PROMPTs and unstable transcripts in the nucleus (Davidson et al., 2019; Preker et al., 2008; Szczepińska et al., 2015). mRNA cytoplasmic turnover depends essentially on XRN1 (Decker & Parker, 1993; Geisler & Coller, 2012; Muhlrad et al., 1994; Nagarajan et al., 2013) and DIS3L1(Staals et al., 2010) or DIS3L2 (Lubas et al., 2013; Malecki et al., 2013). Among deregulated mRNA candidates, MYC was one of the upregulated mRNAs upon knockout of DIS3. Accordingly, it has recently been reported that DIS3 depletion could lead to an increase in MYC levels via the let-7 pathway (Segalla et al., 2015). Therefore, MYC deregulation provides additional confirmation of the validity of our CRISPR-Cas9-mediated DIS3 KO system.

Last but not least, analysis and validation of DIS3 D146N Flp-In T-REx-293 cells are still ongoing and will give us a broad view of DIS3 endoribonucleolytic domain impact on circular and linear RNA expression.

4.6 Subcellular localization of DIS3 and its association with the exosome

It has been reported that in humans, DIS3 is mainly localized in the nucleus, excluded from the nucleolus and present only in a small pool in the cytoplasm (Tomecki et al., 2010). It remains unclear whether in this pool, DIS3 is alone or associated with components of the exosome. Our subcellular fractionation analysis revealed that DIS3 is localized in both compartments and not preferentially in the nucleus as expected from the literature. Regarding three components of the exosome that we tested, EXOSC3 and EXOSC9 were also found in the cytoplasm while EXOSC10 was restricted to the nucleus.

We also investigated DIS3 distribution in cytoplasmic and nuclear glycerol gradients and we confirmed the presence of exosome complexes in both compartments with a preference for the nucleus. Surprisingly, we found more DIS3 in the low-density fractions than in the high-density ones and the levels of free DIS3 higher in the cytoplasmic extract. These observations support the hypothesis that a pool of DIS3 can exist on its own in the cytoplasm and provide an insight into the specific substrate targets. Specifically, the endonucleolytic activity of DIS3 can provide an alternative

entry site and cleavage for highly structured RNAs such as circRNAs (Lebreton et al., 2008; Schneider et al., 2009; Schaeffer et al., 2009). Furthermore, we can speculate that DIS3 does not necessarily need the whole exosome for degrading circRNAs. However, the effects of ectopic expression of tagged proteins in the cells need also to be considered.

Additionally, mass spectrometry analysis and co-immunoprecipitation experiments confirmed our idea of a pool of cytoplasmic free DIS3 and revealed that DIS3 association with the exosome transient. Few peptides arising from exosome components can be found in DIS3 immunoprecipitations and no one of them can be detected by western blot. This finding is consistent with the observations of Tomecki and collegues and of Domanski and LaCava, who both optimized less stringent protocols to purify the exosome components from DIS3 immunoprecipitation (Domanski & LaCava, 2017; Tomecki et al., 2010). The weak interaction of DIS3 with the exosome should be evaluated from a different perspective. It remains possible that *in vivo*, the exosome is a dynamic complex and DIS3 can dynamically associate and dissociate depending on cell conditions or needs as well as different RNA metabolism. This results in two interchangeable pools of DIS3, one free and one associated with exosome. This is also supported by Telekawa and colleagues' work, who argues against a static and uniform model of the exosome complex with spontaneous activity for RNA degradation (Telekawa et al., 2018). Similarly, the exosome was also described as a versatile complex with a fixed scaffold but variable catalytic subunits such as DIS3, DIS3L1 and EXOSC10 (Lykke-Andersen et al., 2011). However, further experiments are necessary to investigate this new insight.

4.7 Cytoplasmic and nuclear interactor partners of DIS3

The identification of nuclear and cytoplasmic partners of DIS3 gave us some hints to better understand DIS3 biological function and regulation. Mass spectrometry analysis identified several proteins that specifically interacts with DIS3 in the cytoplasm or in the nucleus. Interestingly, RioK1 was found as one of top candidates for cytoplasmic interaction partners. RioK1 is an atypical serine/threonine kinase, which plays a key role in the final steps of cytoplasmic maturation of the 40s ribosomal subunit (Ameismeier et al., 2020; Widmann et al., 2012). Specifically, it activates the endonuclease NOB1 by dissociating it from the inhibitor binding partner PNO1, although the protein kinase domain is proposed to act predominantly as an ATPase. In addition to its role in ribosomal biogenesis, RioK1 acts as adaptor protein in the methylosome complex such as PRMT5 which catalyses the symmetrical arginine dimethylation of its different substrate proteins (Guderian et al., 2011). The cytoplasmic interaction of DIS3 with RioK1 opens different perspectives. On one side,

DIS3 could be implicated in cytoplasmic rRNA biogenesis since it has been reported that DIS3 is involved in rRNA biogenesis (Allmang et al., 1999; Philip Mitchell et al., 1996; Schilders et al., 2007; Schillewaert et al., 2012; Tafforeau et al., 2013). On the other side, RioK1 could also activate the endonuclease domain of DIS3 in the similar way it does for the endonuclease PNO1 (Ameismeier et al., 2020; Widmann et al., 2012). Finally, we should also consider DIS3 association with RioK1 and all the components of the PRMT5 complex. It would be interesting to investigate whether DIS3 is a new component of the complex or a substrate to methylate. Further analysis would be necessary to validate these hypotheses.

About the nuclear interactions, our interest was focused on the protein serine/threonine phosphatase PTW/PP1 complex. PTW/PP1 is a stable multimeric complex composed of regulatory subunits PNUTS, Tox4, and Wdr82 and one of PP1 catalytic subunits PPP1CA, PPP1CB or PPP1CC (Lee et al., 2010). All the components of the PTW/PP1 complex were identified in our mass spectrometry analysis of DIS3 from nuclear extracts. Moreover, the following immunoprecipitations and nuclear/cytoplasmic gradient experiments confirmed DIS3 association with two components of the complex preferentially in the nucleus. Taken together these results suggested a possible role of PTW/PP1 complex in dephosphorylating DIS3 in the nucleus and encouraged us to investigate on DIS3 phosphorylation sites. We speculated that post-translational modifications could affect DIS3 nuclear and cytoplasmic function and regulation.

4.8 DIS3 phosphosites and phosphomutants

To analyse whether DIS3 function could be regulated via phosphorylation, we identified nuclear and cytoplasmic phosphorylation sites on ectopic expressed DIS3 by mass spectrometry. Interestingly, although we had a good sequence coverage for both cytoplasmic and nuclear DIS3, only cytoplasmic phospho-sites were identified. In detail, we found five phospho-sites in total, one following the PIN domain (S215) and two clusters in the exoribonucleolytic RNB domain (S633, S634, S730 and S732). The first cluster consists of two consecutive serines S633 and S634, whereas the second cluster consists of serine S730 and tyrosine T732. Notably, all phospho-sites were reported in PhosphoSitePlus® (www.phosphosite.org) except for T732. The previously characterized serine phosphorylation site in the RNB of DIS3, S786 in Drosophila and S814 in fission yeast, was not found in our mass spectrometry data. It is possible that in humans, the equivalent serine is not phosphorylated or phosphorylated only in specific conditions. It often happens that phosphates are lost during sample preparation or mass spectrometry processing.

The specific localization of the two clusters in the RNB domain, one in the catalytic center and the other in a flexible loop, gave us some insights into their potential function. We were wondering whether these specific-localized phosphorylations could affect the exoribonucleolytic activity of DIS3 in the cytoplasm. Indeed, it is known that the addition of a negative charge by a phosphate group can block the binding of the RNA since it is negatively charged or can induce conformational changes of the protein domain. Ser-786 in *Drosophila* and the equivalent Ser-809 in *S. pompe,* are examples of this kind (Snee et al., 2016; Telekawa et al., 2018). These residues are located near the RNB domain of DIS3.When they are phosphorylated, the exoribonucleolytic activity is inhibited but not the endoribonucleolytic one.

To test this for our phosphor-sites, we selected the phospho-sites that were present in all replicates with high scores (S634 and S730). The following studies with phospho-mutant analysis revealed that phosphorylation of S730 inhibits the exoribonuclease activity but not S634. Since S730 is located in a flexible loop, we speculated that the inhibition of the catalytic domain is somewhat due to a conformation change than the positioning of the RNA itself. Although the endonuclease activity remains to be investigated, this funding suggested that phosphorylation in the exoribonucleolytic domain of DIS3 can inhibit its activity in the cytoplasm. The functional relevance of this phosphorylation, as well as the involved kinases, awaits answers. However, one possible role of S730 phosphorylation could be to keep the cytoplasmic free DIS3 in an exoribonucleolytic inactive state until incorporation in the exosome core. As a consequence, the endoribonuclease activity is preferred in the cytoplasm for degrading specific RNAs. Alternatively, the phosphorylation of S730 could induce conformational changes in the exosome core that would favour selected RNA targets toward the endoribonuclease active domain of DIS3 or the other catalytic components. Finally, we could hypothesize that DIS3 phospho-sites are dephosphorylated by the above-mentioned PTW/PP1 complex in the nucleus where the DIS3-exosome performs its main function. Notably, in the specific case of S730 and T732, the phosphatase complex does not need to gain access to the catalytic site since they are located in an exposed loop.

4.9 A model for cytoplasmic degradation of selected circRNAs

Our study provided the first insights into *in vitro* and *in vivo* circRNA degradation potentially mediated by DIS3. Additionally, we characterized DIS3 cytoplasmic and nuclear function with a particular interest in the exosome and in DIS3 interaction partners. Finally, we identified human DIS3 phosphorylation sites and that some of them might inhibit its exoribonucleolytic activity.

Figure 44 presents a suggestive model for cytoplasmic degradation of circRNAs by DIS3. Human DIS3 localizes in both cellular compartments. In the cytoplasm, DIS3 is mainly free and only a few molecules are associated with the exosome. The RNB domain is phosphorylated and its exoribonuclease activity is inhibited. Consequently, DIS3 endoribonucleolytic activity is preferred and circRNAs are degraded rather than linear RNAs. In the nucleus, DIS3 is principally associated with the exosome. The exoribonucleolytic domain is dephosphorylated presumably by PTW/PP1. The exoribonucleolytic activity is preferred to the endoribonucleolytic one. Subsequently, DIS3, together with the exosome, can perform its nuclear function on degrading linear RNAs.

The proposed model revisits the common knowledge of exosome as a static complex with constitutive and spontaneous RNA degradation activity. Accordingly, DIS3 can exist on its own or be associated with the exosome. The RNA substrates selected for degradation depend on DIS3 subcellular localization, phosphorylation and on its exo- and endo- mutually exclusive activities.

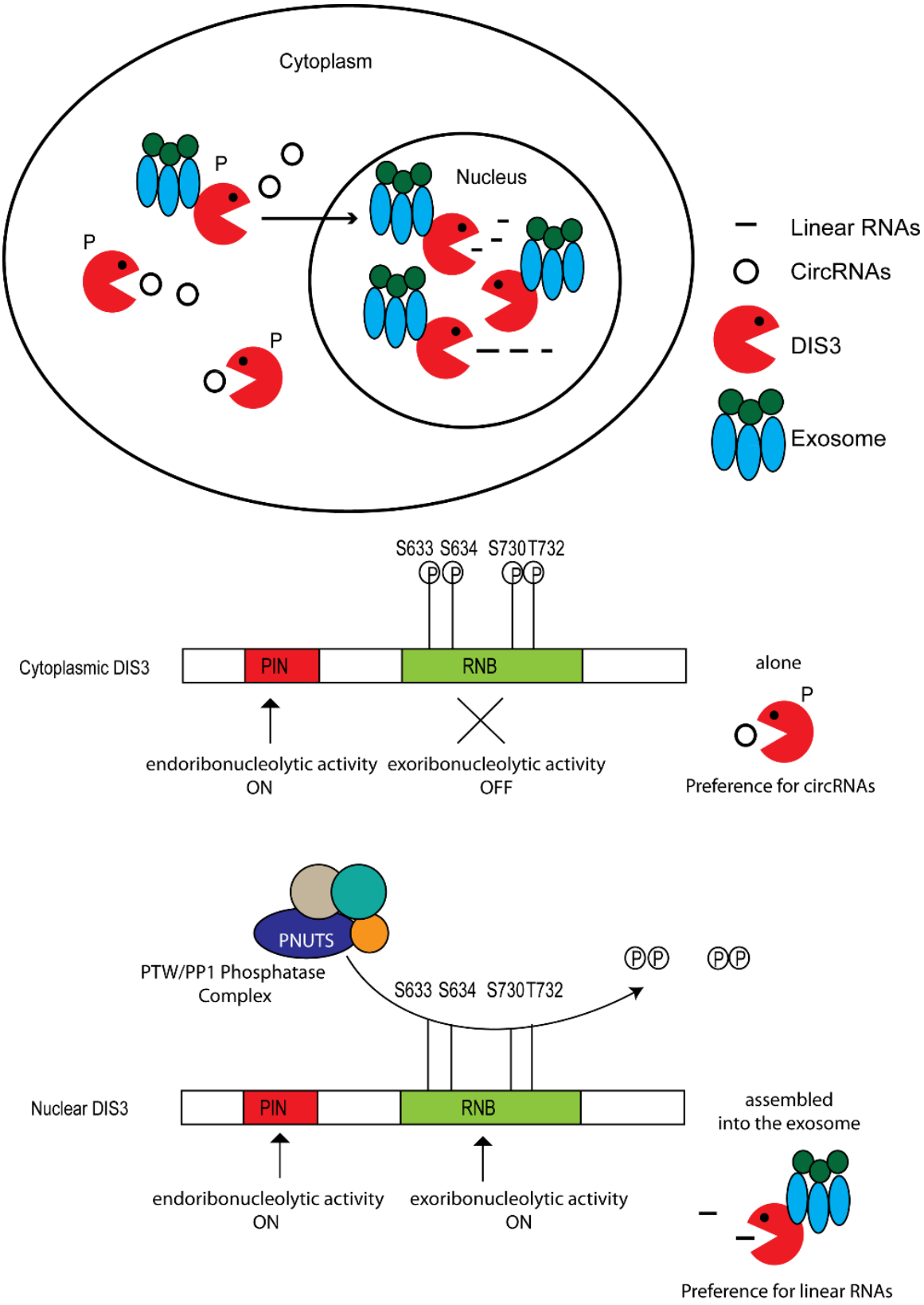

Figure 44. A model for cytoplasmic circRNA degradation. In the cytoplasm, DIS3 is mainly alone and its RNB domain responsible of exonucleolytic activity is phosphorylated and inhibited. As a consequence, endoribonucleolytyc activity is preferred and selected circRNAs are degraded. In the nucleus, DIS3 forms a complex with the exosome and its exonucleolytic domain is dephosphorylated by PTW/PP1 phosphatase complex and activated. DIS3, together with the exosome, can perform its nuclear function by degrading target linear RNAs.

5 Materials and Methods

5.1 Materials

5.1.1 *Instruments*

Table 4. List of instruments

Instrument	**Company**
Branson Sonifier™ S-450A	Emerson (St. Louis, USA)
Centrifuge 5415C	Berthold (Bad Wildbad, Germany)
Centrifuge 5415D	Eppendorf (Hamburg, Germany)
Centrifuge 5430R	Eppendorf (Hamburg, Germany)
Geiger Counter LB123 EG&G	Berthold (Bad Wildbad, Germany)
HeraCell 240i CO2 Incubator	Thermo Fisher Scientific (Waltham, USA)
HeraSafe KS	Thermo Fisher Scientific (Waltham, USA)
Incubator Model B6200	Heraeus (Hanau, Germany)
Innova 44 Incubator Shaker Series	New Brunswick Scientific (Edison, USA)
Lab dancer	VWR (Darmstadt, Germany)
Magnetic stirrer MR 300	Heidolph (Schwabach, Germany)
Milli-Q plus	Merck Millipore (Burlington, USA)
NanoDrop™ 1000 Spectrophotometer	Thermo Fisher Scientific (Waltham, USA)
Odyssey Infrared Imaging System	LI-COR Biosciences (Lincoln, USA)
peqSTAR Thermocycler	PeqLab (Erlangen, Germany)
Personal Molecular Imager™ System	Bio-Rad (Hercules, USA)
Power PAC 200, power supply	Bio-Rad (Hercules, USA)

Power PAC 300, power supply	Bio-Rad (Hercules, USA)
Power supply Power Pack P25	Biometra (Göttingen, Germany)
Quantum ST4	PeqLab (Erlangen, Germany)
Rotanta 460 R	Hettich (Tuttlingen, Deutschland)
Screen Eraser-K	Bio-Rad (Hercules, USA)
SPROUT® MINI CENTRIFUGE	Heathrow Scientific
Thermomixer comfort	Eppendorf (Hamburg, Germany)
Trans-Blot SD	Bio-Rad (Hercules, USA)

5.1.2 *Consumables*

Table 5. List of consumables

Consumable	**Company**
Amersham Hybond ECL Membrane	GE Healthcare (Buckinghamshire, UK)
Molecular Imager FX Imaging Screen-K	Bio-Rad (Hercules, USA)
Plastic pipettes and pipet tips	Sarstedt (Nuembrecht, Germany)
Reaction tubes (1.5 mL and 2 mL)	Eppendorf (Hamburg, Germany)
Tissue culture dishes	Sarstedt (Nuembrecht, Germany)
Tubes (15 mL and 50 mL)	Sarstedt (Nuembrecht, Germany)
Whatman® Cellulose Filter Paper	GE Healthcare (Buckinghamshire, UK)
X-Ray Cassette	CAWO (Schrobenhausen, Germany)

5.1.3 *Softwares*

Table 6. List of softwares

Software	**Company**

Odyssey 3.0.30	LI-COR Biosciences (Lincoln, USA)
Quantity One Version 4.6.9	Bio-Rad (Hercules, USA)
Quantum ST4 v16.04	PeqLab (Erlangen, Germany)

5.1.4 *Kits and solutions*

Table 7. List of kits and solutions

Name	**Manufacturer**	**Application**
First Strand cDNA Synthesis Kit	Thermo Fisher Scientific Inc.	cDNA synthesis for qPCR
Lipofectamine™ 2000	Thermo Fisher Scientific Inc.	Transfection of plasmid DNA
Lipofectamine™ RNAiMAX	Thermo Fisher Scientific Inc.	Transfection of siRNA
NucleoBond®-Xtra-Midi	MACHEREY-NAGEL GmbH & Co. KG (Düren, Germany)	Large scale plasmid purification
NucleoSpin®-Extract	MACHEREY-NAGEL GmbH & Co. KG	DNA purification from agarose gel slices, PCR reactions or other enzymatic reactions
NucleoSpin®-Plasmid	MACHEREY-NAGEL GmbH & Co. KG	Small scale plasmid purification
Passive Lysis 5X Buffer	Promega Corporation (Fitchburg, USA)	Cell lysis for luciferase assays
pGEM®-T Easy Vector System	Promega Corporation	Subcloning of DNA sequences
Phusion™ High-Fidelity DNA Polymerase	Thermo Fisher Scientific Inc.	PCR amplification
Roti®-Phenol/Chloroform/Isoamyl alcohol (25:24:1), pH 4.5-5	Carl Roth GmbH + Co. KG	Extraction of total RNA from immunoprecipitated samples
Roti®-Quant (5X)	Carl Roth GmbH + Co. KG	Protein quantitation according to Bradford
SequaGel® UreaGel™ System	National Diagnostics Inc., (Atlanta, USA)	Denaturing PAGE
SsoFast™ EvaGreen® Supermix	Bio-Rad Laboratories Inc. (Hercules, USA)	qPCR
SuperScript™ III First Strand Synthesis Super Mix	Thermo Fisher Scientific Inc.	cDNA synthesis for small RNA cloning
TRIzol Reagent	Thermo Fisher Scientific Inc.	Extraction of total RNA

5.1.1 *Buffers*

Table 8. List of buffers

Method	Buffer and solution	Components
Western blot	Tris buffered saline (TBS)	10 mM Tris pH 7,5 150 mM NaCl 0,1% (v/v) Tween 20
	TBS-Tween (TBS-T) (10x)	TBS 0,1% (v/v) Tween 20
	SDS running buffer (10x)	200 mM Glycine 25 mM Tris pH 7,5 25 mM SDS
	Laemmli protein sample buffer / SDS sample buffer (5x)	300 mM Tris pH 6,8 10% SDS 62.5% glycerol 1 mg/ml Bromophenol blue 10% mercaptoethanol
	Blocking solution	5% milk powder 0.02% NaN3
	SDS running buffer	25 mM Tris 192 M glycine 0,1% SDS
	Towbin Blotting Buffer (10x)	1,92 M glycine 250 mM Tris
	Towbin Blotting Buffer (1x)	1x Towbin Buffer (10x) 20% methanol

Coomassie staining	Coomassie staining solution	30% ethanol 10% Acetic acid 0,1% Coomassie Brilliant Blue R-250
	Coomassie destaining solution	Ethanol Acetic acid
Northern blot (Urea-PAGE gel)	2x RNA loading dye	99,9 % Formamide 0,025 % Xylene cyanol 0,025 % Bromphenol blue in TBE
	Tris/Borate/EDTA buffer (TBE 1X)	89 mM Tris pH 8,3 89 mM Boric acid 2,5 mM EDTA
	20x SSC	3 M NaCl 0,3 M TriNaCitrate pH 7,0
	50x Denhardt's Solution	1 % Albumin Fraction V 1 % Polyvinylpyrrolidone K30 1 % Ficoll 400
	Hybridization solution	5x SSC 20 mM NaPi, pH 7,2 7 % SDS 1x Denhardt's Solution
	EDC crosslinking solution	61,25 ul Methylimidazole 75 ul 1 M HCl 188,25 mg EDC in 6 ml H2O
	Wash solution 1	5x SSC 1% (w/v) SDS

	Wash solution 2	1x SSC 1% (w/v) SDS
Northern blot (Agarose gel)	Blue juice	3 mL Glycerol (100%) 200 ul 2.5% Bromphenol Blue 6.8 mL RNase-free H2O
	2 x RNA loading dye	450 ul Formamide (100%) 100 ul 10X MOPS 160 ul Formaldehyde (37%) 90 ul RNase-free H2O 200 ul Blue Juice
	MOPS buffer (10x)	200 mM MOPS 20 mM NaAc 10 mM EDTA
	MOPS buffer (1x)	1/10 MOPS buffer (10x) 2% Formaldehyde (37%)
	Wash solution 3	2X SSC 0.1% (w/v) SDS
	Wash solution 4	0.5X SSC 0.1% (w/v) SDS
	Wash solution 5	0.1X SSC 0.1% (w/v) SDS
IP	IP lysis buffer	150 mM KCl 25 mM Tris pH 7,5 2 mM EDTA 1 mM NaF 0,5 % NP-40 1mM DTT

		1mM AEBSF
IP	IP wash buffer	50 mM Tris/HCl pH 7.5 300 mM KCl 1 mM MgCl2 0.5% NP-40
	Phosphate buffered saline (PBS)	140 mM NaCl 10 mM NaH2PO4 2,7 mM KCl 1,8 mM KH2PO4
Cytoplasmic/Nuclear fractionation	Hypotonic lysis buffer (HLB)	10 mM Tris (pH 7.5) 10 mM NaCl 3 mM MgCl2 0.3% (vol/vol) NP-40 10% (vol/vol) glycerol 1mM AEBSF 1mM DTT
	Nuclear lysis buffer (NLB)	20 mM Tris (pH 7.5) 150 mM KCl 3 mM MgCl2 0.3% (vol/vol) NP-40 10% (vol/vol) glycerol
Glycerol gradient	Gradient solution light	10% glycerol 150 mM KCl 50 mM Tris (pH 7.5) 5mM MgCl2
	Gradient solution heavy	40% glycerol 150 mM KCl 50 mM Tris (pH 7.5) 5mM MgCl2
Calcium phosphate transfection	HEPES (2x)	274 mM NaCl 54.6 mM Hepes 1.5 Na2HPO4

5.1.2 *Oligos*

Table 9. Oligos for qRT-PCR

circGSE1-div-Fw	CCATCCTCCAGCTTTGCCG
circGSE1-div-Rev	GTGAGGGGGTTGACGGTG
circDOPEY2-div-Fw	AGGGATCCTCTTCCGTTTACT
circDOPEY2-div-Rev	AGGGTGAGTGGATAATCTGGAG
circCORO1C-div-Fw	ACATGCCCAAGAGGGGACTT
circCORO1C-div-Rev	CAGCAACACCCCATTGCTAGT
circNRIP1-div-Fw	GCTCAGAGCTTGGAGACAGAC
circNRIP1-div-Rev	GGCTGTGTTTCTCCCAAATGTTAAA
GAPDH Fw	TGGTATCGTGGAAGGACTCATGAC
GAPDH Rev	ATGCCAGTGAGCTTCCCGTTCAGC
circSAMD1-div-fw	GAGGCCAGCACCTTTGAG
circSAMD1-div-rev	GGATATGAGGGTGGGAAGGT
circEMSY-div-fw	TGCAGTAACAGCTGTGGTGTC
circEMSY-div-rev	GAAGAGTTTGTTCGCCTTCG
circASCC1-div-fw	GTACTGGCGAAGTGCTCCAT
circASCC1-div-rev	CCCGTCTTGTCCAGGTTTAG
circBPTFdiv-fw	CTCAGAGCCGAGATCCTGAA
circBPTF-div-rev	GTACCTGCATCTGGGGTGAC
circFAM208A-div-fw	GCAGCCTTTATGAAGTTGTGG
circFAM208A-div-rev	CCTGGAGTTAATGGCTGGAA
circPSD3-div-fw	CCATTGCTTCACAAGATGGA
circPSD3-div-rev	CTCCCCATTTCAGAATGAGC

circRERE-div-fw	TTTGCAGGAATGTGTGATGG
circRERE-div-rev	CACACAAAGCAGGAGTTGGA
circSMO-div-fw	TCCTCACTGTGGCAATCCTT
circSMO-div-rev	TGATGTTCTGCACCTCATTCTC
circOXCT1-div-fw	ACACGTCGATCTGACAATGC
circOXCT1-div-rev	ATGGATGTCTTCTGGAGCAAA
linearRERE-fw	GCAGAGACAGTGAAGAAGTCGG
linearRERE-rev	CTTCTTGGAGCTGGTCCTGTCA
linearSMO-fw	AGGCCAGGAGCTGTCCTTCA
linearSMO-rev	TGATGTTCTGCACCTCATTCTC
linearFAM208A-fw	ATGAGAAAGCTCGCCAAAACCAG
linearFAM208A-rev	GCCTATGGATGTCAGCAATGCC
MYC-fw	CACGTCTCCCACACATCAGCA
MYC-rev	CCAACTTGACCCTCTTGGCA
Tubulin-fw	TTGGCCAGATCTTTAGACCAGACAAC
Tubulin-rev	CCGTACCACATCCAGGACAGAATC
HPRT-fw	GCTATAAATTCTTTGCTGACCTGCTG
HPRT-rev	AATTACTTTTATGTCCCCTGTTGACTGG

Table 10. Oligos for cloning linear RNAs and *in vitro* transcription templates

GSE1 linear full fw	GCATGAGCCATGAGCCCAAGTCC
GSE1 linear full rev	CTCTGGGCTCCTCCGCCTGTTTG
GSE1 T7 Fw	TAATACGACTCACTATAGGGCATGAGCCATGAGCCCAAGTCC
NRIP1 linear full fw	GAAGTGTTTGGATTGTGAGC

NRIP linear full rev	CGTCTGTCTCCAAGCTCTGAG
NRIP T7 fw	TAATACGACTCACTATAGGGGAAGTGTTTGGATTGTGAGC
DOPEY2 linear full fw	CACAACCTCCAAGAGGGAAAAC
DOPEY2 linear full rev	TTTGGTGGTTTTAAAGTAAACGG
DOPEY2 T7 fw	TAATACGACTCACTATAGGGCACAACCTCCAAGAGGGAAAAC
CORO1C linear full fw	AAAAATATGCAGGAACCAATTGC
CORO1C linear full rev	CTGGCAATCTCACATTTGTTAAC
CORO1C linear T7 fw	TAATACGACTCACTATAGGGAAAAATATGCAGGAACCAATTGC

Table 11. Oligos for RNAse H assay

Name	**Sequence**
GSE1 antisense	GGCAAAGCTGGAGGATGG
NRIP1 antisense	GGCTGTGTTTCTCCCAAATGTTAAA
DOPEY2 antisense	AGGGTGAGTGGATAATCTGGAG
CORO1C antisense	CAGCAACACCCCATTGCTAGT

Table 12. Oligos for cloning

Number	**Name**	**Sequence**
1	NotI-DIS3 -Fw	attgcggccgcCTCAAGTCCAAGACGTTCTTAA
2	AscI-DIS3-Rev	attggcgcgccCTATTTTCCAAGCTTCATCTTCT
3	Fse1-APEX1-Fw	cgaggccggccCCGAAGCGTGGGAAAAAGG
4	AscI-APEX1-rev	aatggcgcgccCACAGTGCTAGGTATAGGGTGA
5	FseI-AldoA-Fw	cgaggccggccCCCTACCAATATCCAGCACTG
6	AscI-AldoA-rev	ttaggcgcgccTTAATAGGCGTGGTTAGAGACG
7	FseI-G3BP-Fw	cgaggccggccGTGATGGAGAAGCCTAGTCC

8	AscI-G3BP-Rev	attggcgcgccTCACTGCCGTGGCGCAAGCCC
9	FseI- PPP1R8/ARD1-Fw	cgaggccggccGCGGCAGCCGCGAACTCCGGCT
10	AscI- PPP1R8/ARD1-Rev	aatggcgcgccTCAAATCAGCAAGGAAGGTGTGGG
11	FseI-EXOSC1-Fw	cgaggccggccGCGCCACCTGTGAGATACTG
12	AscI-EXOSC1-Rev	aatggcgcgccTTAGGTCTGCAAGAATTCGGGTTG
13	FseI-EXOSC2-Fw	cgaggccggccGCGATGGAGATGAGGCTTCC
14	AscI-EXOSC2-Rev	aatggcgcgccTTATCCCTCCTGTTCCAAAAGCC
15	FseI-Rrp40/EXOSC3-Fw	cgaggccggccGCCGAACCTGCGTCTGTCGCGGC
16	AscI-Rrp40/EXOSC3-Rev	aatggcgcgccTCAACTTTCTGCCAATCTGGAG
17	FseI-EXOSC10-Fw	cgaggccggccGCGCCACCCAGTACCCGGGAGC
18	AscI-EXOSC10-Rev	aatggcgcgccCTATCTCTGTGGCCAGTTGTACC
19	FseI-DIS3L1-Fw	cgaggccggccCTGCAGAAGCGGGAGAAGGTGC
20	AscI-DIS3L1-Rev	aatggcgcgccTCATATTCCATAATTGTTTGAAAC
21	FseI-EXOSC9-Fw	cgaggccggccAAGGAAACGCCACTCTCAAACTG
22	AscI-EXOSC9-Rev	ttaggcgcgccTTAATTGGCAGCTCTCTTCTTTTTTC
23	FseI-PPP1CA-Fw	cgaggccggccTCCGACAGCGAGAAGCTCAAC
24	AscI-PPP1CA-Rev	ttaggcgcgccCTATTTCTTGGCTTTGGCGG
25	FseI-PPP1CB-Fw	cgaggccggccGCGGACGGGGAGCTGAACGTGG
26	AscI-PPP1CB-Rev	ttaggcgcgccTCACCTTTTCTTCGGCGGATTAG
27	FseI-PPP1CC-Fw	cgaggccggccGCGGATTTAGATAAACTCAAC
28	AscI-PPP1CC-Rev	ttaggcgcgccCTATTTCTTTGCTTGCTTTGTG
29	FseI-PNUTS-Fw	cgaggccggccGGTTCGGGTCCCATAGACCC
30	AscI-PNUTS-Rev	ttaggcgcgccCTAGGGCAGGGGGGGCCCATTG
31	FseI-TOX4-Fw	cgaggccggccGAGTTTCCCGGAGGAAATGAC

32	AscI-TOX4-Fev	ttaggcgcgccCTATTTCACAAACACCACTGTG
33	FseI-WDR82-Fw	cgaggccggccAAGCTGACCGACAGCGTGTTGC
34	AscI-WDR82-Rev	ttaggcgcgccGTTGCCCACCATTGATGACTGA
35	BamHI-DIS3-fw	cgcggatccATGGACTACAAGGACGACGATG
36	XhoI-DIS3-Rev	ccgctcgagCTATTTTCCAAGCTTCATCTTC

Table 13. Oligos for mutagenesis pcr

Number	Name	Sequence
35.1	DIS3-mutD146N-fw	CTAATGACAGGAATAATAGAGCGATTCGAGTAGC
36.1	DIS3-mutD146N-rev	GCTACTCGAATCGCTCTATTATTCCTGTCATTAG
37	DIS3-mutD487N-fw	CCAGGATGTACTGATATAAACGATGCTCTACATTGTC
38	DIS3-mutD487N-rev	GACAATGTAGAGCATCGTTTATATCAGTACATCCTGG
39	DIS3-mutS634A-fw	GAAAAAGGGGCTTTGACTCTATCCGCTCCTGAAGTTCGATTC
40	DIS3-mutS634A-rev	GAATCGAACTTCAGGAGCGGATAGAGTCAAAGCCCCTTTTTC
41	DIS3-mutS634E-fw	GAAAAAGGGGCTTTGACTCTATCCGAGCCTGAAGTTCGATTC
42	DIS3-mutS634E-rev	GAATCGAACTTCAGGCTCGGATAGAGTCAAAGCCCCTTTTTC
43	DIS3-mutS730A-fw	CTTTGGATCAGGCCGAAGCTCCTACTTTTCCATATCTAAACAC
44	DIS3-mutS730A-rev	GTGTTTAGATATGGAAAAGTAGGAGCTTCGGCCTGATCCAAAG
45	DIS3-mutS730E-fw	CTTTGGATCAGGCCGAAGAACCTACTTTTCCATATCTAAACAC
46	DIS3-mutS730E-fw	GTGTTTAGATATGGAAAAGTAGGTTCTTCGGCCTGATCCAAAG

Table 14. Oligos for CRISPR/Cas9

47	DIS3-genomicDNA-fw	CCTGGTGTCTCTTCTGCCTTA
48	DIS3-genomicDNA-rev	CTTCTGCACAGCCATGTAAGA
49	DIS3-intron-guideRNA1-sense	caccGTATTAATAAAGGAATACGT

50	DIS3-intron-guideRNA1-antisense	aaacACGTATTCCTTTATTAATAC
51	DIS3 -intron-guideRNA2-sense	caccGATTAGCAAAATTCGGGAGA
52	DIS3-intron-guideRNA2-antisense	aaacTCTCCCGAATTTTGCTAATC

Table 15. Northern blot probes

Name	**sequence**
circGSE1 junction probe	GGGGACTTGGGCTCATGGCTCATGCCTCTGGGCTCCTC CGCCTGTTTGGC
circNRIP1 junction probe	GAAATAGCTCACAATCCAAACACTTCCGTCTGTCTCCA AGCTCTGAGCC
circDOPEY2 junction probe	GTTTTCCCTCTTGGAGGTTGTGTTTGGTGGTTTTAAAGT AAACGG
circCORO1C junction probe	CAATTGGTTCCTGCATATTTTTCTGGCAATCTCACATTT GTTAAC
5.8S rRNA precursor probe 1	GAGGCACCCCCGGGGCGATTGATC
5.8S rRNA precursor probe 2	CCGCCACCCGACGCGTGACCA
5.8S rRNA precursor probe 3	GGCAAGAGGAGGGCGGACGCCGCCGGGTCTGCGCTTA
5.8S rRNA precursor probe 4	GCGATTGATCGGCAAGCGA
5.8S rRNA	CGACGCACGAGCCGAGTGATCCACCGC
U6	GAATTTGCGTGTCATCCTTGCGCAGGGGCCATGCTAA
7sk	ACTCGTATACCCTTGACCGA
7sl	ATCAGCACGGGAGTTTTGACCTGCTCCGTTTCCGACCT GGGCCGGTTCAC

5.1.3 *Plasmids*

Table 16. Plasmids available in the lab

Name	**Description**
Modified pIRES-neo-VP5-Flag/HA-FA	Expression of protein N-terminally fused to Flag-HA
VP5-Flag/HA-FA/GFP	Produced by Dr. Thomas and Dr. Nora Treiber (AG Meister)
VP5-Flag/HA-FA/DIS3L2	Produced by Thomas and Nora Treiber (AG Meister)

pcDNA5-FRT/TO	Inducible expression vector designed for use with the Flp-In™ T-REx™ System
pSpCas9(BB)-2A-Puro (PX459)	Cas9 from S. pyogenes with 2A-Puro, and cloning backbone for sgRNA (V2.0)
pSpCas9(BB)-2A-GFP (PX458)	Cas9 from S. pyogenes with 2A-EGFP, and cloning backbone for sgRNA

Table 17. Cloned Plasmids

Name	Source/plasmid backbone	Cloning oligos	Cloning method
VP5-Flag/HA-FA-DIS3	VP5-Flag/HA-FA	1,2	PCR amplification from cDNA and cloning into VP5-Flag/HA-FA with NotI/AscI
VP5-Flag/HA-FA-DIS3 D146N	VP5-Flag/HA-FA	35.1,36.1	Quick change pcr from VP5-Flag/HA-FA-DIS3
VP5-Flag/HA-FA-DIS3 D487N	VP5-Flag/HA-FA	37,38	Quick change pcr fromVP5-Flag/HA-FA-DIS3
VP5-Flag/HA-FA-DIS3 D146N+D487N	VP5-Flag/HA-FA	35.1,36.1	Quick change pcr from VP5-Flag/HA-FA-DIS3 D487N
VP5-Flag/HA-FA-DIS3 S634A	VP5-Flag/HA-FA	39,40	Quick change pcr from VP5-Flag/HA-FA-DIS3
VP5-Flag/HA-FA-DIS3 S634E	VP5-Flag/HA-FA	41,42	Quick change pcr from VP5-Flag/HA-FA-DIS3
VP5-Flag/HA-FA-DIS3 S730A	VP5-Flag/HA-FA	43,44	Quick change pcr from VP5-Flag/HA-FA-DIS3
VP5-Flag/HA-FA-DIS3 S730E	VP5-Flag/HA-FA	45,46	Quick change pcr from VP5-Flag/HA-FA-DIS3
VP5-Flag/HA-FA-APEX1	VP5-Flag/HA-FA	3,4	Pcr amplification from cDNA and cloning into VP5-Flag/HA-FA with FseI/AscI
VP5-Flag/HA-FA-AldoA	VP5-Flag/HA-FA	5,6	Pcr amplification from cDNA and cloning into VP5-Flag/HA-FA with FseI/AscI
VP5-Flag/HA-FA-G3BP	VP5-Flag/HA-FA	7,8	Pcr amplification from cDNA and cloning into VP5-Flag/HA-FA with FseI/AscI
VP5-Flag/HA-FA-PPP1R8/ARD1	VP5-Flag/HA-FA	9,10	Pcr amplification from cDNA and cloning into VP5-Flag/HA-FA with FseI/AscI
VP5-Flag/HA-FA-EXOSC1	VP5-Flag/HA-FA	11,12	Pcr amplification from cDNA and cloning into VP5-Flag/HA-FA with FseI/AscI
VP5-Flag/HA-FA-EXOSC2	VP5-Flag/HA-FA	13,14	Pcr amplification from cDNA and cloning into VP5-Flag/HA-FA with FseI/AscI
VP5-Flag/HA-FA-Rrp40/EXOSC3	VP5-Flag/HA-FA	15,16	Pcr amplification from cDNA and cloning into VP5-Flag/HA-FA with FseI/AscI

VP5-Flag/HA-FA-EXOSC10	VP5-Flag/HA-FA	17,18	Pcr amplification from cDNA and cloning into VP5-Flag/HA-FA with FseI/AscI
VP5-Flag/HA-FA-DIS3L1	VP5-Flag/HA-FA	19,20	Pcr amplification from cDNA and cloning into VP5-Flag/HA-FA with FseI/AscI
VP5-Flag/HA-FA-EXOSC9	VP5-Flag/HA-FA	21,22	Pcr amplification from cDNA and cloning into VP5-Flag/HA-FA with FseI/AscI
VP5-Flag/HA-FA-PPP1CA	VP5-Flag/HA-FA	23,24	Pcr amplification from cDNA and cloning into VP5-Flag/HA-FA with FseI/AscI
VP5-Flag/HA-FA-PPP1CB	VP5-Flag/HA-FA	25,26	Pcr amplification from cDNA and cloning into VP5-Flag/HA-FA with FseI/AscI
VP5-Flag/HA-FA-PPP1CC	VP5-Flag/HA-FA	27,28	Pcr amplification from cDNA and cloning into VP5-Flag/HA-FA with FseI/AscI
VP5-Flag/HA-FA-PNUTS	VP5-Flag/HA-FA	29,30	Pcr amplification from cDNA and cloning into VP5-Flag/HA-FA with FseI/AscI
VP5-Flag/HA-FA-TOX4	VP5-Flag/HA-FA	31,32	Pcr amplification from cDNA and cloning into VP5-Flag/HA-FA with FseI/AscI
VP5-Flag/HA-FA-WDR82	VP5-Flag/HA-FA	33,34	Pcr amplification from cDNA and cloning into VP5-Flag/HA-FA with FseI/AscI
pcDNA5-FRT/TO-DIS3	pcDNA5-FRT/TO	36,37	Pcr amplification from VP5-Flag/HA-FA-DIS3 and cloning into pcDNA5-FRT/TO with BamHI/XhoI
pcDNA5-FRT/TO-DIS3-D146N	pcDNA5-FRT/TO	36,37	Pcr amplification from VP5-Flag/HA-FA-DIS3 D146N and cloning into pcDNA5-FRT/TO with BamHI/XhoI
PX459-intron guideRNA1	PX459	49,50	Oligos annealing and cloning into PX459 with BbsI according to Zhang lab cloning protocol
PX459-intron guideRNA1	PX459	51,52	Oligos annealing and cloning into PX459 with BbsI according to Zhang lab cloning protocol

5.1.4 *Antibodies*

Table 18. Antibodies

Antibody	Origin	properties	Source	Dilution
HA	Mouse	Monoclonal	Covance (Princeton, Usa)	1:1000
α-tubulin	Mouse	Polyclonal	Sigma Aldrich (Munich, Germany)	1:10000
β-tubulin	Rabbit	Monoclonal	Abcam (Cambridge UK)	1:1000
GAPDH	Rabbit	Polyclonal	Santa Cruz Biotechnology (Dallas, USA)	1:500
β-actin	Mouse	Monoclonal	Abcam (Cambridge, UK)	1:10000
Lamin A/C	Rabbit	Polyclonal	Santa Cruz Biotechnology (Dallas, USA)	1:1000
NONO	Mouse	Monoclonal	BD Bioscience (San Jose, USA)	1:1000
EXOSC3	Rabbit	Polyclonal	Bethyl laboratories (Mongomery,Texas, USA)	1:1000
EXOSC9	Mouse	Monoclonal	Proteintech Group, Europe (Manchester)	1:20000
EXOSC10	Rabbit	Polyclonal	Proteintech Group, Europe (Manchester)	1:1000
DIS3	Rabbit	Polyclonal	Bethyl laboratories (Mongomery,Texas, USA)	1:1000
PPP1CA	Mouse	Monoclonal	Proteintech Group, Europe (Manchester)	1:5000
PPP1R10	Rabbit	Polyclonal	Proteintech Group, Europe (Manchester)	1:1000
Goat-anti-rabbit 680		Secondary antibody	Li-Cor Biosciences (Lincoln, USA)	1:15000
Goat-anti-rabbit 800		Secondary antibody	Li-Cor Biosciences (Lincoln, USA)	1:15000
Goat-anti-mouse 680		Secondary antibody	Li-Cor Biosciences (Lincoln, USA)	1:15000
Goat-anti-mouse 800		Secondary antibody	Li-Cor Biosciences (Lincoln, USA)	1:15000
Goat-anti-rat 680		Secondary antibody	Li-Cor Biosciences (Lincoln, USA)	1:15000
Goat-anti-rat 800		Secondary antibody	Li-Cor Biosciences (Lincoln, USA)	1:15000

5.1.5 *Cell lines and bacteria strand*

Table 19. Cell lines and bacteria strand

Cell line	Description	Growth medium
HEK293T	Originally referred as 293tsA1609neo, is a highly transfectable derivative of human embryonic kidney 293 cells and contains the SV40 T-antigen.	DMEM
Flp-In™ T-REx™ 293	Derived from 293 human embryonic kidney cells and contains pFRT⁄lacZeo and pcDNA™6⁄TR (from the T-REx™ System) stably integrated. Used to rapid generate stable cell lines with homogenous expression of the protein of interest.	DMEM
Bacteria strand	**Description**	**Antibiotic Resistance**
XL1-Blue	endA1 gyrA96(nalR) thi-1 recA1 relA1 lac glnV44 F'[::Tn10 proAB+ $lacI^q$ Δ(lacZ)M15] hsdR17(rK-mK+)	Ampicillin

5.2 Methods

5.2.1 *Cell based methods*

5.2.1.1 Mammalian cells and grown

HEK 293 cells were maintained under standard culture conditions with Dulbecco's modified Eagle's medium DMEM plus 10% FBS, 1% Penicillin/Streptomycin (P/S) antibiotics mix at 37°C and 5% CO2.

Flp-In™ T-REx™-293 cell lines were cultivated in DMEM medium supplemented with 10% FBS, 1% P/S, 100 μg/ml Zeocin and 15 μg/ml blasticidin.

Stable Flp-In™ T-REx™-293 expression cell lines were cultivated in DMEM medium supplemented with 10% FBS, 1% P/S, 100-200 μg/ml hygromycin B and 15 μg/ml blasticidin.

5.2.1.2 Preparation of whole cell extracts

A confluent 15cm plate of cells was washed with cold 1xPBS. Using a cell scraper, the cells were detached from the plate and transferred into a reaction tube. The cells were then centrifuged at 500 x g for 5 min at 4°C. The cell pellet was thoroughly resuspended in 1 ml of IP lysis buffer (25 mM Tris-HCl, pH 7.4, 150 mM KCl, 0.5 % NP-40, 2 mM EDTA, 1 mM NaF). After incubating for 20 minutes on ice, the sample was centrifuged at full speed for 20 minutes at 4°C. The supernatant was then subjected to immunoprecipitation experiments or directly loaded onto a SDS gel.

5.2.1.3 Preparation of subcellular extracts

For nuclear and cytoplasmic fractionation, an adapted protocol from Gagnon et al. was used (Gagnon et al., 2014). 15 cm confluent HEK293T cell plates were washed with 1 x PBS and trypsinazed. To remove any clumps, the cell suspension was passed through a cell strainer and washed again with cold PBS. After centrifugation at 100g for 5 min, the cell pellet was resuspended by gently pipetting with 1ml of ice-cold Hypotonic Lysis Buffer (HLB) for every 75 mg of cells or every 10 million of cells and incubated on ice for 8 min. Afterwards the cell suspension was centrifuged at 800 g at 4° for 8 min. The supernatant that corresponds to the cytoplasmic fraction was transferred to a new tube. The pellet that correspond to the nuclear fraction was washed for four time with HLB by pipetting gently and centrifuging at 200 g for 2 min at 4°. The nuclei pellet was then resuspended in 0,5 ml Nuclear Lysis Buffer (NLB) for every 75mg of cells or every 10 million of cells. If necessary, the nuclei suspension was additional sonicated on ice 1-3 times at 20% power for 15s. Cytoplasmic and nuclear fractions were centrifuged at 15000g for 15 min at 4° and the supernatants were transferred in new tubes.

5.2.1.4 Cell transfection with calcium phosphate

HEK 293T cells were transfected using calcium phosphate. Per 15 cm plate, 10 µg DNA and 123 µl of 2 M CaCl2 were filled up to 1 ml with water in a reaction tube. Afterwards, 1 ml of 2x HEPES were added dropwise into the DNA-containing solution. The mixture was incubated for 10 minutes at room temperature and then added to the cells. The cells were harvested after 24-28 hours. Per 10 cm plate, half of the reagents were used.

5.2.1.5 Cell transfection with Lipofectamin 2000

Plasmid transfection was conducted with Lipofectamine 2000 according to the supplier's protocol. 800.000 cells were seeded into 6-wells plates in DMEM media without antibiotics. 2,5 µg of the

plasmid of interest was added to 250 µl of Opti-MEM. In a second tube, 5 µl of Lipofectamine 2000 was added into 250 µl of Opti-MEM. The mixture was incubated at RT for 5 mins. After incubation, both tubes were mixed together and incubated at room temperature for further 15 minutes. 500 µl of the mixture was added drop-by-drop to the cells. 24 hours post-transfection, the medium was removed and replaced with 2ml of fresh DMEM with 10% FBS and 1% PS. The cells were incubated for 16 hours.

5.2.1.6 Generation of stable cell lines

For generation of stable mammalian cell lines, we used The Flp-In™ T-REx™ System that exhibits tetracycline-inducible expression of a gene of interest from a specific genomic location. Stable Flp-In™ T-REx™-293 were generated by cotransfection of pcDNA™5/FRT/TO expression construct of the gene of interest and the Flp recombinase vector, the pOG44 plasmid. The cells were transfected in 6 well-plates with Lipofectamine 2000 according to the supplier's protocol. One day after, the cells were splitted in 10 cm plates and selected using hygromycin B (100-200 µM). Single hygromycin-resistant, blasticidin-resistant foci were isolated and expanded to generate individual clonal cell lines. The positive clones were tested for the expression of the protein of interest by induction with tetracycline. Tetracycline was added to the final concentration of 1 µM and the cells were incubated for 24 hours at 37° before harvesting. The expression of the protein of interest was verified by Western Blot. The clones were maintained in the same medium as used for selection.

5.2.1.7 Generation of CRISPR-Cas9 Knockout cell lines

For generation of CRISPR-cas9 Knockout cell lines, we used the Flp-In T-Rex HEK293 stable cell lines previously described. 150000 T-Rex HEK293 cells were plated the day before transfection in 12 well-plates in DMEM without antibiotics. The cells were transfected with 1 µg of puromycin resistant px459 plasmid expressing two guide RNAs using the lipofectamine 2000, according to the manufactur's protocol. 24hr post-transfection, the medium was removed and replaced with complete medium containing 6 µg/ml puromycin for selection. After one day, the medium was replaced with DMEM in order to make recovery the resistant cells. When the cells were confluent, a second forward transfection was performed followed by another puromycin selection. The cells were then manually sorted one cell per well into 96-well plates. Single colony were expanded and tested for knockout by genomic PCR and western blotting.

5.2.2 *RNA based methods*

5.2.2.1 RNA extraction

RNA extraction from mammalian cells was done with TRIzol reagent (Life Technologies, Carlsbad, USA) or NucleoSpin RNA Kit (Macherey-Nagel, Düren, Germany) following the manufacturer's protocol. After isolation, RNA was resuspended and stored in H2O. RNA concentration and quality for qPCR from cells and mouse tissues was determined using NanoDrop 1000 Spectrophotometer (Thermo Scientific, Rockford, USA). RNA quality for Northern Blot was additionally checked by nucleic acid staining of gels before Northern Blot in TBE supplemented with 5 µl/100ml ethidium bromide. For MOPS Agarose, RNA was stained with 2,3 µl EtBr (400µg/ml) each sample before loading into Agarose gel. RNA for deep sequencing RNA-seq was analysed using Bioanalyzer 2100 (Agilent Technologies, Santa Clara, USA).

5.2.2.2 Phenol/chloroform RNA extraction

Phenol/chloroform RNA extraction was used to purify the RNA of interest from reactin mixtures. The reaction volume was always adjusted to 200 µl by adding nuclease free water. The RNA was extracted with 1:1 volume (200 µl) of Roti®-phenol/chloroform/isoamyl alcohol solution. The simples were mixed vigorously and centrifuged for 10 min at 17,000 rcf. The aqueous phase was collected and transferred in a new tube. The RNA was precipitated o/n at -20 °C by adding 3 volume of 100% ethanol, 1 µl of glycogen as carrier and 0.1 volume of 3M Sodium acetate. The RNA pellet was collected by full-speed centrifugation at 4 °C for 30 min. The supernatant was discarded, and the pellet was washed twice with 1 ml 70% ethanol. The air-dried RNA pellet was resuspended in water.

5.2.2.3 Denaturing Polyacrylamide gel electrophoresis (PAGE)

SequaGel UreaGel system (National Diagnostics, Atlanta, USA) was used to prepare polyacrylamide urea gels for electrophoresis of RNA. For linear and circular RNA and for small RNA detection, 6 % gels were prepared by mixing 14,4 ml concentrate, 39,6 ml diluent and 6 ml 10x TBE buffer with 50 µl TEMED and 500 µl 10 % APS. After polymerization for at least 1 h, gels were pre-run at 400 V for 20 min in TBE buffer prior to loading of RNA. Gel pockets were rinsed directly before loading to remove the excess of urea. 5 to 20 µg RNA were mixed with 2x RNA sample buffer, heated for 2-3 min at 95 ◦C and loaded. Electrophoresis was performed in 1x TBE buffer at 400 Voltage. For linear and circular RNA detection, gels were run at 400 V until xylene cyanol reaches about 1 cm from pocket bottom. In 6 % gels, bromophenol blue migrates at about 26 nt and xylene cyanol at about 106

nt. No further marker for RNA length determination was used. Disassembled gels were ethidium bromide stained and used for Northern Blot or to isolated RNA bands.

5.2.2.4 Denaturing Agarose gel electrophoresis

For preparing agarose gels, 1% of agarose was dissolved in water by heating. Once cooled down to 65°C approximately, 1x MOPS buffer and 2% Formaldehyde (37%) were added. After polymerization, the gels were pre-run for 15-30 minutes at 70 V in 1x MOPS buffer. 10 µl of 2x RNA loading dye were mixed with 10 µl of 20 µg of RNA samples, heated for 10 min at 65 °C and put on ice. 3 µl of EtBr (400 µg/ µl) were added directly into the samples before loading into the gels. The gels were run at 70 V until the bromophenol blue reaches about 4 cm above the end of the gel.

5.2.2.5 Northern Blot: Semidry transfer of RNA from Urea PAGE

After disassembling polyacrylamide urea gels, RNA was blotted semi-dry onto a Hybond-N membrane (GE Healthcare, Little Chalfont, UK). The blot was done at 20 V for 30 min using H2O as transfer buffer. RNA was subsequently chemically crosslinked using EDC crosslinking solution for 1 h at 50 ◦C.

5.2.2.6 Northern Blot: Capillary transfer of RNA from agarose gels

After disassembling, agarose gels were washed in 50mM NaOH for 30 minutes, in 50mM Tris pH 7.5 for 30 minutes and in 20xSSC for 30 minutes. RNA was transferred onto a Hybond-N membrane by capillary transfer. A glass plate was put on two trays filled with 20XSSC. Two strips of Whatman paper were wetted with 2xSSC and laid over the plate in order that both ends were hanging into 20XSSC. The gel was put on the wet strips with the upper side down. A pre-cut Hybond-N membrane was soaked into Milli-Q water and into 2xSSC. The membrane was put exactly on the gel. After removing all bubbles, three 2xSSC-wetted pieces of Whatman paper of the size of the gel were placed on the membrane. A stack of towel papers was put on top with a second glass plate and an additional weight of 500 g. The transfer was set at room temperature overnight, preferably for 18 hours. The transfer was checked UV light. The RNA was crosslinked to the membrane using the UV Stratalinker at 254 nm.

After crosslinking, the membrane was pre-hybridized in a cylindrical bottle containing 20-30ml of hybridization solution and placed, in which the membrane and then placed in a hybridization oven at 42-60oC for 60 minutes.

5.2.2.7 Northern Blot: 32P-Labeling of probes

DNA oligonucleotides, which were used as Northern blot probes, were labelled by incubating 20 pmol of the oligonucleotides with 20 µCi of γ-32P-ATP (HARTMANN ANALYTIC GmbH, Braunschweig, Germany) and 0.5 U/µl T4 PNK in 1X PNK buffer A (Thermo Fisher Scientific Inc.) in a total volume of 20 µl. Following 30-60 min incubation at 37°C, the reaction was stopped by adding 30 µl of a 30 mM EDTA solution (pH 8.0). Unincorporated nucleotides were separated on a G-25 column (GE Healthcare) according to the manufacturer's instructions.

The cDNA probes were prepared using Megaprime DNA-Labelling Systems kit (Amersham). Afterward, the reaction was stopped with 5 µl of 200 mM EDTA. The cDNA probes were purified using the Illustra MicroSpin G-25.

The DNA probes were directly added to the prehybridized membranes and incubated o/n at 50 °C on a turning wheel with about 50 ml of hybridization solution. The cDNA probes were denatured by heating at 95 °C for 5 min and then immediately placed on ice for 5 min. The DNA probes were directly added to the prehybridized membranes and incubated o/n at 60 °C on a turning wheel with about 50 ml of hybridization solution.

5.2.2.8 Northern Blot: wash and detection

The membrane labelled with DNA probes was washed twice with Northern Blot wash solution 1 and once with Northern Blot wash solution 2. Each wash was performed in a turning wheel at 50 °C for 10 min.

The membrane labelled with cDNA probes was washed once with Northern Blot wash solution 3, once with Northern Blot wash solution 4 and once with Northern Blot wash solution 5. Each wash was performed in a turning wheel at 60. Liquid was discarded and membrane was wrapped in saran for exposure. Signals were detected either by exposure to a Imaging Screen-K (Kodak, Rochester, USA) and read out with Personal Molecular Imager System (Bio-Rad, Hercules, USA).

5.2.2.9 In vitro transcription

In vitro transcriptions of the linear RNAs were performed from PCR amplified DNA with the T7 promoter sequence. *In vitro* transcriptions were performed in 500 µl reaction volumes containing 1 µg DNA, 0.1 mg/ml self-made T7 RNA polymerase, 1x T7 reaction buffer, 25 mM MgCl2, 10 mM each NTP and 2 U/ml thermostable inorganic pyrophosphatase (England Biolabs Inc.) for 4 h or o/n at 37°C. Afterwards, the reaction was digested with 1 µl of 1U/unit DNase I (Thermo Scientific) for

15 mins at 37 °C. *In vitro* transcribed RNAs were purified by PAGE on a 6% polyacrylamide urea gel and precipitated. The RNAs were then dissolved in water.

5.2.2.10 Dephosphorylation of RNA

Dephosphorylation of *in vitro* transcribed RNAs was performed in 100 µl reaction volumes containing 10 µg RNA, 2.5µl of 10U/µl Alkaline Phosphatase, Calf Intestinal (CIP) (England Biolabs Inc.) and 1µl RiboLock RNase Inhibitor (Thermo Fisher Scientific Inc.). The reaction was carried out for 1hr at 37°C. The dephosphorylated RNAs were extracted by phenol-chloroform, precipitated with ethanol-ammonium acetate and resuspended in 30 µl of water.

5.2.2.11 32P-Labeling of RNA

10 µl (about 3µg RNA) of the previous dephosphorylated RNAs were labelled with 20 µCi of γ-32P-ATP and 2 µl T4 PNK in 1X PNK buffer A supplemented with 1 µl RiboLock in a total volume of 20 µl. The reaction was performed at 37°C and stopped by adding 30 µl of a 30 mM EDTA solution (pH 8.0). Unincorporated nucleotides were separated on a G-25 column (GE Healthcare) according to the manufacturer's instructions. The labelled RNAs were additionally purified by phenol-chloroform extraction, precipitated with ethanol-ammonium acetate and resuspended in 30 µl of water.

5.2.2.12 In vitro circularization of RNAs

32-Labelled linear RNA was denaturated at 75 °C for 3 minutes in the presence of 10% dimethyl sulfoxide (DMSO) and slowly cooled down to 16 °C. The ligation was performed in 100 µl reaction volumes containing 5 µl T4 RNA ligase, 10mM ATP, 1X T4 RNA ligase buffer and 1 µl RiboLock o/n at 16 °C. Reaction products were resolved in 6% polyacrylamide urea gels. The circular RNA gel bands were eluted in 300 µl of elution buffer containing 300mM Nacl and 2mM o/n at 4 °C with shaking. Circular RNAs were precipitated with ethanol and resuspended in water.

5.2.2.13 RNA degradation assays

In vitro enzymatic degradation assays were performed in 20 µl reaction volumes containing 10mM Tris-HCl pH 8.0, 75 mM NaCl, and 1 mM 2-mercaptoethanol with $MnCl_2$ at final concentration of 3mM or $MgCl_2$ at final concentration 0.5 mM. 1 Bq/cm^2 of 32-labelled linear or circular RNAs and purified recombinant or 20µl resin-immobilized immunoprecipitated proteins were used. Reaction mixtures were incubated at 37 °C for the indicated durations and stopped with the addiction of 1

volume of 2x RNA sample buffer supplemented with 20mM EDTA. Reactions products were resolved in in 6% denaturing polyacrylamide urea gels.

5.2.2.14 RNase R treatment

50ng of purified linear or circular RNA were treated with or without 0.1 U RNase R (Epicentre) in 10 µl 1x RNase R reaction volume for 20 min at 37 °C. After the addition of 2x RNA sample buffer, RNA was separated by 6% denaturing polyacrylamide gel and detected by northern blotting.

5.2.2.15 RNase H treatment

RNase H assays were performed in 15 µl total reaction volume. 100 ng of purified linear or circular RNA and 1 µl of 10 µM antisense oligonucleotide were heat denaturated 2 min at 95 °C, 2 min at 75 °C and slowly cooled down at 37 ° C. 1x RNase H buffer was added followed by incubation at 37 °C for 20 min. 2.5 U RNase H (Thermo Fisher) was added followed by incubation for an additional 40 min. After the addition of 2x RNA sample buffer, RNA was separated by 6% denaturing polyacrylamide gel and detected by northern blotting.

5.2.2.16 Half-life experiments

To determine RNA decay rates, cells were treated with actinomycin D (10 µg/mL final concentration) and collected at the indicated time points. RNA was extracted and determined by Northern blotting.

5.2.2.17 RT-PCR assays

Total RNA was preferentially extracted using NucleoSpin RNA Kit (Macherey-Nagel, Düren, Germany). 1 µg RNA was used for cDNA synthesis using First Strand cDNA Synthesis Kit (Thermo Scientific, Rockford, USA). Divergent primers were designed to specific span the circular splicing junction. For semiquantitative RT-PCR, PCR products were resolved in 2% agarose gels. For splice site analysis and mapping, PCR product were gel purified and sequenced.
Quantitative Real time PCR was carried out using SsoFast EvaGreen (Bio-Rad) or the Takyon Mix (Eurogentec) on the CFX96 Touch Real-Time PCR Detection System (Bio-Rad). The relative expression level of circular RNA and linear RNA was normalized to GAPDH and calculated by the ΔΔCt method.

5.2.2.18 Sequencing library preparation

The rRNA-depleted RNA library was prepared from total RNA using Universal RNA-Seq with NuQuant® (TECAN) according to manufacturer's protocol. Specifically, 100 ng of total RNA spiked with ERCC RNA Spike was used. CDNA libraries were sequenced on an Illumina NovaSeq 600 S1 in 200 cycle runs (2x100bp).

5.2.3 *Protein based methods*

5.2.3.1 Determination of protein concentration

The protein concentration of cell lysates was determined by a Bradford Protein Assay (Biorad) according to the relative protocol (Bradford, 1976). Briefly, 1 µl of protein sample was diluted in 1 ml of Roti®-Quant solution (Carl Roth GmbH + Co. KG), the resultant blue colour was measured at 595 nm.

5.2.3.2 Immunoprecipitation (IP)

Anti-FLAG M2 agarose beads (Sigma-Aldrich) was used for IP of FLAG/HA-tagged proteins overexpressed in HEK293T cells. For each immunoprecipitation one 1 or 2 dishes (150 mm diameter) were lysed on ice in 1 ml IP lysis buffer and 30 µl of Anti-FLAG M2 beads were washed twice with 1 ml PBS. Lysates were centrifugated full speed at 4 °C for 20 minutes and the supernatants were transferred in new tubes. Input samples were collected, supplemented with LDS sample buffer, heated at 95 °C for 5 mins and store and at -20 °C. The lysate was added to the beads and incubated at 4 °C under rotation for 2-3 h. The beads were centrifuged for 1 min at 1,000 g and the supernatant was discarded. The beads were washed four times with 1ml IP wash buffer and once with 1ml ice cold PBS. After the first washing step, the beads were transferred to new reaction tubes to minimize contamination by unspecific protein binding to the tube material. The beads were resuspended in 100 µl of PBS or degradation buffer. A 20 µl aliquot was taken for western blot analysis.

5.2.3.3 SDS-PAGE

Protein were resolved on 10 or 12% SDS PAGE gels. NuPAGE® 4-12% Bis-Tris Gel (Invitrogen, Life Technologies) was used for samples prepared for Mass Spec. The proteins were visualized with Coomassie. 50-100 µg proteins or 1/5 total IP simples were mixed with 5x Laemmeli buffer, heated at 95 °C for 5 mins and loaded onto self-made SDS-PAGE gels. Gels were run in SDS-running buffer

at constant voltage of 180V for about 2 hours until the bromophenol blue reached the bottom of the gel.

5.2.3.4 Comassie staining

SDS-gels were immersed in a Coomassie staining solution and shaked for 30-60 min. The gels were washed and transferred in destaining solution for 4-24 hours. Bands started to appear in 1-2 hours. It was destained until background was clear.

5.2.3.5 Western Blot

The proteins were transferred onto an Amersham Hybond-ECL membrane (GE Healthcare) by electro-blotting. The transfer was carried in Towbin buffer for 1 min/kDa constant at 1 mA/cm2. The membrane was blocked in TBS containing 0.1% Tween20 and 5% milk powder and subsequently incubated with the primary antibody overnight at 4°C. After three washing steps with TBS containing 0.1% Tween 20, the secondary antibody was added for 1 hour at RT. After three washing steps with TBS containing 0.1% Tween 20, the membrane was scanned on a LI-COR reader.

5.2.3.6 Ammonium sulfate precipitation

5ml cytoplasm lysates (5x 150 mm diameter plates) were transferred in a baker containing a stirrer bar and placed at 4 C° on a magnetic stirrer. While the samples were stirring, a saturated solution of Ammonium Sulfate (AS) was added slowly and drop by drop to bring the final concentration of 20%, 30% and 50% saturation based on the tables of *Wood, 1996*. Once the total volume of AS was added, the beakers were stirring for 30 min at 4 °C. The samples were then centrifuged at about 10000 g for 10 min. The pellets represented the 20%, 30% and 50% saturated AS pellets and were dissolved in 500 µl PBS. The volume of the corresponding supernatants was determined and again a AS saturated solution was added slowly with rapid mixing to raise each to 10 % or 20 % higher level of saturation. The samples were stirred for 30 min at 4 °C and centrifuged at about 10000 g for 10 min. The pellets were the 20-30%, 30-50% and 50-70% saturated AS cuts. Like before, the pellets were dissolved in PBS and dialysed overnight using kit. The different AS saturated fractions were tested for *in vitro* RNA degradation assays with the addition of 5mM ATP and 7.5 mM MgCl2.

5.2.3.7 Glycerol density gradient

A 10 % and 40% glycerol solutions were prepared with 150 mM KCl, 50mM Tris/HCl pH 7.5 and 5mM MgCl2. About 6 ml of 10% glycerol solution was add to a 14x89mm Beckman polyallomer

ultracentrifuge tube. About 6ml of 40% glycerol solution was added beneath the 10% glycerol solution using a syringe with long needle. 10-40% glycerol gradient was prepared using the Bio Comp Gradient Master instrument (long cap, 10-40% Glycerol v/v). About 500 µl of sample was load by gently pipetting onto the top of the gradient. The gradient was run on a SW41 rotor in a pre-cooled Beckman Optima L Series ultracentrifuge with this setting conditions: minimum acceleration; no brake; 4 °C; 40000 RPM; 18 hr. When the run was completed, fractions of about 500-700 µl were collected by gently pipetting in circles and were tested for enzymatic degradation assays with the addition of 5mM ATP and 7.5 mM MgCl2.

5.2.3.8 Mass-spectrometric analyses

Gel bands were excised and transferred into 2ml micro tubes (Eppendorf) and washed:

- 1 hr min with 50 mM NH4HCO3,
- 1 hr with 50 mM NH4HCO3/ acetonitrile (3/1)
- 30 min with 10 mM NH4HCO3/ acetonitrile (1/1)
- 10 min with Acetonitrile

The gels samples were lyophilized for 30min/1hr.

Free cysteines were reduced with 200 µl 1mg/ml DTT solved in 50 mM NH4HCO3 (57 °C/ 35 min) and carbamidomethylated with 200 µl 5 mg/ml Iodoacetamide (RT/ 35 min) solved in 50 mM NH4HCO3. Gel slices were washed again and lyophilized. Proteins were subjected to in-gel tryptic digest overnight at 37 °C with 0,04 µg/µl Trypsin Gold mass spectrometry grade (Promega) solved in 50mM NH4HCO3. The For the elution step, the supernatant of the tryptic digest was collected. The remaining gel slices were eluted once with 50 mM NH4HCO3 (37°C/ 300rpm/ 1hr) and another time with 50 mM NH4HCO3/ acetonitrile (1/1). The 3 eluates were combined togheter and lyophilized. Further processing was executed by Dr. Astrid Bruckmann or Eduard Hochmuth.

5.2.4 *DNA Based Methods*

5.2.4.1 Determination of nucleic acid concentration

The concentration and purity of DNAs and RNAs were determined by measuring the absorbance of 1-2 µl of the samples with the Nanodrop® ND-1000 spectrophotometer (Thermo Fisher Scientific Inc).

5.2.4.2 Genomic DNA extraction

For screening of CRISPR/Cas9 knockout clones, genomic DNA (gDNA) was extracted from human cell lines. Confluent cells from 6-well plates were pelleted by centrifugation at 500 g for 5 min, 4°C. The cell pellet was resuspended in 500 µl Proteinase K buffer and incubated o/n at 50°C. 400 µl isopropanol was added and the mixture was incubated for 1 h at -20°C. The sample was centrifuged for 15 min at full speed and the supernatant was discarded. The pellet was washed once with 1 ml 70% ethanol. The gDNA pellet was air-dried and dissolved in 100 µL H_2O by shaking at 500 rpm o/n at 37°C.

5.2.4.3 Polymerase Chain Reaction (PCR)

Amplification of DNA fragments was performed with the Phusion™ High-Fidelity (HF) DNA Polymerase (Thermo Fisher Scientific Inc.) according to the manufacturer's instruction and with the primers listed. The standard PCR reaction mixture consisted of the following components:

Components	**Volume [µl]**
HF/GC Phusion Buffer (5x)	10
Primer forward (10 µM)	2.5
Primer reverse (10 µM)	2.5
dNTPs (10 µM)	1
DMSO	1.5
Phusion Polymerase (2 U/µL)	0.5
Template	250 ng genomic DNA or 50 ng plasmid DNA or 1 µl cDNA
H_2O	up to 50

PCRs were performed with the following cycling conditions, whereby the annealing temperature was determined for each primer pair with the Tm calculator tool (Thermo Fisher Scientific Inc.):

Step	**Temperature**	**Time**	
Initialization	98 °C	30 s	
Denaturation	98 °C	10 s	30-35 cycles
Annealing	variable (52 – 65 °C)	30 s	
Elongation	72 °C	30s/kb	
Final elongation	72 °C	10 min	
Store	4 °C	∞	

PCR products were resolved on 0.5-2% (w/v) agarose gels by electrophoresis in 1X TBE buffer. The gels contained 0.1 µg/ml EtBr for the visualization of the DNA under UV light. When required, bands

of the correct size were excised from the gel and the DNA was extracted with the NucleoSpin®-Extract kit (MACHEREY-NAGEL GmbH & Co. KG) according to the manufacturer's protocol.

5.2.4.4 Site-directed mutagenesis (quick change)

Point-mutations were introduced to plasmids using primers (with the desired mutation) that amplifies the entire plasmid template. The parent template was removed using the restriction enzyme DpnI, a methylation-dependent endonuclease.

The PCR reaction and cycling conditions for quick change are listed below:

Components	**Volume [µl]**
HF/GC Phusion Buffer (5x)	10
Primer forward (10 µM)	1
Primer reverse (10 µM)	1
dNTPs (10 µM)	1
DMSO	1.5
Phusion Polymerase (2 U/µL)	0.5
Template	50 ng plasmid DNA
H_2O	up to 50

Step	**Temperature**	**Time**	
Initialization	98 °C	30 s	
Denaturation	98 °C	10 s	18 cycles
Annealing	55°	30 s	
Elongation	72 °C	1min/kb	
Final elongation	72 °C	10 min	
Store	4 °C	∞	

5.2.4.5 Agarose gel electrophoresis

DNA fragments were resolved on 0.8-2% (w/v) agarose gels by electrophoresis in 1X TBE buffer. The gels contained 0.1 µg/ml EtBr for the visualization of the DNA under UV light. If required, bands of the correct size were excised from the gel and the DNA was extracted with the NucleoSpin®-Extract kit (MACHEREY-NAGEL GmbH & Co. KG) according to the manufacturer's instruction.

5.2.4.6 Molecular Cloning-Restriction Digest of DNA and Dephosphorylation of Linearized Vectors

Restriction digest of purified PCR products (ca. 500ng) or plasmid DNA (ca. 5 µg) was performed for >1h at 37°C with the FastDigest™ restriction enzyme system (Thermo Fisher Scientific Inc.) in a reaction volume of 30 µl. To prevent re-ligation of empty plasmid, the 5' ends of the linearized

plasmid DNA were dephosphorylated with the FastAP thermosensitive alkaline phosphatase (Thermo Fisher Scientific Inc.) according to the manufacturer's instruction. Digested PCR fragments were directly purified with the NucleoSpin®-Extract kit (MACHEREY-NAGEL GmbH & Co. KG). Digested plasmids were first run on agarose gel electrophoresis and then purified with NucleoSpin®-Extract kit.

5.2.4.7 DNA Insert and Vector Ligation

DNA fragments were ligated into linearized, dephosphorylated vectors using the T4 DNA ligase (Thermo Fisher Scientific Inc.). For standard cloning, 3 insert : 1 vector molar ratio was used. The amount of insert necessary for the reaction was calculated with the formula:

$$ng\ (Insert) = ng\ (Vector) \times 4\ \times \frac{length\ (Insert)}{length\ (Vector)}$$

Ligation was performed with the following conditions:

Component	**Volume [µL]**
T4 DNA Ligase Buffer (10x)	1
T4 DNA Ligase (5 U/µL)	1
Plasmid DNA	50/100 ng)
Insert DNA	variable
H_2O	up to 10

The reaction mixture was incubated at room temperature (RT) for at least 1 h or overnight (o/n).

5.2.4.8 Transformation and cultivation of E. coli

Chemically competent *E. coli* XL1-Blue cells were used for molecular cloning. Bacteria cells were transformed with plasmids by heat-shock method. Briefly, 50 µl of thawed suspension cells were gently mix with the appropriate amount of plasmids or ligation reaction. The mixture of competent cells/DNA was incubated for 20 min on ice. The cells were exposed to heat shock for 45s at 42° and placed back on ice for 5 minutes. 1ml of LB medium without antibiotics was added to the transformed cells followed by growth at 37° in a shaking incubator for at least 30 min. This recovery phase can be omitted if the antibiotic selection is ampicillin (Amp). The bacteria cells were centrifuged at 5000 rcf and resuspended in 100 µl of LB medium. The bacteria were plated on LB-Agar plates containing

an appropriate selection antibiotic. LB plates were incubated overnight at 37°. The following day, single colonies were picked and shaken at 37° overnight into 5 ml of LB medium with the appropriate antibiotic.

5.2.4.9 Extraction of Plasmid DNA from E. coli and Test Digest

Plasmid DNA were isolated from *E. coli* with NucleoSpin Plasmid kit (Macherey-Nagel) and resuspended in 30 µl of water. Prior to sequencing, a test digest with restriction enzymes was performed in order to verify that the vector backbone and the insert were of the expected sizes. About 5 µl of the purified Plasmid DNA was digested using the FastDigest™ restriction enzyme system (Thermo Fisher Scientific Inc.) in a reaction volume of 20 µl and run on agarose gel. Positive clones were verified by Sanger sequencing.
NucleoBond®-Xtra-Midi kit (MACHEREY-NAGEL GmbH & Co. KG) was used for transfection-grade plasmid DNA. In this case, 150-200 ml of overnight culture was prepared.

6 Supplementary Data

6.1 Supplemental Figures

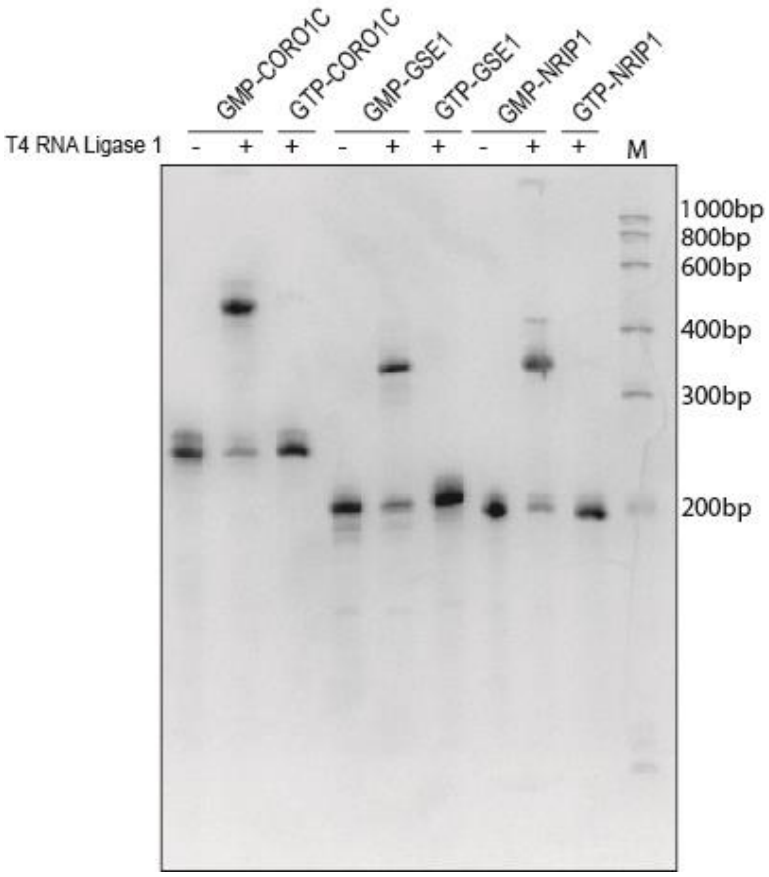

Supplemental Figure 1. *In vitro* circularization was analyzed by 6% denaturing polyacrylamide gel electrophoresis (PAGE). RNAs were synthesized by *in vitro* transcription under excess of GMP and ligated by T4 RNA ligase I. Two different controls were used: the ligation assay without enzyme (-GMP) and the triphosphorylated RNAs with enzyme (GTP +). No circular signal can be observed in the controls.

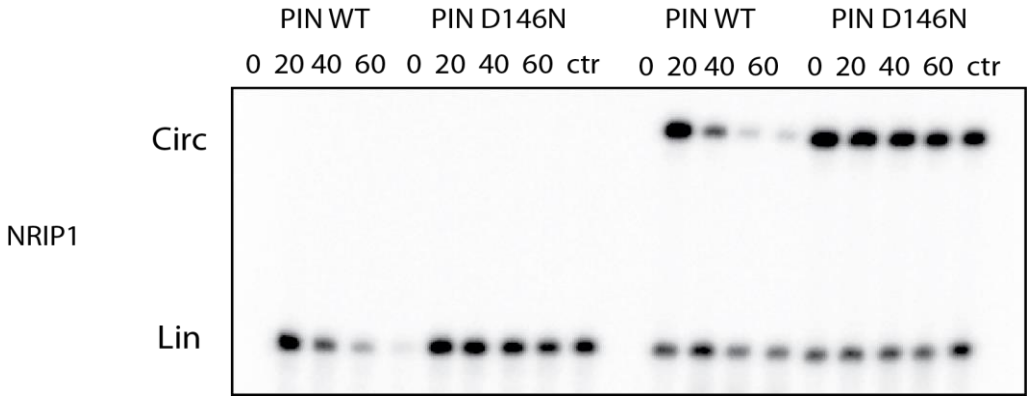

Supplemental Figure 2. Gel-electrophoresis analysis generated by the incubation of labelled linear and circular NRIP with different versions of human DIS3 PIN domain at different time points.

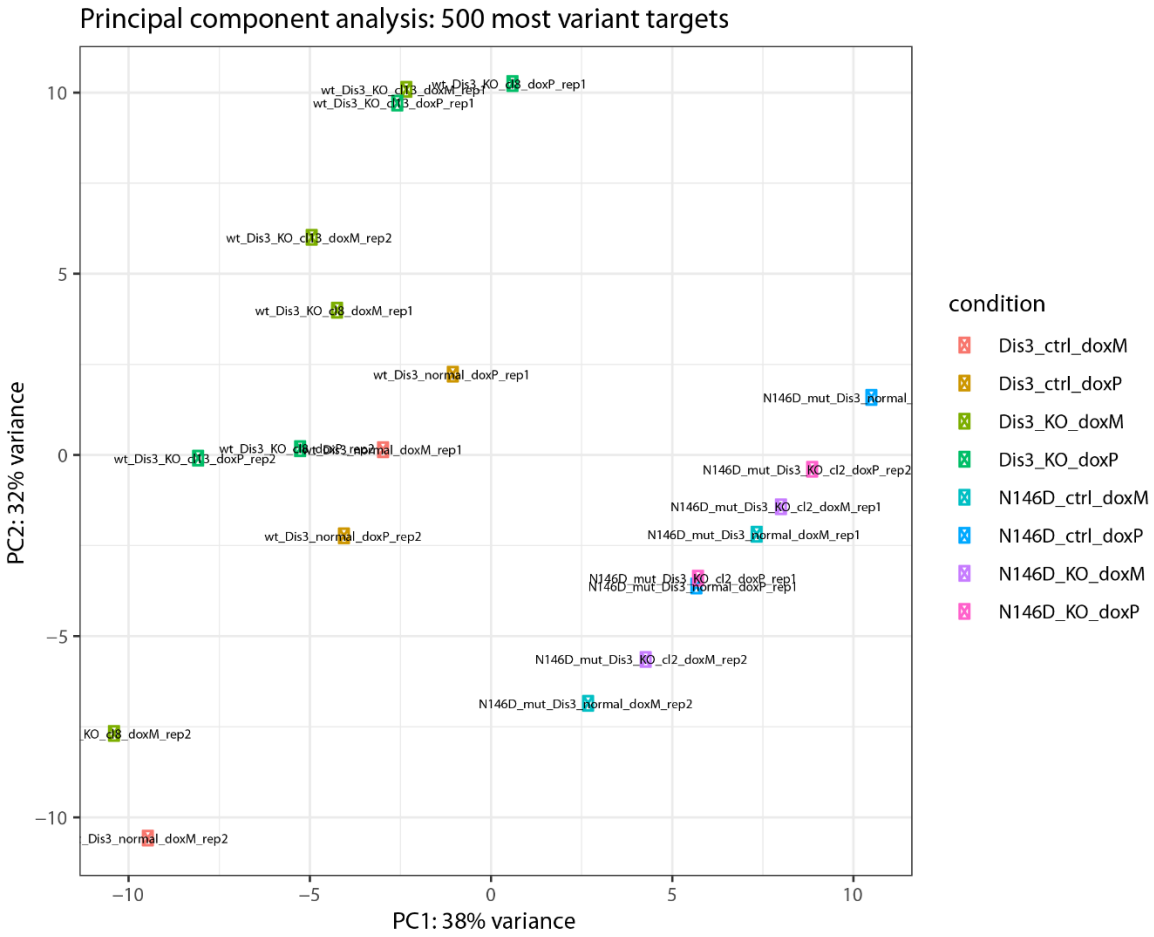

Supplemental Figure 3. Principle component analysis (PCA) of all libraries prepared for deep sequencing from our CRISPR/knockout model. DoxM: Dox (-). DoxP: Dox (+). Analysis performed by Gerhard Lehmann.

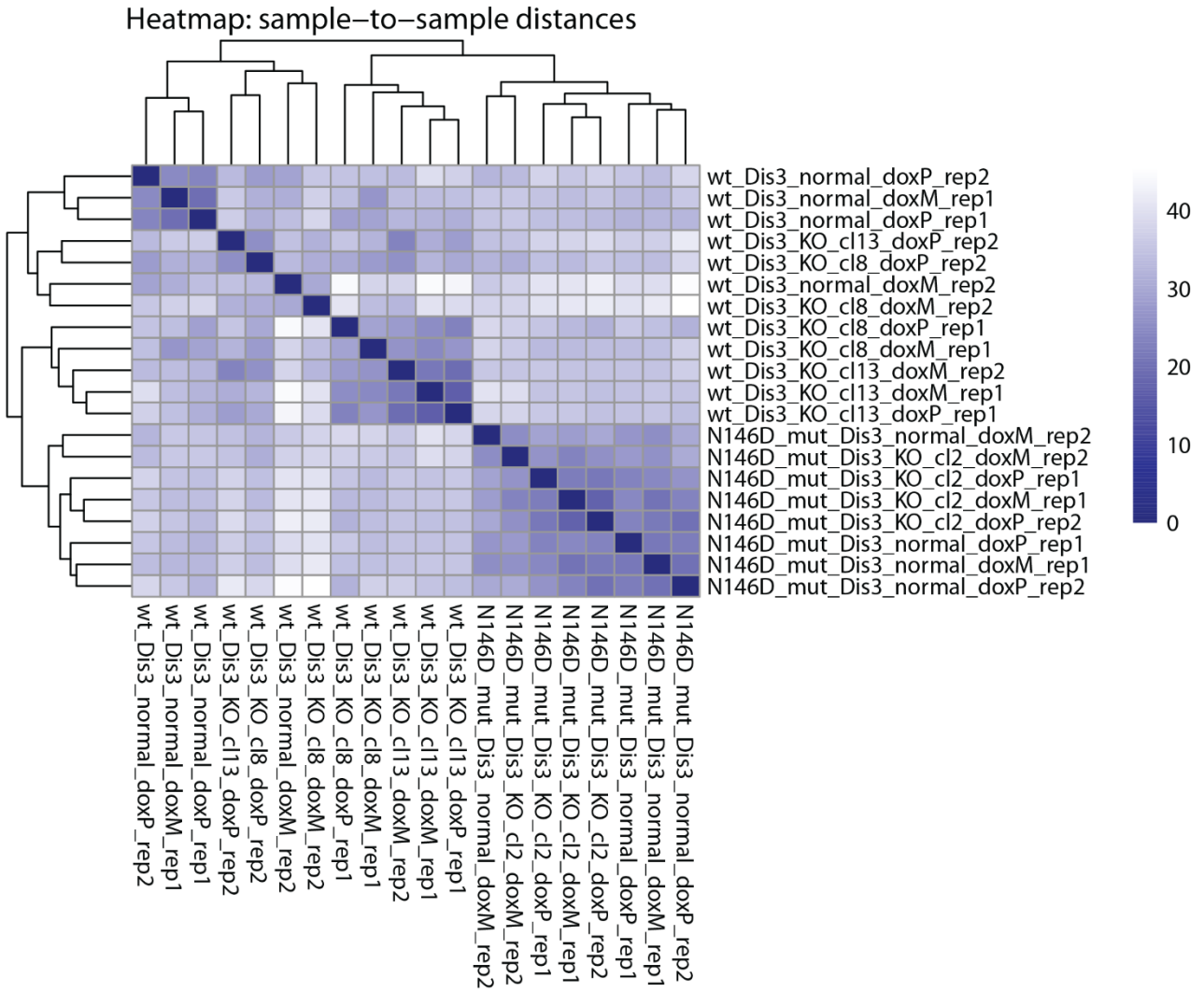

Supplemental Figure 4. Distance plot of all libraries prepared for deep sequencing from our CRISPR/knockout model. DoxM: Dox (-). DoxP: Dox (+). Analysis performed by Gerhard Lehmann.

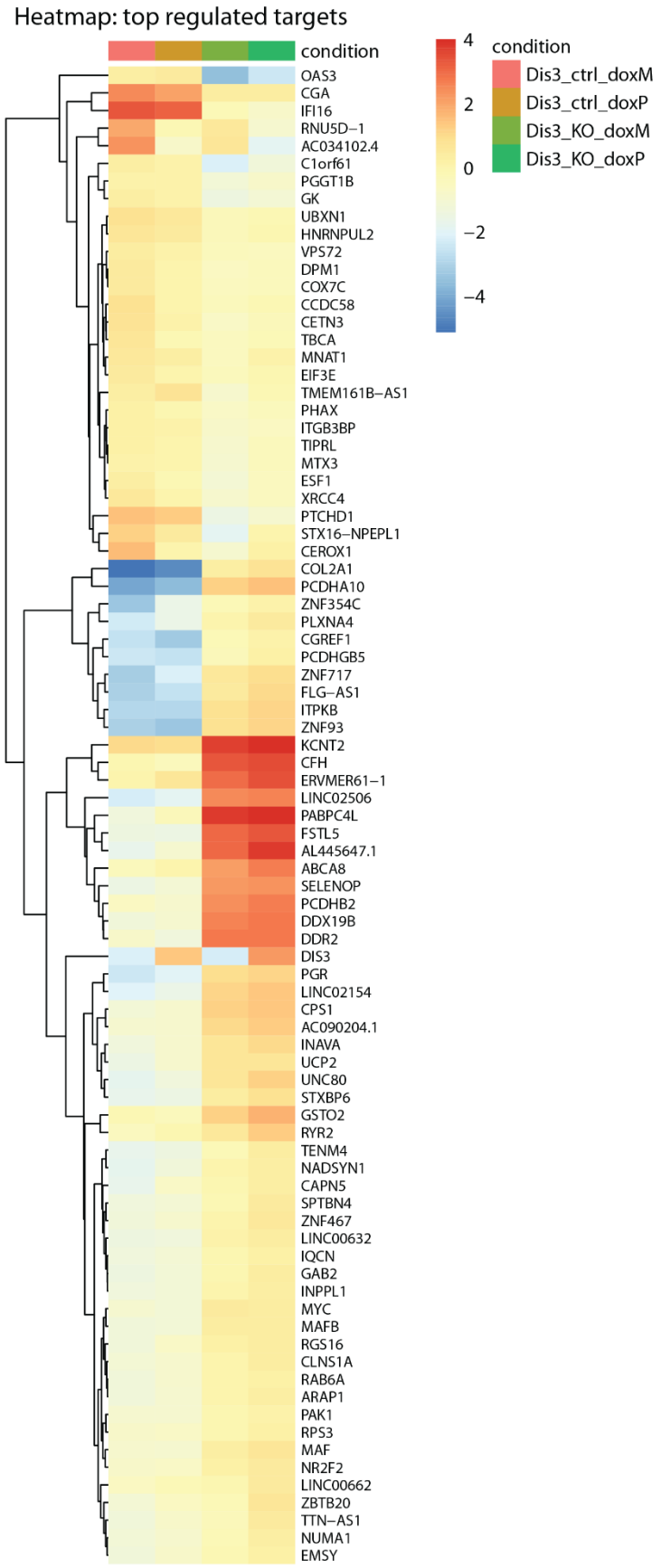

Supplemental Figure 5. Heatmap of most variant linear RNAs from deep sequencing data of DIS3 WT control vs DIS3 WT KO. DoxM: Dox (-). DoxP: Dox (+). Analysis performed by Gerhard Lehmann.

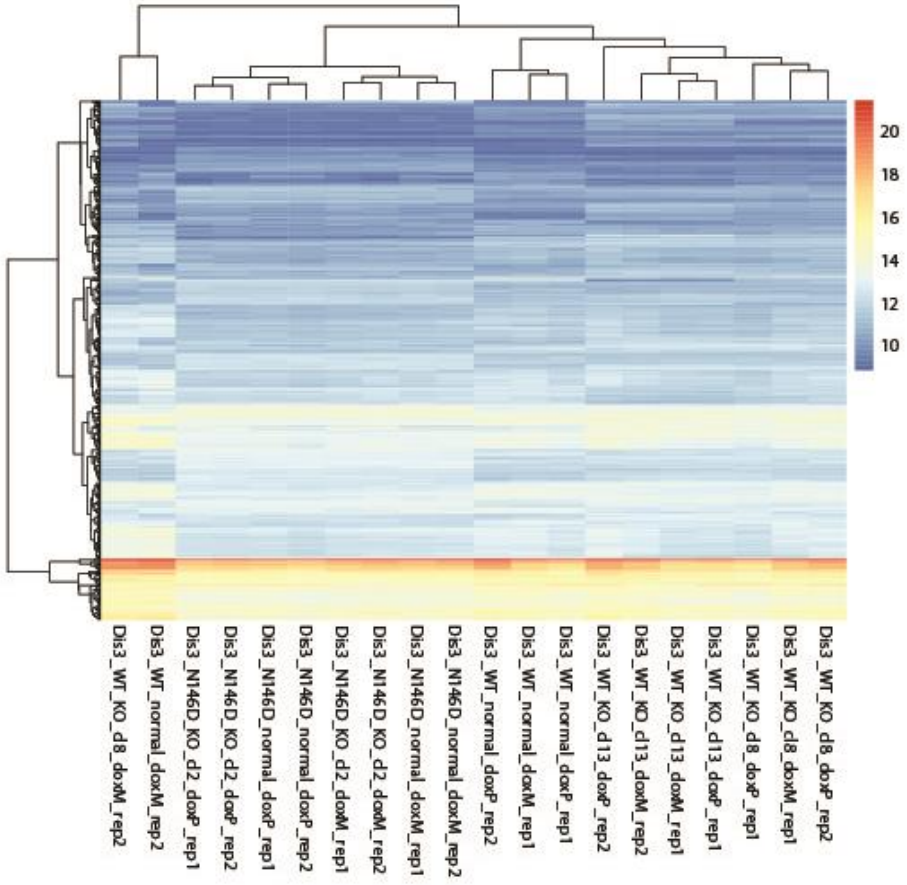

Supplemental Figure 6. Clustering of the 500 most variable genes for all sequencing samples. Analysis performed by Petar Glazar from Nikolaus Rajewsky lab.

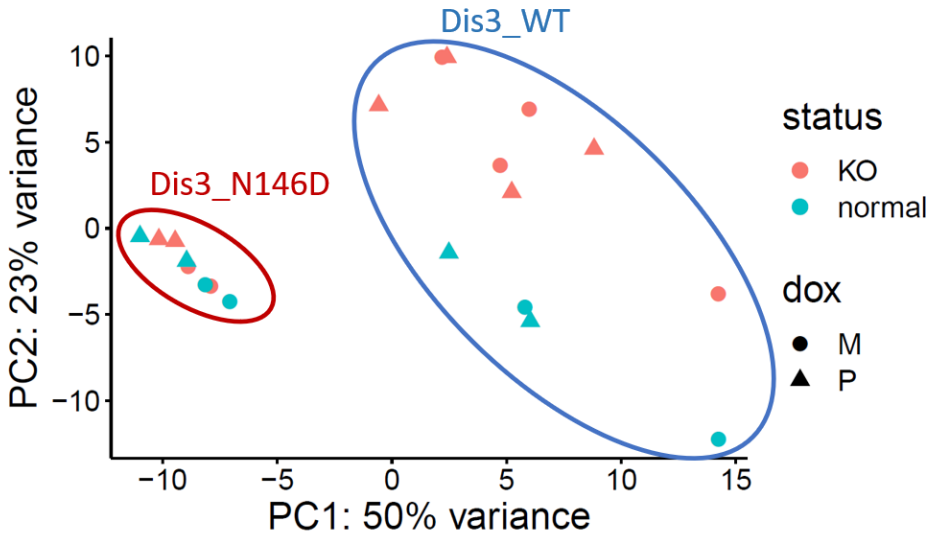

Supplemental Figure 7. Principle component analysis (PCA) of all sequencing samples. WT DIS3 simples and D146N DIS3 simples are represented by red and blue circle respectively. Analysis performed by Petar Glazar from Nikolaus Rajewsky lab.

6.2 Supplemental Tables

Supplemental Table 1. Summary of the endoribonuclease candidates found by mass spec.

Accession	Gene	Description	MW [kDa]	Scores	#Peptides	SC [%]
sp|Q9Y2L1|RRP44_HUMAN	DIS3	Exosome complex exonuclease RRP44	108.9	180.5	5	7.5
sp|P04075|ALDOA_HUMAN	ALDOA	Fructose-bisphosphate aldolase A	39.4	686.6	8	34.9
sp|Q13283|G3BP1_HUMAN	G3BP1	Ras GTPase-activating protein-binding protein 1	52.1	403.3	9	28.8
sp|Q12972|PP1R8_HUMAN	PPP1R8	Nuclear inhibitor of protein phosphatase 1	38.5	87.4	2	10.8
sp|P27695|APEX1_HUMAN	APEX1	DNA-(apurinic or apyrimidinic site) lyase	35.5	87.0	2	10.1
sp|P39748|FEN1_HUMAN	FEN1	Flap endonuclease 1	42.6	132.9	3	12.4

Supplemental Table 2. Information regarding the deep sequencing of rRNA-depleted transcriptome libraries (part 1).

Sample	**total_reads**	**perc_ mapped genome**	**perc_uniq**	**perc_multi**	**perc_ unmapped genome**
DIS3_N146D_KO_cl2_doxM_rep1	72511325	95.8	83.97	11.83	4.2
DIS3_N146D_KO_cl2_doxM_rep2	78727881	94.48	86.74	7.74	5.52
DIS3_N146D_KO_cl2_doxP_rep1	57236136	95.19	84.81	10.38	4.81
DIS3_N146D_KO_cl2_doxP_rep2	68444356	94.92	85.39	9.53	5.08
DIS3_N146D_normal_doxM_rep1	61415321	94.92	84.71	10.21	5.08
DIS3_N146D_normal_doxM_rep2	117989742	95.34	86.69	8.65	4.66
DIS3_N146D_normal_doxP_rep1	66809867	95.36	86	9.35	4.64
DIS3_N146D_normal_doxP_rep2	70203584	96.23	89.91	6.32	3.77
DIS3_WT_KO_cl13_doxM_rep1	86197716	96.29	86.41	9.88	3.71
DIS3_WT_KO_cl13_doxM_rep2	81980183	95.91	86.75	9.16	4.09
DIS3_WT_KO_cl13_doxP_rep1	94499228	95.43	86.61	8.81	4.57
DIS3_WT_KO_cl13_doxP_rep2	90603268	96.2	83.23	12.98	3.8
DIS3_WT_KO_cl8_doxM_rep1	79357152	96.06	80	16.06	3.94

DIS3_WT_KO_cl8_doxM_rep2	63611309	96.13	78.26	17.87	3.87
DIS3_WT_KO_cl8_doxP_rep1	87293909	95.5	89.15	6.35	4.5
DIS3_WT_KO_cl8_doxP_rep2	82676878	94.86	85.93	8.94	5.14
DIS3_WT_normal_doxM_rep1	88522526	96.22	81.34	14.88	3.78
DIS3_WT_normal_doxM_rep2	71192084	96.09	76.63	19.46	3.91
DIS3_WT_normal_doxP_rep1	87565801	95.92	87.62	8.3	4.08
DIS3_WT_normal_doxP_rep2	80952303	95.97	86.63	9.33	4.03

Supplemental Table 3. Information regarding the deep sequencing of rRNA-depleted transcriptome libraries (part 2).

sample	**n_mapped_ genome**	**n_ genes**	**n_ circRNAs**	**circRNA_ reads**	**rRNA%**
DIS3_N146D_KO_cl2_doxM_rep1	69463121	41206065	1378	22220	8.83
DIS3_N146D_KO_cl2_doxM_rep2	74381962	42505343	1030	28915	4.49
DIS3_N146D_KO_cl2_doxP_rep1	54483155	35517936	592	19579	7.57
DIS3_N146D_KO_cl2_doxP_rep2	64964276	40266089	1652	21082	6.43
DIS3_N146D_normal_doxM_rep1	58293588	34258678	1244	19722	7.01
DIS3_N146D_normal_doxM_rep2	112493340	61083388	890	50520	5.4
DIS3_N146D_normal_doxP_rep1	63708595	41550145	1018	31395	6.3
DIS3_N146D_normal_doxP_rep2	67556168	44640633	2208	28223	3.6
DIS3_WT_KO_cl13_doxM_rep1	83004089	55261669	2282	30410	6.88
DIS3_WT_KO_cl13_doxM_rep2	78624182	46961041	2391	39498	5.41
DIS3_WT_KO_cl13_doxP_rep1	90176113	55355220	2592	37289	5.57
DIS3_WT_KO_cl13_doxP_rep2	87163137	45542337	1256	35945	8.53
DIS3_WT_KO_cl8_doxM_rep1	76233154	45112340	3386	52650	12.51
DIS3_WT_KO_cl8_doxM_rep2	61151210	30421939	912	42910	11.62
DIS3_WT_KO_cl8_doxP_rep1	83368626	51040076	1984	21683	3.61
DIS3_WT_KO_cl8_doxP_rep2	78430262	43676787	1406	38172	5.58
DIS3_WT_normal_doxM_rep1	85178137	50697963	2713	39125	11.32
DIS3_WT_normal_doxM_rep2	68407813	32913192	827	36693	12.6
DIS3_WT_normal_doxP_rep1	83993050	52941379	2496	38196	5.22

DIS3_WT_normal_doxP_rep2	77688652	42126989	2022	36731	5.38

Supplemental Table 4. Summary of the circRNA candidates from the sequencing data.

circRNA (gene)	lenght (bp)	circRNA ID	position
SAMD11	353	hsa_circ_0009189	chr1:935772-939412
OXCT1	516	hsa_circ_0004873	chr5:41794003-41807438
SMO	727	hsa_circ_0001742	chr7:129205203-129206587
EMSY	537	not annoted	chr11:76463821-76472840
ASCC1	277	hsa_circ_0018736	chr10:72196811-72203524
BPTF	1227	hsa_circ_0000798	chr17:67945409-67948306
FAM208A	1037	hsa_circ_0001315	chr3:56660731-56673725
RERE	708	hsa_circ_0009117	chr1:8495063-8614686
PSD3	448	hsa_circ_0004458	chr8:18799295-18804898

Supplemental Table 5. Mass spectrometry data: top proteins identified exclusively in the cytoplasm from Flag IP DIS3 (HEK293T).

Number	**Accession**	**Gene**	**Description**	**Score**	**Peptides**	**SC %**
1	sp|Q9Y2L1|RRP44_HUMAN	DIS3	Exosome complex exonuclease RRP44	13331.8	146	79.4
2	**sp|O14744|ANM5_HUMAN**	**PRMT5**	**Protein arginine N-methyltransferase 5**	**5420.9**	**67**	**73.8**
3	**sp|Q9BQA1|MEP50_HUMAN**	**WDR77**	**Methylosome protein 50**	**2180.9**	**29**	**93.6**
4	**sp|Q9BRS2|RIOK1_HUMAN**	**RIOK1**	**Serine/threonine-protein kinase RIO1**	**1794.9**	**31**	**37.0**
5	sp|Q9BVA1|TBB2B_HUMAN	TUBB2B	Tubulin beta-2B chain OS=Homo sapiens	1564.2	29	55.7
6	sp|P60709|ACTB_HUMAN	ACTB	Actin, cytoplasmic 1 OS=Homo sapiens	1370.1	18	46.1
7	sp|P46020|KPB1_HUMAN	PHKA1	Phosphorylase b kinase regulatory subunit alpha, skeletal muscle isoform	1025.0	23	26.6
8	sp|P68366|TBA4A_HUMAN	TUBA4A	Tubulin alpha-4A chain	992.0	19	47.1
9	sp|Q15750|TAB1_HUMAN	TAB1	TGF-beta-activated kinase 1 and MAP3K7-binding protein 1	974.1	17	45.0
10	sp|Q93079|H2B1H_HUMAN	HIST1H2BH	Histone H2B type 1-H	895.7	12	27.0
11	sp|P29144|TPP2_HUMAN	TPP2	Tripeptidyl-peptidase 2	890.4	21	21.8

12	sp|P19474|RO52_HUMAN	TRIM21	E3 ubiquitin-protein ligase TRIM21	872.5	17	35.2
13	**sp|P54105|ICLN_HUMAN**	**CLNS1A**	**Methylosome subunit pICln**	**855.9**	**15**	**59.5**
14	sp|Q93100|KPBB_HUMAN	PHKB	Phosphorylase b kinase regulatory subunit beta	849.3	21	28.6
15	sp|Q13509|TBB3_HUMAN	TUBB3	Tubulin beta-3 chain OS=Homo sapiens OX=9606 GN=TUBB3 PE=1 SV=2	837.8	16	29.3
16	sp|Q9Y4E8|UBP15_HUMAN	USP15	Ubiquitin carboxyl-terminal hydrolase 15	807.4	20	30.1
17	sp|Q9P219|DAPLE_HUMAN	CCDC88C	Protein Daple	778.5	17	12.6
18	sp|Q9P2R3|ANFY1_HUMAN	ANKFY1	Rabankyrin-5	737.7	16	18.7
19	**sp|Q13464|ROCK1_HUMAN**	**ROCK1**	**Rho-associated protein kinase 1**	**705.8**	**17**	**16.2**
20	sp|P46019|KPB2_HUMAN	PHKA2	Phosphorylase b kinase regulatory subunit alpha, liver isoform	694.3	19	18.2
21	sp|P35573|GDE_HUMAN	AGL	Glycogen debranching enzyme	693.3	17	14.7
22	sp|Q9Y2H1|ST38L_HUMAN	STK38	Serine/threonine-protein kinase 38-like	660.3	15	34.7
23	sp|O95071|UBR5_HUMAN	UBR5	E3 ubiquitin-protein ligase UBR5	655.0	14	7.3
24	sp|O43318|M3K7_HUMAN	MAP3K7	Mitogen-activated protein kinase kinase kinase 7	646.4	14	27.2
25	sp|P15735|PHKG2_HUMAN	PHKG2	Phosphorylase b kinase gamma catalytic chain, liver/testis isoform	579.1	12	36.0
26	sp|P14625|ENPL_HUMAN	HSP90B1	Endoplasmin	555.9	11	18.4
27	sp|Q99460|PSMD1_HUMAN	PSMD1	26S proteasome non-ATPase regulatory subunit 1	547.8	11	13.3
28	sp|O43242|PSMD3_HUMAN	PSMD3	26S proteasome non-ATPase regulatory subunit 3	497.0	12	26.8
29	sp|O00231|PSD11_HUMAN	PSMD11	26S proteasome non-ATPase regulatory subunit 11	479.7	9	29.1
30	sp|Q15057|ACAP2_HUMAN	ACAP2	Arf-GAP with coiled-coil, ANK repeat and PH domain-containing protein 2	471.8	10	15.0
31	sp|P62195|PRS8_HUMAN	PSMC5	26S proteasome regulatory subunit 8	445.1	10	32.0
32	sp|P26640|SYVC_HUMAN	VARS	Valine--tRNA ligase	432.8	10	11.2
33	sp|P18669|PGAM1_HUMAN	E2F7	Phosphoglycerate mutase 1	426.4	9	44.5
34	sp|Q96AV8|E2F7_HUMAN	PGAM1	Transcription factor E2F7	421.7	10	13.7
35	sp|A6NCN2|KR87P_HUMAN	KRT87P	Putative keratin-87	421.4	7	24.7
36	sp|P23526|SAHH_HUMAN	AHCY	Adenosylhomocysteinase	398.2	8	22.7
37	sp|P35998|PRS7_HUMAN	PSMC2	26S proteasome regulatory subunit 7	394.8	9	21.9
38	sp|P23381|SYWC_HUMAN	WARS	Tryptophan--tRNA ligase, cytoplasmic	384.0	9	24.8

39	sp|P10644|KAP0_HUMAN	PRKAR1A	cAMP-dependent protein kinase type I-alpha regulatory subunit	367.4	8	28.3
40	sp|P48594|SPB4_HUMAN	SERPINB4	Serpin B4	367.0	9	24.6
41	sp|P22234|PUR6_HUMAN	PAICS	Multifunctional protein ADE2	361.7	7	22.8
42	sp|Q7Z353|HDX_HUMAN	HDX	Highly divergent homeobox	357.1	7	13.3
43	sp|Q9Y6Y0|NS1BP_HUMAN	IVNS1ABP	Influenza virus NS1A-binding protein	355.4	8	17.9
44	sp|P49321|NASP_HUMAN	NASP	Nuclear autoantigenic sperm protein	354.0	9	15.2
45	sp|Q9P1Y5|CAMP3_HUMAN	CAMSAP3	Calmodulin-regulated spectrin-associated protein 3	349.3	9	10.9
46	sp|P62333|PRS10_HUMAN	PSMC6	26S proteasome regulatory subunit 10B	344.9	7	30.1
47	sp|Q12931|TRAP1_HUMAN	TRAP1	Heat shock protein 75 kDa, mitochondrial	342.4	7	13.5
48	sp|Q14697|GANAB_HUMAN	GANAB	Neutral alpha-glucosidase AB	342.3	9	13.0
49	sp|P29401|TKT_HUMAN	TKT	Transketolase	341.8	9	21.3
50	sp|Q9Y6A5|TACC3_HUMAN	TACC3	Transforming acidic coiled-coil-containing protein 3	330.8	7	14.8
51	sp|P50395|GDIB_HUMAN	GDI2	Rab GDP dissociation inhibitor beta	314.7	7	22.5
52	sp|P00491|PNPH_HUMAN	PNP	Purine nucleoside phosphorylase	309.3	7	31.5
53	sp|Q15181|IPYR_HUMAN	PPA1	Inorganic pyrophosphatase	290.3	7	30.4
54	sp|P51665|PSMD7_HUMAN	PSMD7	26S proteasome non-ATPase regulatory subunit 7	288.6	7	28.4
55	sp|P22392|NDKB_HUMAN	NME2	Nucleoside diphosphate kinase B	282.9	7	47.4
56	sp|P43686|PRS6B_HUMAN	PSMC4	26S proteasome regulatory subunit 6B	274.2	6	27.0
57	sp|Q9UNM6|PSD13_HUMAN	PSMD13	26S proteasome non-ATPase regulatory subunit 13	271.3	6	25.3
58	sp|P48556|PSMD8_HUMAN	PSMD8	26S proteasome non-ATPase regulatory subunit 8	264.2	6	19.7
59	sp|P27824|CALX_HUMAN	CANX	Calnexin	255.4	7	14.2
60	sp|P35606|COPB2_HUMAN	COPB2	Coatomer subunit beta'	244.1	7	9.8
61	sp|O00232|PSD12_HUMAN	PSMD12	26S proteasome non-ATPase regulatory subunit 12	243.4	6	16.2
62	sp|Q15008|PSMD6_HUMAN	PSMD6	26S proteasome non-ATPase regulatory subunit 6	231.3	6	17.2
63	**sp|Q9ULX3|NOB1_HUMAN**	**NOB1**	**RNA-binding protein NOB1**	**65.2**	**2**	**7.8**
64	**sp|Q9NRX1|PNO1_HUMAN**	**PNO1**	**RNA-binding protein PNO1**	**40.9**	**1**	**5.6**
65	sp|Q15024|EXOS7_HUMAN	EXOSC7	Exosome complex component RRP42	30.7	1	8.2

Supplemental Table 6. Mass spectrometry data: top proteins identified exclusively in the nucleus from Flag IP DIS3 (HEK293T).

Number	Accension	Gene	Description	Score	Peptides	SC %
1	**sp|Q9Y2L1|RRP44_HUMAN**	**DIS3**	**Exosome complex exonuclease RRP44**	**2126.9**	**38**	**43.6**
2	sp|Q16643|DREB_HUMAN	DBN1	Drebrin	3213.4	33	65.9
3	sp|P08754|GNAI3_HUMAN	GNAI3	Guanine nucleotide-binding protein G(i) subunit alpha	2704.6	35	63.0
4	sp|Q96SB3|NEB2_HUMAN	PPP1R9B	Neurabin-2	2525.2	36	48.1
5	sp|Q16891|MIC60_HUMAN	IMMT	MICOS complex subunit MIC60	2450	31	46.2
7	sp|Q9UHB6|LIMA1_HUMAN	LIMA1	LIM domain and actin-binding protein 1	2313.5	33	43.7
8	sp|P04899|GNAI2_HUMAN	GNAI2	Guanine nucleotide-binding protein G(i) subunit alpha-2	2285.9	34	63.4
9	**sp|P62136|PP1A_HUMAN**	**PPP1CA**	**Serine/threonine-protein phosphatase PP1-alpha catalytic subunit**	**2199.4**	**33**	**70.6**
10	sp|P10809|CH60_HUMAN	HSPD1	60 kDa heat shock protein, mitochondrial	2196.7	37	62.8
11	**sp|Q9Y2L1|RRP44_HUMAN**	**DIS3**	**Exosome complex exonuclease RRP44**	**2126.9**	**38**	**43.6**
12	sp|Q9NVI7|ATD3A_HUMAN	ATAD3A	ATPase family AAA domain-containing protein 3A	2096.5	34	40.1
13	sp|P61978|HNRPK_HUMAN	HNRNPK	Heterogeneous nuclear ribonucleoprotein K	2073.5	28	55.7
14	**sp|P62140|PP1B_HUMAN**	**PPP1CB**	**Serine/threonine-protein phosphatase PP1-beta catalytic subunit**	**2072.6**	**32**	**67.9**
15	sp|Q15233|NONO_HUMAN	NONO	Non-POU domain-containing octamer-binding protein	2030.6	34	47.6
16	sp|Q5T9A4|ATD3B_HUMAN	ATAD3B	ATPase family AAA domain-containing protein 3B	2000.8	33	44.0
17	sp|Q8NI35|INADL_HUMAN	PATJ	InaD-like protein	1998.5	35	34.8
18	sp|P12814|ACTN1_HUMAN	ACTN1	Alpha-actinin-1 OS=Homo sapiens	1992.3	35	39.3
19	**sp|P36873|PP1G_HUMAN**	**PPP1CC**	**Serine/threonine-protein phosphatase PP1-gamma catalytic subunit**	**1964.5**	**30**	**66.6**
20	sp|P22626|ROA2_HUMAN	HNRNPA2B1	Heterogeneous nuclear ribonucleoproteins A2/B1	1937	27	71.1
21	sp|Q9NNW5|WDR6_HUMAN	WDR6	WD repeat-containing protein 6	1931.9	37	41.1
22	**sp|Q6UXN9|WDR82_HUMAN**	**WDR82**	**WD repeat-containing protein 82**	**193.8**	**5**	**12.8**

23	sp|Q9HAV0|GBB4_HUMAN	GNB4	Guanine nucleotide-binding protein subunit beta-4	1924	28	54.7
24	sp|O43491|E41L2_HUMAN	EPB41L2	Band 4.1-like protein 2	1891.3	37	45.4
25	sp|P26599|PTBP1_HUMAN	PTBP1	Polypyrimidine tract-binding protein 1	1873.1	27	62.5
26	sp|Q86YQ8|CPNE8_HUMAN	CPNE8	Copine-8	1852.3	30	54.4
27	sp|Q8WWI1|LMO7_HUMAN	LMO7	LIM domain only protein 7	1812.8	35	29.2
28	sp|P28290|ITPI2_HUMAN	ITPRID2	Protein ITPRID2	1783.9	31	35.3
29	sp|P07437|TBB5_HUMAN	TUBB	Tubulin beta chain	1779.1	31	62.8
30	sp|P06576|ATPB_HUMAN	ATP5F1B	ATP synthase subunit beta, mitochondrial	1763	32	69.4
31	sp|P20700|LMNB1_HUMAN	LMNB1	Lamin-B1	1744	32	46.2
32	sp|Q5M775|CYTSB_HUMAN	SPECC1	Cytospin-B	1740.6	32	31.6
33	sp|P55072|TERA_HUMAN	VCP	Transitional endoplasmic reticulum ATPase	1713.9	35	48.4
34	sp|P07948|LYN_HUMAN	LYN	Tyrosine-protein kinase Lyn	1694.5	34	61.1
35	sp|P47756|CAPZB_HUMAN	CAPZB	F-actin-capping protein subunit beta	1687.2	32	63.9
36	sp|P52272|HNRPM_HUMAN	HNRNPM	Heterogeneous nuclear ribonucleoprotein M	1684.2	33	38.6
37	sp|P49792|RBP2_HUMAN	RANBP2	E3 SUMO-protein ligase RanBP2	1682.3	37	16.6
38	sp|P63096|GNAI1_HUMAN	GNAI1	Guanine nucleotide-binding protein G(i) subunit alpha-1 OS=Homo sapiens OX=9606 GN=GNAI1 PE=1 SV=2	1682	28	60.2
39	sp|P17844|DDX5_HUMAN	DDX5	Probable ATP-dependent RNA helicase DDX5	1671.7	28	46.6
40	sp|P68371|TBB4B_HUMAN	TUBB4B	Tubulin beta-4B chain TUBB4B	1667.6	29	56.6
41	sp|P07947|YES_HUMAN	YES1	Tyrosine-protein kinase Yes	1652.8	31	49.5
42	sp|Q86V48|LUZP1_HUMAN	LUZP1	Leucine zipper protein 1 LUZP1	1616.7	31	38.4
43	sp|Q9ULV4|COR1C_HUMAN	CORO1C	Coronin-1C	1595	28	42.6
44	sp|Q8N3R9|MPP5_HUMAN	MPP5	MAGUK p55 subfamily member 5	1594.7	30	53.5
45	sp|Q14980|NUMA1_HUMAN	NUMA1	Nuclear mitotic apparatus protein 1	1583.7	31	23.1
46	sp|Q86VI3|IQGA3_HUMAN	IQGAP3	Ras GTPase-activating-like protein IQGAP3	1503	32	26.1
47	sp|P52732|KIF11_HUMAN	PE	Kinesin-like protein KIF11	1460.5	30	40.2
48	sp|Q96H55|MYO19_HUMAN	MYO19	Unconventional myosin-XIX	1444.7	28	35.8
49	sp|O75533|SF3B1_HUMAN	SF3B1	Splicing factor 3B subunit 1	1434	30	31.0
50	sp|P68104|EF1A1_HUMAN	EEF1A1 PE	Elongation factor 1-alpha 1	1417.1	27	47.0
51	sp|Q9P0K7|RAI14_HUMAN	RAI14	Ankycorbin	1398.3	28	36.5

52	sp|Q02218|ODO1_HUMAN	OGDH	2-oxoglutarate dehydrogenase, mitochondrial	1362.9	30	34.2
53	sp|Q9Y4I1|MYO5A_HUMAN	MYO5A	Unconventional myosin-Va	1327	28	18.1
54	sp|Q96T37|RBM15_HUMAN	RBM15	RNA-binding protein 15	233.9	6	7.3
55	**sp|Q96QC0|PP1RA_HUMAN**	**PPP1R10**	**Serine/threonine-protein phosphatase 1 regulatory subunit 10**	**119.7**	**3**	**5.9**
56	sp|Q13868|EXOS2_HUMAN	EXOSC2	Exosome complex component RRP4	115.8	2	9.2
57	sp|Q9NPD3|EXOS4_HUMAN	EXOSC4	Exosome complex component RRP41	93.8	2	12.7
58	sp|Q5RKV6|EXOS6_HUMAN	EXOSC6	Exosome complex component MTR3	88.6	2	9.6
59	sp|Q9NQT5|EXOS3_HUMAN	EXOSC3	Exosome complex component RRP40	76	1	7.6
60	**sp|O94842|TOX4_HUMAN**	**TOX4**	**TOX high mobility group box family member 4**	**61.8**	**1**	**1.6**
61	sp|Q9NQT4|EXOS5_HUMAN	EXOSC5	Exosome complex component RRP46	51.9	1	5.1
62	sp|Q15007|FL2D_HUMAN	EXOSC5	Pre-mRNA-splicing regulator WTAP	46.9	1	3.8
63	sp|Q96B26|EXOS8_HUMAN	EXOSC8	Exosome complex component RRP43	43.5	1	9.8
64	sp|Q06265|EXOS9_HUMAN	EXOSC9	Exosome complex component RRP45	31.9	1	2.5

7 Abbreviations

3’ss	3’splice site
5’ss	5’splice site
AEBSF	4-(2-aminoethyl)benzenesulfonyl fluoride hydrochloride
AGO	Argonaute
Ala	alanine
Amp	ampicillin
APS	ammonium persulphate
ATP	adenosine triphosphate
bp	base pair(s)
BSA	bovine serum albumin
cDNA	complementary DNA
ceRNA	competing endogenous RNA
circRNA	circular RNA
ciRNA	Intronic circRNA
CoIP	Co-ImmunoPrecipitation
CRISPR	Clustered Regularly Interspaced Short Palindromic Repeats
Ctrl	Control
D. melanogaster	*Drosophila melanogaster*
DANN	deoxyribonucleic acid
DAPI	4’,6-diamidino-2-phenylindole
DMEM	Dulbecco’s Modified Eagle Medium
dNTP	deoxynucleoside triphosphate
dNTP	Deoxynucleoside triphosphate
Dox	Doxycycline
ds	double-stranded
DTT	Dithiothreitol
DTT	dithiothreitol
E. coli	Escherichia coli
ecircRNA	Exonic circRNA
EDC	1-ethyl-3-(3-dimethyl-aminopropyl)-carbodiimid
EDTA	ethylenediaminetetraacetic acid
EIciRNA	Exonic-Intronic circRNA
eIF	eukaryotic initiation factor
EtBr	ethidium bromide
FBS	fetal bovie serum
FH	Flag/HA
Fig.	Figure
GAPDH	glyceraldehyde 3-phosphate dehydrogenase
GDP	guanosine diphosphate
GFP	green fluorescent protein

Glu	glutamate
GTP	guanosine triphosphate
HA	Human influenza hemagglutinin
HEK293(T)	Human embryonic kidney 293
HeLa	Henrietta Lacks
HEPES	4-(2-hydroxyethyl)-1-piperazineethanesulfonic acid
IP	Immunoprecipitation
IRES	ribosomal entry sites
IVT	*in vitro* transcription
kDa	kilodalton
kDa	Kilodalton
KO	Knockout
lnRNA	long Non-coding RNA
m^6A	N6-methyladenosine
m7G	7-methylguanosine
miR	microRNA
miRNA	microRNA
ml	Milliliter
mM	Millimolar
mRNA	Messenger RNA
Mut	Mutant
ncRNA	noncoding RNA
NLS	nuclear export signal
nt (s)	nucleotides(s)
o/n	overnight
ORF	Open Reading Frame
PAGE	polyacrylamide gel electrophoresis
PCR	polymerase chain reaction
PolII	RNA Polymerase II
Poly(A)	polyadenilation
Pre-mRNA	Precursor mRNA
RNA	Ribonucleic acid
RNase	Ribonuclease
RNA-seq	RNA-sequencing
RNB	Exoribonuclease domain
RNB	RNA binding protein
RNP	Ribonucleoprotein
RRM	RNA recognition motif
rRNA	Ribosomal RNA
S. cerevisiae	*Saccharomyces cerevisiae*
S. pompe	*Saccharomyces pompe*
SDS	sodium dodecyl sulfate
Ser	Serine
siRNA	small interfering RNA
snRNA	Small nuclear RNA
snRNP	Small nuclear ribonucleoprotein
SR	Serine and arginine-rich
Suppl. Figure	Supplemental Figure

TBE	Tris/Borate/EDTA buffer
TBS	Tris buffered saline
TBS(-T)	Tris-buffered saline (containing Tween 20)
tRNA	Transfer RNA
Tyr	Tyrosine
UTR	untranslated region
UV	Ultraviolet
WB	Western blot
WT	Wildtype
µl	Microliter
µM	Micromolar

8 Index of Figures

9 Index of Tables

10 References

Abdelmohsen, K., Panda, A. C., Munk, R., Grammatikakis, I., Dudekula, D. B., De, S., Kim, J., Noh, J. H., Kim, K. M., Martindale, J. L., & Gorospe, M. (2017). Identification of HuR target circular RNAs uncovers suppression of PABPN1 translation by CircPABPN1. *RNA Biology*, *14*(3), 361–369. https://doi.org/10.1080/15476286.2017.1279788

Abe, N., Kodama, A., & Abe, H. (2018). Preparation of circular RNA in vitro. In *Methods in Molecular Biology* (Vol. 1724, pp. 181–192). Humana Press Inc. https://doi.org/10.1007/978-1-4939-7562-4_15

Abe, N., Matsumoto, K., Nishihara, M., Nakano, Y., Shibata, A., Maruyama, H., Shuto, S., Matsuda, A., Yoshida, M., Ito, Y., & Abe, H. (2015). Rolling Circle Translation of Circular RNA in Living Human Cells. *Scientific Reports*, *5*(1), 1–9. https://doi.org/10.1038/srep16435

Ahn, S. H., Kim, M., & Buratowski, S. (2004). Phosphorylation of Serine 2 within the RNA Polymerase II C-Terminal Domain Couples Transcription and 3′ End Processing. *Molecular Cell*, *13*(1), 67–76. https://doi.org/10.1016/S1097-2765(03)00492-1

Aktaş, T., Ilik, I. A., Maticzka, D., Bhardwaj, V., Pessoa Rodrigues, C., Mittler, G., Manke, T., Backofen, R., & Akhtar, A. (2017). DHX9 suppresses RNA processing defects originating from the Alu invasion of the human genome. *Nature*, *544*(7648), 115–119. https://doi.org/10.1038/nature21715

Allmang, C., Kufel, J., Chanfreau, G., Mitchell, P., Petfalski, E., & Tollervey, D. (1999). Functions of the exosome in rRNA, snoRNA and snRNA synthesis. *EMBO Journal*, *18*(19), 5399–5410. https://doi.org/10.1093/emboj/18.19.5399

Ameismeier, M., Zemp, I., van den Heuvel, J., Thoms, M., Berninghausen, O., Kutay, U., & Beckmann, R. (2020). Structural basis for the final steps of human 40S ribosome maturation. *Nature*, *587*(7835), 683–687. https://doi.org/10.1038/s41586-020-2929-x

Andersson, R., Refsing Andersen, P., Valen, E., Core, L. J., Bornholdt, J., Boyd, M., Heick Jensen, T., & Sandelin, A. (2014). Nuclear stability and transcriptional directionality separate functionally distinct RNA species. *Nature Communications*, *5*. https://doi.org/10.1038/ncomms6336

Ashwal-Fluss, R., Meyer, M., Pamudurti, N. R., Ivanov, A., Bartok, O., Hanan, M., Evantal, N., Memczak, S., Rajewsky, N., & Kadener, S. (2014). CircRNA Biogenesis competes with Pre-mRNA splicing. *Molecular Cell*, *56*(1), 55–66. https://doi.org/10.1016/j.molcel.2014.08.019

Aubert, M., O'donohue, M. F., Lebaron, S., & Gleizes, P. E. (2018). Pre-ribosomal RNA processing in human cells: From mechanisms to congenital diseases. In *Biomolecules* (Vol. 8, Issue 4). MDPI AG. https://doi.org/10.3390/biom8040123

Aufiero, S., van Den Hoogenhof, M. M. G., Reckman, Y. J., Beqqali, A., van der Made, I., Kluin, J., Khan, M. A. F., Pinto, Y. M., & Creemers, E. E. (2018). Cardiac circRNAs arise mainly from constitutive exons rather than alternatively spliced exons. *RNA*, *24*(6), 815–827. https://doi.org/10.1261/rna.064394.117

Bachmayr-Heyda, A., Reiner, A. T., Auer, K., Sukhbaatar, N., Aust, S., Bachleitner-Hofmann, T., Mesteri, I., Grunt, T. W., Zeillinger, R., & Pils, D. (2015). Correlation of circular RNA abundance with proliferation - Exemplified with colorectal and ovarian cancer, idiopathic lung fibrosis, and normal human tissues. *Scientific Reports*, *5*(1), 8057. https://doi.org/10.1038/srep08057

Bahn, J. H., Zhang, Q., Li, F., Chan, T.-M., Lin, X., Kim, Y., Wong, D. T. W., & Xiao, X. (2015). The Landscape of MicroRNA, Piwi-Interacting RNA, and Circular RNA in Human Saliva. *Clinical Chemistry*, *61*(1), 221–230. https://doi.org/10.1373/clinchem.2014.230433

Barbagallo, D., Caponnetto, A., Cirnigliaro, M., Brex, D., Barbagallo, C., D'Angeli, F., Morrone, A., Caltabiano, R., Barbagallo, G. M., Ragusa, M., Di Pietro, C., Hansen, T. B., & Purrello, M. (2018). CircSMARCA5 inhibits migration of glioblastoma multiforme cells by regulating a molecular axis involving splicing factors SRSF1/SRSF3/PTB. *International Journal of Molecular Sciences*, *19*(2). https://doi.org/10.3390/ijms19020480

Barnes, T., Kim, W. C., Mantha, A. K., Kim, S. E., Izumi, T., Mitra, S., & Lee, C. H. (2009). Identification of Apurinic/apyrimidinic endonuclease 1 (APE1) as the endoribonuclease that cleaves c-myc mRNA. *Nucleic Acids Research*, *37*(12), 3946–3958. https://doi.org/10.1093/nar/gkp275

Barrett, S. P., Wang, P. L., & Salzman, J. (2015). Circular RNA biogenesis can proceed through an exon-containing lariat precursor. *ELife*, *4*(JUNE), 1–18. https://doi.org/10.7554/eLife.07540

Barzilay, G., Mol, C. D., Robson, C. N., Walker, L. J., Cunningham, R. P., Tainer, J. A., & Hickson, I. D. (1995). Identification of critical active-site residues in the multifunctional human DNA

repair enzyme HAP1. *Nature Structural Biology*, *2*(7), 561–568. https://doi.org/10.1038/nsb0795-561

Begum, S., Yiu, A., Stebbing, J., & Castellano, L. (2018). Novel tumour suppressive protein encoded by circular RNA, circ-SHPRH, in glioblastomas. In *Oncogene* (Vol. 37, Issue 30, pp. 4055–4057). Nature Publishing Group. https://doi.org/10.1038/s41388-018-0230-3

Behm-Ansmant, I., Kashima, I., Rehwinkel, J., Saulière, J., Wittkopp, N., & Izaurralde, E. (2007). mRNA quality control: An ancient machinery recognizes and degrades mRNAs with nonsense codons. In *FEBS Letters* (Vol. 581, Issue 15, pp. 2845–2853). FEBS Lett. https://doi.org/10.1016/j.febslet.2007.05.027

Bisbal, C., & Silverman, R. H. (2007). Diverse functions of RNase L and implications in pathology. *Biochimie*, *89*(6–7), 789–798. https://doi.org/10.1016/j.biochi.2007.02.006

Bonneau, F., Basquin, J., Ebert, J., Lorentzen, E., & Conti, E. (2009). The Yeast Exosome Functions as a Macromolecular Cage to Channel RNA Substrates for Degradation. *Cell*, *139*(3), 547–559. https://doi.org/10.1016/j.cell.2009.08.042

Braun, J. E., Truffault, V., Boland, A., Huntzinger, E., Chang, C. Te, Haas, G., Weichenrieder, O., Coles, M., & Izaurralde, E. (2012). A direct interaction between DCP1 and XRN1 couples mRNA decapping to 5′ exonucleolytic degradation. *Nature Structural and Molecular Biology*, *19*(12), 1324–1331. https://doi.org/10.1038/nsmb.2413

Braunschweig, U., Barbosa-Morais, N. L., Pan, Q., Nachman, E. N., Alipanahi, B., Gonatopoulos-Pournatzis, T., Frey, B., Irimia, M., & Blencowe, B. J. (2014). Widespread intron retention in mammals functionally tunes transcriptomes. *Genome Research*, *24*(11), 1774–1786. https://doi.org/10.1101/gr.177790.114

Bremer, K. A., Stevens, A., & Schoenberg, D. R. (2003). An endonuclease activity similar to Xenopus PMR1 catalyzes the degradation of normal and nonsense-containing human β-globin mRNA in erythroid cells. *RNA*, *9*(9), 1157–1167. https://doi.org/10.1261/rna.5720303

Calfon, M., Zeng, H., Urano, F., Till, J. H., Hubbard, S. R., Harding, H. P., Clark, S. G., & Ron, D. (2002). IRE1 couples endoplasmic reticulum load to secretory capacity by processing the XBP-1 mRNA. *Nature*, *415*(6867), 92–96. https://doi.org/10.1038/415092a

Cañete-Soler, R., Reddy, K. S., Tolan, D. R., & Zhai, J. (2005). Aldolases A and C are ribonucleolytic components of a neuronal complex that regulates the stability of the light-neurofilament mRNA. *Journal of Neuroscience*, *25*(17), 4353–4364. https://doi.org/10.1523/JNEUROSCI.0885-

05.2005

Capel, B., Swain, A., Nicolis, S., Hacker, A., Walter, M., Koopman, P., Goodfellow, P., & Lovell-Badge, R. (1993). Circular transcripts of the testis-determining gene Sry in adult mouse testis. *Cell*, *73*(5), 1019–1030. https://doi.org/10.1016/0092-8674(93)90279-Y

Cech, T. R., Zaug, A. J., & Grabowski, P. J. (1981). In vitro splicing of the ribosomal RNA precursor of tetrahymena: Involvement of a guanosine nucleotide in the excision of the intervening sequence. *Cell*, *27*(3 PART 2), 487–496. https://doi.org/10.1016/0092-8674(81)90390-1

Chang, A. C. Y., Sohlberg, B., Trinkle-Mulcahy, L., Claverie-Martin, F., Cohen, P., & Cohen, S. N. (1999). Alternative splicing regulates the production of ARD-1 endoribonuclease and NIPP-1, an inhibitor of protein phosphatase-1, as isoforms encoded by the same gene. *Gene*, *240*(1), 45–55. https://doi.org/10.1016/S0378-1119(99)00435-7

Chapman, M. A., Lawrence, M. S., Keats, J. J., Cibulskis, K., Sougnez, C., Schinzel, A. C., Harview, C. L., Brunet, J. P., Ahmann, G. J., Adli, M., Anderson, K. C., Ardlie, K. G., Auclair, D., Baker, A., Bergsagel, P. L., Bernstein, B. E., Drier, Y., Fonseca, R., Gabriel, S. B., … Golub, T. R. (2011). Initial genome sequencing and analysis of multiple myeloma. *Nature*, *471*(7339), 467–472. https://doi.org/10.1038/nature09837

Chen, Chang You, & Sarnow, P. (1995). Initiation of protein synthesis by the eukaryotic translational apparatus on circular RNAs. *Science*, *268*(5209), 415–417. https://doi.org/10.1126/science.7536344

Chen, Ching Yi, Gherzi, R., Ong, S. E., Chan, E. L., Raijmakers, R., Pruijn, G. J. M., Stoecklin, G., Moroni, C., Mann, M., & Karin, M. (2001). AU binding proteins recruit the exosome to degrade ARE-containing mRNAs. *Cell*, *107*(4), 451–464. https://doi.org/10.1016/S0092-8674(01)00578-5

Chen, I., Chen, C. Y., & Chuang, T. J. (2015). Biogenesis, identification, and function of exonic circular RNAs. In *Wiley Interdisciplinary Reviews: RNA* (Vol. 6, Issue 5, pp. 563–579). Blackwell Publishing Ltd. https://doi.org/10.1002/wrna.1294

Chen, L. L. (2016). The biogenesis and emerging roles of circular RNAs. In *Nature Reviews Molecular Cell Biology* (Vol. 17, Issue 4, pp. 205–211). Nature Publishing Group. https://doi.org/10.1038/nrm.2015.32

Chen, L. L. (2020). The expanding regulatory mechanisms and cellular functions of circular RNAs. In *Nature Reviews Molecular Cell Biology* (Vol. 21, Issue 8, pp. 475–490). Nature Research.

https://doi.org/10.1038/s41580-020-0243-y

Chen, Y. G., Kim, M. V., Chen, X., Batista, P. J., Aoyama, S., Wilusz, J. E., Iwasaki, A., & Chang, H. Y. (2017). Sensing Self and Foreign Circular RNAs by Intron Identity. *Molecular Cell*, *67*(2), 228-238.e5. https://doi.org/10.1016/j.molcel.2017.05.022

Chernokalskaya, E., Dubell, A. N., Cunningham, K. S., Hanson, M. N., Dompenciel, R. E., & Schoenberg, D. R. (1998). A polysomal ribonuclease involved in the destabilization of albumin mRNA is a novel member of the peroxidase gene family. *RNA*, *4*(12), 1537–1548. https://doi.org/10.1017/S1355838298980451

Chiu, A. C., Suzuki, H. I., Wu, X., Mahat, D. B., Kriz, A. J., & Sharp, P. A. (2018). Transcriptional Pause Sites Delineate Stable Nucleosome-Associated Premature Polyadenylation Suppressed by U1 snRNP. *Molecular Cell*, *69*(4), 648-663.e7. https://doi.org/10.1016/j.molcel.2018.01.006

Chou, K. M., Kukhanova, M., & Cheng, Y. C. (2000). A novel action of human apurinic/apyrimidinic endonuclease. Excision of L-configuration deoxyribonucleoside analogs from the 3' termini of DNA. *Journal of Biological Chemistry*, *275*(40), 31009–31015. https://doi.org/10.1074/jbc.M004082200

Claverie-Martin, F., Wang, M., & Cohen, S. N. (1997). ARD-1 cDNA from human cells encodes a site-specific single-strand endoribonuclease that functionally resembles Escherichia coli RNase E. *Journal of Biological Chemistry*, *272*(21), 13823–13828. https://doi.org/10.1074/jbc.272.21.13823

Cocquerelle, C., Mascrez, B., Hétuin, D., & Bailleul, B. (1993). Mis-splicing yields circular RNA molecules. *The FASEB Journal*, *7*(1), 155–160. https://doi.org/10.1096/fasebj.7.1.7678559

Conn, S. J., Pillman, K. A., Toubia, J., Conn, V. M., Salmanidis, M., Phillips, C. A., Roslan, S., Schreiber, A. W., Gregory, P. A., & Goodall, G. J. (2015). The RNA binding protein quaking regulates formation of circRNAs. *Cell*, *160*(6), 1125–1134. https://doi.org/10.1016/j.cell.2015.02.014

Conn, V. M., Hugouvieux, V., Nayak, A., Conos, S. A., Capovilla, G., Cildir, G., Jourdain, A., Tergaonkar, V., Schmid, M., Zubieta, C., & Conn, S. J. (2017). A circRNA from SEPALLATA3 regulates splicing of its cognate mRNA through R-loop formation. *Nature Plants*, *3*. https://doi.org/10.1038/nplants.2017.53

Coughlin, D. J., Pleiss, J. A., Walker, S. C., Whitworth, G. B., & Engelke, D. R. (2008). Genome-wide search for yeast RNase P substrates reveals role in maturation of intron-encoded box C/D

small nucleolar RNAs. *Proceedings of the National Academy of Sciences of the United States of America*, *105*(34), 12218–12223. https://doi.org/10.1073/pnas.0801906105

Cunningham, K. S., Hanson, M. N., & Schoenberg, D. R. (2001). Polysomal ribonuclease 1 exists in a latent form on polysomes prior to estrogen activation of mRNA decay. *Nucleic Acids Research*, *29*(5), 1156–1162. https://doi.org/10.1093/nar/29.5.1156

Danan, M., Schwartz, S., Edelheit, S., & Sorek, R. (2012). Transcriptome-wide discovery of circular RNAs in Archaea. *Nucleic Acids Research*, *40*(7), 3131–3142. https://doi.org/10.1093/nar/gkr1009

Davidson, L., Francis, L., Cordiner, R. A., Eaton, J. D., Estell, C., Macias, S., Cáceres, J. F., & West, S. (2019). Rapid Depletion of DIS3, EXOSC10, or XRN2 Reveals the Immediate Impact of Exoribonucleolysis on Nuclear RNA Metabolism and Transcriptional Control. *Cell Reports*, *26*(10), 2779-2791.e5. https://doi.org/10.1016/j.celrep.2019.02.012

Decker, C. J., & Parker, R. (1993). A turnover pathway for both stable and unstable mRNAs in yeast: Evidence for a requirement for deadenylation. *Genes and Development*, *7*(8), 1632–1643. https://doi.org/10.1101/gad.7.8.1632

Demple, B., & Sung, J. S. (2005). Molecular and biological roles of Ape1 protein in mammalian base excision repair. *DNA Repair*, *4*(12), 1442–1449. https://doi.org/10.1016/j.dnarep.2005.09.004

Di Timoteo, G., Dattilo, D., Centrón-Broco, A., Colantoni, A., Guarnacci, M., Rossi, F., Incarnato, D., Oliviero, S., Fatica, A., Morlando, M., & Bozzoni, I. (2020). Modulation of circRNA Metabolism by m6A Modification. *Cell Reports*, *31*(6). https://doi.org/10.1016/j.celrep.2020.107641

Domanski, M., & LaCava, J. (2017). Affinity Purification of the RNA Degradation Complex, the Exosome, from HEK-293 Cells. *BIO-PROTOCOL*, *7*(8). https://doi.org/10.21769/bioprotoc.2238

Dong, B., Niwa, M., Walter, P., & Silverman, R. H. (2001). Basis for regulated RNA cleavage by functional analysis of RNase L and Ire1p. *RNA*, *7*(3), 361–373. https://doi.org/10.1017/S1355838201002230

Dong, B., & Silverman, R. H. (1997). A bipartite model of 2-5A-dependent RNase L. *Journal of Biological Chemistry*, *272*(35), 22236–22242. https://doi.org/10.1074/jbc.272.35.22236

Dou, Y., Cha, D. J., Franklin, J. L., Higginbotham, J. N., Jeppesen, D. K., Weaver, A. M., Prasad, N.,

Levy, S., Coffey, R. J., Patton, J. G., & Zhang, B. (2016). Circular RNAs are down-regulated in KRAS mutant colon cancer cells and can be transferred to exosomes. *Scientific Reports*, *6*. https://doi.org/10.1038/srep37982

Du, W. W., Fang, L., Yang, W., Wu, N., Awan, F. M., Yang, Z., & Yang, B. B. (2017). Induction of tumor apoptosis through a circular RNA enhancing Foxo3 activity. *Cell Death and Differentiation*, *24*(2), 357–370. https://doi.org/10.1038/cdd.2016.133

Du, W. W., Yang, W., Liu, E., Yang, Z., Dhaliwal, P., & Yang, B. B. (2016). Foxo3 circular RNA retards cell cycle progression via forming ternary complexes with p21 and CDK2. *Nucleic Acids Research*, *44*(6), 2846–2858. https://doi.org/10.1093/nar/gkw027

Dziembowski, A., Lorentzen, E., Conti, E., & Séraphin, B. (2007). A single subunit, Dis3, is essentially responsible for yeast exosome core activity. *Nature Structural and Molecular Biology*, *14*(1), 15–22. https://doi.org/10.1038/nsmb1184

Eberle, A. B., Lykke-Andersen, S., Mühlemann, O., & Jensen, T. H. (2009). SMG6 promotes endonucleolytic cleavage of nonsense mRNA in human cells. *Nature Structural and Molecular Biology*, *16*(1), 49–55. https://doi.org/10.1038/nsmb.1530

Eisenberg, E., & Levanon, E. Y. (2018). A-to-I RNA editing - Immune protector and transcriptome diversifier. In *Nature Reviews Genetics* (Vol. 19, Issue 8, pp. 473–490). Nature Publishing Group. https://doi.org/10.1038/s41576-018-0006-1

Enuka, Y., Lauriola, M., Feldman, M. E., Sas-Chen, A., Ulitsky, I., & Yarden, Y. (2016). Circular RNAs are long-lived and display only minimal early alterations in response to a growth factor. *Nucleic Acids Research*, *44*(3), 1370–1383. https://doi.org/10.1093/nar/gkv1367

Errichelli, L., Dini Modigliani, S., Laneve, P., Colantoni, A., Legnini, I., Capauto, D., Rosa, A., De Santis, R., Scarfò, R., Peruzzi, G., Lu, L., Caffarelli, E., Shneider, N. A., Morlando, M., & Bozzoni, I. (2017). FUS affects circular RNA expression in murine embryonic stem cell-derived motor neurons. *Nature Communications*, *8*. https://doi.org/10.1038/ncomms14741

Esakova, O., & Krasilnikov, A. S. (2010). Of proteins and RNA: The RNase P/MRP family. In *RNA* (Vol. 16, Issue 9, pp. 1725–1747). Cold Spring Harbor Laboratory Press. https://doi.org/10.1261/rna.2214510

Fan, H., Goodier, J. L., Chamberlain, J. R., Engelke, D. R., & Maraia, R. J. (1998). 5′ Processing of tRNA Precursors Can Be Modulated by the Human La Antigen Phosphoprotein. *Molecular and Cellular Biology*, *18*(6), 3201–3211. https://doi.org/10.1128/mcb.18.6.3201

Fischer, J. W., Busa, V. F., Shao, Y., & Leung, A. K. L. (2020). Structure-Mediated RNA Decay by UPF1 and G3BP1. *Molecular Cell*, *78*(1), 70-84.e6. https://doi.org/10.1016/j.molcel.2020.01.021

Frischmeyer, P. A., Van Hoof, A., O'Donnell, K., Guerrerio, A. L., Parker, R., & Dietz, H. C. (2002). An mRNA surveillance mechanism that eliminates transcripts lacking termination codons. *Science*, *295*(5563), 2258–2261. https://doi.org/10.1126/science.1067338

Fu, H., Feng, J., Liu, Q., Sun, F., Tie, Y., Zhu, J., Xing, R., Sun, Z., & Zheng, X. (2009). Stress induces tRNA cleavage by angiogenin in mammalian cells. *FEBS Letters*, *583*(2), 437–442. https://doi.org/10.1016/j.febslet.2008.12.043

Gabriel, A. F., Costa, M. C., & Enguita, F. J. (2020). Circular RNA-centered regulatory networks in the physiopathology of cardiovascular diseases. In *International Journal of Molecular Sciences* (Vol. 21, Issue 2, p. 456). MDPI AG. https://doi.org/10.3390/ijms21020456

Gagnon, K. T., Li, L., Janowski, B. A., & Corey, D. R. (2014). Analysis of nuclear RNA interference in human cells by subcellular fractionation and Argonaute loading. In *Nature Protocols* (Vol. 9, Issue 9, pp. 2045–2060). Nature Publishing Group. https://doi.org/10.1038/nprot.2014.135

Gallouzi, I., Parker, F., Chebli, K., Maurier, F., Labourier, E., Barlat, I., Capony, J.-P., Tocque, B., & Tazi, J. (1998). A Novel Phosphorylation-Dependent RNase Activity of GAP-SH3 Binding Protein: a Potential Link between Signal Transduction and RNA Stability. *Molecular and Cellular Biology*, *18*(7), 3956–3965. https://doi.org/10.1128/mcb.18.7.3956

Gao, X., & Xu, Z. (2008). Mechanisms of action of angiogenin. In *Acta Biochimica et Biophysica Sinica* (Vol. 40, Issue 7, pp. 619–624). Acta Biochim Biophys Sin (Shanghai). https://doi.org/10.1111/j.1745-7270.2008.00442.x

Garneau, N. L., Wilusz, J., & Wilusz, C. J. (2007). The highways and byways of mRNA decay. In *Nature Reviews Molecular Cell Biology* (Vol. 8, Issue 2, pp. 113–126). Nature Publishing Group. https://doi.org/10.1038/nrm2104

Geisler, S., & Coller, J. (2012). XRN1: A Major 5' to 3' Exoribonuclease in Eukaryotic Cells. In *Enzymes* (Vol. 31, pp. 97–114). Academic Press. https://doi.org/10.1016/B978-0-12-404740-2.00005-7

Gill, T., Cai, T., Aulds, J., Wierzbicki, S., & Schmitt, M. E. (2004). RNase MRP Cleaves the CLB2 mRNA To Promote Cell Cycle Progression: Novel Method of mRNA Degradation. *Molecular and Cellular Biology*, *24*(3), 945–953. https://doi.org/10.1128/mcb.24.3.945-953.2004

Glavan, F., Behm-Ansmant, I., Izaurralde, E., & Conti, E. (2006). Structures of the PIN domains of SMG6 and SMG5 reveal a nuclease within the mRNA surveillance complex. *EMBO Journal*, *25*(21), 5117–5125. https://doi.org/10.1038/sj.emboj.7601377

Graham, A. C., Davis, S. M., & Andrulis, E. D. (2009). Interdependent Nucleocytoplasmic Trafficking and Interactions of Dis3 with Rrp6, the Core Exosome and Importin-α3. *Traffic*, *10*(5), 499–513. https://doi.org/10.1111/j.1600-0854.2009.00888.x

Graham, A. C., Kiss, D. L., & Andrulis, E. D. (2006). Differential distribution of exosome subunits at the nuclear lamina and in cytoplasmic foci. *Molecular Biology of the Cell*, *17*(3), 1399–1409. https://doi.org/10.1091/mbc.E05-08-0805

Gross, H. J., Domdey, H., Lossow, C., Jank, P., Raba, M., Alberty, H., & Sänger, H. L. (1978). Nucleotide sequence and secondary structure of potato spindle tuber viroid. *Nature*, *273*(5659), 203–208. https://doi.org/10.1038/273203a0

Grundmann, U., Römisch, J., Siebold, B., Bohn, H., & Amann, E. (1990). Cloning and Expression of a cDNA Encoding Human Placental Protein 11, a Putative Serine Protease with Diagnostic Significance as a Tumor Marker. *DNA and Cell Biology*, *9*(4), 243–250. https://doi.org/10.1089/dna.1990.9.243

Gruner, H., Cortés-López, M., Cooper, D. A., Bauer, M., & Miura, P. (2016). CircRNA accumulation in the aging mouse brain. *Scientific Reports*, *6*(1), 1–14. https://doi.org/10.1038/srep38907

Gu, S. Q., Bakthavachalu, B., Han, J., Patil, D. P., Otsuka, Y., Guda, C., & Schoenberg, D. R. (2012). Identification of the human PMR1 mRNA endonuclease as an alternatively processed product of the gene for peroxidasin-like protein. *RNA*, *18*(6), 1186–1196. https://doi.org/10.1261/rna.031369.111

Gu, S. Q., Gallego-Perez, D., McClory, S. P., Shi, J., Han, J., Lee, L. J., & Schoenberg, D. R. (2016). The human PMR1 endonuclease stimulates cell motility by down regulating miR-200 family microRNAs. *Nucleic Acids Research*, *44*(12), 5811–5819. https://doi.org/10.1093/nar/gkw497

Guderian, G., Peter, C., Wiesner, J., Sickmann, A., Schulze-Osthoff, K., Fischer, U., & Grimmler, M. (2011). RioK1, a new interactor of protein arginine methyltransferase 5 (PRMT5), competes with pICln for binding and modulates PRMT5 complex composition and substrate specificity. *Journal of Biological Chemistry*, *286*(3), 1976–1986. https://doi.org/10.1074/jbc.M110.148486

Gudipati, R. K., Xu, Z., Lebreton, A., Séraphin, B., Steinmetz, L. M., Jacquier, A., & Libri, D. (2012). Extensive Degradation of RNA Precursors by the Exosome in Wild-Type Cells. *Molecular Cell*,

48(3), 409–421. https://doi.org/10.1016/j.molcel.2012.08.018

Guo, J. U., Agarwal, V., Guo, H., & Bartel, D. P. (2014). Expanded identification and characterization of mammalian circular RNAs. *Genome Biology*, *15*(7). https://doi.org/10.1186/s13059-014-0409-z

Guo, Y., Wei, X., & Peng, Y. (2020). Structure-Mediated Degradation of CircRNAs. In *Trends in Cell Biology* (Vol. 30, Issue 7, pp. 501–503). Elsevier Ltd. https://doi.org/10.1016/j.tcb.2020.04.001

Halbach, F., Reichelt, P., Rode, M., & Conti, E. (2013). The Yeast Ski Complex: Crystal Structure and RNA Channeling to the Exosome Complex. *Cell*, *154*, 814–826. https://doi.org/10.1016/j.cell.2013.07.017

Hansen, T. B. (2021). Signal and noise in circRNA translation. *Methods*. https://doi.org/10.1016/j.ymeth.2021.02.007

Hansen, Thomas B. (2018). Characterization of circular RNA concatemers. In *Methods in Molecular Biology* (Vol. 1724, pp. 143–157). Humana Press Inc. https://doi.org/10.1007/978-1-4939-7562-4_12

Hansen, Thomas B., Jensen, T. I., Clausen, B. H., Bramsen, J. B., Finsen, B., Damgaard, C. K., & Kjems, J. (2013). Natural RNA circles function as efficient microRNA sponges. *Nature*, *495*(7441), 384–388. https://doi.org/10.1038/nature11993

Hansen, Thomas B., Kjems, J., & Damgaard, C. K. (2013). Circular RNA and miR-7 in Cancer. In *Cancer Research* (Vol. 73, Issue 18, pp. 5609–5612). Cancer Res. https://doi.org/10.1158/0008-5472.CAN-13-1568

Hansen, Thomas B, Wiklund, E. D., Bramsen, J. B., Villadsen, S. B., Statham, A. L., Clark, S. J., & Kjems, J. (2011). miRNA-dependent gene silencing involving Ago2-mediated cleavage of a circular antisense RNA. *The EMBO Journal*, *30*(21), 4414–4422. https://doi.org/10.1038/emboj.2011.359

He, Y., Huang, H., Jin, L., Zhang, F., Zeng, M., Wei, L., Tang, S., Chen, D., & Wang, W. (2020). CircZNF609 enhances hepatocellular carcinoma cell proliferation, metastasis, and stemness by activating the Hedgehog pathway through the regulation of miR-15a-5p/15b-5p and GLI2 expressions. *Cell Death and Disease*, *11*(5). https://doi.org/10.1038/s41419-020-2441-0

Ho-Xuan, H., GlaÅar, P., Latini, C., Heizler, K., Haase, J., Hett, R., Anders, M., Weichmann, F.,

Bruckmann, A., Van Den Berg, D., Hüttelmaier, S., Rajewsky, N., Hackl, C., & Meister, G. (2020). Comprehensive analysis of translation from overexpressed circular RNAs reveals pervasive translation from linear transcripts. *Nucleic Acids Research*, *48*(18), 10368–10382. https://doi.org/10.1093/nar/gkaa704

Ho-Xuan, H., Lehmann, G., Glazar, P., Gypas, F., Eichner, N., Heizler, K., Schlitt, H. J., Zavolan, M., Rajewsky, N., Meister, G., & Hackl, C. (2020). Gene Expression Signatures of a Preclinical Mouse Model during Colorectal Cancer Progression under Low-Dose Metronomic Chemotherapy. *Cancers*, *13*(1), 49. https://doi.org/10.3390/cancers13010049

Holdt, L. M., Stahringer, A., Sass, K., Pichler, G., Kulak, N. A., Wilfert, W., Kohlmaier, A., Herbst, A., Northoff, B. H., Nicolaou, A., Gäbel, G., Beutner, F., Scholz, M., Thiery, J., Musunuru, K., Krohn, K., Mann, M., & Teupser, D. (2016). Circular non-coding RNA ANRIL modulates ribosomal RNA maturation and atherosclerosis in humans. *Nature Communications*, *7*(1), 1–14. https://doi.org/10.1038/ncomms12429

Holloway, D. E., Shapiro, R., Hares, M. C., Leonidas, D. D., & Acharya, K. R. (2002). Guest-host crosstalk in an angiogenin - RNase a chimeric protein. *Biochemistry*, *41*(33), 10482–10489. https://doi.org/10.1021/bi026151r

Hou, D., Ruiz, M., & Andrulis, E. D. (2012). The ribonuclease Dis3 is an essential regulator of the developmental transcriptome. *BMC Genomics*, *13*(1). https://doi.org/10.1186/1471-2164-13-359

Houseley, J., LaCava, J., & Tollervey, D. (2006). RNA-quality control by the exosome. In *Nature Reviews Molecular Cell Biology* (Vol. 7, Issue 7, pp. 529–539). Nature Publishing Group. https://doi.org/10.1038/nrm1964

Huang, C., Liang, D., Tatomer, D. C., & Wilusz, J. E. (2018). A length-dependent evolutionarily conserved pathway controls nuclear export of circular RNAs. *Genes and Development*, *32*(9–10), 639–644. https://doi.org/10.1101/gad.314856.118

Huntzinger, E., Kashima, I., Fauser, M., Saulière, J., & Izaurralde, E. (2008). SMG6 is the catalytic endonuclease that cleaves mRNAs containing nonsense codons in metazoan. *RNA*, *14*(12), 2609–2617. https://doi.org/10.1261/rna.1386208

Irvine, K., Stirling, R., Hume, D., & Kennedy, D. (2004). Rasputin, more promiscuous than ever: A review of G3BP. In *International Journal of Developmental Biology* (Vol. 48, Issue 10, pp. 1065–1077). Int J Dev Biol. https://doi.org/10.1387/ijdb.041893ki

Isken, O., & Maquat, L. E. (2007). Quality control of eukaryotic mRNA: Safeguarding cells from abnormal mRNA function. In *Genes and Development* (Vol. 21, Issue 15, pp. 1833–1856). Genes Dev. https://doi.org/10.1101/gad.1566807

Ivanov, A., Memczak, S., Wyler, E., Torti, F., Porath, H. T., Orejuela, M. R., Piechotta, M., Levanon, E. Y., Landthaler, M., Dieterich, C., & Rajewsky, N. (2015). Analysis of intron sequences reveals hallmarks of circular RNA biogenesis in animals. *Cell Reports*, *10*(2), 170–177. https://doi.org/10.1016/j.celrep.2014.12.019

Izumi, T., Brown, D. B., Naidu, C. V., Bhakat, K. K., MacInnes, M. A., Saito, H., Chen, D. J., & Mitra, S. (2005). Two essential but distinct functions of the mammalian abasic endonuclease. *Proceedings of the National Academy of Sciences of the United States of America*, *102*(16), 5739–5743. https://doi.org/10.1073/pnas.0500986102

Jackson, R. J., Hellen, C. U. T., & Pestova, T. V. (2010). The mechanism of eukaryotic translation initiation and principles of its regulation. In *Nature Reviews Molecular Cell Biology* (Vol. 11, Issue 2, pp. 113–127). Nature Publishing Group. https://doi.org/10.1038/nrm2838

Jakobi, T., Czaja-Hasse, L. F., Reinhardt, R., & Dieterich, C. (2016). Profiling and Validation of the Circular RNA Repertoire in Adult Murine Hearts. In *Genomics, Proteomics and Bioinformatics* (Vol. 14, Issue 4, pp. 216–223). Beijing Genomics Institute. https://doi.org/10.1016/j.gpb.2016.02.003

Jeck, W. R., & Sharpless, N. E. (2014). Detecting and characterizing circular RNAs. In *Nature Biotechnology* (Vol. 32, Issue 5, pp. 453–461). Nature Publishing Group. https://doi.org/10.1038/nbt.2890

Jeck, W. R., Sorrentino, J. A., Wang, K., Slevin, M. K., Burd, C. E., Liu, J., Marzluff, W. F., & Sharpless, N. E. (2013). Circular RNAs are abundant, conserved, and associated with ALU repeats. *RNA*, *19*(2), 141–157. https://doi.org/10.1261/rna.035667.112

Kadaba, S., Krueger, A., Trice, T., Krecic, A. M., Hinnebusch, A. G., & Anderson, J. (2004). Nuclear surveillance and degradation of hypomodified initiator tRNA Met in S. cerevisiae. *Genes and Development*, *18*(11), 1227–1240. https://doi.org/10.1101/gad.1183804

Kanno, S. I., Iwai, S., Takao, M., & Yasui, A. (1999). Repair of apurinic/apyrimidinic sites by UV damage endonuclease; a repair protein for UV and oxidative damage. *Nucleic Acids Research*, *27*(15), 3096–3103. https://doi.org/10.1093/nar/27.15.3096

Kelly, S., Greenman, C., Cook, P. R., & Papantonis, A. (2015). Exon Skipping Is Correlated with

Exon Circularization. *Journal of Molecular Biology*, *427*(15), 2414–2417. https://doi.org/10.1016/j.jmb.2015.02.018

Khabar, K. S. A., Siddiqui, Y. M., Al-Zoghaibi, F., Al-Haj, L., Dhalla, M., Zhou, A., Dong, B., Whitmore, M., Paranjape, J., Al-Ahdal, M. N., Al-Mohanna, F., Williams, B. R. G., & Silverman, R. H. (2003). RNase L mediates transient control of the interferon response through modulation of the double-stranded RNA-dependent protein kinase PKR. *Journal of Biological Chemistry*, *278*(22), 20124–20132. https://doi.org/10.1074/jbc.M208766200

Kilchert, C., Wittmann, S., & Vasiljeva, L. (2016). The regulation and functions of the nuclear RNA exosome complex. In *Nature Reviews Molecular Cell Biology* (Vol. 17, Issue 4, pp. 227–239). Nature Publishing Group. https://doi.org/10.1038/nrm.2015.15

Kim, W. C., King, D., & Lee, C. H. (2010). RNA-cleaving properties of human apurinic/apyrimidinic endonuclease 1 (APE1). *International Journal of Biochemistry and Molecular Biology*, *1*(1), 12–25. www.ijbmb.org

Kim, Y. K. I., & Maquat, L. E. (2019). UPFront and center in RNA decay: UPF1 in nonsense-mediated mRNA decay and beyond. In *RNA* (Vol. 25, Issue 4, pp. 407–422). Cold Spring Harbor Laboratory Press. https://doi.org/10.1261/rna.070136.118

Kirsebom, L. A. (2007). RNase P RNA mediated cleavage: Substrate recognition and catalysis. *Biochimie*, *89*(10), 1183–1194. https://doi.org/10.1016/j.biochi.2007.05.009

Kiss, D. L., & Andrulis, E. D. (2010). Genome-wide analysis reveals distinct substrate specificities of Rrp6, Dis3, and core exosome subunits. *RNA*, *16*(4), 781–791. https://doi.org/10.1261/rna.1906710

Kjems, J., & Garrett, R. A. (1988). Novel splicing mechanism for the ribosomal RNA intron in the archaebacterium desulfurococcus mobilis. *Cell*, *54*(5), 693–703. https://doi.org/10.1016/S0092-8674(88)80014-X

Kleaveland, B., Shi, C. Y., Stefano, J., & Bartel, D. P. (2018). A Network of Noncoding Regulatory RNAs Acts in the Mammalian Brain. *Cell*, *174*(2), 350-362.e17. https://doi.org/10.1016/j.cell.2018.05.022

Kobyłecki, K., Drążkowska, K., Kuliński, T. M., Dziembowski, A., & Tomecki, R. (2018). Elimination of 01/A′-A0 pre-rRNA processing by-product in human cells involves cooperative action of two nuclear exosome-associated nucleases: RRP6 and Dis3. *RNA*, *24*(12), 1677–1692. https://doi.org/10.1261/rna.066589.118

Kramer, M. C., Liang, D., Tatomer, D. C., Gold, B., March, Z. M., Cherry, S., & Wilusz, J. E. (2015). Combinatorial control of Drosophila circular RNA expression by intronic repeats, hnRNPs, and SR proteins. *Genes and Development*, *29*(20), 2168–2182. https://doi.org/10.1101/gad.270421.115

Kristensen, Lasse S., Andersen, M. S., Stagsted, L. V. W., Ebbesen, K. K., Hansen, T. B., & Kjems, J. (2019). The biogenesis, biology and characterization of circular RNAs. In *Nature Reviews Genetics* (Vol. 20, Issue 11, pp. 675–691). Nature Publishing Group. https://doi.org/10.1038/s41576-019-0158-7

Kristensen, Lasse Sommer, Okholm, T. L. H., Venø, M. T., & Kjems, J. (2018). Circular RNAs are abundantly expressed and upregulated during human epidermal stem cell differentiation. *RNA Biology*, *15*(2), 280–291. https://doi.org/10.1080/15476286.2017.1409931

Kuninger, D. T., Izumi, T., Papaconstantinou, J., & Mitra, S. (2002). Human AP-endonuclease 1 and hnRNP-L interact with a nCaRE-like repressor element in the AP-endonuclease 1 promoter. In *Nucleic Acids Research* (Vol. 30, Issue 3, pp. 823–829). Oxford University Press. https://doi.org/10.1093/nar/30.3.823

LaCava, J., Houseley, J., Saveanu, C., Petfalski, E., Thompson, E., Jacquier, A., & Tollervey, D. (2005). RNA degradation by the exosome is promoted by a nuclear polyadenylation complex. *Cell*, *121*(5), 713–724. https://doi.org/10.1016/j.cell.2005.04.029

Laneve, P., Gioia, U., Ragno, R., Altieri, F., Di Franco, C., Santini, T., Arceci, M., Bozzoni, I., & Caffarelli, E. (2008). The tumor marker human placental protein 11 is an endoribonuclease. *Journal of Biological Chemistry*, *283*(50), 34712–34719. https://doi.org/10.1074/jbc.M805759200

Lasda, E., & Parker, R. (2016). Circular RNAs co-precipitate with extracellular vesicles: A possible mechanism for circrna clearance. *PLoS ONE*, *11*(2). https://doi.org/10.1371/journal.pone.0148407

Lebreton, A., Tomecki, R., Dziembowski, A., & Séraphin, B. (2008). Endonucleolytic RNA cleavage by a eukaryotic exosome. *Nature*, *456*(7224), 993–996. https://doi.org/10.1038/nature07480

Lee, G., Bratkowski, M. A., Ding, F., Ke, A., & Ha, T. (2012). Elastic coupling between RNA degradation and unwinding by an exoribonuclease. *Science*, *336*(6089), 1726–1729. https://doi.org/10.1126/science.1216848

Lee, J. H., You, J., Dobrota, E., & Skalnik, D. G. (2010). Identification and characterization of a

novel human PP1 phosphatase complex. *Journal of Biological Chemistry*, *285*(32), 24466–24476. https://doi.org/10.1074/jbc.M110.109801

Lee, K. P. K., Dey, M., Neculai, D., Cao, C., Dever, T. E., & Sicheri, F. (2008). Structure of the Dual Enzyme Ire1 Reveals the Basis for Catalysis and Regulation in Nonconventional RNA Splicing. *Cell*, *132*(1), 89–100. https://doi.org/10.1016/j.cell.2007.10.057

Legnini, I., Di Timoteo, G., Rossi, F., Morlando, M., Briganti, F., Sthandier, O., Fatica, A., Santini, T., Andronache, A., Wade, M., Laneve, P., Rajewsky, N., & Bozzoni, I. (2017). Circ-ZNF609 Is a Circular RNA that Can Be Translated and Functions in Myogenesis. *Molecular Cell*, *66*(1), 22-37.e9. https://doi.org/10.1016/j.molcel.2017.02.017

Li, W. M., Barnes, T., & Lee, C. H. (2010). Endoribonucleases - enzymes gaining spotlight in mRNA metabolism. *FEBS Journal*, *277*(3), 627–641. https://doi.org/10.1111/j.1742-4658.2009.07488.x

Li, X., Liu, C. X., Xue, W., Zhang, Y., Jiang, S., Yin, Q. F., Wei, J., Yao, R. W., Yang, L., & Chen, L. L. (2017). Coordinated circRNA Biogenesis and Function with NF90/NF110 in Viral Infection. *Molecular Cell*, *67*(2), 214-227.e7. https://doi.org/10.1016/j.molcel.2017.05.023

Li, Yan, Zheng, Q., Bao, C., Li, S., Guo, W., Zhao, J., Chen, D., Gu, J., He, X., & Huang, S. (2015). Circular RNA is enriched and stable in exosomes: A promising biomarker for cancer diagnosis. In *Cell Research* (Vol. 25, Issue 8, pp. 981–984). Nature Publishing Group. https://doi.org/10.1038/cr.2015.82

Li, Yawei, Zheng, F., Xiao, X., Xie, F., Tao, D., Huang, C., Liu, D., Wang, M., Wang, L., Zeng, F., & Jiang, G. (2017). Circ HIPK 3 sponges miR-558 to suppress heparanase expression in bladder cancer cells . *EMBO Reports*, *18*(9), 1646–1659. https://doi.org/10.15252/embr.201643581

Li, Z., Huang, C., Bao, C., Chen, L., Lin, M., Wang, X., Zhong, G., Yu, B., Hu, W., Dai, L., Zhu, P., Chang, Z., Wu, Q., Zhao, Y., Jia, Y., Xu, P., Liu, H., & Shan, G. (2015). Exon-intron circular RNAs regulate transcription in the nucleus. *Nature Structural and Molecular Biology*, *22*(3), 256–264. https://doi.org/10.1038/nsmb.2959

Liang, D., Tatomer, D. C., Luo, Z., Wu, H., Yang, L., Chen, L. L., Cherry, S., & Wilusz, J. E. (2017). The Output of Protein-Coding Genes Shifts to Circular RNAs When the Pre-mRNA Processing Machinery Is Limiting. *Molecular Cell*, *68*(5), 940-954.e3. https://doi.org/10.1016/j.molcel.2017.10.034

Liang, D., & Wilusz, J. E. (2014). Short intronic repeat sequences facilitate circular RNA production.

Genes and Development, *28*(20), 2233–2247. https://doi.org/10.1101/gad.251926.114

Liu, C. X., Li, X., Nan, F., Jiang, S., Gao, X., Guo, S. K., Xue, W., Cui, Y., Dong, K., Ding, H., Qu, B., Zhou, Z., Shen, N., Yang, L., & Chen, L. L. (2019). Structure and Degradation of Circular RNAs Regulate PKR Activation in Innate Immunity. *Cell*, *177*(4), 865-880.e21. https://doi.org/10.1016/j.cell.2019.03.046

Liu, H., Rodgers, N. D., Jiao, X., & Kiledjian, M. (2002). The scavenger mRNA decapping enzyme DcpS is a member of the HIT family of pyrophosphatases. *EMBO Journal*, *21*(17), 4699–4708. https://doi.org/10.1093/emboj/cdf448

Liu, Q., Greimann, J. C., & Lima, C. D. (2006). Reconstitution, Activities, and Structure of the Eukaryotic RNA Exosome. *Cell*, *127*(6), 1223–1237. https://doi.org/10.1016/j.cell.2006.10.037

Lorentzen, E., Basquin, J., Tomecki, R., Dziembowski, A., & Conti, E. (2008). Structure of the Active Subunit of the Yeast Exosome Core, Rrp44: Diverse Modes of Substrate Recruitment in the RNase II Nuclease Family. *Molecular Cell*, *29*(6), 717–728. https://doi.org/10.1016/j.molcel.2008.02.018

Lorentzen, E., Dziembowski, A., Lindner, D., Seraphin, B., & Conti, E. (2007). RNA channelling by the archaeal exosome. *EMBO Reports*, *8*(5), 470–476. https://doi.org/10.1038/sj.embor.7400945

Lubas, M., Damgaard, C. K., Tomecki, R., Cysewski, D., Jensen, T. H., & Dziembowski, A. (2013). Exonuclease hDIS3L2 specifies an exosome-independent 3′-5′ degradation pathway of human cytoplasmic mRNA. *EMBO Journal*, *32*(13), 1855–1868. https://doi.org/10.1038/emboj.2013.135

Lukiw, W. J. (2013). Circular RNA (circRNA) in Alzheimer's disease (AD). In *Frontiers in Genetics* (Vol. 4, Issue DEC). Frontiers Media SA. https://doi.org/10.3389/fgene.2013.00307

Lykke-Andersen, S., Tomecki, R., Jensen, T. H., & Dziembowski, A. (2011). The eukaryotic RNA exosome: Same scaffold but variable catalytic subunits. In *RNA Biology* (Vol. 8, Issue 1, pp. 61–66). Taylor and Francis Inc. https://doi.org/10.4161/rna.8.1.14237

Mackie, G. A. (1998). Ribonuclease E is a 5'-end-dependent endonuclease. *Nature*, *395*(6703), 720–723. https://doi.org/10.1038/27246

Makino, D. L., Baumgärtner, M., & Conti, E. (2013). Crystal structure of an rna-bound 11-subunit eukaryotic exosome complex. *Nature*, *495*(7439), 70–75. https://doi.org/10.1038/nature11870

Malecki, M., Viegas, S. C., Carneiro, T., Golik, P., Dressaire, C., Ferreira, M. G., & Arraiano, C. M.

(2013). The exoribonuclease Dis3L2 defines a novel eukaryotic RNA degradation pathway. *EMBO Journal*, *32*(13), 1842–1854. https://doi.org/10.1038/emboj.2013.63

Malet, H., Topf, M., Clare, D. K., Ebert, J., Bonneau, F., Basquin, J., Drazkowska, K., Tomecki, R., Dziembowski, A., Conti, E., Saibil, H. R., & Lorentzen, E. (2010). RNA channelling by the eukaryotic exosome. *EMBO Reports*, *11*(12), 936–942. https://doi.org/10.1038/embor.2010.164

Memczak, S., Jens, M., Elefsinioti, A., Torti, F., Krueger, J., Rybak, A., Maier, L., Mackowiak, S. D., Gregersen, L. H., Munschauer, M., Loewer, A., Ziebold, U., Landthaler, M., Kocks, C., Le Noble, F., & Rajewsky, N. (2013). Circular RNAs are a large class of animal RNAs with regulatory potency. *Nature*, *495*(7441), 333–338. https://doi.org/10.1038/nature11928

Memczak, S., Papavasileiou, P., Peters, O., & Rajewsky, N. (2015). Identification and Characterization of Circular RNAs As a New Class of Putative Biomarkers in Human Blood. *PLOS ONE*, *10*(10), e0141214. https://doi.org/10.1371/journal.pone.0141214

Meyer, K. D., Patil, D. P., Zhou, J., Zinoviev, A., Skabkin, M. A., Elemento, O., Pestova, T. V., Qian, S. B., & Jaffrey, S. R. (2015). 5′ UTR m6A Promotes Cap-Independent Translation. *Cell*, *163*(4), 999–1010. https://doi.org/10.1016/j.cell.2015.10.012

Mitchell, Phil. (2014). Exosome substrate targeting: The long and short of it. *Biochemical Society Transactions*, *42*(4), 1129–1134. https://doi.org/10.1042/BST20140088

Mitchell, Philip, Petfalski, E., & Tollervey, D. (1996). The 3′ end of yeast 5.8S rRNA is generated by an exonuclease processing mechanism. *Genes and Development*, *10*(4), 502–513. https://doi.org/10.1101/gad.10.4.502

Moteki, S., & Price, D. (2002). Functional coupling of capping and transcription of mRNA. *Molecular Cell*, *10*(3), 599–609. https://doi.org/10.1016/S1097-2765(02)00660-3

Muhlrad, D., Decker, C. J., & Parker, R. (1994). Deadenylation of the unstable mRNA encoded by the yeast MFA2 gene leads to decapping followed by 5’ → 3’ digestion of the transcript. *Genes and Development*, *8*(7), 855–866. https://doi.org/10.1101/gad.8.7.855

Mukherjee, D., Gao, M., O’Connor, J. P., Raijmakers, R., Pruijn, G., Lutz, C. S., & Wilusz, J. (2002). The mammalian exosome mediates the efficient degradation of mRNAs that contain AU-rich elements. *EMBO Journal*, *21*(1–2), 165–174. https://doi.org/10.1093/emboj/21.1.165

Müller, S., & Appel, B. (2017). In vitro circularization of RNA. In *RNA Biology* (Vol. 14, Issue 8, pp. 1018–1027). Taylor and Francis Inc. https://doi.org/10.1080/15476286.2016.1239009

Murakami, H., Goto, D. B., Toda, T., Chen, E. S., Grewal, S. I., Martienssen, R. A., & Yanagida, M. (2007). Ribonuclease Activity of Dis3 Is Required for Mitotic Progression and Provides a Possible Link between Heterochromatin and Kinetochore Function. *PLoS ONE*, *2*(3), e317. https://doi.org/10.1371/journal.pone.0000317

Nagarajan, V. K., Jones, C. I., Newbury, S. F., & Green, P. J. (2013). XRN 5'→3' exoribonucleases: Structure, mechanisms and functions. In *Biochimica et Biophysica Acta - Gene Regulatory Mechanisms* (Vol. 1829, Issues 6–7, pp. 590–603). Elsevier. https://doi.org/10.1016/j.bbagrm.2013.03.005

Nigro, J. M., Cho, K. R., Fearon, E. R., Kern, S. E., Ruppert, J. M., Oliner, J. D., Kinzler, K. W., & Vogelstein, B. (1991). Scrambled exons. *Cell*, *64*(3), 607–613. https://doi.org/10.1016/0092-8674(91)90244-S

Obi, P., & Chen, Y. G. (2021). The design and synthesis of circular RNAs. *Methods*. https://doi.org/10.1016/j.ymeth.2021.02.020

Ohkura, H., Adachi, Y., Kinoshita, N., Niwa, O., Toda, T., & Yanagida, M. (1988). Cold-sensitive and caffeine-supersensitive mutants of the Schizosaccharomyces pombe dis genes implicated in sister chromatid separation during mitosis. *The EMBO Journal*, *7*(5), 1465–1473. https://doi.org/10.1002/j.1460-2075.1988.tb02964.x

Ok Hyun Park, A., Ha, H., Lee, Y., Ho Boo, S., Hoon Kwon, D., Kyu Song, H., Ki Kim Correspondence, Y., Hyun Park, O., & Ki Kim, Y. (2019). Endoribonucleolytic Cleavage of m 6 A-Containing RNAs by RNase P/MRP Complex. *Molecular Cell*, *74*, 494–507. https://doi.org/10.1016/j.molcel.2019.02.034

Pamudurti, N. R., Bartok, O., Jens, M., Ashwal-Fluss, R., Stottmeister, C., Ruhe, L., Hanan, M., Wyler, E., Perez-Hernandez, D., Ramberger, E., Shenzis, S., Samson, M., Dittmar, G., Landthaler, M., Chekulaeva, M., Rajewsky, N., & Kadener, S. (2017). Translation of CircRNAs. *Molecular Cell*, *66*(1), 9-21.e7. https://doi.org/10.1016/j.molcel.2017.02.021

Park, O. H., Ha, H., Lee, Y., Boo, S. H., Kwon, D. H., Song, H. K., & Kim, Y. K. (2019). Endoribonucleolytic Cleavage of m6A-Containing RNAs by RNase P/MRP Complex. *Molecular Cell*, *74*(3), 494-507.e8. https://doi.org/10.1016/j.molcel.2019.02.034

Pastori, R. L., Moskaitis, J. E., Buzek, S. W., & Schoenberg, D. R. (1991). Coordinate estrogen-regulated instability of serum protein-coding messenger RNAs in Xenopus laevis. *Molecular Endocrinology*, *5*(4), 461–468. https://doi.org/10.1210/mend-5-4-461

Pastori, R. L., Moskaitis, J. E., & Schoenberg, D. R. (1991). Estrogen-Induced Ribonuclease Activity in Xenopus Liver. *Biochemistry*, *30*(43), 10490–10498. https://doi.org/10.1021/bi00107a018

Petkovic, S., & Müller, S. (2018). Synthesis and engineering of circular RNAs. In *Methods in Molecular Biology* (Vol. 1724, pp. 167–180). Humana Press Inc. https://doi.org/10.1007/978-1-4939-7562-4_14

Pirouz, M., Munafò, M., Ebrahimi, A. G., Choe, J., & Gregory, R. I. (2019). Exonuclease requirements for mammalian ribosomal RNA biogenesis and surveillance. *Nature Structural and Molecular Biology*, *26*(6), 490–500. https://doi.org/10.1038/s41594-019-0234-x

Piwecka, M., Glažar, P., Hernandez-Miranda, L. R., Memczak, S., Wolf, S. A., Rybak-Wolf, A., Filipchyk, A., Klironomos, F., Jara, C. A. C., Fenske, P., Trimbuch, T., Zywitza, V., Plass, M., Schreyer, L., Ayoub, S., Kocks, C., Kühn, R., Rosenmund, C., Birchmeier, C., & Rajewsky, N. (2017). Loss of a mammalian circular RNA locus causes miRNA deregulation and affects brain function. *Science*, *357*(6357). https://doi.org/10.1126/science.aam8526

Preker, P., Nielsen, J., Kammler, S., Lykke-Andersen, S., Christensen, M. S., Mapendano, C. K., Schierup, M. H., & Jensen, T. H. (2008). RNA exosome depletion reveals transcription upstream of active human promoters. *Science*, *322*(5909), 1851–1854. https://doi.org/10.1126/science.1164096

Preußer, C., Hung, L. H., Schneider, T., Schreiner, S., Hardt, M., Moebus, A., Santoso, S., & Bindereif, A. (2018). Selective release of circRNAs in platelet-derived extracellular vesicles. *Journal of Extracellular Vesicles*, *7*(1). https://doi.org/10.1080/20013078.2018.1424473

Robinson, S. R., Oliver, A. W., Chevassut, T. J., & Newbury, S. F. (2015). The 3’ to 5’ exoribonuclease DIS3: From structure and mechanisms to biological functions and role in human disease. In *Biomolecules* (Vol. 5, Issue 3, pp. 1515–1539). MDPI AG. https://doi.org/10.3390/biom5031515

Ron, D., & Hubbard, S. R. (2008). How IRE1 Reacts to ER Stress. In *Cell* (Vol. 132, Issue 1, pp. 24–26). Elsevier B.V. https://doi.org/10.1016/j.cell.2007.12.017

Rossi, F., Legnini, I., Megiorni, F., Colantoni, A., Santini, T., Morlando, M., Di Timoteo, G., Dattilo, D., Dominici, C., & Bozzoni, I. (2019). Circ-ZNF609 regulates G1-S progression in rhabdomyosarcoma. *Oncogene*, *38*(20), 3843–3854. https://doi.org/10.1038/s41388-019-0699-4

Russo, N., Shapiro, R., Acharya, K. R., Riordan, J. F., & Vallee, B. L. (1994). Role of glutamine-117

in the ribonucleolytic activity of human angiogenin. *Proceedings of the National Academy of Sciences of the United States of America*, *91*(8), 2920–2924. https://doi.org/10.1073/pnas.91.8.2920

Rybak-Wolf, A., Stottmeister, C., Glažar, P., Jens, M., Pino, N., Giusti, S., Behm, M., Bartok, O., Ashwal-Fluss, R., Herzog, M., Schreyer, L., Papavasileiou, P., Ivanov, A., Öhman, M., Refojo, D., Kadener, S., & Rajewsky, N. (2014). Circular RNAs in the Mammalian Brain Are Highly Abundant, Conserved, and Dynamically Expressed. *Molecular Cell*, *58*(5), 870–885. https://doi.org/10.1016/j.molcel.2015.03.027

Salzman, J., Chen, R. E., Olsen, M. N., Wang, P. L., & Brown, P. O. (2013). Cell-Type Specific Features of Circular RNA Expression. *PLoS Genetics*, *9*(9). https://doi.org/10.1371/journal.pgen.1003777

Salzman, J., Gawad, C., Wang, P. L., Lacayo, N., & Brown, P. O. (2012). Circular RNAs are the predominant transcript isoform from hundreds of human genes in diverse cell types. *PLoS ONE*, *7*(2). https://doi.org/10.1371/journal.pone.0030733

Sanger, H. L., Klotz, G., Riesner, D., Gross, H. J., & Kleinschmidt, A. K. (1976). Viroids are single stranded covalently closed circular RNA molecules existing as highly base paired rod like structures. *Proceedings of the National Academy of Sciences of the United States of America*, *73*(11), 3852–3856. https://doi.org/10.1073/pnas.73.11.3852

Schaeffer, D., Tsanova, B., Barbas, A., Reis, F. P., Dastidar, E. G., Sanchez-Rotunno, M., Arraiano, C. M., & Van Hoof, A. (2009). The exosome contains domains with specific endoribonuclease, exoribonuclease and cytoplasmic mRNA decay activities. *Nature Structural and Molecular Biology*, *16*(1), 56–62. https://doi.org/10.1038/nsmb.1528

Scherbik, S. V., Paranjape, J. M., Stockman, B. M., Silverman, R. H., & Brinton, M. A. (2006). RNase L Plays a Role in the Antiviral Response to West Nile Virus. *Journal of Virology*, *80*(6), 2987–2999. https://doi.org/10.1128/jvi.80.6.2987-2999.2006

Schilders, G., van Dijk, E., & Pruijn, G. J. M. (2007). C1D and hMtr4p associate with the human exosome subunit PM/Scl-100 and are involved in pre-rRNA processing. *Nucleic Acids Research*, *35*(8), 2564–2572. https://doi.org/10.1093/nar/gkm082

Schillewaert, S., Wacheul, L., Lhomme, F., & Lafontaine, D. L. J. (2012). The Evolutionarily Conserved Protein LAS1 Is Required for Pre-rRNA Processing at Both Ends of ITS2. *Molecular and Cellular Biology*, *32*(2), 430–444. https://doi.org/10.1128/mcb.06019-11

Schneider, C., Anderson, J. T., & Tollervey, D. (2007). The Exosome Subunit Rrp44 Plays a Direct Role in RNA Substrate Recognition. *Molecular Cell*, *27*(2), 324–331. https://doi.org/10.1016/j.molcel.2007.06.006

Schneider, C., Kudla, G., Wlotzka, W., Tuck, A., & Tollervey, D. (2012). Transcriptome-wide Analysis of Exosome Targets. *Molecular Cell*, *48*(3), 422–433. https://doi.org/10.1016/j.molcel.2012.08.013

Schneider, C., Leung, E., Brown, J., & Tollervey, D. (2009). The N-terminal PIN domain of the exosome subunit Rrp44 harbors endonuclease activity and tethers Rrp44 to the yeast core exosome. *Nucleic Acids Research*, *37*(4), 1127–1140. https://doi.org/10.1093/nar/gkn1020

Segalla, S., Pivetti, S., Todoerti, K., Chudzik, M. A., Giuliani, E. C., Lazzaro, F., Volta, V., Lazarevic, D., Musco, G., Muzi-Falconi, M., Neri, A., Biffo, S., & Tonon, G. (2015). The ribonuclease DIS3 promotes let-7 miRNA maturation by degrading the pluripotency factor LIN28B mRNA. *Nucleic Acids Research*, *43*(10), 5182–5193. https://doi.org/10.1093/nar/gkv387

Sidrauski, C., & Walter, P. (1997). The transmembrane kinase Ire1p is a site-specific endonuclease that initiates mRNA splicing in the unfolded protein response. *Cell*, *90*(6), 1031–1039. https://doi.org/10.1016/S0092-8674(00)80369-4

Smith, S. B., Kiss, D. L., Turk, E., Tartakoff, A. M., & Andrulis, E. D. (2011). Pronounced and extensive microtubule defects in a Saccharomyces cerevisiae DIS3 mutant. *Yeast*, *28*(11), 755–769. https://doi.org/10.1002/yea.1899

Snee, M. J., Wilson, W. C., Zhu, Y., Chen, S. Y., Wilson, B. A., Kseib, C., O'Neal, J., Mahajan, N., Tomasson, M. H., Arur, S., & Skeath, J. B. (2016). Collaborative control of cell cycle progression by the RNA exonuclease Dis3 and ras is conserved across species. *Genetics*, *203*(2), 749–762. https://doi.org/10.1534/genetics.116.187930

Staals, R. H. J., Bronkhorst, A. W., Schilders, G., Slomovic, S., Schuster, G., Heck, A. J. R., Raijmakers, R., & Pruijn, G. J. M. (2010). Dis3-like 1: A novel exoribonuclease associated with the human exosome. *EMBO Journal*, *29*(14), 2358–2367. https://doi.org/10.1038/emboj.2010.122

Stagsted, L. V. W., Nielsen, K. M., Daugaard, I., & Hansen, T. B. (2019). Noncoding AUG circRNAs constitute an abundant and conserved subclass of circles. *Life Science Alliance*, *2*(3). https://doi.org/10.26508/lsa.201900398

Starke, S., Jost, I., Rossbach, O., Schneider, T., Schreiner, S., Hung, L. H., & Bindereif, A. (2015).

Exon circularization requires canonical splice signals. *Cell Reports*, *10*(1), 103–111. https://doi.org/10.1016/j.celrep.2014.12.002

Stevens, A., Wang, Y., Bremer, K., Zhang, J., Hoepfner, R., Antoniou, M., Schoenberg, D. R., & Maquat, L. E. (2002). β-globin mRNA decay in erythroid cells: UG site-preferred endonucleolytic cleavage that is augmented by a premature termination codon. *Proceedings of the National Academy of Sciences of the United States of America*, *99*(20), 12741–12746. https://doi.org/10.1073/pnas.192442399

Stoll, L., Sobel, J., Rodriguez-Trejo, A., Guay, C., Lee, K., Venø, M. T., Kjems, J., Laybutt, D. R., & Regazzi, R. (2018). Circular RNAs as novel regulators of β-cell functions in normal and disease conditions. *Molecular Metabolism*, *9*, 69–83. https://doi.org/10.1016/j.molmet.2018.01.010

Su, Z., Kuscu, C., Malik, A., Shibata, E., & Dutta, A. (2019). Angiogenin generates specific stress-induced tRNA halves and is not involved in tRF-3-mediated gene silencing. *Journal of Biological Chemistry*, *294*(45), 16930–16941. https://doi.org/10.1074/jbc.RA119.009272

Surono, A., Takeshima, Y., Wibawa, T., Ikezawa, M., Nonaka, I., & Matsuo, M. (1999). Circular dystrophin RNAs consisting of exons that were skipped by alternative splicing. *Human Molecular Genetics*, *8*(3), 493–500. https://doi.org/10.1093/hmg/8.3.493

Symmons, M. F., & Luisi, B. F. (2009). Through Ancient Rings Thread Programming Strings. In *Structure* (Vol. 17, Issue 11, pp. 1429–1431). Cell Press. https://doi.org/10.1016/j.str.2009.10.006

Synowsky, S. A., van den Heuvel, R. H. H., Mohammed, S., Pijnappel, W. W. M. P., & Heck, A. J. R. (2006). Probing genuine strong interactions and post-translational modifications in the heterogeneous yeast exosome protein complex. *Molecular and Cellular Proteomics*, *5*(9), 1581–1592. https://doi.org/10.1074/mcp.M600043-MCP200

Szczepińska, T., Kalisiak, K., Tomecki, R., Labno, A., Borowski, L. S., Kulinski, T. M., Adamska, D., Kosinska, J., & Dziembowski, A. (2015). DIS3 shapes the RNA polymerase II transcriptome in humans by degrading a variety of unwanted transcripts. *Genome Research*, *25*(11), 1622–1633. https://doi.org/10.1101/gr.189597.115

Tafforeau, L., Zorbas, C., Langhendries, J. L., Mullineux, S. T., Stamatopoulou, V., Mullier, R., Wacheul, L., & Lafontaine, D. L. J. (2013). The complexity of human ribosome biogenesis revealed by systematic nucleolar screening of pre-rRNA processing factors. *Molecular Cell*,

51(4), 539–551. https://doi.org/10.1016/j.molcel.2013.08.011

Tan, W. L. W., Lim, B. T. S., Anene-Nzelu, C. G. O., Ackers-Johnson, M., Dashi, A., See, K., Tiang, Z., Lee, D. P., Chua, W. W., Luu, T. D. A., Li, P. Y. Q., Richards, A. M., & Foo, R. S. Y. (2017). A landscape of circular RNA expression in the human heart. *Cardiovascular Research*, *113*(3), 298–309. https://doi.org/10.1093/cvr/cvw250

Tanaka, N., Nakanishi, M., Kusakabe, Y., Goto, Y., Kitade, Y., & Nakamura, K. T. (2004). Structural basis for recognition of 2′,5′-linked oligoadenylates by human ribonuclease L. *EMBO Journal*, *23*(20), 3929–3938. https://doi.org/10.1038/sj.emboj.7600420

Telekawa, C., Boisvert, F. M., & Bachand, F. (2018). Proteomic profiling and functional characterization of post-translational modifications of the fission yeast RNA exosome. *Nucleic Acids Research*, *46*(21), 11169–11183. https://doi.org/10.1093/nar/gky915

Tirasophon, W., Lee, K., Callaghan, B., Welihinda, A., & Kaufman, R. J. (2000). The endoribonuclease activity of mammalian IRE1 autoregulates its mRNA and is required for the unfolded protein response. *Genes and Development*, *14*(21), 2725–2736. https://doi.org/10.1101/gad.839400

Tomecki, R., Drazkowska, K., Kucinski, I., Stodus, K., Szczesny, R. J., Gruchota, J., Owczarek, E. P., Kalisiak, K., & Dziembowski, A. (2014). Multiple myeloma-associated hDIS3 mutations cause perturbations in cellular RNA metabolism and suggest hDIS3 PIN domain as a potential drug target. *Nucleic Acids Research*, *42*(2), 1270–1290. https://doi.org/10.1093/nar/gkt930

Tomecki, R., Kristiansen, M. S., Lykke-Andersen, S., Chlebowski, A., Larsen, K. M., Szczesny, R. J., Drazkowska, K., Pastula, A., Andersen, J. S., Stepien, P. P., Dziembowski, A., & Jensen, T. H. (2010). The human core exosome interacts with differentially localized processive RNases: HDIS3 and hDIS3L. *EMBO Journal*, *29*(14), 2342–2357. https://doi.org/10.1038/emboj.2010.121

Tourrière, H., Gallouzi, I., Chebli, K., Capony, J. P., Mouaikel, J., van der Geer, P., & Tazi, J. (2001). RasGAP-Associated Endoribonuclease G3BP: Selective RNA Degradation and Phosphorylation-Dependent Localization. *Molecular and Cellular Biology*, *21*(22), 7747–7760. https://doi.org/10.1128/mcb.21.22.7747-7760.2001

Towler, B. P., Jones, C. I., Viegas, S. C., Apura, P., Waldron, J. A., Smalley, S. K., Arraiano, C. M., & Newbury, S. F. (2015). The 3'-5' exoribonuclease Dis3 regulates the expression of specific microRNAs in Drosophila wing imaginal discs. *RNA Biology*, *12*(7), 728–741.

https://doi.org/10.1080/15476286.2015.1040978

Van Eynde, A., Pérez-Callejón, E., Schoenmakers, E., Jacquemin, M., Stalmans, W., & Bollen, M. (1999). Organization and alternate splice products of the gene encoding nuclear inhibitor of protein phosphatase-1 (NIPP-1). *European Journal of Biochemistry*, *261*(1), 291–300. https://doi.org/10.1046/j.1432-1327.1999.00272.x

Venø, M. T., Hansen, T. B., Venø, S. T., Clausen, B. H., Grebing, M., Finsen, B., Holm, I. E., & Kjems, J. (2015). Spatio-temporal regulation of circular RNA expression during porcine embryonic brain development. *Genome Biology*, *16*(1). https://doi.org/10.1186/s13059-015-0801-3

Verduci, L., Ferraiuolo, M., Sacconi, A., Ganci, F., Vitale, J., Colombo, T., Paci, P., Strano, S., Macino, G., Rajewsky, N., & Blandino, G. (2017). The oncogenic role of circPVT1 in head and neck squamous cell carcinoma is mediated through the mutant p53/YAP/TEAD transcription-competent complex. *Genome Biology*, *18*(1). https://doi.org/10.1186/s13059-017-1368-y

Walker, B. A., Wardell, C. P., Melchor, L., Hulkki, S., Potter, N. E., Johnson, D. C., Fenwick, K., Kozarewa, I., Gonzalez, D., Lord, C. J., Ashworth, A., Davies, F. E., & Morgan, G. J. (2012). Intraclonal heterogeneity and distinct molecular mechanisms characterize the development of t(4;14) and t(11;14) myeloma. *Blood*, *120*(5), 1077–1086. https://doi.org/10.1182/blood-2012-03-412981

Wang, M., & Cohen, S. N. (1994). ard-1: A human gene that reverses the effects of temperature-sensitive and deletion mutations in the Escherichia coli rne gene and encodes an activity producing RNase E-like cleavages. *Proceedings of the National Academy of Sciences of the United States of America*, *91*(22), 10591–10595. https://doi.org/10.1073/pnas.91.22.10591

Wang, P. L., Bao, Y., Yee, M.-C., Barrett, S. P., Hogan, G. J., Olsen, M. N., Dinneny, J. R., Brown, P. O., & Salzman, J. (2014). Circular RNA Is Expressed across the Eukaryotic Tree of Life. *PLoS ONE*, *9*(3), e90859. https://doi.org/10.1371/journal.pone.0090859

Wang, Y., & Wang, Z. (2015). Efficient backsplicing produces translatable circular mRNAs. *RNA*, *21*(2), 172–179. https://doi.org/10.1261/rna.048272.114

Wasmuth, E. V., & Lima, C. D. (2012). Exo- and Endoribonucleolytic Activities of Yeast Cytoplasmic and Nuclear RNA Exosomes Are Dependent on the Noncatalytic Core and Central Channel. *Molecular Cell*, *48*(1), 133–144. https://doi.org/10.1016/j.molcel.2012.07.012

Weng, W., Wei, Q., Toden, S., Yoshida, K., Nagasaka, T., Fujiwara, T., Cai, S., Qin, H., Ma, Y., &

Goel, A. (2017). Circular RNA ciRS-7 — A promising prognostic biomarker and a potential therapeutic target in colorectal cancer. *Clinical Cancer Research*, *23*(14), 3918–3928. https://doi.org/10.1158/1078-0432.CCR-16-2541

Werfel, S., Nothjunge, S., Schwarzmayr, T., Strom, T. M., Meitinger, T., & Engelhardt, S. (2016). Characterization of circular RNAs in human, mouse and rat hearts. *Journal of Molecular and Cellular Cardiology*, *98*, 103–107. https://doi.org/10.1016/j.yjmcc.2016.07.007

Wesselhoeft, R. A., Kowalski, P. S., & Anderson, D. G. (2018). Engineering circular RNA for potent and stable translation in eukaryotic cells. *Nature Communications*, *9*(1). https://doi.org/10.1038/s41467-018-05096-6

Wesselhoeft, R. A., Kowalski, P. S., Parker-Hale, F. C., Huang, Y., Bisaria, N., & Anderson, D. G. (2019). RNA Circularization Diminishes Immunogenicity and Can Extend Translation Duration In Vivo. *Molecular Cell*, *74*(3), 508-520.e4. https://doi.org/10.1016/j.molcel.2019.02.015

Westholm, J. O., Miura, P., Olson, S., Shenker, S., Joseph, B., Sanfilippo, P., Celniker, S. E., Graveley, B. R., & Lai, E. C. (2014). Genome-wide Analysis of Drosophila Circular RNAs Reveals Their Structural and Sequence Properties and Age-Dependent Neural Accumulation. *Cell Reports*, *9*(5), 1966–1980. https://doi.org/10.1016/j.celrep.2014.10.062

Widmann, B., Wandrey, F., Badertscher, L., Wyler, E., Pfannstiel, J., Zemp, I., & Kutay, U. (2012). The kinase activity of human Rio1 is required for final steps of cytoplasmic maturation of 40S subunits. *Molecular Biology of the Cell*, *23*(1), 22–35. https://doi.org/10.1091/mbc.E11-07-0639

Wilson, D. M., Takeshita, M., Grollman, A. P., & Demple, B. (1995). Incision activity of human apurinic endonuclease (Ape) at abasic site analogs in DNA. *Journal of Biological Chemistry*, *270*(27), 16002–16007. https://doi.org/10.1074/jbc.270.27.16002

Wilusz, J. E., Freier, S. M., & Spector, D. L. (2008). 3′ End Processing of a Long Nuclear-Retained Noncoding RNA Yields a tRNA-like Cytoplasmic RNA. *Cell*, *135*(5), 919–932. https://doi.org/10.1016/j.cell.2008.10.012

Wu, X., Xiao, S., Zhang, M., Yang, L., Zhong, J., Li, B., Li, F., Xia, X., Li, X., Zhou, H., Liu, D., Huang, N., Yang, X., Xiao, F., & Zhang, N. (2021). A novel protein encoded by circular SMO RNA is essential for Hedgehog signaling activation and glioblastoma tumorigenicity. *Genome Biology*, *22*(1). https://doi.org/10.1186/s13059-020-02250-6

Xiao, M. S., & Wilusz, J. E. (2019). An improved method for circular RNA purification using RNase R that efficiently removes linear RNAs containing G-quadruplexes or structured 3’ ends. *Nucleic*

Acids Research, *47*(16), 8755–8769. https://doi.org/10.1093/nar/gkz576

Yamasaki, S., Ivanov, P., Hu, G. F., & Anderson, P. (2009). Angiogenin cleaves tRNA and promotes stress-induced translational repression. *Journal of Cell Biology*, *185*(1), 35–42. https://doi.org/10.1083/jcb.200811106

Yang, F., & Schoenberg, D. R. (2004). Endonuclease-mediated mRNA decay involves the selective targeting of PMR1 to polyribosome-bound substrate mRNA. *Molecular Cell*, *14*(4), 435–445. https://doi.org/10.1016/j.molcel.2004.05.001

Yang, Y., Fan, X., Mao, M., Song, X., Wu, P., Zhang, Y., Jin, Y., Yang, Y., Chen, L. L., Wang, Y., Wong, C. C. L., Xiao, X., & Wang, Z. (2017). Extensive translation of circular RNAs driven by N 6 -methyladenosine. *Cell Research*, *27*(5), 626–641. https://doi.org/10.1038/cr.2017.31

Ye, C. Y., Chen, L., Liu, C., Zhu, Q. H., & Fan, L. (2015). Widespread noncoding circular RNAs in plants. *New Phytologist*, *208*(1), 88–95. https://doi.org/10.1111/nph.13585

Yoo, C. J., & Wolin, S. L. (1997). The yeast La protein is required for the 3' endonucleolytic cleavage that matures tRNA precursors. *Cell*, *89*(3), 393–402. https://doi.org/10.1016/S0092-8674(00)80220-2

Yoshida, H., Matsui, T., Yamamoto, A., Okada, T., & Mori, K. (2001). XBP1 mRNA is induced by ATF6 and spliced by IRE1 in response to ER stress to produce a highly active transcription factor. *Cell*, *107*(7), 881–891. https://doi.org/10.1016/S0092-8674(01)00611-0

You, X., Vlatkovic, I., Babic, A., Will, T., Epstein, I., Tushev, G., Akbalik, G., Wang, M., Glock, C., Quedenau, C., Wang, X., Hou, J., Liu, H., Sun, W., Sambandan, S., Chen, T., Schuman, E. M., & Chen, W. (2015). Neural circular RNAs are derived from synaptic genes and regulated by development and plasticity. *Nature Neuroscience*, *18*(4), 603–610. https://doi.org/10.1038/nn.3975

Yu, C. Y., Li, T. C., Wu, Y. Y., Yeh, C. H., Chiang, W., Chuang, C. Y., & Kuo, H. C. (2017). The circular RNA circBIRC6 participates in the molecular circuitry controlling human pluripotency. *Nature Communications*, *8*(1), 1–15. https://doi.org/10.1038/s41467-017-01216-w

Zaphiropoulos, P G. (1997). Exon skipping and circular RNA formation in transcripts of the human cytochrome P-450 2C18 gene in epidermis and of the rat androgen binding protein gene in testis. *Molecular and Cellular Biology*, *17*(6), 2985–2993. https://doi.org/10.1128/mcb.17.6.2985

Zaphiropoulos, Peter G. (1996). Circular RNAs from transcripts of the rat cytochrome P450 2C24

gene: Correlation with exon skipping. *Proceedings of the National Academy of Sciences of the United States of America*, *93*(13), 6536–6541. https://doi.org/10.1073/pnas.93.13.6536

Zekri, L., Chebli, K., Tourrière, H., Nielsen, F. C., Hansen, T. V. O., Rami, A., & Tazi, J. (2005). Control of Fetal Growth and Neonatal Survival by the RasGAP-Associated Endoribonuclease G3BP. *Molecular and Cellular Biology*, *25*(19), 8703–8716. https://doi.org/10.1128/mcb.25.19.8703-8716.2005

Zeng, K., Chen, X., Xu, M., Liu, X., Hu, X., Xu, T., Sun, H., Pan, Y., He, B., & Wang, S. (2018). CircHIPK3 promotes colorectal cancer growth and metastasis by sponging miR-7 article. *Cell Death and Disease*, *9*(4). https://doi.org/10.1038/s41419-018-0454-8

Zeng, Y., Du, W. W., Wu, Y., Yang, Z., Awan, F. M., Li, X., Yang, W., Zhang, C., Yang, Q., Yee, A., Chen, Y., Yang, F., Sun, H., Huang, R., Yee, A. J., Li, R. K., Wu, Z., Backx, P. H., & Yang, B. B. (2017). A circular RNA binds to and activates AKT phosphorylation and nuclear localization reducing apoptosis and enhancing cardiac repair. *Theranostics*, *7*(16), 3842–3855. https://doi.org/10.7150/thno.19764

Zhang, M., Huang, N., Yang, X., Luo, J., Yan, S., Xiao, F., Chen, W., Gao, X., Zhao, K., Zhou, H., Li, Z., Ming, L., Xie, B., & Zhang, N. (2018). A novel protein encoded by the circular form of the SHPRH gene suppresses glioma tumorigenesis. *Oncogene*, *37*(13), 1805–1814. https://doi.org/10.1038/s41388-017-0019-9

Zhang, X. O., Wang, H. Bin, Zhang, Y., Lu, X., Chen, L. L., & Yang, L. (2014a). Complementary sequence-mediated exon circularization. *Cell*, *159*(1), 134–147. https://doi.org/10.1016/j.cell.2014.09.001

Zhang, X. O., Wang, H. Bin, Zhang, Y., Lu, X., Chen, L. L., & Yang, L. (2014b). Complementary sequence-mediated exon circularization. *Cell*, *159*(1), 134–147. https://doi.org/10.1016/j.cell.2014.09.001

Zhang, Y., Xue, W., Li, X., Zhang, J., Chen, S., Zhang, J. L., Yang, L., & Chen, L. L. (2016). The Biogenesis of Nascent Circular RNAs. *Cell Reports*, *15*(3), 611–624. https://doi.org/10.1016/j.celrep.2016.03.058

Zhang, Y., Zhang, X. O., Chen, T., Xiang, J. F., Yin, Q. F., Xing, Y. H., Zhu, S., Yang, L., & Chen, L. L. (2013). Circular Intronic Long Noncoding RNAs. *Molecular Cell*, *51*(6), 792–806. https://doi.org/10.1016/j.molcel.2013.08.017

Zhao, J., Lee, E. E., Kim, J., Yang, R., Chamseddin, B., Ni, C., Gusho, E., Xie, Y., Chiang, C. M.,

Buszczak, M., Zhan, X., Laimins, L., & Wang, R. C. (2019). Transforming activity of an oncoprotein-encoding circular RNA from human papillomavirus. *Nature Communications*, *10*(1). https://doi.org/10.1038/s41467-019-10246-5

Zheng, Q., Bao, C., Guo, W., Li, S., Chen, J., Chen, B., Luo, Y., Lyu, D., Li, Y., Shi, G., Liang, L., Gu, J., He, X., & Huang, S. (2016). Circular RNA profiling reveals an abundant circHIPK3 that regulates cell growth by sponging multiple miRNAs. *Nature Communications*, *7*(1), 1–13. https://doi.org/10.1038/ncomms11215

Zuo, Y., & Deutscher, M. P. (2001). Exoribonuclease superfamilies: Structural analysis and phylogenetic distribution. *Nucleic Acids Research*, *29*(5), 1017–1026. https://doi.org/10.1093/nar/29.5.1017

11 Contributions

Prof. Dr. Remco Sprangers kindly provided recombinant proteins and contributed to the project with discussions. Protein purifications were performed by Anna-Lisa Fuchs.

Astrid Bruckmann and Eduard Hochmuth performed all mass-spectrometric measurements and analysis.

RNA-seq experiments were performed together with the group of Prof. Dr. Nikolaus Rajewsky at the Max-Delbrück Center for Molecular Medicine (Berlin, Germany).

Data analysis of linear RNA sequencing data was performed by Gerhard Lehmann (Gunter Meister lab).

Data analysis of circular RNA sequencing data was performed by Petar Glazar in the group of Prof. Dr. Nikolaus Rajewsky.

Figure 32 and Mass spectrometry analysis were done with the support of Simone Larivera.